Investigating the effects of targeting nitric oxide pathways in a kainic acid mouse model of epileptogenesis

Thesis submitted in accordance with the requirements of the

University of Liverpool for the degree of

Doctor in Philosophy

by

Karen Tse

March 2015

Declaration

This thesis is the result of my own work. The material presented within this thesis is, to the best of my knowledge, original and has not been submitted in whole or part of a degree in any other university.

Karen Tse

The research presented in this thesis was carried out in the Wolfson Centre for Personalised Medicine, Department of Molecular and Clinical Pharmacology, Institute of Translational Medicine and the Duncan Building, Department of Musculoskeletal Biology, Institute of Ageing and Chronic Disease, University of Liverpool, United Kingdom.

Acknowledgements

To begin with, I would like to thank my supervisors, Graeme J Sills, Thimmasettappa Thippeswamy and Richard Barrett-Jolley for their guidance and support in the last 3-4 years. I would also like to thank Dr Thippeswamy for securing the funding at the University of Liverpool and Biotechnology and Biological Sciences Research Council Centre for the work in this thesis. I would also like to thank Dr Deb Simpson and Professor Rob Beynon for their help and guidance on the proteomics work. Special thanks to Will Redfern who recommended me to the PhD programme.

I would like to extend my gratitude to Professor Matthew Walker, Dr Mala Shah and Dr Rob Wykes at University College London for their guidance on my EEG model. This also goes to Gail Calvert from Meso Scale Discovery for her help with the multiplex kit, and Dean Plumbley from the University of Manchester for his help with the coastline analysis. I would also like to thank all other PhD students for their help and support during my time at Liverpool. I thank Ed Beamer for training me at the start of my PhD, Gurpreet Ghattaoraya for his programming skills and Lauren Walker for enlightening me of the reality dealing with clinical epilepsy.

I have made many friends throughout my PhD and I thank all of them for the good memories during one of the toughest journey of my life. Thanks to Hayley for keeping me company in the dark room and wait for blots to appear, Gurpreet and Philippe for keeping me company at the Wolfson Centre while I wrote my thesis and Lauren for letting me spend time with her girls when I needed a break from writing.

Finally, I'd like to thank my godparents, mum and brothers for their encouragement and support. I would like to dedicate this thesis to my godfather, who constantly reassured me that there will be light at the end of the tunnel.

Table of Contents

List of figures

List of tables

List of abbreviations

AEDs	Antiepileptic drugs
AGC	Automatic gain control
AMPA	α-amino-2-hydroxy-5-methyl-4-isoxazolepropionic acid
ANOVA	Analysis of Variance
ATP	Adenosine triphosphate
AUC	Area under the curve
BBB	Blood-brain-barrier
BSA	Bovine serum albumin
CA1	*Cornu Ammonis* 1 etc..
CAG	Chrom alum gelatine
Chapsyn	Channel-associated proteins of synapse
CID	Collisional-induced dissociation
CNS	Central nervous system
CREB	Cyclic adenosine monophosphate response element-binding protein
CY3	Cyanine 3
DAPI	4',6-diamidino-2-phenylindole
DG	Dentate gyrus
DSI	Data Scientific International
EDTA	Ethylenediaminetetraacetic acid
EEG	Electroencephalography
eNOS	Endothelial nitric oxide synthase
FITC	Fluorescein isothiocyanate
GABA	γ-aminobutyric acid
GAPDH	Glyceraldehyde-3-phosphate dehydrogenase
HCD	Higher energy collisional dissociation
HPLC	High performance liquid chromatography
HRP	Horse-radish peroxidase
IHC	Immunohistochemistry
IFN-γ	Interferon-γ
IL-1	Interleukin-1 etc..
ILAE	International League Against Epilepsy
i.m.	Intramuscular
iNOS	Inducible nitric oxide synthase
i.p.	Intraperitoneal
KA	Kainic acid
KC/GRO	Keratinocyte-derived cytokine/growth-related oncogene
K_{ir}4.1	Inwardly-rectifying potassium channel 4.1
LAP	Latency-associated peptide
LC-MS	Liquid chromatography-mass spectrometry
LPS	Lipopolysaccharide
LTBP	Latency binding protein
MALDI-TOF	Matrix-assisted laser desorption ionisation time-of-flight
MS	Mass spectrometry
MSD	Meso Scale Discovery
NADPH	Nicotinamide adenine dinucleotide phosphate
NMDA	*N*-methyl-D-aspartate

NMDAR	NMDA receptor
nNOS	Neuronal nitric oxide synthase
NO	Nitric oxide
NOS	NO synthase
NR2B	NMDAR subunit 2B fusion protein
PBS	Phosphate buffered saline
PFA	Paraformaldehyde
PSD95	Post-synaptic density 95 protein
PSD95BP	PSD95 blocking peptide
R^2	Coefficient of determination
ROS	Reactive oxygen species
Sb	Subiculum
s.c.	Subcutaneous
SD	Standard deviation
SDS-PAGE	Sodium dodecyl sulphate-polyacrylamide gel electrophoresis
SE	*Status epilepticus*
SEM	Standard error of mean
SRS	Spontaneous recurrent seizures
STRING	Search Tool for the Retrieval of Interacting Genes/Proteins
T_h	Helper T cells
TBS	Tris buffered saline
TBST	TBS with Tween 20
TFA	Trifluoroacetic acid
TGFβ1	Transforming growth factor β1
TGFβRI	Transforming growth factor β receptor 1
TLE	Temporal lobe epilepsy
TNF-α	Tumour necrosis factor-α
UniProt	Universal Protein Resource

Publications and proceedings arising from this thesis

Published literature

- **Tse K**, Puttachary S, Beamer E, Sills GJ, Thippeswamy T (2014) Advantages of Repeated Low Dose against Single High Dose of Kainate in C57BL/6J Mouse Model of Status Epilepticus: Behavioral and Electroencephalographic Studies. *PLoS ONE* 9(5): e96622. Doi:10.1371/journal.pone.0096622

Manuscripts in preparation

- **Tse K**, Simpson D, Beynon R, Sills GJ, Thippeswamy T (2015) The proteomic profile of the hippocampus: confounding effects of intracranial surgery in a mouse model of epileptogenesis.

Published abstracts

- **Tse K**, Simpson D, Beynon R, Sills GJ, Thippeswamy T (2013) Confounding effects of intracranial procedures in a kainate model of epileptogenesis *British Neurosci. Assoc. Abstr., Vol.22: P545*

Other abstracts

- **Tse K**, Sills GJ, Thippeswamy T (2013) The effects of PSD95 blocking peptide and 1400W dihydrochloride on electrographic spikes in a kainate mouse model of epilepsy *Proceedings of the ILAE British Chapter Annual Scientific Meeting, Glasgow*
- **Tse K**, Beamer E, Simpson D, Beynon R, Sills GJ, Thippeswamy T (2012) Proteomics and immunohistochemical analyses of astrogliosis in a mouse model of epileptogenesis *Proceedings of the ProteoMMX 2.0, Strictly Quantitative Symposium, Chester*

Abstract

Epilepsy is one of the most common chronic neurological disorders, and the symptomatic form is characterised by the occurrence of spontaneous recurrent seizures following a neurological insult. One third of epilepsy patients are resistant to antiepileptic drugs (AEDs), therefore the development of novel treatments is required. Glutamate is implicated in epilepsy however, only a few glutamate receptor antagonists have been successful in epilepsy trials. An indirect means of modifying glutamate-mediated excitation, such as targeting nitric oxide (NO), might be a reasonable alternative approach. Selectively targeting NO signalling pathway by two drug interventions was investigated in this thesis. Post-synaptic density 95 blocking peptide (PSD95BP) is a protein that uncouples GluN2 subunits of the N-methyl-D-aspartate (NMDA) subtype of glutamate receptor from neuronal NO synthase to prevent downstream neurotoxic signalling of NO. In contrast, 1400W is a highly specific inducible NO synthase inhibitor that binds to the guanidine recognition site of the enzyme, competing with L-arginine and preventing neurotoxic production of NO. These compounds are effective in animal models of stroke and were tested here in a C57BL/6J mouse model of epileptogenesis. Kainic acid (KA) is widely used to induce *status epilepticus* (SE) in animals and the resulting neuropathology mimics that seen in humans with temporal lobe epilepsy. Repeated low dose administration of KA via intraperitoneal injection every 30 minutes consistently induced generalised seizures but was associated with inter-animal variability in KA sensitivity, acute seizure severity and mortality rate. Extra-dural telemetry electrodes were implanted in mice for electroencephalography (EEG) recordings. Two algorithms, measuring spike frequency and EEG coastline respectively, were used to quantify epileptiform activity. Mice that received drug interventions following KA-induced SE had significantly lower mean spike frequency and fewer extended coastline epochs per day than the control group at both 7 and 14 days after the initial insult. Label-free proteomics quantification showed significant changes to the hippocampal protein profile as a result of both PSD95BP and 1400W administration following KA-induced seizures. Drug treatment, singly or in combination, also reversed the effects of KA on the expression of both transforming growth factor β1 and inwardly rectifying potassium channel 4.1 in the hippocampus. Surgical implantation of extra-dural electrodes significantly lowered the seizure threshold to KA and was associated with an increase in brain expression of pro-inflammatory cytokines, suggesting that careful consideration is required in studies involving intracranial surgery to assess epileptogenesis or AED effects. Current research investigating novel therapeutic agents is focusing on non-NMDA glutamate receptors, such as α-amino-3-hydroxy-5-methyl-4-isoxazolepropionic acid and kainate receptors, as potential AED targets. There are no compounds targeting the NO signalling pathway currently being investigated for the treatment of epilepsy. The data reported in this thesis give cause for optimism but further studies are needed to fully investigate the antiepileptic and possible antiepileptogenic properties of PSD95BP and 1400W and true efficacy will ultimately require clinical evaluation.

Chapter 1

Introduction

1.1. Epilepsy

1.1.1. Overview

Epilepsy is one of the most common chronic neurological disorders worldwide and includes a number of conditions with the principal characteristics of spontaneous and recurrent seizures that arise as a result of prolonged and synchronised neuronal discharges (Chang and Lowenstein, 2003; Aroniadou-Anderjaska et al., 2008; Vincent and Mulle, 2009). The most current International League Against Epilepsy (ILAE) operational clinical definition of epilepsy is the occurrence of "at least two unprovoked (or reflex) seizures occurring more than 24 hours apart" or "one unprovoked seizure and a probability of further seizures that are similar to the general recurrence risk (at least 60%) after two unprovoked seizures, occurring over the next 10 years" (ILAE, 2014). Epilepsy usually presents in childhood or during adolescence but can occur for the first time at any age (Lindsay et al., 2010).

1.1.2. Epidemiology and aetiology

Approximately 5% of the world's population will experience a single seizure during their lives but only 0.5% will develop spontaneous recurrent seizures (SRS) (Lindsay et al., 2010). In developed countries, the incidence is approximately 1 in 2000 people annually and in poorer, developing countries, there are higher incidences affecting approximately 1 in 100 people per year (Sander, 2003). The reasons for the increase in incidence in developing countries are attributed to the poorer health status of the patients and health care availability (Birbeck, 2010).

Amongst epilepsy patients, the overall prognosis for seizure treatment is good, with 70% of patients well-controlled with antiepileptic drugs (AEDs) (Sander, 2003; Lindsay et al., 2010). However, the remaining 30% are resistant to drug treatment (Lindsay et al., 2010), and the new discovery of AEDs has thus far failed to significantly improve the prognosis of drug-resistant epilepsy (Herman, 2010). Non-pharmacological treatments of epilepsy, such as vagal nerve stimulation, ketogenic diet, transcranial magnetic stimulation are also considered

as alternatives to antiepileptic pharmacotherapy and have been shown to be as effective as pharmacotherapy in some patients (Wolf and Okujava, 1999; Saxena and Nadkami, 2011). Despite being the most common neurological disorder, there is still a lack of understanding of the epidemiology of epilepsy due to heterogeneity of the syndrome (Sander, 2003).

There are three aetiological classes of epilepsy, idiopathic, symptomatic and cryptogenic. Idiopathic epilepsy cases are believed to be mainly genetically related and comprise of approximately 30% of all clinical cases and represent self-limited epilepsy syndromes with strictly defined clinical and electroencephalography (EEG) findings but with no other neurological findings (Sander, 2003; Berkovic et al., 2006; Shorvon, 2011). Symptomatic epilepsy, which also constitutes approximately 30% of epilepsy cases, generally arises from an identifiable insult to the brain associated with gross pathological abnormalities, indicative of underlying disease or condition (Sander, 2003; Shorvon, 2011). Seizures triggered by the insult are acute symptomatic seizures and do not constitute as epilepsy until SRS occur (Sander, 2003). Some of the primary causes of symptomatic epilepsy include traumatic brain injury, stroke, tumours and central nervous system (CNS) infections (Sander, 2003; Dudek and Staley, 2011). Cryptogenic epilepsies are those that resemble symptomatic epilepsies in their phenomenology but in which the presumed lesion remains elusive on brain imaging (Shorvon, 2011).

Epileptic seizures are classified into two broad groups – generalised and partial. Generalised seizures result from convulsive discharges that start from deeper midline structures, and arise in both cerebral hemispheres simultaneously, and can manifest as generalised tonic, clonic or tonic-clonic convulsions with the loss of consciousness (Sharma et al., 2007; Lindsay et al., 2010). Other generalised seizure types, such as absence and myoclonic, do not possess a major convulsive component. Generalised seizures generally exhibit no evidence of local onset (Dingledine et al., 1990). In contrast, partial seizures are caused by attacks stemming from focal neurological lesions but can spread across the entire brain (Chang and Lowenstein, 2003) and may gradually develop into secondary

generalised seizures (Sharma et al., 2007). Complex partial seizures are the most frequent single seizure type; they occur when a partial seizure is accompanied by impaired consciousness and they most commonly develop from the mesial temporal lobe (Samuel, 2000; Lindsay et al., 2010). The mechanisms underlying partial seizures are not very well understood, despite being the most common seizure disorder in adults and accounting for up to 50% of incident and 60% of prevalent epilepsy cases (Samuel, 2000; Chang and Lowenstein, 2003).

1.1.3. Temporal lobe epilepsy

Temporal lobe epilepsy (TLE) is the most common and arguably most important type of symptomatic partial epilepsy and is often characterised by mesial temporal sclerosis with complex recurrent partial seizures (Samuel, 2000; Williams et al., 2009). TLE is a progressive disease with silent intervals and progressive elaboration of seizures (French et al., 1993). In some cases, epileptiform activity spreads to other limbic structures including the amygdala complex and the medial entorhinal cortex, causing secondary generalised tonic-clonic seizures (Vincent and Mulle, 2009).

TLE is invariably treated with AEDs, which provide only symptomatic intervention rather than disease-modifying treatment (Herman, 2002; Sharma et al., 2007). TLE is often resistant to AED therapy (Samuel, 2000; Aroniadou-Anderjaska et al., 2008) and symptomatic partial epilepsy in general is more likely to be drug-resistant than idiopathic epilepsy (Kwan and Brodie 2004; Gilioli et al, 2012). The current alternative therapeutic approach for drug-resistant TLE is surgical resection of specific structural lesions in the hippocampus, which is located in the mesial temporal lobe of the brain, with the elimination of seizures in up to 80% of patients (Schmidt and Löscher, 2003; Buckmaster, 2004). Nevertheless, there can be risks of causing immediate and permanent loss of a patient's ability to make new memories, as the hippocampus is responsible for memory formation (Buckmaster, 2004). The potential adverse outcome of surgery makes surgical resection treatment for TLE less than ideal, meaning that it remains useful to develop novel drug treatments that can prevent "epileptogenesis" or the development of epilepsy (see below). Studying the

molecular mechanisms of epileptogenesis would facilitate the identification of a mechanistic target or biomarker involved in the epileptogenic process, which can then be targeted for drug development. Currently, clinical studies on the process of epileptogenesis rely on self-reporting of seizures from patients that may have post-seizure amnesia or unnoticed attacks that may have occurred during the night (Sridharan, 2002). Unreported attacks, together with the lack of continuous EEG monitoring and the use of therapy to suppress seizures has prevented the collection of quantitative clinical data on the development and progression of epilepsy (Williams et al., 2009). As an alternative, animal models can be used to provide insights into the temporal features of acquired epilepsy (Williams et al., 2009).

1.2. Epileptogenesis

1.2.1. Overview

The initial brain insult in symptomatic epilepsy that ultimately causes partial seizures is commonly followed by a latent period or "silent interval", during which there is no seizure activity until the first appearance of SRS (Walker et al., 2002; Chang and Lowenstein, 2003; Williams et al., 2009). Partial seizures can induce molecular and cellular changes to the brain, and the alterations in the surviving neurons that eventually lead to SRS is a measure of epileptogenesis (Walker et al., 2002; Aroniadou-Anderjaska et al., 2008). Epileptogenesis occurs during the latent period and is the process by which surviving injured neurons progressively form hyperexcitable, epileptic neuronal networks (Aroniadou-Anderjaska et al., 2008). The latent period does not, however, define the duration of epileptogenesis (Williams et al., 2009), as epileptogenesis can continue after the onset of SRS (Williams et al., 2007; 2009). The latent period is known to be highly variable in rat models of epileptogenesis and the unpredictability of the onset of SRS originally suggested that epileptogenesis occurred only during the latent period (Williams et al., 2009). However, there is now strong evidence to support the suggestion that development of symptomatic epilepsy is continuous and/or progressive and persists after the onset of clinical seizures (Williams et al., 2009).

The understanding of epileptogenesis fundamentally comes from animal models investigating brain trauma, stroke or *status epilepticus* (SE)-induced epileptogenesis, and most models produce alterations in the brain similar to those found in resected temporal lobe tissue of patients with drug-resistant epilepsy (Pitkänen and Lukasiuk, 2009). The understanding of cellular and molecular mechanisms of epileptogenesis is still incomplete and requires further investigation to help target the development of preventive therapeutic approaches (Herman, 2002; Friedman et al., 2009). The latent period in particular is considered to be a window of opportunity for intervention designed to retard or prevent the subsequent development of epilepsy. Animal models have been widely used in the past to study cellular and molecular mechanisms of TLE and can also be used to test potential novel anticonvulsant or antiepileptogenic therapies (Löscher, 2002; Buckmaster, 2004; Löscher, 2011; Bauer and Norwood, 2013). Currently, administration of AEDs following acute brain insults has failed to prevent chronic epilepsy, indicating that present AEDs are antiepileptic but not antiepileptogenic, most likely because they were not designed for that purpose (Herman, 2002; Walker et al., 2002).

Present AEDs are used to treat the acute symptoms of seizures and do not affect the development of chronic epilepsy (Smith et al, 2007). Traditional AEDs were mostly discovered by chance, rather than designed (Baker and Jacoby, 2013; Brodie, 2010). Phenobarbital was given to epilepsy patients for sedative purposes; the accompanying anticonvulsant effect was purely fortuitous (Brodie, 2010). Carbamazepine was synthesised as an atypical antipsychotic and only later recognised to have anticonvulsant properties (Brodie, 2010). Valproic acid was initially used as a solvent to dissolve drugs of interest in an epilepsy drug screening study; its antiepileptic effects were realised when all animals in the screening study, including vehicle-treated controls, were protected against seizures (Brodie, 2010). Subsequently identified AEDs were identified and screened as part of the Anticonvulsant Drug Development Programme (Smith et al, 2007) using target-orientated design, modification of existing molecules and systematic screening against a range of animal seizure models (Brodie, 2010).

Using this discovery process, the identified AEDs share similar mechanistic characteristics in decreasing neuronal excitation or increasing neuronal inhibition (Smith et al, 2007) but they do not modify the course of epilepsy or prevent the development of epilepsy (Smith et al, 2007).

1.2.2. Animal models of epileptogenesis

Countless animal models have been used in epilepsy research, most of which are acute models of single seizures rather than chronic models of epileptogenesis (Löscher, 2011). Chronic models of epileptogenesis, where animals develop SRS, can be spontaneous, as in the case of using mutant or transgenic animals with inherent epilepsy, or can be acquired, in which an initial brain insult is induced either chemically or electrically or by direct brain trauma (Löscher, 2011). Chronic epilepsy models with induced SE are considered to have the greatest resemblance to human TLE (Löscher, 2011). Currently, the most widely used chemicals to induce SE in animals are pilocarpine and kainic acid (KA) (Löscher, 2002). Pilocarpine, a cholinergic muscarinic agonist, and KA, an excitotoxic glutamate analogue, can be administered systemically, intracerebrally or intracerebroventricularly. Both chemicals, when administered systemically, target the hippocampus as the seizure onset zone (Lévesque and Avoli, 2013). The neuropathology arising from pilocarpine or KA-induced epilepsy includes mossy fibre sprouting in the dentate gyrus (DG), neuronal loss in thalamus, *substantia nigra*, amygdala, hippocampal formation, olfactory cortices and neocortex, marked atrophy and dendritic sprouting in the sensorimotor cortex, and reorganisation and neuroplasticity of neocortical networks (Curia et al., 2008; Lévesque and Avoli, 2013). These effects are similar to the neuropathology of patients with TLE, which is characterised by neuronal loss in the hippocampal formation, aberrant mossy fibre sprouting in the molecular layer of DG and granule cell dispersion (Berkovic et al, 1991; Buckmaster, 2012; Lévesque and Avoli, 2013).There are also differences between chemical-induced epilepsy models and TLE patients. Seizure propagation is faster in animal models than in humans and TLE patients generally have lateraliesd foci and lesions, whereas seizure onsets and lesions are equal in both hemispheres in rodents (Jefferys, 2014).

Despite showing similarities in seizure onset region and in their neuropathological characteristics, there are differences between pilocarpine and KA in their blood-brain-barrier (BBB) penetration and the duration of the latent period that follows the initial SE. The opening of the BBB has been suggested to be a major precipitating factor in the induction of acute seizures (Marchi et al., 2011; Lévesque and Avoli, 2013). Pilocarpine is generally co-administered with compounds, such as lithium, bradykinin or histamine, that enhance BBB permeability in order to induce epileptiform activity at lower doses (Müller et al., 2009; Lévesque and Avoli, 2013). KA, on the other hand, is able to temporarily increase BBB permeability independently during acute seizures (Zucker et al., 1983; Williams et al., 2009). Pilocarpine-induced SE is reported to be far more intense than that induced by KA and therefore the onset of SRS is likely to occur earlier (Williams et al., 2009). Pilocarpine-treated rats show presence of spontaneous seizures during the first week following SE (Jung et al, 2007), whereas KA-treated rats show first spontaneous motor seizures beyond 7 days after SE (Hellier et al, 1999). Although lower doses can extend the latent period to SRS and lower the mortality rate, the average latency is still shorter for pilocarpine than for KA-treated rats (Curia et al, 2008; Glien et al, 2001; Hellier et al, 1998). Evidence of a shortened latent period in the pilocarpine model could potentially mean a limited window of opportunity to investigate potential antiepileptogenic agents, where the intervention is administered after the initial acute neurological insult. Nevertheless, both pilocarpine and KA have short latent period compared to human TLE, which can in some cases take 20+ years to develop following a complex febrile seizure (Williams et al, 2007). Shorter latent period is even less characteristic of human TLE (White, 2002), therefore, the KA model of epileptogenesis may be considered to be more suitable for investigating antiepileptogenic properties of drug interventions and more consistent with the human disorder it is intended to model.

1.3. Neurotransmission in epilepsy

Epilepsy can develop from an imbalance of excitatory and inhibitory neurotransmission. Epilepsy occurs when there is an increase in neuronal activity caused by either an abnormally high level of excitatory neurotransmission or a decrease in inhibitory neurotransmission (Bradford, 1995). The abnormal amplification and synchronisation of neuronal firing that causes seizures, and also changes in amino acid content in brain tissues following the onset of epileptic seizures, involves the interaction of inhibitory neurotransmitter, γ-aminobutyric acid (GABA), and excitatory neurotransmitter, glutamate (Bradford, 1995). Almost all excitatory CNS neurotransmission is controlled by glutamate. It is acknowledged as the most important transmitter for normal brain function (Purves et al., 2001) and is one of the most important factors in regulating the physiological balance of CNS function. Glutamate is implicated in several neurological disorders, including epilepsy (Danysz et al., 1995). Excessive release of glutamate and prolonged excitatory synaptic transmission is toxic to neurons due to the resulting influx of calcium (Cao et al., 2005). The accumulation of calcium causes destruction of transporter proteins on pre-synaptic glial cells that are responsible for the uptake of glutamate from the synaptic cleft, hence causing a "feed-forward" excitotoxic mechanism of excessive stimulation of glutamate receptors (Nelson et al., 2003).

A transient increase in extracellular glutamate levels in the brain has been observed in epileptic patients during spontaneous seizures (Chapman, 2000). Excitatory glutamatergic mechanisms play a key role in the pathophysiology of epileptogenesis (Chapman, 2000) and may be involved at 3 different levels – chronic sub-convulsive hyperactivity in the epileptic focus; amplified excitatory activity leading to initiation of seizures and recruitment of excitatory neurons adjacent to the focus; and propagation of the hyperactivity to precipitate a generalised seizure (Bradford, 1995). Increased extracellular glutamate at the epileptic focus occurs at the onset of epileptic hyperactivity in animal models of epilepsy, and may precipitate further glutamate release (Bradford, 1995). Altering glutamate levels by manipulating glutamate transporter expression can

induce or suppress epileptic seizures in genetic models of epilepsy (Chapman, 2000).

Glutamate activates 3 major types of ionotropic receptors, *N*-methyl-D-aspartate (NMDA), α-amino-2-hydroxy-5-methyl-4-isoxazolepropionic acid (AMPA) and KA (Danysz et al., 1995) and these receptors are expressed mainly in the CNS (Figure 1.1).

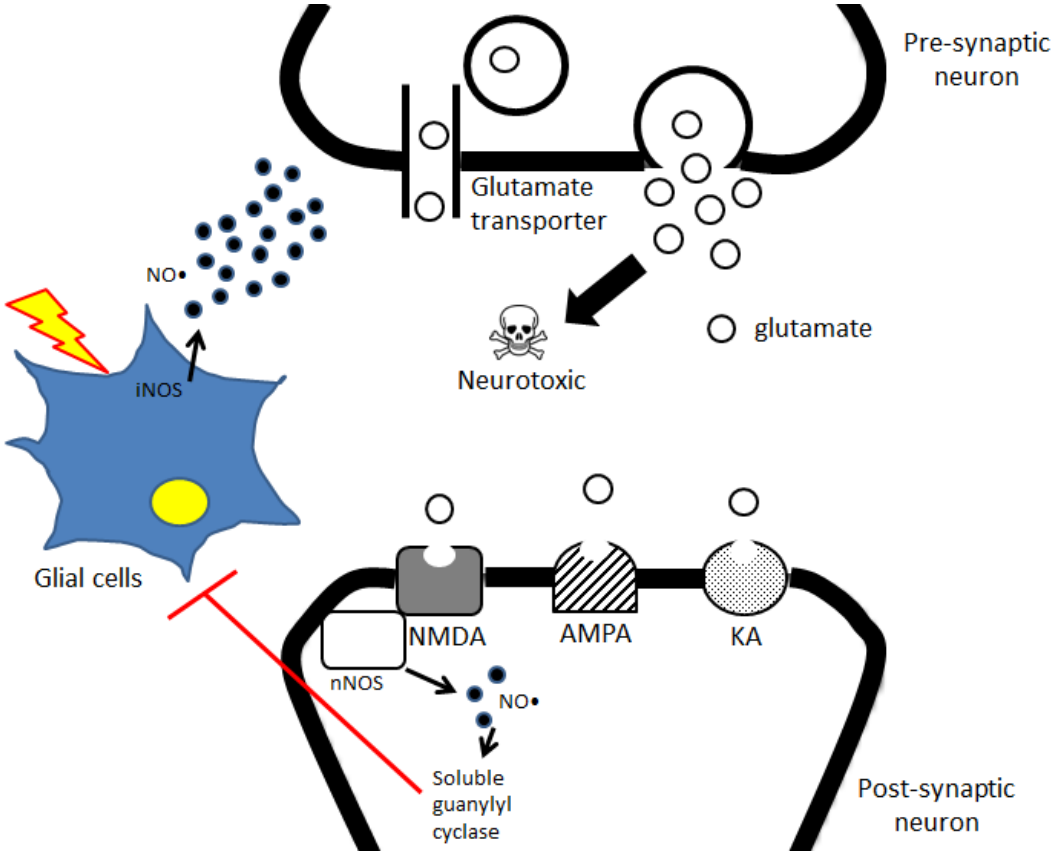

Figure 1.1. A schematic diagram illustrating synaptic neurotransmission. Neurons release glutamate from the pre-synaptic termimal and glutamate transporters are responsible for the uptake of glutamate back into the pre-synaptic terminal. Extracellular glutamate binds to glutamate receptors, *N*-methyl-D-aspartate (NMDA), α-amino-2-hydroxy-5-methyl-4-isoxazolepropionic acid (AMPA) or kainate (KA) on the post-synaptic neuron. At physiological conditions, neuronal nitric oxide synthase (nNOS) that is closely associated with NMDA receptors, produces endogenous low levels of nitric oxide (NO•) which exerts neuroprotective effects by activating soluble guanylyl cyclase. This activation can block glial cell activation, causing anti-inflammatory effects. In the event of a neurological insult, glial cells up-regulate inducible nitric oxide synthase (iNOS) activity that results in higher concentrations of NO• that can cause acute glutamate release from neurons, which leads to neurotoxicity. Image adapted from Araque et al (1999).

NMDA receptors (NMDAR) are involved in synaptic plasticity and long-term potentiation (Cull-Candy et al, 2001), and theiractivation largely mediates glutamate excitotoxicity and neuronal damage, and is involved in a variety of neurological disorders, including epilepsy (Danysz et al., 1995; Dingledine et al., 1999; Zhou and Zhu, 2009).

Glutamate receptors are an obvious therapeutic target in the search for new epilepsy drugs. However, until the recent advent of perampanel, which is an antagonist at AMPA receptors, few glutamate receptor agents had been successful in epilepsy trials (Dingledine et al., 1999). Competitive and uncompetitve NMDA receptor antagonists did not show convincing anticonvulsant activity but did cause severe neuropsychological adverse effects in healthy volunteers (Loscher, 1998). This prompted researchers to look at alternative, indirect means of modifying glutamate neurotoxicity. One such approach was to focus on nitric oxide, which is known to be a mediator of downstream signalling following glutamate activation (Dawson et al., 1991).

1.4. Nitric oxide

1.4.1. Overview

Nitric oxide (NO) is a gaseous chemical messenger molecule with many roles in the CNS and is typically produced endogenously at low levels (Nelson et al., 2003; Cherian et al., 2006; Benarroch, 2011). At physiological concentrations, NO exerts neuroprotective effects by inducing a structural change to NMDAR, and down-regulating its activity (Nelson et al., 2003). When produced in excess, NO can cause acute glutamate release from neurons and astrocytes, which leads to neurotoxicity (Dawson and Dawson, 1996) (Figure 1.1). NO induces cell death in a manner that is very similar to glutamate-induced cell death (Cao et al., 2005). Deficiency of NO is also associated with vasoconstriction of cerebral vessels, which can result in decreased cerebral blood flow and ischemia (Cherian et al., 2006). Developing novel drugs that target NO signalling has the potential to

benefit on its neuroprotective properties and prevent glutamate-induced neurotoxicity but also creates a risk of NO deficiency that can be equally detrimental. This balance between efficacy and toxicity may only allow a small therapeutic window, which can make this a risky target for drug development. However, by identifying the therapeutic range, given the appropriate therapeutic dose levels and the use of appropriate biomarkers for the treatment, it may be possible achieve efficacious levels and minimise toxicity.

1.4.2. Nitric oxide synthase

NO is not stored in synaptic vesicles and does not undergo exocytosis or act on membrane-bound receptors (Dawson et al., 1992; Dawson and Dawson, 1996). Rather, NO is synthesised on demand (Dawson and Dawson, 1996) and is rapidly neutralised by haemoglobin, methylene blue and superoxide anion, with a half-life of 3 to 5 seconds (Dawson et al., 1992; Rodeberg et al., 1995). NO is membrane permeable and diffuses from one neuron to another and acts on intracellular components (Dawson and Dawson, 1996). NO activity is regulated by its synthesis from the terminal guanidine group of L-arginine to a ω-hydroxyl-L-arginine intermediate compound, a reaction that is catalysed by the enzyme NO synthase (NOS). This reaction uses molecular oxygen and nicotinamide adenine dinucleotide phosphate (NADPH) to oxidise the substrate to L-citrulline and NO (Rodeberg et al., 1995; Dawson and Dawson, 1996; Benarroch, 2011). There are two types of NOS - constitutive and inducible. Constitutive forms include neuronal nitric oxide synthase (nNOS) and endothelial nitric oxide synthase (eNOS). Within the neurons, nNOS is mainly found in the cytoplasm but is concentrated at the post-synaptic membrane, closely associated with NMDAR (Cherian et al., 2006; Brown, 2010) (Figure 1.1). In the endothelium, eNOS produces NO and causes increased vascular blood flow, as NO is a potent vasodilator (Cherian et al., 2006). In contrast, inducible nitric oxide synthase (iNOS) is expressed predominantly in inflammatory cells, with NO production induced by pro-inflammatory cytokines or bacterial lipopolysaccharide (LPS) (Nomura and Kitamura, 1993; Kato et al., 2005; Benarroch, 2011).

1.4.3. Nitric oxide production under physiological conditions

NO is produced by most tissues in the body, however NO concentrations are highest in the brain (Cherian et al., 2006). All three isoforms of NOS can be expressed in the CNS, but under normal circumstances nNOS and eNOS predominate (Dawson and Dawson, 1996). eNOS regulates cerebral blood flow and BBB permeability (Dawson and Dawson, 1996; Kato et al., 2005; Parathath et al., 2007). Chemical signals in blood vessels activate eNOS by eliciting an increase in intracellular calcium (Benarroch, 2011). In contrast, nNOS regulates synaptic potentiation and plasticity, and modifies release of glutamate in the brain (Dawson and Dawson, 1996; Kato et al., 2005; Parathath et al., 2007). The mechanism of nNOS activation in neurons is through calcium influx via NMDAR (Dawson et al., 1992; Cherian et al., 2006; Benarroch, 2011). NO production by nNOS is activated by the binding of calcium to calmodulin (Nelson et al., 2003; Cao et al., 2005) (Figure 1.2).

The expression of nNOS is regulated by the activation of cyclic adenosine monophosphate response element-binding protein (CREB) by the calcium-calmodulin complex following calcium influx (Benarroch, 2011). At the post-synaptic density synapse, nNOS and calmodulin form a macromolecular complex via post-synaptic density 95 protein (PSD95). This complex promotes the calcium-calmodulin interaction with nNOS (Benarroch, 2011) (Figure 1.2). NO can act as a negative feedback system by oxidising some redox sites within the NMDAR and inhibiting calcium influx (Lipton and Stamler, 1994; De Luca et al., 2006).

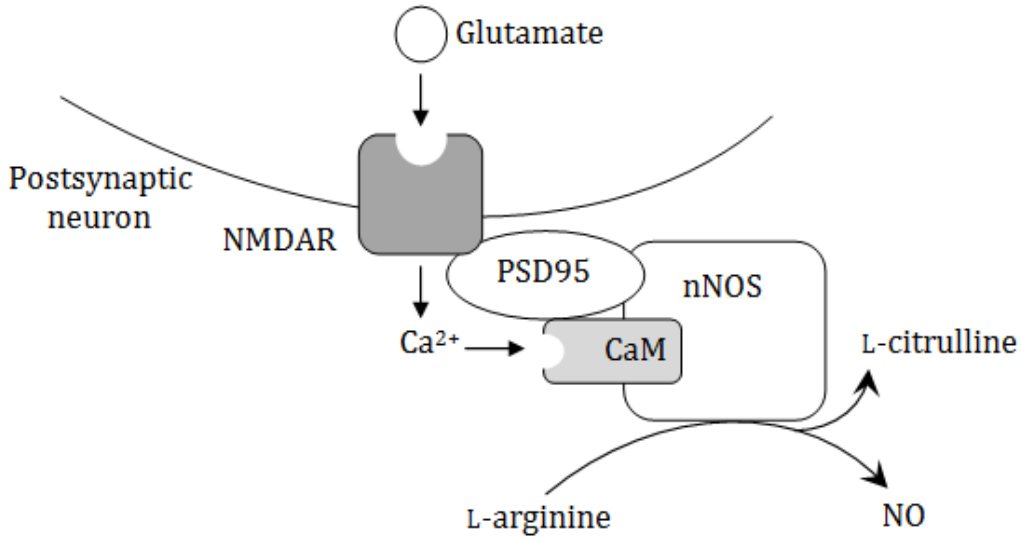

Figure 1.2. A schematic diagram illustrating the mechanism of neuronal nitric oxide synthase (nNOS) activation in postsynaptic neurons through calcium (Ca^{2+}) influx via the N-methyl-D-aspartate receptor (NMDAR), converting L-arginine to L-citrulline and nitric oxide (NO). NO production from nNOS is activated by binding of Ca^{2+} to calmodulin (CaM). CaM and nNOS form a macromolecular complex via post-synaptic density 95 (PSD95), which promotes the Ca^{2+}-CaM interaction with nNOS. Image adapted from previous publications (Dawson et al., 1992; Benarroch, 2011).

1.4.4. Nitric oxide production in neurological disease states

The activity of both constitutive forms of NOS can react rapidly to changes in physiological conditions, allowing transient increase in low levels of NO. In contrast, iNOS, when induced, produces higher concentrations of NO but over longer periods of time (Benarroch, 2011). iNOS expression in the brain is almost undetectable under normal physiological conditions but in several disease states, glial cells (specifically microglia and astrocytes) are triggered by pathogens, insult or hypoxia, and induce iNOS activity (Nelson et al., 2003; Cherian et al., 2006; Benarroch, 2011) (Figure 1.1). iNOS, once induced, is continuously activated without further induction (Nomura and Kitamura, 1993; Cherian et al., 2006; Benarroch, 2011). During an immune reaction, cytokines are produced to counteract pathogens and to coordinate a T-cell response. The increase in pro-inflammatory cytokines activates nuclear factor kB which induces iNOS

transcription in the nucleus (Nelson et al., 2003; Cherian et al., 2006; Benarroch, 2011). Hypoxia also induces iNOS via hypoxia-inducible factor-1 (Benarroch, 2011).

1.4.5. Neurotoxic properties of nitric oxide

The mechanisms of action of NO are mediated by different pathways, hence NO can be neuroprotective or neurotoxic depending on its concentration and cellular production (Benarroch, 2011). Low levels of NO are produced within seconds by nNOS and eNOS under normal physiological conditions. This transient increase in NO exerts neuroprotective and anti-apoptotic effects via a rapid and short-lasting activation of soluble guanylyl cyclase (Benarroch, 2011) (Figures 1.1 and 1.3).

This leads to the formation of cyclic guanosine monophosphate (cGMP) and activation of protein kinase G, which causes the inhibition of intracellular calcium release and regulates downstream transcription factors such as CREB, through phosphorylation by cGMP-dependent protein kinases (Dawson et al., 1992; Benarroch, 2011; Pilz and Casteel, 2003) (Figure 1.3). In the CNS, NO is the major activator of cGMP formation (Dawson and Dawson, 1996). This pathway modulates its effects on synaptic activity and vascular relaxation and its neuroprotective effects (Benarroch, 2011). Soluble guanylyl cyclase activation can also block astrocyte and microglial activation, causing anti-inflammatory effects (Brown, 2010) (Figure 1.1).

The neurotoxic effects of NO have been implicated in the pathogenesis of cerebral ischemia, neuroinflammation, brain tumours, neurodegenerative diseases and neurological disorders i.e. epilepsy (Kato et al., 2005; Brown, 2010). In the disease state, an excess production of NO can be both beneficial and detrimental due to the complex roles of NO under normal physiological conditions. NO itself is mildly toxic with limited number of potential cellular targets (Dawson and Dawson, 1996), but at high intracellular levels, NO may lead to nitrosative stress that is potentiated by the concomitant excessive production of reactive oxygen species (Dawson and Dawson, 1996; Benarroch, 2011).

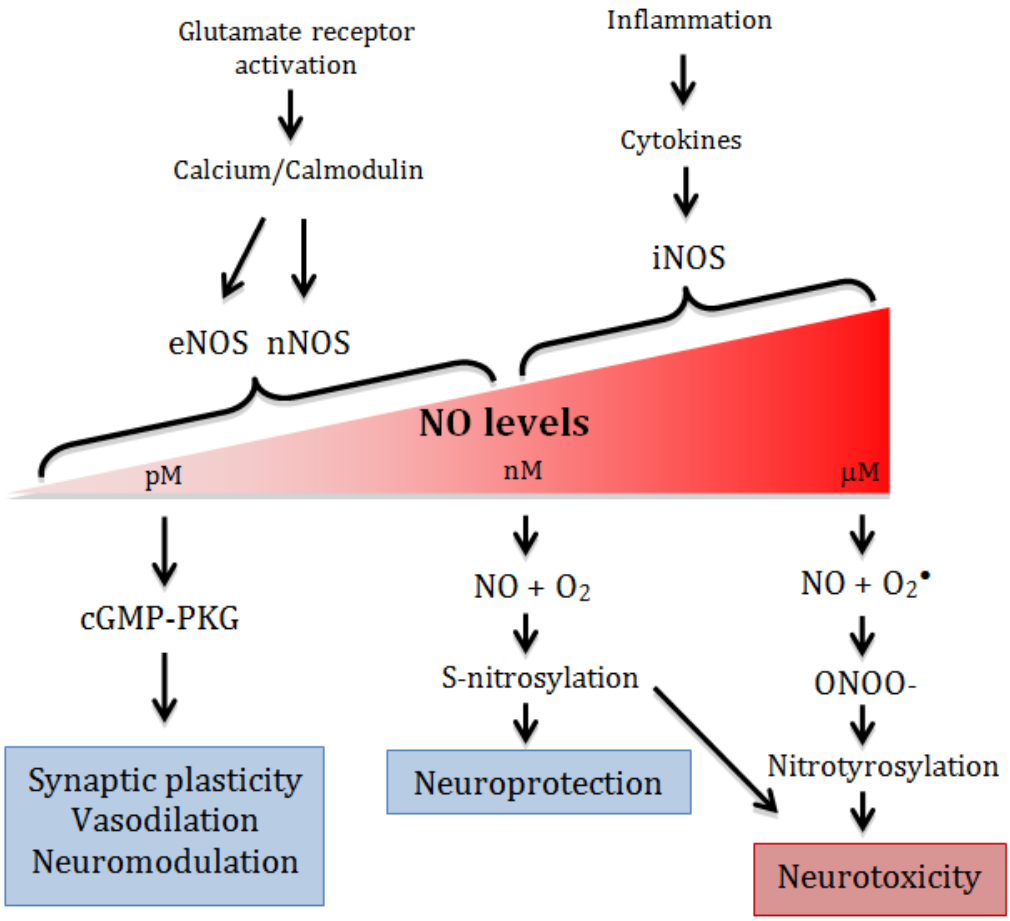

Figure 1.3. A schematic diagram illustrating the neuroprotective and neurotoxic properties of nitric oxide (NO) depending on its level of synthesis from neuronal nitric oxide synthase (nNOS), endothelial nitric oxide synthase (eNOS) and inducible nitric oxide synthase (iNOS). nNOS is activated through calcium influx via glutamate receptor activation and binding of calcium to calmodulin. eNOS is activated by an increase in intracellular calcium. iNOS expression is triggered by a neurological insult and the resulting increase in inflammatory cytokines induces iNOS transcription. The transient increase in NO by nNOS and eNOS leads to cyclic guanosine monophosphate and protein kinase G complex activation (cGMP-PKG). This pathway regulates the production of NO and its effects on synaptic plasticity, vasodilation and neuromodulation. S-nitrosylation occurs when NO combines with oxygen (O_2), which reversibly interacts with thiols to form S-nitrosothiol. The S-nitrosylation process causes neuroprotection at low levels of NO, while excess S-nitrosylation causes neurotoxicity. Nitrotyrosylation occurs when NO reacts with superoxide anion ($O_2^{\bullet}$) to produce peroxynitrite (ONOO-) that causes multiple neurotoxic effects via oxidative and nitrosative stress. Image adapted from (Benarroch, 2011)).

A chronic increase in NO causes neurotoxic and apoptotic effects via S-nitrosylation and nitrotyrosylation (Benarroch, 2011) (Figure 1.3). S-nitrosylation occurs when NO combines with oxygen to produce nitrosonium ion, which reversibly interacts with thiols to form S-nitrosothiol (Benarroch, 2011) (Figure 1.3). It is this S-nitrosylation process that causes a structural change to the transmembrane calcium channel proteins of the NMDAR and down-regulates receptor activity, which reduces calcium influx and exerts neuroprotection at low levels of NO (Nelson et al., 2003; Benarroch, 2011). Excess S-nitrosylation, however, causes neurotoxicity (Brown, 2010) (Figure 1.3). Nitrotyrosylation occurs when NO reacts with superoxide anion to produce peroxynitrite, a potent oxidant involved in neurotoxicity that spontaneously isomerises to nitrate tyrosine residues of proteins forming 3-nitrotyrosine. This causes multiple neurotoxic effects via oxidative and nitrosative stress (Benarroch, 2011) (Figure 1.3). Nitrosative stress contributes to the development of neurodegenerative disorders (Brown, 2010).

NO toxicity mediated by the induction of iNOS by pro-inflammatory cytokines is exacerbated by concurrent excessive production of NO from the calcium-sensitive activation of nNOS through the overstimulation of NMDARs, leading to calcium overload in the cell (Zhou and Zhu, 2009; Benarroch, 2011). Following a neurological insult, the homeostatic balance between endogenous antioxidants and reactive oxygen species (ROS) becomes unequal. iNOS is expressed as a result of increased ROS production and a decreased antioxidant defence. This results in oxidative stress that causes molecular damage and cell death (Nelson et al., 2003).

NO can also cause mitochondrial inhibition, glutamate release and subsequent excitotoxic neuronal death via glutamate receptor activation (Brown, 2010). High levels of NO causes acute glutamate release from neurons, resulting from either the inhibition of mitochondrial respiration followed by reversal of glutamate uptake, or by direct activation of vesicular exocytosis by modifying protein thiols (Brown, 2010). High NO levels can also induce acute glutamate release from astrocytes by causing intracellular calcium release followed by

calcium activation of vesicular exocytosis (Brown, 2010). Under normal physiological conditions, glutamate is localised mainly in presynaptic vesicles. Following its release during depolarising events it is efficiently removed from the synapse by glutamate transporters and re-packaged back into presynaptic vesicles (Figure 1.1). However, excessive release of glutamate leads to accumulation in the extracellular space, mediating cell death via NMDAR activation and the consequent increase in intracellular calcium levels in a process termed "excitotoxicity" (Dawson and Dawson, 1996; Brown, 2010).

BBB disruptions are associated with excitotoxicity following neurotrauma or inflammatory reactions (Wong et al., 2004). Following neurological insult, astrocytes and microglia become activated around the insult sites in the brain leading to elevated iNOS expression in glia (Nomura and Kitamura, 1993). The high concentrations of NO produced elicit neuronal death by causing inhibition of mitochondrial respiration in neurons, which in turn leads to neuronal depolarisation and glutamate release, therefore causing further excitotoxicity (Nomura and Kitamura, 1993; Brown, 2010). Excess NO can also compromise BBB integrity, which further compounds the cellular damage following glutamate release but the mechanism involved is poorly understood (Wong et al., 2004; Parathath et al., 2007).

1.4.6. Nitric oxide levels following acute neurological insult

NOS expression has been shown to increase in the cerebral cortex of patients with epilepsy (González-Hernández et al., 2000). NO produced by nNOS and eNOS is shown to peak immediately after a neurological insult, with a later peak of NO produced by iNOS following an interval of relative NO deficiency (Cherian et al., 2006). This low level in the intervening period is associated with low cerebral blood flow (Cherian et al., 2006). Following an insult, eNOS activity is believed to be beneficial, since genetically-modified rodents deficient in eNOS show more extensive neuronal damage than wild-type rodents following both experimental cerebral ischemia and traumatic brain injury (Huang et al., 1996; Parmentier et al., 1999; Jafarian-Tehrani et al., 2005). On the other hand, nNOS contributes to neurotoxicity within minutes following an insult (Cherian et al.,

2006). An increase in NO levels in the hippocampus of mice has been observed after KA administration (Kato et al., 2005). NO formation has also been shown to increase during KA-induced seizures in rat brain, but is not believed to be involved in the regulation of seizure generation and propagation (Milatovic et al., 2002). Pre-treatment with NOS inhibitors has been reported to reverse the increase in NO levels seen after KA administration *in vivo*, however, these inhibitors did not show any anti-seizure properties (Kato et al., 2005). The effect of NOS inhibitors is controversial in the literature, with reports suggesting both pro- and anti-convulsant activity, depending on dosage, time of administration and the animal species used (Przegaliński et al., 1994; Dawson and Dawson, 1996; Przegaliński et al., 1996; Kato et al., 2005). This can be explained by the fact that non-specific NOS inhibitors have effects on cerebral blood flow mediated via inhibition of eNOS, resulting in greater neuronal damage than is observed with convulsant agents such as KA alone (Dawson and Dawson, 1996; Kato et al., 2005). This finding emphasises the importance of specificity amongst NOS inhibitors. Targeting NO synthesis via highly specific inhibition of either nNOS or iNOS may be able to prevent excitotoxicity mediated via NMDAR or inflammation, respectively. These inhibitors can then be evaluated for potential antiepileptic or antiepileptogenic properties.

1.5. Pharmacological neuroprotection by disrupting nitric oxide synthesis

1.5.1. Post-synaptic density 95 blocking peptide

Post-synaptic density (PSD) is a cytoskeletal adapter specialisation, involved in anchoring neurotransmitter receptors and regulating the response of post-synaptic neurons to synaptic stimulation (Chen et al., 2006). PSD is composed of 4 major types of molecules – membrane-bound, cytoskeletal, scaffolding proteins and modulatory enzymes (Forder and Tymianski, 2009). Of all PSD proteins, PSD95 plays an important organisational role by coupling NMDAR to intracellular proteins and signalling enzymes (Forder and Tymianski, 2009). PSD95 is an essential synaptic adapter protein that binds to NMDAR subunits and activates the NMDAR-mediated cascade of downstream events, and thus has roles in

synaptic plasticity, neuronal ionic excitability and seizure susceptibility (Chen et al., 2006). Proteins from the same family as PSD95 are called channel-associated proteins of synapses (chapsyns), and it consists of four proteins: SAP90/PSD95, SAP97, PSD93/chapsyn-110 and SAP102 (Dingledine et al., 1999). These proteins can bind to the C termini of NMDAR subunits (Dingledine et al., 1999). PSD95 is an abundant cytoskeletal protein found mainly in the postsynaptic fraction of synaptosomes, although it can also be found presynaptically (Dingledine et al., 1999). PSD95 is also a multidomain protein that serves as a central mediator of assembly of the PSD complex (Cao et al., 2005). PSD95 contains 3 PDZ domains – PDZ1, PDZ2 and PDZ3. The PDZ domain is a structural domain shared by 3 proteins, PSD95, *Drosophilia* disc large tumor suppressor, Dlg1, and zonula occludens-1 protein, zo-1, and its name is derived from the first letter of each protein in that order (Kennedy, 1995).

PSD95 is central to the activation of nNOS. NO cannot be stored in the cells and must be generated on demand; this requires that nNOS is either bound to membranes directly or is anchored by adapter proteins to the membrane (Zhou and Zhu, 2009). PSD95 assembles in a tight ternary complex with nNOS and NMDAR subunit 2B (NR2B) fusion protein, by interacting with the C-terminal of the NMDAR subunit 2 (NR2) via the PDZ1 and PDZ2 domains, and interacting with nNOS via the PDZ2 domain (Christopherson et al., 1999; Dingledine and McBain, 1999; Cao et al., 2005). The NMDAR is therefore able to activate nNOS by coupling with PSD95 (Forder and Tymianski, 2009). The PDZ3 domain of PSD95 is not known to have any importance in glutamate-induced neuronal cell death (Cao et al., 2005).

NMDAR antagonists have been studied as potential antiepileptic agents in rodent models of epilepsy (Dingledine et al., 1990; Danysz et al., 1995; Brandt et al., 2003) and are shown to be weak AEDs when administered after SE (Brandt et al., 2003; Aroniadou-Anderjaska et al., 2008). Excitotoxic brain damage and epileptogenesis are likely to be controlled by different molecular pathways, therefore neuroprotective compounds may not necessarily be efficacious as AEDs in the treatment of epilepsy (Vincent and Mulle, 2009). NMDAR antagonists may

potentially be more effective as antiepileptogenic agents for the prevention of epilepsy. However, the development of a treatment that competitively blocks the NMDAR is unlikely to progress beyond clinical trials because of its neurotoxic side effects and the profound disturbances on normal brain function that would outweigh its therapeutic value (Dingledine and McBain, 1999; Löscher, 2002; Vincent and Mulle, 2009). Different NMDAR antagonists exert different impairment of NMDA receptor function. One of the variations depends on the off-rate of the compound (Sleigh et al, 2014). Ketamine, an open channel blocker, selectively influences the action of NMDAR by blocking the receptor when opened for prolonged period of time in pathological states, and has minimal effects when opened transiently at physiological states (Sleigh et al, 2014). However, ketamine also has a slow off-rate, which means ketamine remains trapped in the closed ion channel and causes a prolonged tonic blockade that disrupts physiological and pathological function (Sleigh et al, 2014). Antagonists with fast off-rate are able to escape from the ion channel before it closes, therefore preserving some physiological NMDA function with fewer adverse effects (Sleigh et al, 2014). Memantine, a low affinity open-channel blocker with a fast off-rate only blocks NMDA receptors when open for a pathologically prolonged time and has minimal effect when NMDA receptor is only transiently open in physiological states (Lipton, 2007). This mechanism is comparable to the effects of persistent sodium channel blockers (Devor, 2006), hence some NMDA antagonists maybe expected to have more adverse effects than sodium channel blockers. Therefore, selectively blocking the downstream signalling of NMDAR, by suppressing the expression of nNOS or PSD95, without affecting NMDAR itself might also reduce the vulnerability of neurons to NMDA-mediated toxicity and thus avoid the profound consequences of glutamatergic inhibition (Sun et al., 2008; Vincent and Mulle, 2009).

The NMDAR-PSD95-nNOS complex has been shown to be important in mediating excitotoxic damage (Cui et al., 2007). Peptides that selectively disrupt the interaction of the NMDAR with PSD95 protein have shown to reduce excitotoxic neuronal loss after ischaemia, without blocking excitatory neurotransmission (Sun et al., 2008; Forder and Tymianski, 2009; Vincent and Mulle, 2009). The

inhibition of nNOS has also been shown to have antiepileptic properties in the early phases of epileptogenesis in a mouse KA model (Beamer et al., 2012). However, inhibiting nNOS directly may also cause disturbance in physiological functions with undesirable long-term side effects, such as affecting learning and memory (Hopper and Garthwaite, 2006; Taqatqeh et al, 2009; Forstermann and Sessa, 2011). Interfering with nNOS-PSD95 interaction may be preferable and has been shown to reduce NO production without affecting nNOS function (Cui et al., 2007; Zhou and Zhu, 2009).

Disruption of the interaction between NR2B and PSD95 can be achieved by introducing a peptide that mimics the NMDAR subunit 2 (NR2) C-terminal interaction of NMDAR with the PDZ domain of PSD95. This peptide is termed NR2B9c as it comprises nine C-terminal (9c) residues of the NR2B subunit but is often referred to as PSD95 blocking peptide (PSD95BP) (Cui et al., 2007; Forder and Tymianski, 2009). To achieve BBB permeability, NR2B9c was fused to the cell membrane protein transduction domain of a human immunodeficiency virus type 1 Tat protein (Schwarze et al., 1999; Cui et al., 2007; Sun et al., 2008), hence PSD95BP is also named Tat-NR2B9c in some literature (Aarts et al., 2002; Cui et al., 2007; Forder and Tymianski, 2009; Cook et al., 2012). PSD95BP given intravenously at a dose of 7.6 mg/kg to rodents has been shown to exclusively block the PDZ domain of PSD95 and nNOS only, and uncouple NMDAR and nNOS without blocking other cellular interactions (Cui et al., 2007).

PSD95BP is the first pharmacological compound that has shown efficacy when administered after the ischemic insult in a primate model of stroke (Forder and Tymianski, 2009; Cook et al., 2012). PSD95BP has also been tested during the early phases of epileptogenesis in a KA mouse model of epilepsy, using EEG as a surrogate marker of outcome (Beamer, 2013). The administration of PSD95BP one hour after KA-induced SE significantly reduced epileptiform spike frequency during the subsequent 3-12 hours (Beamer, 2013). To my knowledge, PSD95BP has not been tested in any other animal model of epilepsy or against any other aspect of epileptogenesis.

1.5.2. 1400W dihydrochloride

N-(3-(aminomethyl)benzyl)acetamidine, also known as 1400W, is a highly selective, cell and tissue permeable iNOS inhibitor (Parmentier et al., 1999; Alderton et al., 2001). 1400W is currently the most selective known iNOS inhibitor and is at least 100-fold more selective in reducing vascular injury from LPS-induced iNOS in rats than previous iNOS inhibitors, such as aminoguanidine which also had inhibitory effects on nNOS and eNOS (Laszlo et al., 1995; Garvey et al., 1997). 1400W is 5000-fold more selective for iNOS than for eNOS, and 200-fold more selective for iNOS than for nNOS (Garvey et al., 1997). The inhibition of iNOS by 1400W has a slow onset and is NADPH-dependent (Garvey et al., 1997). Its mechanism of inhibition involves competition with L-arginine and is considered to be either irreversible or only very slowly reversible (Garvey et al., 1997; Alderton et al., 2001). Irreversible or very slowly reversible inhibitors can have prolonged effects, which may be therapeutically advantageous in some circumstances. However they may also cause more undesirable side effects as they permanently abolish the function of the respective enzyme and make the treatment of overdose problematic. The amidine moiety of 1400W is a structural analogue of guanidine, which is the functional group on the side chain of arginine (Garvey et al., 1997). 1400W binds to the guanidine recognition site of the enzyme, preventing the production of NO from L-arginine (Garvey et al., 1997). It shows biological activity with selectivity for iNOS in rat tissues and prevents microvasculature injury in an *in vivo* rat model (Garvey et al., 1997).

An inflammatory response is one of the events that is activated following a neurological insult and NO is known to play a crucial role in neuroinflammation. The induction of iNOS during epileptogenesis has been reported in various rodent models of epilepsy (Park et al., 2001; Rehni et al., 2009). The production of NO by iNOS can be detrimental to the brain, depending on the time of production (Jafarian-Tehrani et al., 2005). In *in vitro* models, induction of iNOS in glial cells following LPS challenge has an onset at around 4 hours and peaks at 24 hours, while NO levels increase linearly from 4 to 72 hours after LPS insult in the presence of L-arginine (Nomura and Kitamura, 1993). The induction of iNOS has been shown to cause neuronal cell death up to 72 hours after LPS insult in

primary rat mixed glial-neuronal cultures (Dawson and Dawson, 1996). Following acute ischemia, when the first dose of 1400W was administered at 20 mg/kg immediately or 1 hour after the insult and then subsequent doses administered between 24 – 72 hours after the insult, studies have shown improved pathological outcome in a rat model of stroke (Armengou et al., 2003; Pérez-Asensio et al., 2005; O'Neill et al., 2011). iNOS inhibition is shown to be neuroprotective when an initial dose of 20 mg/kg 1400W was given immediately following traumatic brain injury in rats, and subsequent doses were administered between 18 – 72 hours after the injury (Jafarian-Tehrani et al., 2005). However, when iNOS inhibition occurred beyond 72 hours after the injury, no neuroprotective role against traumatic brain injury in rodents was observed (Jafarian-Tehrani et al., 2005). Based on the results from *in vitro* and *in vivo* studies, it would appear that inhibition of iNOS at any point up to 72 hours after an insult is likely to protect against neuronal damage.

1400W has been tested during the early phases of epileptogenesis in a KA mouse model of epilepsy, using EEG as a surrogate marker of outcome (Beamer, 2013). No change in EEG spike frequency was observed for up to 7 days after KA-induced SE (Beamer, 2013). To my knowledge, the effect of 1400W in other models of epilepsy or beyond the initial 7 days in models of epileptogenesis has not been investigated.

1.6. Aim of thesis

The potential for NO to cause neurotoxicity can be potentiated by: (1) transient, low concentration production of NO from nNOS following activation of NMDAR, and (2) sustained, high concentration production of NO from iNOS following its induction by pro-inflammatory cytokines. As such, it is possible that selective inhibition of nNOS or iNOS (or both simultaneously) will have therapeutic benefit in neurological disorders, including epilepsy, that are known to be associated with a change in expression of brain NO (Alderton et al., 2001). To date, selective inhibition of NO synthesis has not been systemically investigated for the treatment of epilepsy. Furthermore, many studies have explored

antiepileptogenic properties of novel therapeutic agents but most have administered those agents prior to the initial brain insult (i.e. the initial SE), thereby failing to distinguish between direct effects modifying the disease course and indirect effects which simply modified the severity of the precipitating injury (Löscher, 2002). Administration of antiepileptogenic agents after the initial insult is not commonly performed and to my knowledge, there is currently no potential antiepileptogenic agent that targets NO signalling pathway.

The aim of my PhD was to explore the effects of PSD95BP and 1400W in a mouse model of epileptogenesis and to identify the protein pathways involved. The overall objective was to determine whether PSD95, and its coupling of NMDAR and nNOS, or iNOS, whose expression is induced following brain insults, might represent novel targets for the treatment of TLE. Administering PSD95BP and 1400W after the initial neurological insult in this project was designed to improve the clinical relevance and to avoid any confounding effects of insult modification.

Chapter 2

Methodology

2.1. Kainic acid model of epileptogenesis

2.1.1. Animals

Adult male C57BL/6J mice (weight range between 25-30g) were purchased from Charles River Laboratories, Margate, UK. All animals were habituated in their housing environment in groups of five per cage for at least 7 days before any experimental procedures were performed. All animals used were housed under standard conditions in the Biomedical Services Unit, University of Liverpool, with 12h light/dark cycle and access to food and water *ad libitum*.

2.1.2. Reagents

KA (Abcam, Cambridge, UK) was formulated to 2.5mg/ml with distilled water and sonicated for approximately 15 minutes until the powder was dissolved. KA was prepared and used on the day of a study. Diazepam ampoules (Hameln Pharmaceuticals, Gloucester, UK) and sodium pentobarbitone (Pentoject®; Animalcare Limited, York, UK), were purchased by the Named Veterinary Surgeon, Biomedical Services Unit, University of Liverpool.

2.1.3. Seizure induction protocol

All *in vivo* experimental procedures were carried out in accordance with the Animals (Scientific Procedures) Act, 1986. Where possible, experiments were designed and have been reported in accordance with the principles of the ARRIVE guidelines (Kilkenny et al, 2010). Prior to the induction of seizures, all animals were weighed and separated into individual cages, with access to food and water *ad libitum*. All animals were single-housed for the duration of seizure induction until the end of the experiment when sacrificed. The first dose of KA administration started from between 8:30am-9:00am for all animals. KA was administered by the same experimenter for all experiments. KA-treated mice received 5mg/kg KA via intraperitoneal (i.p.) injection every 30 minutes until the onset of generalised seizures. Behavioural indicators of seizure severity were scored using the modified Racine scale (Racine, 2002) characterised as follows: Stage 1, animals displayed mouth and facial twitching; Stage 2, animals displayed head nodding with myoclonic twitching and tremor; Stage 3, animals displayed

forelimb clonus with a lordotic posture; Stage 4, animals reared with concomitant forelimb clonus; Stage 5, generalised clonic convulsion when animals displayed exaggerated activity (i.e. exaggerated running or jumping) (Hellier et al., 1998; Williams et al., 2009; Macias et al., 2013). All behavioural assessments were conducted by the same experimenter. The dosing of KA in individual animals was discontinued after each had experienced a generalised seizure consistent with Stage 5 of the modified Racine scale. Two hours after the onset of the first Stage 5 seizure, all mice (KA-treated animals and their vehicle-treated counterparts) were administered 10mg/kg diazepam intramuscularly (i.m.) in order to standardise the duration of acute KA-induced seizures. The use of diazepam at this dose and at this time-point does not interfere with subsequent epileptogenesis or the development of associated neuropathology (Ben-Ari et al., 1980; Halonen et al., 2001; Aroniadou-Anderjaska et al., 2008).

2.1.4. Euthanasia

Mice were euthanised according to The Humane Killing of Animals under Schedule 1 to the Animals (Scientific Procedures) Act, 1986. On the day of euthanasia, mice were administered an overdose of sodium pentobarbitone (60mg/kg, i.p.) and death was confirmed with exsanguination. There is no evidence that sodium pentobarbitone used at this dose and at this time-point had any effect on subsequent analysis of blood or tissue samples obtained from the animals.

2.2. Electroencephalography

2.2.1. Surgery

C57BL/6J mice were implanted with a telemetry device (Physiotel® transmitter, TA10ETA-F20, Data Science International (DSI), Amsterdam, The Netherlands) to allow freely-moving remote EEG recording. Animals were placed individually in a clear induction chamber and anaesthesia was induced with 3% isoflurane in 100% oxygen with a delivery rate of 2 litre per minute until the loss of the pinch reflex. The animals were then transferred to an anaesthetic mask and anaesthesia was maintained with 2% isoflurane in 100% oxygen with a flow rate

of 2 litre per minute for the duration of the pre-operative procedures. The head of the animal was shaved and iodine (Videne®, Adams Healthcare, UK) used to disinfect the scalp. Animals were then administered a prophylactic antibiotic, enrofloxacin (5mg/kg, subcutaneously (s.c.); Baytril®, Bayer Health group, Germany), and an analgesic, buprenorphine (0.3mg/kg, i.m.; Vetergesic®, Reckitt Benckiser Healthcare, UK), prior to surgery.

After the pre-operative preparation, animals were transferred to the operating theatre and anaesthesia was maintained with 2% isoflurane in 100% oxygen with a flow rate of 2 litre per minute via the anaesthetic mask throughout surgery. An incision was made through the skin, muscle and connective tissue over the skull. A pocket was also created in the flank of the animal, by s.c. tunnelling, where the transmitter unit was placed. One ml of sterile 0.9% saline solution was added to the pocket for lubrication and local hydration. Burr holes, each of 2mm diameter, were drilled using a high-speed drill with a rose-head nail bilaterally over the hippocampal region, approximately 5mm cranial to lambda and 2mm lateral to the midline over each hemisphere. No stereotactic apparatus was used but drill sites were pre-marked using a permanent pen and the head of the animal was held securely during drilling. The rubber insulation covering the electrode terminals of the transmitter was removed, and the exposed terminals were placed directly onto the surface of the *dura mater*. Electrodes were secured and terminals insulated using dental cement made from Alphracryl Rapid Repair mixed with methylacrylate (National Dental Supplies, Southport, U.K.).

After the electrode terminals were fixed and the transmitter inserted into the s.c. pocket, the scalp incision was sutured using Polysorb 4.0 absorbable sutures and reinforced with Vetbond™ Tissue adhesive (3M Animal Care Products, USA). Animals were then given saline (0.5ml s.c.) for rehydration and placed in an incubator set at 30-35^{o}C for warmth during recovery from anaesthesia. Animals were given soft food and housed individually during recovery from surgery. Post-operative care consisted of daily monitoring of food/water intake and of body weight and continued until individual body weight, excluding the weight of the transmitter unit, returned to its pre-operative level.

2.2.2. Data Scientific International system and micro1401 set-up

DSI PhysioTel® Implantable Telemetry devices were used for remote EEG monitoring from conscious laboratory animals. The transmitters (ETA-F20) are designed to measure bi-potential parameters, including EEG, in small to medium sized laboratory animals. Each transmitter unit is flat-shaped, 3.9g in weight, 1.9cc in volume, has 1 bi-potential channel, and has a battery life of 4 months. The transmitter unit has an outer material of silicon elastomer and its on-off mechanism is magnetically actuated. The transmitter signal was sensed by RMC-1 DSI receiver pads, processed via signal analog adapters to the DSI Data Exchange Matrix system and the micro1401 data acquisition hardware (Cambridge Electronic Design, Cambridge, UK). Six receiver pads were connected to the hardware to allow six animals to be monitored simultaneously. The micro1401 hardware was connected to a laptop equipped with Spike2 version 3 software (Cambridge Electronic Design) via a USB cable for recording. Spike2 software was set to record waveforms at 250Hz continuously for all 6 channels with data files automatically saved after every hour of recording.

2.2.3. Video recording for behavioural analysis

Four dome CCD cameras (Sony, UK) with built-in infra-red were placed next to each cage, filming across to allow the behaviour of up to 4 mice to be monitored concurrently with EEG recordings continuously over a 28 day period (Figure 2.1). The cameras were connected to a H.264 network digital video surveillance recorder that allowed video files to be exported and played back on the computer.

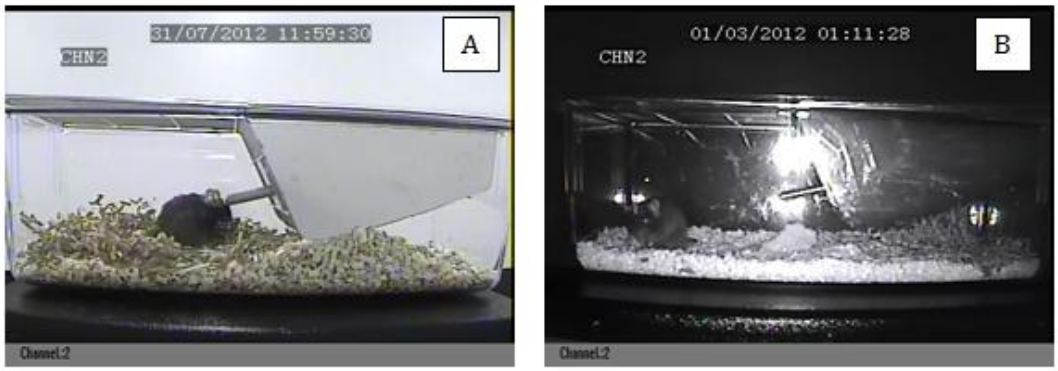

Figure 2.1. Representative images of a C57BL/6J mouse per cage in one channel under video monitoring with the CCD camera filming across the cage (A) during the day and (B) at night using built-in infra-red light.

2.2.4. EEG analysis

Data sorting and filtering using Spike2 and MATLAB software

Raw EEG data were saved in SMR format compatible with Spike2 software. Each data file was then exported as a plain text file at an output sample rate of 100Hz using Spike2 version 5. These files were imported into MATLAB (The MathWorks, Massachusetts, USA) and sorted into individual channels according to the respective receiver pad. Data for each channel were then individually sampled at 100Hz into EEGLAB (Delorme and Makeig, 2004), a MATLAB toolbox for processing continuous electrophysiological data, for 1Hz high pass filtering before re-imported back into MATLAB for spike counting. Artefacts were detected by manually scrolling through the data for each channel. Any sections of the waveforms with exceedingly high amplitudes that were beyond the range limit of the EEGLAB toolbox were removed. The data sorting and filtering processes were eventually automated using programming to increase efficiency. Raw EEG data files were sorted into individual channels using Python (See Appendix for full script). The data filtering process was also automated using programming in MATLAB (See Appendix for full script).

Spike frequency analysis using MATLAB

The spike counting was performed in a semi-automated manner using MATLAB. A spike in extradural EEG represents a combination of extensive simultaneous recordings from all surrounding neurons at the *dura mater* in contact with the electrode terminals (Telenczuk et al, 2015). Each spike was counted using the *'findpeaks'* toolbox in MATLAB to count local maxima or peaks by comparing each element of data to its neighbouring values. When an element of data is larger than both of its neighbouring elements, that element of data is classified as a local peak. Within the toolbox, a name-value pair argument was added to set a threshold, which was determined by the data collected before KA was administered (baseline data). The standard deviation (SD) of the baseline data was multiplied and used as the name-value pair argument to determine the number of spikes present in the baseline data that were beyond the set threshold. The cut off spike frequency for the threshold was set to be ≤5spikes/minute for all channels as this was the average number of spikes in every minute of all the baseline data. This threshold was used to standardise the spike frequency after KA was administered for all animals. For spike counting, a *'minimum peak height'* threshold was specified as a real-valued scalar. In other words, *'findpeaks'* would only return local maxima that exceeded the *'minimum peak height'* threshold value. This method was subsequently automated using programming in MATLAB (See Appendix for full script).

Coastline analysis using EEG Analyser (Java)

The EEG Analyser version 1.0 program (See Appendix for the coastline analysis script) calculates coastline metrics based on the following equation (White et al., 2006).

$$CoastLine = \sum_{i=1}^{3000} ABS(x_i - x_{i-1})$$

x represents the voltage of the filtered EEG data, *i* indicates the data point of each epoch, *ABS* means all values are made absolute to account for and eliminate any negative values the program may generate, since coastline value should always

be a positive number. Coastline values are calculated between each consecutive data point in each epoch with a total of 3000 data points, which is equivalent to 30 seconds of EEG data collected at 100Hz; thus 120 coastlines were generated per hour of EEG and these were exported to text file. A program to automatically sort all exported text files onto Microsoft Excel was created using Python to increase efficiency due to the large amount of data generated (See Appendix for the Python script).

2.3. Bradford protein assay

2.3.1. Reagents

Bovine serum albumin (BSA) standards were prepared using a stock solution containing 4000µg/ml BSA (Sigma Aldrich, UK). Bradford reagent was also purchased from Sigma Aldrich, UK.

2.3.2. Protein quantification

BSA standards were diluted with distilled water to concentrations ranging from 100 – 1400µg/ml. A 10µl volume of each sample and BSA standards were added in duplicate to individual wells of a 96-well plate. A 200µl volume of Bradford reagent was added to each well and the 96-well plate left to incubate at room temperature for 5 minutes. The maximum absorbance frequency for each sample was measured at 595nm using a multimode plate reader (DTX 880; Beckman Coulter, USA) and protein content of samples was determined by comparison to a standard curve generated using a serial dilution of BSA.

2.4. Proteomics

2.4.1. Reagents

Ammonium bicarbonate (Sigma Aldrich, UK) was formulated to 25mM with distilled water. Rapigest SF (Waters MS Technologies, Manchester, UK) was formulated to 1% w/v with 25mM ammonium bicarbonate. Dithiothreitol (Melford Laboratories, UK) was formulated to 9.2mg/ml with 25mM ammonium bicarbonate. Iodoacetamide (Sigma Aldrich, UK) was formulated to 33mg/ml

with 25mM ammonium bicarbonate. Trypsin (Sigma Aldrich, UK) was formulated to 0.2µg/µl in 50mM acetic acid (Sigma Aldrich, UK). Trifluoroacetic acid (TFA), high performance liquid chromatography (HPLC) grade acetonitrile and formic acid were all purchased from Sigma Aldrich, UK. Bradford assay reagent (Pierce Coomassie Plus) was purchased from Thermo Scientific, UK.

2.4.2. Tissue homogenisation and digestion

Hippocampi were dissected out from the extracted brains and homogenised in 500µl of ice-cold 25mM ammonium bicarbonate for 30s using a TissueRuptor (Qiagen, UK). A 10µl aliquot of the resulting homogenate representing a pre-acidification digest, was analysed by sodium dodecyl sulphate-polyacrylamide gel electrophoresis (SDS-PAGE) to compare the presence of proteins with the post-acidification digest. For digestion, 15µl of homogenate was diluted to 160µl with 25mM ammonium bicarbonate in an Eppendorf® LoBind tube (Sigma Aldrich, UK) and 10µl of 1% (w/v) Rapigest SF was added. Digested samples were then heated to 80^{o}C for 10 min. A 10µl volume of 9.2mg/ml dithiothreitol was added to each tube and samples held at 60^{o}C for 10 min. Thereafter, 10µl of 33mg/ml iodoacetamide was added and samples were incubated at room temperature in the dark for a further 30 min. A 10ml aliquot of 0.2µg/µl trypsin was then added to each tube and the samples incubated at 37^{o}C overnight. All samples were diluted 300-fold with distilled water for protein quantification using Bradford protein assay. The 96-well plate was measured using a spectrophotometer (Multiskan™ FC Microplate Photometer; Thermo Scientific, UK) and the protein content of each sample was determined as previously described.

After overnight incubation, 2µl of 99% (v/v) TFA was added to each digest for acidification and the samples incubated at 37^{o}C for 45 min. Samples were then centrifuged at 17,000 x *g* for 45 min and the resulting supernatant was transferred to an Eppendorf® LoBind 0.5mL tube. The centrifugation step was repeated and 10µl of resulting supernatant was transferred to a total recovery vial for liquid chromatography-mass spectrometry (LC-MS) analysis. In addition, 10µl of the post-acidification resulting supernatant was then analysed by SDS-

PAGE to confirm complete digestion and absence of protein in comparison to the pre-acidification digest.

2.4.3. Liquid chromatography separation

All peptide separations were carried out using a nanoAcquity UPLC™ system (Waters MS Technologies, Manchester, UK). For each analysis, 1µl of sample digest was loaded onto a trapping column (C_{18}, 180mm x 20mm, Waters), using partial loop injections for 3 minutes at 5µl/min with an aqueous solution containing 0.1% (v/v) TFA and 2% (v/v) HPLC grade acetonitrile. The sample was resolved on an analytical column (nanoAcquity UPLC™ HSS T3 column, C_{18} 150mm x 75mm inner diameter, 1.8µm, Waters) using a gradient mobile phase which comprised a mixture of aqueous (A) and organic (B) solvents. Solvent A was HPLC grade water with 0.1% (v/v) formic acid (Sigma Aldrich, UK), and solvent B was HPLC grade acetonitrile with 0.1% (v/v) formic acid. Separations were performed by applying a linear gradient of 3% to 40% solvent B over 30 min followed by a washing step (5 min at 99% solvent(B) and an equilibration step (15 min at 3.8% solvent(B), and using a flow rate of 300nl/min. The equivalent of 1µg of protein for each sample was injected.

2.4.4. Mass spectrometry

Orbitrap Velos™ mass spectrometry

The Orbitrap Velos™ instrument (Thermo Fisher, UK) was operated in the data dependent mode to automatically switch between full scan mass spectrometry (MS) and tandem MS (MS/MS) acquisition. Survey full scan MS spectra (*m/z* 350-2000) were acquired in the Orbitrap with 30,000 resolution (*m/z* 400) after accumulation of ions to $1x10^6$ target value based on predictive automatic gain control (AGC) values from the previous full scan. The 20 most intense multiply charged ions ($z \geq 2$) were sequentially isolated and fragmented in the linear ion trap by collisional-induced dissociation (CID) with a fixed injection time of 100 ms. Dynamic exclusion was set to 20s. Typical mass spectrometric conditions were as follows: spray voltage, 1.5kV, no sheath and auxillary gas flow; heated capillary temperature, 200°C; normalised CID collision energy 35%. The MS/MS

ion selection threshold was set to 500 counts and 1.2Da isolation width was set. A metal-coated picotip (New Objective, Aquilant Scientific, UK) was used in the nanospray assembly and was maintained at a voltage of 1500V.

Q Exactive™ mass spectrometry

The Q Exactive™ instrument (Thermo Fisher, UK) was operated in the data dependent mode to automatically switch between full scan MS and MS/MS acquisition. Survey full scan MS spectra (*m/z* 300-2000) were acquired in the Orbitrap with 70,000 resolution (*m/z* 200) after accumulation of ions to $1x10^6$ target value based on predictive AGC values from the previous full scan. Dynamic exclusion was set to 20s. The 10 most intense multiply charged ions ($z \geq 2$) were sequentially isolated and fragmented in the octopole collision cell by higher energy collisional dissociation (HCD) with a fixed injection time of 100 ms and 35,000 resolution. Typical mass spectrometric conditions were as follows: spray voltage, 1.9kV, no sheath and auxillary gas flow; heated capillary temperature, 275°C; normalised HCD collision energy 30%. The MS/MS ion selection threshold was set to 1×10^4 counts. A 2Da isolation width was set.

2.5. Western blot

2.5.1. Reagents

Homogenisation buffer consisted of 25mM ammonium bicarbonate (Sigma Aldrich, UK) supplemented with 10% (v/v) protease inhibitor cocktail (Sigma Aldrich, UK). The cocktail contains 4-benzenesulfonyl fluoride hydrochloride at 2mM, aprotinin at 0.3µM, bestatin at 130mM, E-64 at 14mM, leupeptin at 1mM and ethylenediaminetetraacetic acid (EDTA) at 1mM. Reducing buffer consisted of 30:70 (v/v) NuPAGE® Sample Reducing Agent (10X)/NuPAGE® LDS Sample Buffer (4X). Running buffer was prepared by 1:20 dilution of NuPAGE® MOPS SDS Running Buffer (20X) in distilled water, with NuPAGE® antioxidant (1:400) added, as necessary. Transfer buffer was prepared by 1:20 dilution of NuPAGE® Transfer Buffer (20X) in 80:20 (v/v) distilled water/methanol, supplemented with 1:1000 NuPAGE® antioxidant to enhance transfer of proteins to membranes. A 10X stock of Tris buffered saline (TBS 10X) was prepared with 8%

sodium chloride (Sigma Aldrich, UK), 0.2% potassium chloride (Fisher Scientific, UK), 3.03% Trizma Base (Sigma Aldrich, UK) and pH adjusted to 7.4 using 0.1M hydrochloric acid. TBS with Tween 20 (TBST) comprised 10% of TBS 10X and 0.1% Tween 20 (Sigma Aldrich, UK) prepared in distilled water. Stripping buffer consisted of 2% SDS (Fisher Scientific, UK), 12.5% Tris HCl (1M, pH 6.8, Sigma Aldrich, UK) and 0.7% β-mercaptoethanol (Sigma Aldrich, UK) in distilled water. Chemiluminescence substrate solution consisted of 50:50 (v/v) mix of Reagent A (luminol) and Reagent (enhancer) from the Novex® ECL horse-radish peroxidase (HRP) Chemiluminescent Substrate Reagent Kit. All reagents, unless stated otherwise, were purchased from Life Technologies, UK.

2.5.2. Tissue homogenisation

Brain tissue samples for western blot analysis were thawed on ice and homogenised in 500µl of homogenisation buffer using a TissueRuptor, as described previously. Homogenates were then centrifuged at 14,000 x *g* for 10 minutes at 4°C and the supernatants isolated. Bradford protein assay was performed on each supernatant to determine the amount of protein present, as described in section 2.3. Thereafter, supernatants were aliquoted into microcentrifuge tubes and stored at -20°C.

2.5.3. Western blot protocol

Sample loading, gel electrophoresis, protein transfer to membrane

Supernatants were thawed on ice and the volume required from each sample to achieve the requisite amount of protein for each assay was aliquoted into individual microcentrifuge tubes. A 5µl volume of reducing buffer mix was added to each sample and heated at 85°C for 5 minutes to denature the proteins. Reduced and denatured samples were then cooled on ice for 10 minutes and vortex with a whirlmixer.

Reduced and denatured samples were loaded onto the gel (NuPAGE® Novex® 4-12% Bis-Tris gel, Invitrogen, UK) with a prism protein ladder, which contains 11 proteins that resolve into bands in the range of 10 to 175kDa (Abcam, UK) for

comparative purposes added on the first lane. After all samples were loaded, running buffer (1X) supplemented with antioxidant was first added to the running tank from the upper cathode buffer chamber of the gel electrophoresis running tank (XCell SureLock™ Mini-Cell, Invitrogen, UK) until completely filled. The external anode chamber was then filled with running buffer (1X) without antioxidant, until the buffer reached the level of wells of the gel. The power lead was connected to a PowerPac™ 300 (Bio-Rad, UK) set at 90V and the gel run for 10 minutes until the lanes had run straight. Thereafter, the voltage was increased to 170V and the gel run for an additional 45 minutes.

After gel electrophoresis, the gel was placed in the transfer gel sandwich within the gel holder cassette and inserted into the module of the transfer tank (Mini Trans-Blot® Cell, Bio-Rad, UK), filled with 1X transfer buffer. The tank was connected to a PowerPac™ set at 80V and run for 1.5 hours.

Blocking procedures and antibody incubations

Ponceau S dye (Sigma Aldrich, UK) was added to the membrane in a plastic tray until the whole membrane was fully stained to check the uniformity and effectiveness of the transfer of proteins to the membrane. The dye was subsequently washed off using TBST before blocking the membrane with 5% skim milk powder prepared in TBST (Sigma Aldrich, UK) at 4^{o}C overnight under gentle shaking to prevent non-specific binding of the primary antibodies to be added later. After blocking, the milk powder solution was discarded and diluted primary antibodies prepared in 5% skim milk in TBST were added to the membrane and incubated at room temperature for 1 hour under gentle shaking. After incubation with primary antibodies, the membrane was rinsed with TBST for 20 minutes (with TBST replaced every 5 minutes) to remove any unbound primary antibodies. After rinsing, TBST was discarded and diluted secondary antibodies prepared in 5% skim milk in TBST were added and incubated at room temperature for 1 hour under gentle shaking. The secondary antibodies were chosen based on the species-specific portion of the primary antibody and were all horseradish peroxidase-linked in order to cleave a chemiluminescent agent. After the incubation of secondary antibodies, the membrane was rinsed with

TBST for 20 minutes, as previously described, to remove any unbound secondary antibodies.

Chemiluminescence detection of proteins, film exposure and development

After rinsing, the membrane was incubated for 1 minute in 1ml of pre-mixed chemiluminescence substrate solution. Excess substrate solution was then drained from the membrane using paper towels. The membrane was then placed between 2 sheets of acetate in a development folder, with photographic film (Carestream® Kodak® BioMax® light film, Sigma Aldrich, UK) placed on top of the acetate sandwich and exposed by closing the development folder for the optimum exposure time of each assay. After exposure, the film was placed in a tray with developer (Carestream® Kodak® autoradiography GBX developer/replenisher, Sigma Aldrich, UK) diluted to 1:4.5 with water, until blots appeared on the film. The film was then immediately rinsed in a tray filled with water before being placed into another tray with fixative (Carestream® Kodak® autoradiography GBX fixer/replenisher, Sigma Aldrich, UK), also diluted to 1:4.5 with water. The film was left immersed in the fixative tray for 5-10 minutes.

Membrane stripping and reprobing with loading control

After the exposure of blots for the protein of interest, the membrane was stripped to remove any detection antibodies and chemiluminescence substrates. The membrane was then blotted for the loading control, glyceraldehyde-3-phosphate dehydrogenase (GAPDH), which was used as a housekeeping protein against which the levels of the proteins of interest were normalised. Stripping was carried out by placing the membrane in a plastic tray with stripping buffer and washing for 45 minutes at 60^{o}C under gentle shaking. After stripping, the buffer was discarded and the membrane rinsed using TBST for 20 minutes, as previously described. The membrane was then blocked with 5% skim milk powder solution in TBST for 1 hour at room temperature under gentle shaking. The milk solution used for blocking was then discarded and anti-GAPDH mouse monoclonal antibody (Abcam, UK) diluted to 1:5000 using 5% skim milk in TBST was added. The primary antibody was incubated for 1 hour at room temperature under gentle shaking and was then washed for 20 minutes using TBST, as

described previously. After rinsing, goat anti-mouse secondary HRP antibody (Abcam, UK) diluted to 1:5000 in 5% skim milk in TBST was added and the membrane incubated for 1 hour at room temperature under gentle shaking. Thereafter, the membrane was once again rinsed with TBST for 20 minutes, with the TBST solution replaced every 5 minutes. Chemiluminescence detection of GAPDH, film exposure and development was as previously described. The optimum film exposure for GAPDH was 5 minutes. All antibody dilutions were kept in 4^{o}C and re-used within 1 week of dilution in order to minimise the effect of degradation.

2.5.4. Analysis

All developed films were scanned using a GS-800™ Calibrated Densitometer (Bio-Rad, UK) and captured using Quantity One® 1-D Analysis Software (Bio-Rad, UK). Images were quantified using the '1D electrophoresis gel and western blot analysis' within TotalLab Quant tools applications (TotalLab Ltd, UK), with densitometric quantitation of band volumes exported into Microsoft Excel.

2.6. Meso Scale Discovery Proinflammatory Panel 1 mouse V-PLEX kit

2.6.1. Reagents

Tris lysis buffer consisted of 150mM sodium chloride (Fisher Scientific, UK), 20mM Tris (Fisher Scientific, UK) adjusted to pH 7.5, 1mM EDTA, 1mM ethyleneglycoltetraacetic acid and 1% Triton-X-100. One PBS tablet was dissolved in 200mL of distilled water to yield 0.01M phosphate buffer. Wash buffer consisted of PBS with 0.05% Tween 20. All reagents were purchased from Sigma Aldrich, UK, unless stated otherwise.

2.6.2. Tissue homogenisation and sample preparation

Brain tissue samples were thawed on ice and weighed. Tris lysis buffer containing 1:50 protease inhibitor was added to each sample at a volume of 10µl per mg of tissue. Samples were then homogenised using a TissueRuptor, sonicated to remove bubbles and then centrifuged at 10,000 x *g* for 20 minutes at

4°C. The resulting supernatants were aliquoted and the protein content in one aliquot from each sample were determined using a Bradford assay, as described in section 2.3. All brain supernatants were diluted to 1:50 with distilled water prior to protein assay. Plasma samples for MSD V-PLEX assay were prepared by thawing on ice, vortexing and centrifuging at 13,000 x *g* for 10 minutes at 4°C.

2.6.3. Meso Scale Discovery reagents preparation

Preparation of standards solution, detection antibody solution and read buffer was performed in accordance with the manufacturer's instructions (Meso Scale Discovery (MSD) kit reference K15048D-1). All reagents from the kit were allowed to warm at room temperature prior to preparation. The "multi-analyte lyophilised calibrator" supplied by MSD is the standards stock that contains the highest concentration of all the cytokines in the assay. The calibrator was reconstituted in 1000µl of Diluent 41 (MSD, USA), mixed by vortexing and left for 5 minutes before serial dilution. A series of standards was prepared by serial dilution of the calibrator by adding 100ml of the calibrator to 300ml of Diluent 41, vortex-mixing, and repeating the process 5 times to generate a total of 7 standards. Diluent 41 alone was used as the blank. The kit provided 10 separate detection antibodies, 60µl of each at 50X stock solution. All detection antibody solutions were combined together (600µl) and added to 2400ml of Diluent 45 (MSD, USA) for a 1:50 dilution. Reader buffer T 4X stock solution (MSD, USA) was diluted to 1:2 with distilled water prior to use.

2.6.4. Protocol

The assay was performed in accordance with the manufacturer's instructions (MSD kit reference K15048D-1). The standards, blank and samples solution were measured in duplicates, with 50µl of each solution added to an allocated well within the customised 96-well plate before sealing the plate with an adhesive plate seal and incubating at room temperature with shaking for 2 hours. After incubation, the plate was washed for 3 times by adding 150µl wash buffer per well and emptying after each wash. Thereafter, 25µl of the diluted detection antibody was added to each well, the plate resealed with an adhesive plate seal, and incubated at room temperature with shaking for a further 2 hours. After

antibody incubation, the plate was washed 3 times, as previously described, and then 150µl of 2X read buffer T was added to each well. The plate was then placed on the MSD instrument and read immediately.

2.6.5. Meso Scale Discovery instrument

The reading of the V-Plex plate was performed using the MSD SECTOR Imager 2400 according to the manufacturer's manual (MSD, USA). The plate possessed a MSD barcode label that allowed the SECTOR Imager to detect the type of plate being run. The data generated were automatically analysed with a template using the Discovery Workbench version 4.0 software.

2.7. Immunohistochemistry

2.7.1. Reagents

PBS used for immunohistochemistry (IHC) consisted of stock A/stock B/distilled water (140:360:500 v/v), adjusted to pH 7.2 with 0.9% sodium chloride (Fisher Scientific, UK). Stock A consisted of 2.76% (w/v) of sodium dihydrogen orthophosphate monohydrate (VWR International Ltd, UK) in distilled water. Stock B consisted of 7.164% (w/v) of di-sodium hydrogen orthophosphate dodecahydrate (Fisher Scientific, UK) in distilled water. Paraformaldehyde (PFA; Sigma Aldrich, UK) was dissolved in PBS to a concentration of 4% at 60^{o}C while stirring, and adjusted to pH 7 with 1M sodium hydroxide. Gelatin solution comprised 15% sucrose (Fisher Scientific, UK), 0.1% sodium azide (Fisher Scientific, UK) and 7.5% gelatin from porcine skin (Sigma Aldrich, UK) prepared in PBS, heated at 45-50^{o}C with stirring. Chrom Alum Gelatin (CAG) solution was prepared by dissolving gelatin from porcine skin to a concentration of 3% in distilled water at 60^{o}C, adding chromium potassium sulphate (0.5%, Sigma Aldrich, UK) to a final concentration of 0.5% and stirring until dissolved, and then adding a few crystals of thymol (Sigma Aldrich, UK) as a preservative. Donkey serum (Santa Cruz Biotechnology, UK) was diluted to a concentration of 0.5% in PBS to make the blocking solution. Antibody diluting fluid was prepared with 0.25% donkey serum, 0.25% sodium azide (Fisher Scientific, UK), and 0.2% Triton-X-100 (Sigma Aldrich, UK) prepared in PBS.

2.7.2. Brain perfusion, gelatin embedding and cryostat sectioning

Brain perfusion

Animals were anaesthetised with 5 mg/kg sodium pentobarbitone (i.p.), with anaesthesia confirmed by loss of the pinching reflex. Animals were exsanguinated by cardiac perfusion with PBS, followed by perfusion-fixation with 4% PFA. Brains were then removed and further fixed by immersion in 4% PFA solution for 4 hours, before then immersing in 20% sucrose.

Gelatin embedding

After sucrose had diffused throughout the tissue, brains were immersed in warm gelatin solution and placed in an incubator at 40^{o}C for 3 hours. The gelatin solution containing the intact brain was then allowed to cool at room temperature before being chilled at 4^{o}C overnight. The resulting solidified gelatin with embedded brains was trimmed into a block and attached to a 'Disc cork for Cryostat' (20mm diameter x 3mm depth, Fisher Scientific, UK) using Tissue-Tek® O.C.T.™ Compound (Sakura, The Netherlands) before being snap-frozen with isopentane cooled in liquid nitrogen.

Cryostat sectioning

Superfrost™ microscope slides (Fisher Scientific, UK) were dipped in warm CAG solution (40-50^{o}C), drained onto paper towels and left to air dry overnight before being used for mounting sections. Serial cryostat sections of whole brains were cut coronally from rostral to caudal at -20^{o}C and at 12µm thickness per section throughout the septal and temporal extension of the hippocampus using a Leica CM1950 cryostat (Leica Biosystems, UK). Each frozen section was mounted on a warm CAG-coated Superfrost™ slide kept in room temperature, which allowed the section to instantaneously melt and adhere to the slide. The first 10 sections were mounted on 10 separate slides, as the first specimen on each slide. The subsequent 10 sections were then mounted sequentially as the second specimen on each of the 10 slides. This method of mounting continued until there were at least 4 sections on each slide to ensure that each slide had an equivalent cross-

section of the brain. After mounting, the slides and remaining uncut tissue were stored in -20°C.

2.7.3. Protocol

Frozen sections mounted on slides were thawed for 20 minutes at room temperature. Slides were aligned with Shandon® Sequenza coverplates (Thermo Scientific, UK) and attached to the Shandon® Sequenza slide rack (Thermo Scientific, UK). Brain sections on the slides were then washed with PBS to remove any fixatives or excess PFA from the earlier perfusion by filling the cover-plates with PBS and allowing them to drain. This was repeated five times. A 70ml volume of blocking solution was then added and the slide rack was incubated at 4°C for 1.5 hours. Thereafter, 70ml of diluted primary antibody of interest (prepared in antibody diluting fluid) was added to the slides and left overnight at 4°C. Slides were then washed with PBS continuously for 1 hour to remove any unbound primary antibodies before adding 70ml of diluted secondary antibody conjugated with a fluorophore, again prepared in antibody diluting fluid. The secondary antibody was selected according to the species of the host animal in which the primary antibody was raised. The slides were then incubated at 4°C for 1.5 hour before being washed with PBS continuously for 1 hour to remove any unbound secondary antibodies. After washing, slides were mounted using one drop of Vectashield® Mounting Medium containing 4',6-diamidino-2-phenylindole (DAPI; Vector Laboratories, UK) per microscope slide and a coverslip was placed over the stained sections. Slides were stored in 4°C until examined under a microscope.

2.7.4. Fluorescence microscope

A Zeiss Axioimager microscope was connected to an X-Cite 120 Fluorescence Illumination System for fluorescence imaging and a camera connected to a computer pre-installed with Axiovision 4.8.2 Release software was used to capture the images. Microscope slides were placed onto the mechanical stage and secured with the slide holder. The objective lens was selected to 20× magnification with a theoretical resolution limit of 0.50mm. The appropriate filter position was chosen to visualise the fluorophore of interest using the

eyepiece. Two fluorophores, fluorescein isothiocyanate (FITC; Jackson ImmunoResearch Laboratories, USA) and cyanine 3 (CY3; Jackson ImmunoResearch Laboratories, USA), conjugated with the secondary antibodies raised against different animal species were used for double-staining. FITC is a green fluorescent dye with excitation and emission spectrum peak wavelengths of approximately 492nm and 520nm, respectively (Imhof et al., 1999). CY3 is a red fluorescent dye with excitation and emission spectrum wavelengths of approximately 550nm and 570nm, respectively (Mujumdar et al., 1993). DAPI, present in the mounting medium, is a blue fluorescent stain that binds to DNA, with excitation and emission spectrum peak wavelengths of 360nm and 460nm, respectively. When capturing an image on the microscope, the light path was switched from the eyepiece to the camera in order for the image to be captured and exported to TIFF images using the Axiovision software.

2.7.5. Analysis

All TIFF images were imported to Image Processing and Analysis in Java (ImageJ) version 1.48 and the images were analysed according to the area and the percentage of the stained cells. The "quantify gray value" function was used to quantify the area of the gray levels at the pixel intensity adjusted to a set value to standardise the intensity level for the images. A different threshold intensity was set for each protein of interest. The number of cells stained with the protein of interest was manually counted using the cell counter plugin on ImageJ and quantified in relation to the number of DAPI-positive cells.

2.7.6. Determination of optimum antibodies dilutions for immunohistochemistry

The primary antibody for albumin was detectable at the dilution range of 1:200 to 1:1000, with the secondary antibody dilution of 1:150 to 1:500 (Figure 2.2). The primary antibody dilution at 1:200 and secondary antibody dilution at 1:500 were chosen as they gave the least background staining. The detection of transforming growth factor β1 (TGFβ1) increased with rising dilutions of the primary antibody from 1:20 to 1:5. The primary antibody dilution at 1:10 and secondary antibody dilution at 1:150 were chosen as they gave minimal

background staining with clear visualisation of TGFβ1 (Figure 2.2). Similarly, for transforming growth factor β receptor I (TGFβRI), the primary antibody dilution at 1:10 and secondary antibody dilution at 1:150 were chosen as they gave minimal background staining with clearer visualisation of TGFβRI (Figure 2.2). For K_{ir}4.1, the highest primary antibody dilution tested at 1:150 and the highest secondary antibody dilution tested at 1:150 were chosen as they gave the brightest visualisation of the K_{ir}4.1 stained cells (Figure 2.2).

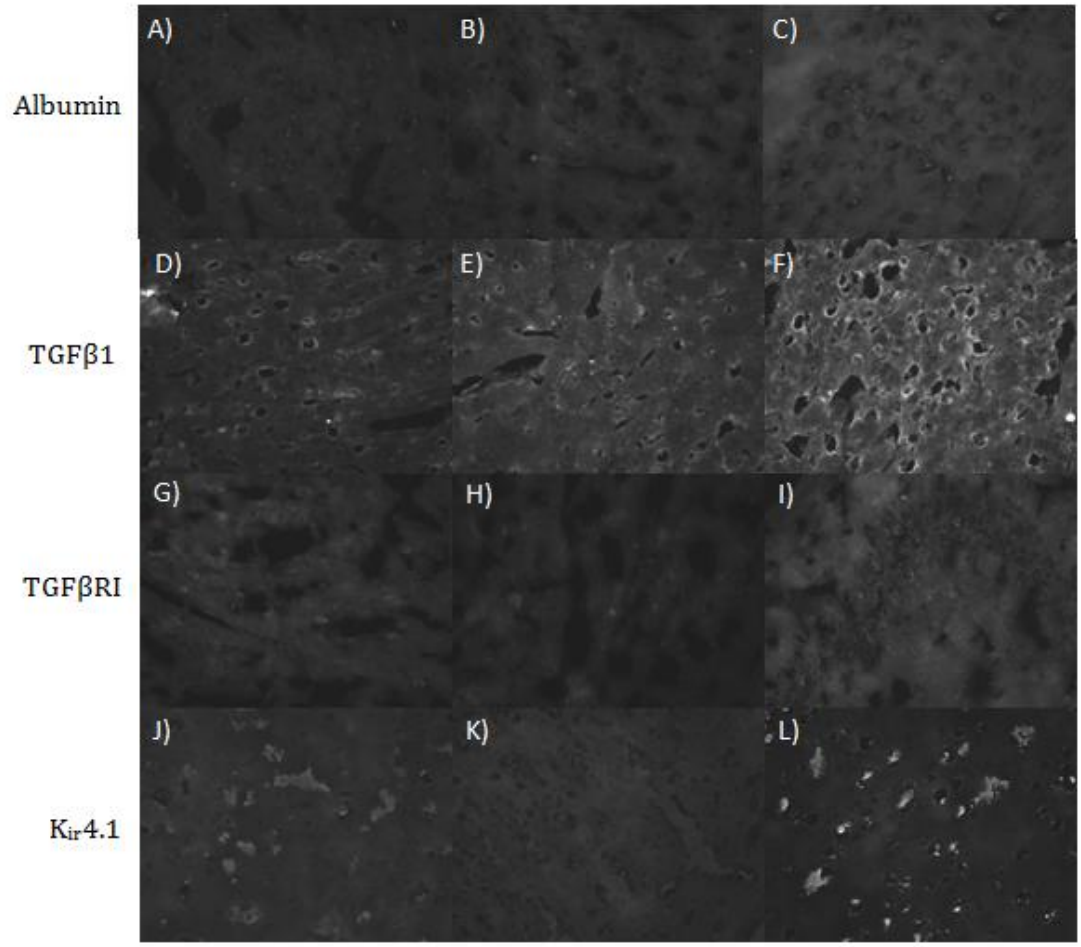

Figure 2.2. Paraformaldehyde-fixed gelatin-embedded mouse brain tissue were cut coronally and stained with albumin, transforming growth factor β1 (TGFβ1), transforming growth factor β receptor 1 (TGFβRI) and inwardly-rectifying potassium channel (K_{ir}4.1). Albumin was stained using mouse-raised primary antibody and anti-mouse secondary antibody conjugated with cyanine fluorophore. (A) Primary 1:1000, secondary 1:500. (B) Primary 1:500, secondary 1:250. (C) Primary 1:200, secondary 1:150. TGFβ1 was stained using rabbit-raised primary antibody and anti-rabbit secondary antibody conjugated with cyanine fluorophore. (D) Primary 1:20, secondary 1:300. (E) Primary 1:10, secondary 1:150. (F) Primary 1:5, secondary 1:150. TGFβRI was stained using rabbit-raised primary antibody and anti-rabbit secondary antibody cyanine fluorophore. (G) Primary 1:20, secondary 1:300. (H) Primary 1:10, secondary 1:150. (I) Primary 1:5, secondary 1:150. K_{ir}4.1 was stained using guinea pig-raised primary antibody and anti-guinea pig secondary antibody conjugated with cyanine fluorophore. (J) Primary 1:300, secondary 1:300. (K) Primary 1:150, secondary 1:300. (L) Primary 1:150, secondary 1:150.

Chapter 3
Acute behavioural seizures in a kainic acid model of epileptogenesis

3.1. Introduction

3.1.1. Kainic acid

KA has been used extensively as a chemoconvulsant in rodent models of epileptogenesis (Sperk et al., 1983; Sperk, 1994) to study the mechanisms of neurodegeneration (Wang et al., 2005) and specifically TLE (Nadler, 1981). It is a selective KA receptor agonist and a cyclic analogue of L-glutamate, which mimics the excitatory effects of glutamate (Nadler, 1981; Sharma et al., 2007) and causes sustained neuronal depolarisation that leads to acute seizure generation in animals following systemic or central administration (Sharma et al., 2007). Excessive glutamatergic activity induces neuronal pathology and can lead to hyperexcitability and epilepsy. Neuronal damage with KA is exacerbated due to excessive glutamate release associated with epileptic seizures (Aroniadou-Anderjaska et al., 2008). KA is 30- to 50-fold more potent than glutamate (London and Coyle, 2005; Wang et al., 2005) and can cause a cascade of cellular events leading to neuronal cell death (Wang et al., 2005) (Figure 3.1).

The KA model is based upon SE as the precipitating neurological insult, associated with prolonged and repetitive seizure activity within the limbic system (Hellier et al., 1998). When administered to experimental animals, KA has been shown to elicit a pattern of post-SE neuronal cell loss and astrogliosis similar to the neuropathology observed in human TLE (Nadler, 1981; Vincent and Mulle, 2009). Most animal models are focused on reproducing hippocampal sclerosis to study the pathogenesis of TLE in patients. Hippocampal lesions that develop in animals following acute seizures induced by KA are similar to the hippocampal sclerosis observed in patients with TLE (Sharma et al., 2007). Hippocampal sclerosis involves extensive loss of neurons in *Cornu Ammonis* 1 (CA1) and *Cornu Ammonis* 3 (CA3) regions, together with pyramidal cells and interneurons in the hilus of the DG (Berkovic et al., 1991; Buckmaster, 2004; Vincent and Mulle, 2009).

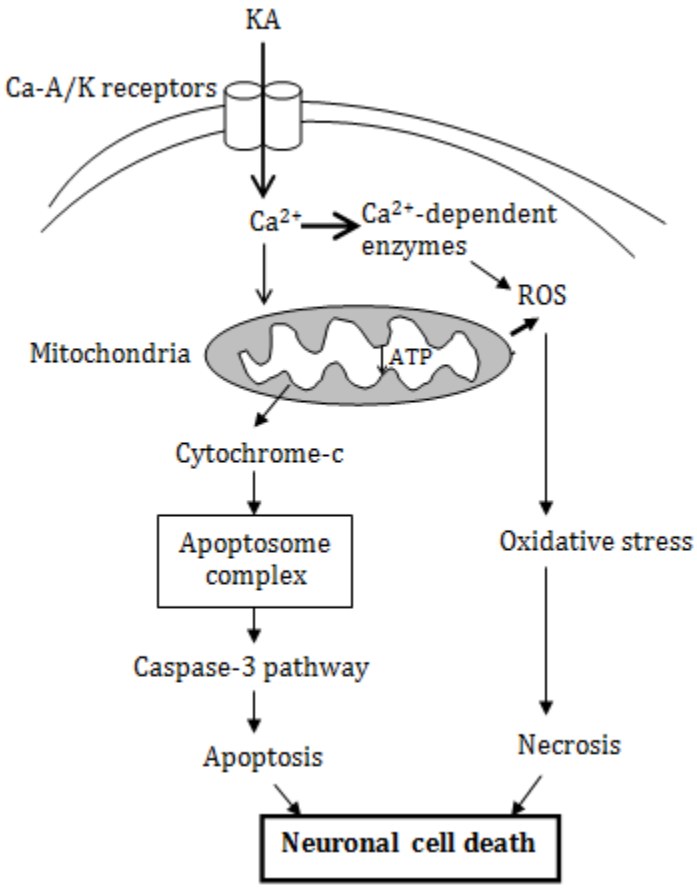

Figure 3.1. Schematic diagram showing the pathway of kainic acid (KA)-induced neuronal cell death. KA stimulates AMPA and KA receptors (Ca-A/K receptors) that are permeable to calcium (Ca^{2+}), leading to rapid Ca^{2+} entry. This activates Ca^{2+}-dependent enzymes that generate reactive oxygen species (ROS). Excessive Ca^{2+} and ROS lead to the breakdown of the mitochondrial membrane potential and open the mitochondrial permeability transition pores to release cytochrome-c. This release forms the apoptosome complex and activates the caspase-3 pathway, leading to apoptosis and neuronal cell death. Ca^{2+} overload could also cause mitochondrial damage and decrease in adenosine triphosphate (ATP). This causes the increase in ROS which leads to oxidative stress, necrosis and neuronal cell death. Image adapted from (Wang et al., 2005).

The hippocampus, particularly CA3 pyramidal cells, is susceptible to the epileptogenic effect of KA (Vincent and Mulle, 2009). KA has also been shown to cause necrosis, demyelination, astrogliosis, perivenous haemorrhages and vascular sprouting in the pyriform cortex, amygdala, olfactory bulb and olfactory tubercle (Sperk et al, 1983). KA induces epileptiform seizures that originate in the CA3 region of the hippocampus and extend to other limbic structures and cause excitotoxic cell death in CA3 and CA1 hippocampal subfields and within the

hilus of the DG (Nadler et al., 1978; Ben-Ari et al., 1980; Schwob et al., 1980; Nadler, 1981; Vincent and Mulle, 2009). CA3 acts as the pacemaker for the generation of synchronised activities that propagate to CA1 and other limbic regions (Ben-Ari and Cossart, 2000).

KA receptors are highly expressed in the hippocampus and are assembled from combinations of 5 receptor subunits, GluK1-5, also referred to as GluR5, GluR6, GluR7, KA1 and KA2 (Carta et al., 2014). The GluK1 subunit is expressed in GABA-ergic interneurons throughout the hippocampus (Carta et al., 2014). The GluK2 subunit is highly expressed in the principal cell layers of CA1-CA3 pyramidal cells, the DG and in interneurons (Carta et al., 2014). The GluK3 subunit is predominantly expressed in the DG (Carta et al., 2014). The GluK4 subunit is highly expressed in CA3 pyramidal cells but only weakly expressed in CA1 and the DG (Rattka et al., 2013; Carta et al., 2014), and the GluK5 subunit is the most abundantly expressed subunit, present in all subregions and highly expressed in both CA1 and CA3 pyramidal cells (Rattka et al., 2013; Carta et al., 2014). The high expressions of GluK2, GluK4- and GluK5-containing receptors render the CA3 region highly susceptible to the excitotoxic effects of KA and make the hippocampus the principal target for seizure onset of KA agonists (Rattka et al., 2013; Carta et al., 2014).

In addition to the loss of pyramidal cells and interneurons, mossy fibre sprouting occurs in both humans with TLE and in animal models of TLE. Mossy fibres originating from dentate granule cells form an aberrant glutamatergic network within the DG, with increased KA receptor subunit expression leading to the formation of a functional recurrent excitatory circuit. This facilitates the generation of epileptiform activity in the hippocampus by reducing the threshold for granule cell synchronisation (Sharma et al., 2007; Vincent and Mulle, 2009; Carta et al., 2014). The clinical manifestation of TLE in patients is usually an acute neurological insult followed by a latent period of a few months to several years before the development of SRS (French et al., 1993; Sharma et al., 2007). Administration of KA closely mimics this clinical scenario, albeit over a much shorter timescale by causing repetitive seizures or SE in rodents that represents

the initial insult, followed by a latent period of several weeks preceding the development of epilepsy (Sperk, 1994; Hellier et al., 1998; Brandt et al., 2003; McCord et al., 2008). SE is a relatively rare cause of epilepsy in patients and may not be a condition that best represents human epileptogenesis. However, these models have contributed to the understanding of the molecular and cellular changes in TLE that can be used to test hypotheses for developing therapeutic prevention of epilepsy (Pitkänen and Lukasiuk, 2009).

3.1.2. Route of kainic acid administration

Various routes of KA administration have been reported to induce acute seizures in rodents, including intracerebral (Schwob et al., 1980) (both hippocampal (Cavalheiro et al., 1982; Rattka et al., 2013) or amygdaloid (Ben-Ari et al., 1980)), intranasal (Chen et al., 2002; 2004) and systemic (Schwob et al., 1980; Hellier et al., 1998). The morphological, behavioural and epileptogenic features of KA administered intracerebrally or systemically are similar, except for the extent of neuropathological damage (Ben-Ari et al., 1980; Pitkänen and Lukasiuk, 2009; Lévesque and Avoli, 2013). The pattern of neuropathological lesions induced by systemic administration of KA is similar to that seen after intrahippocampal administration, but with more symmetrical bilateral damage and with damage extending to extrahippocampal regions (Ben-Ari et al., 1980; Schwob et al., 1980; Sperk et al., 1983). The extent of damage to these regions depends on the severity of seizure activity (Sperk et al., 1983). Systemic administration of KA produces neuronal damage in limbic structures with hippocampal pyramidal neurons being the most vulnerable (Vincent and Mulle, 2009). The extent of neuronal damage in the brain of an animal treated systemically with KA is more widespread and more severe than that observed in humans with TLE (Rattka et al., 2013), but the semiology of the acute seizures and the chronic nature of the resulting epilepsy appears to be similar (Hellier et al., 1998). Intracerebral administration of KA has also been shown to be a useful model of epileptogenesis that produces less extensive damage in the brain and which might be a better representation of human TLE (Rattka et al., 2013). However, substantial variability in the pattern of neuronal degeneration has been reported (Schwob et al., 1980). Although the systemic KA model produces more severe acute seizure

activity and greater pathological damage in the limbic system than is seen in humans, it is a more convenient way to administer KA than the intracerebral route, allowing multiple animals to be injected at the same time and without the need for surgical intervention (Sperk, 1994; Lévesque and Avoli, 2013). Due to the possibility of post-surgical complications and the technical difficulty involved in intracerebral administration of KA to a large number of animals, the systemic route was preferred for this project.

3.1.3. C57BL/6J mice

The C57BL/6 mouse is the most commonly used inbred strain across scientific disciplines and the substrain, C57BL/6J, has been used widely in several seizure models (Ferraro et al., 1995; Schauwecker and Steward, 1997; Benkovic et al., 2004; Wang et al., 2005; Mekada et al., 2009). C57BL/6J is known as a seizure-resistant strain compared to other inbred mouse strains because C57BL/6J mice are more resistant to seizure-induced neuronal excitotoxicity than some inbred strains, such as FVB/N, despite experiencing a similar seizure severity (Seyfried et al., 1980; Green and Seyfried, 1991; McKhann et al., 2003; McLin and Steward, 2006; Vincent and Mulle, 2009). However, it has been shown that the limited seizure activity induced by KA in C57BL/6J mice can cause significant excitotoxic neuronal damage, suggesting that the damage occurs as a result of the direct neurotoxic effect of KA, and not as a result of the severity of the acute seizures that are elicited (Benkovic et al., 2004). It has also been suggested that C57BL/6J mice show similar neurodegeneration following KA-induced seizures as other strains, but that they recover more rapidly and to a greater degree than other mouse strains (Benkovic et al., 2004). Genetic factors may be relevant in determining the extent of hippocampal damage following acute seizures in resistant strains like C57BL/6J (Vincent and Mulle, 2009). On occasion, strains that are more sensitive to KA-induced seizures show no pyramidal cell loss or mossy fibre reorganisation, whilst more resistant strains can exhibit extensive pyramidal cell loss and mossy fibre sprouting (Vincent and Mulle, 2009). Differences in excitotoxic cell death following KA administration may result from genetically determined differences in intracellular cascades, together with

differential levels of glutamate receptor expression between strains of mice, underlying the variation in their seizure susceptibility (Vincent and Mulle, 2009).

3.1.4. Repeated low doses of kainic acid

Systemic administration of KA has been given as a single bolus injection or in multiple injections to induce acute seizures in rodents. Single injection of KA in rats is associated with a higher mortality rate of up to 30% compared to 15% seen with multiple doses (Hellier et al., 1998; Sharma et al., 2007; Lévesque and Avoli, 2013). Single dose KA also results in a smaller proportion of animals subsequently developing epilepsy. Most epilepsy models involving systemic administration of KA use a 60 to 120 minute period of SE as the initial insult and employ compounds such as diazepam to terminate the SE and thereby standardise the duration of SE amongst animals. Diazepam may also help reduce the mortality associated with chemically induced SE (Löscher and Brandt, 2010). Unlike the single bolus dose approach, the repeated low-dose method of KA administration is tailored to the behaviour of the animal, decreasing the probability of an overdose while ensuring animals have a sufficiently long duration of acute seizures to maximise the likelihood of them later developing epilepsy (Hellier et al., 1998). This method of administration allows a slower diffusion of KA into the brain and extends overall exposure to KA (Hellier et al., 1998).

Another disadvantage of the single bolus dose of KA is that not all animals develop acute seizures upon administration of KA, possibly due to the variable absorption of KA or its penetration into the brain (Pitkänen et al., 2005; Lévesque and Avoli, 2013). Multiple dose models are more reliable at maximising seizure activity by titrating the KA dose based on observed acute seizure severity in individual animals and by ensuring that all animals have a similar severity of seizures. This results in a higher survival rate, which is important from both experimental and animal husbandry perspectives, and the resulting histopathological changes more closely resemble those seen in human mesial temporal sclerosis (Hellier et al., 1998; McKhann et al., 2003). However, the multiple dosing approach introduces a different variability, with animals

potentially exposed to quite different total doses of KA (Lévesque and Avoli, 2013) and this requires careful consideration in experimental design and data interpretation.

The multiple dosing regimen of KA not only improves the survival rate of animals but can also determine the severity of the resulting epilepsy. Post-SE models of TLE are considered to be good models for studying epileptogenesis, as they produce short latent periods and high incidences of SRS after the initial neurological insults (Löscher and Brandt, 2010). This can shorten the study duration whilst achieving higher success rate of animals developing epilepsy.

In summary, systemic KA administration using a repeated low-dose regimen maximises survival, enhances the proportion of animals experiencing acute seizures, standardises seizure severity during the SE period, and ultimately the resulting epilepsy mimics human TLE and shares important neuropathological features. As such, this model was chosen for the investigations of epileptogenesis reported in this thesis. The C57BL/6J mouse was specifically chosen as a result of the large volume of published data available regarding behavioural and neuropathological changes in response to KA and the molecular mechanisms involved in epileptogenesis in this strain.

3.1.5. Overview

An animal model of disease should be designed carefully to mimic the human condition as closely as possible in order to address specific questions regarding the disease state. No animal model of epileptogenesis can completely match the complex aetiology of human epilepsy, but it can contribute to the understanding of the mechanisms of epileptogenesis (Herman, 2002; Löscher, 2011). There are differences between humans and experimental animal models in terms of the manifestation of epilepsy, duration and mechanisms of epileptogenesis, and the relative contribution of individual neurobiological pathways to the development of epilepsy (Aroniadou-Anderjaska et al., 2008). These differences may also be dependent on the brain region and type of neurological insult involved. It is vital to understand the molecular and cellular alterations that arise from a

neurological insult and that specifically lead to the development of epilepsy in some cases and brain repair in others (Löscher and Brandt, 2010). The use of experimental models to replicate the behavioural, electroencephalographic and histopathological features of human epilepsy is necessary to understand the anatomical region of the seizure onset and molecular mechanisms underlying epileptogenesis (Lévesque and Avoli, 2013).

3.2. Materials and methods

3.2.1. Animals

All experimental procedures were performed in accordance with the Animal (Scientific Procedures) Act, 1986 (UK). All methodological details regarding the source of animals, their housing conditions and KA-induced seizures are provided in section 2.1. The C57BL/6J strain was introduced to Charles River in 2004 and breeding was conducted in accordance with The Jackson Laboratory genetic management system (Charles River Laboratories, UK).

3.2.2. Behavioural assessment for acute seizures

The preparation of KA and the induction of seizures are described in sections 2.1.1 and 2.1.2. For this project, a 2-hour period of acute seizures was used for all mice. After the onset of the first Stage 5 generalised seizures (see below/described in section 2.2.3), the dosing of KA was discontinued and animals' behaviour was assessed continuously for 2 hours. The most severe seizure severity during every 5-minute epoch was recorded based on the modified Racine scale, with the following criteria: stage 1 (non-convulsive) – mouth and facial twitching; stage 2 (non-convulsive) – head nodding with myoclonic twitching and tremor; stage 3 (convulsive) – forelimb clonus with a lordotic posture; stage 4 (convulsive) – rearing with concomitant forelimb clonus; stage 5 (convulsive) - generalised clonic convulsion with exaggerated activity.

3.2.3. Seizure severity quantification

Seizure severity was quantified using the modified Racine scores recorded during each 5-minute epoch and summing the total score for the 2-hour acute seizure period between onset of the first generalised seizure and diazepam administration. The lowest score of 0 would indicate no abnormal behaviour observed during the SE period. The highest score of 120 would indicate at least one Stage 5 seizure every 5 minutes for the whole 2-hour SE period. Thus, seizure severity for each individual animal is indicated by the total cumulative modified Racine score over the 2-hour SE period. Since only the highest scoring seizure in each epoch was recorded, the maximum score in any given 5-minute period was 5 irrespective of how many acute seizures occurred in that period or their individual severity. This quantification was used to investigate the variation of behavioural seizures with respect to the difference in total KA doses administered to individual animals.

3.3. Results

During this project, KA was administered (i.p.) to a total of 187 C57BL/6J mice using the repeated low dose regimen described in section 2.2.3. These mice were delivered in 19 separate batches from Charles River (UK), according to experimental need. All mice experienced Stage 5 generalised convulsive seizures after receiving KA.

3.3.1. Mortality

A total of 11 mice died following KA administration, with a variable mortality rate between batches of animals. The overall mean mortality rate of animals after receiving KA was 5.9%. The highest mortality rate of 22.2% was seen in batch 7 with 2 mice from a total of 9 that died after receiving KA (Figure 3.2). In all cases, mortality occurred after the onset of Stage 5 generalised seizures and prior to the administration of diazepam, and was associated with convulsive seizures.

3.3.2. KA sensitivity variation

When administered i.p. at 5mg/kg every 30 minutes, the cumulative KA dose required to reach the first Stage 5 generalised seizure in C57BL/6J mice ranged from 15 to 55mg/kg (Figure 3.3). More than 90% of animals required ≤35mg/kg of total KA dose (Figure 3.4). The KA sensitivity also varied between batches of animals, even when ordered at the same age and weight range from the same supplier (Figure 3.5).

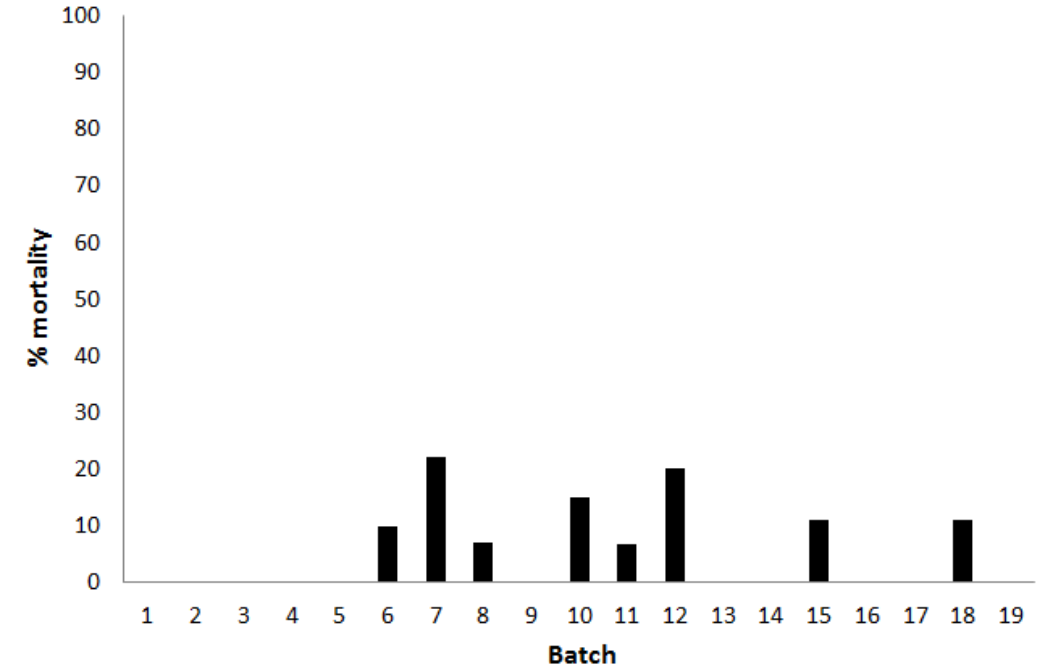

Figure 3.2. The mortality rate, expressed as a percentage of all kainic acid-treated animals, presented by batch number.

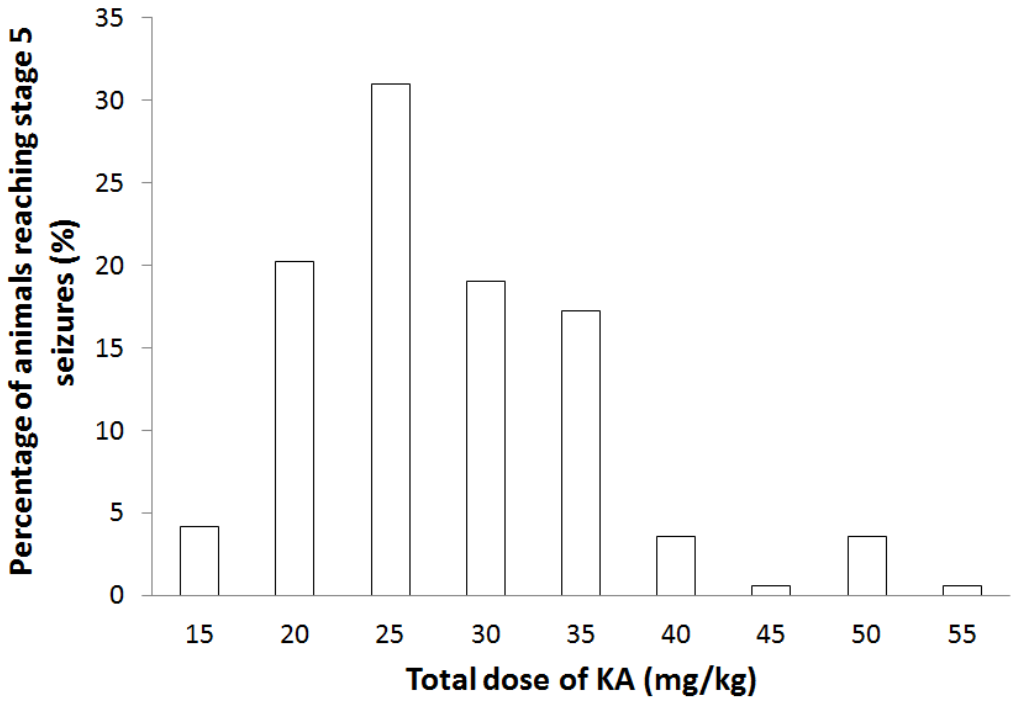

Figure 3.3. Total kainic acid (KA) dose (mg/kg) required to induce generalised convulsive seizures in all C57BL/6J mice (n=187) following repeated intraperitoneal administration of KA at 5mg/kg every 30 minutes. Data are expressed as the percentage of animals that reached Stage 5 seizures, with dose reported as a categorical variable.

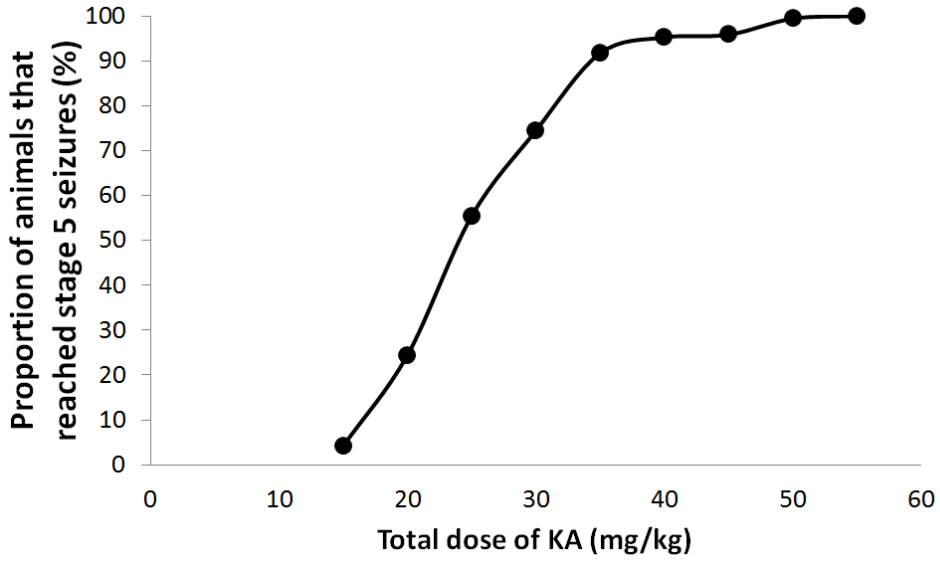

Figure 3.4. Dose-response relationship between total kainic acid (KA) dose (mg/kg) and proportion of all C57BL/6J mice (n=187) experiencing Stage 5 generalised convulsive seizures following repeated intraperitoneal administration of KA at 5mg/kg every 30 minutes. Data are expressed as the proportion of animals that reached Stage 5 seizures, with dose reported as a continuous variable.

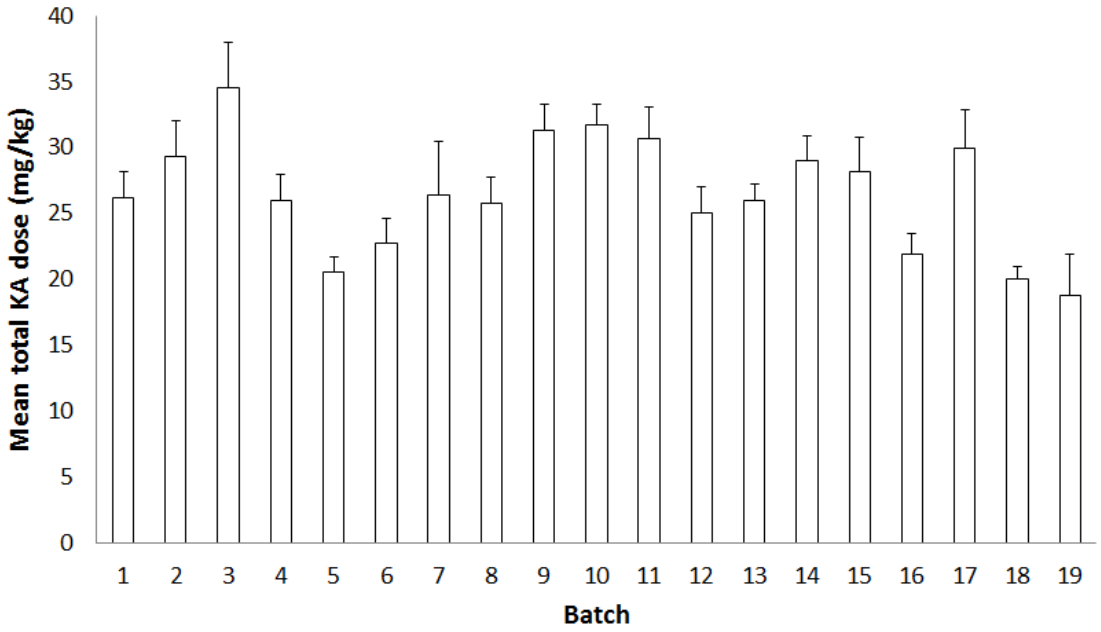

Figure 3.5. Comparative kainic acid (KA) sensitivity in different batches of C57BL/6J mice purchased from Charles River, UK. Data are expressed as mean total KA dose (± SEM) required to induce generalised convulsive seizures following repeated intraperitoneal injection of KA at 5mg/kg every 30 minutes. Batch size ranged n=4 to n=17.

3.3.3. Seizure severity variation

During the 2-hour seizure assessment period, all animals had at least one occurrence of a generalised seizure hence the lowest possible seizure severity score is 5. A cumulative behaviour score (calculated from 24 separate 5-minute epochs over the 2-hour assessment period) of less than 50 was indicative of mice that either had occasional episodes of convulsive seizures (scores 3-5) with behaviour returning to normal in-between (score 0) or that remained in non-convulsive states (scores 1-2) for the majority of the period. A behavioural score of between 50 and 100 was typically indicative of animals experiencing multiple episodes of generalised seizures and spending the majority of the time in convulsive seizure states. A behavioural score of above 100 was recorded in animals with the most severe seizures; these animals generally had one or more Stage 4 or 5 seizures every 5 minutes throughout the assessment period (Figure 3.6). Comparison of seizure severity score and total dose of KA showed no strong correlation (R^2 = 0.0128; Figure 3.6). Higher doses of KA were not associated

with increased seizure severity, and seizure severities at a given dose varied widely (Figure 3.6).

3.4. Discussion

KA is a chemoconvulsant that consistently induces generalised convulsive seizures in mice when administered systemically. However, there was considerable inter-animal variation in the sensitivity to KA and in the severity of acute seizures caused by KA in the C57BL/6J mice used in this study. Rates of mortality also differed between different batches of animals. This variation appears to be consistent with published literature on the variability of response to KA (Schwob et al., 1980; Hellier et al., 1998; McKhann et al., 2003). The overall mortality rate of C57BL/6J mice in this study is lower than the 15% mortality rate reported in rats following repeated doses of KA (Hellier et al., 1998). Mice require a range of doses of KA to induce generalised seizures (Figure 3.3). Those that had onset of generalised seizures at the same dose of KA also had different seizure severities over the 2-hour period thereafter (Figure 3.6).

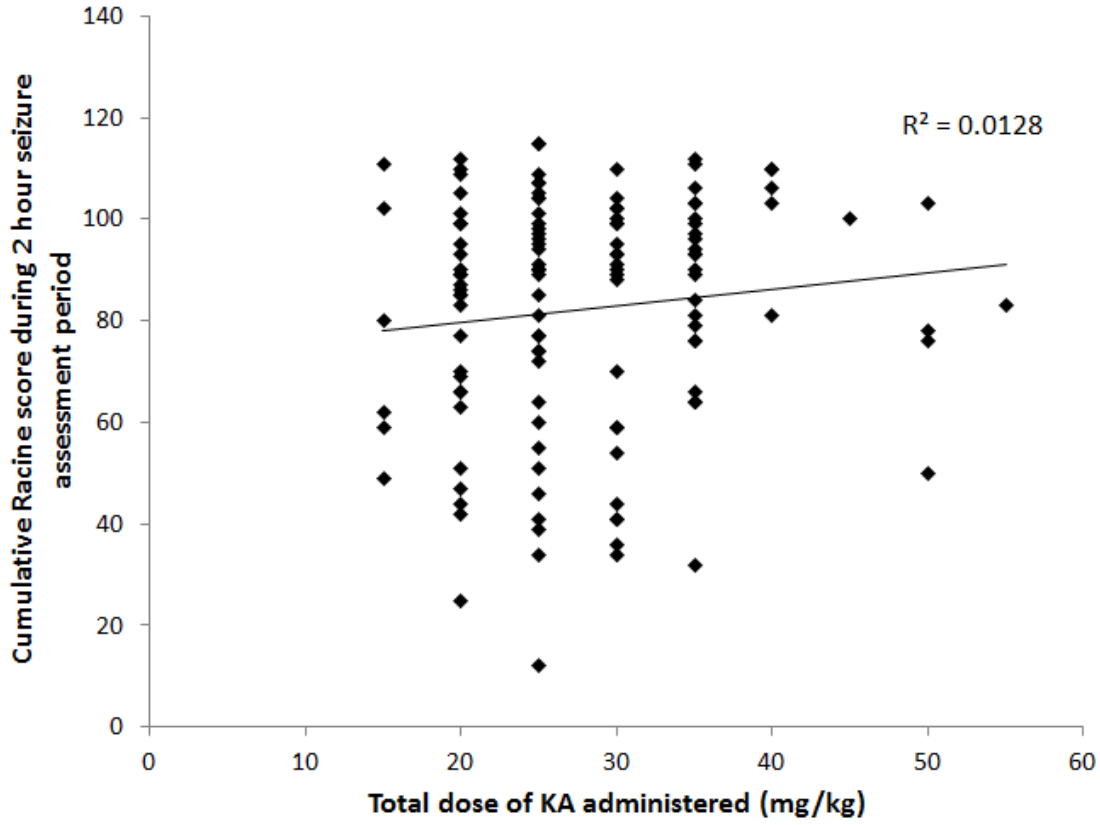

Figure 3.6. Correlation between seizure severity score and total dose of kainic acid (KA) required to induce generalised convulsive seizures following intraperitoneal administration of KA at 5mg/kg every 30 minutes. Each datapoint represents a single animal (n=187). Pearson's product-moment correlation is illustrated by the solid line, with the corresponding correlation co-efficient reported.

There was no correlation between the total dose of KA and the cumulative seizure severity during the 2-hour assessment period after the onset of the first generalised seizure (Figure 3.6). The cause of this variability in seizure severity is unknown. It could simply be due to variability of KA concentration in the brain but this has not been investigated. There is some evidence that low concentrations of KA can generate acute seizures whilst higher concentrations can lead to overall conduction block (Ben-Ari and Cossart, 2000). This may partly explain the lack of association between the dose of KA and seizure severity. Systemic KA administration has been shown to induce dose-dependent behavioural effects in other rodents (Giorgi et al., 2005) but this was not observed in this model using C57BL/6J mice and a repeated low-dose treatment regimen. The variation in the seizure response to KA was not only observed between individual animals given the same doses but also the mean dose

required to induce generalised seizures was significantly different between batches of animals from the same breeding facility. All mice were outsourced from the same supplier rather than bred in-house, and always ordered at a specific body weight range. Given the extensive use of C57BL/6J mice in biomedical research and the high demand on their supply, it is unlikely that batches of animals were always derived from exactly the same breeding stock. On that basis, subtle genetic variations between breeding lines may explain at least some of the intra-strain differences observed (Watkins-Chow et al., 2008).

Although the repeated low dose KA regimen was used in an attempt to ensure that all mice consistently achieved generalised seizures, this introduced variability in terms of the total KA dose to which each animal was exposed. It has been reported that different doses of KA can trigger different degrees of brain damage and different forms of neuronal death (Vincent and Mulle, 2009). A moderate KA dose of 12 mg/kg when given i.p. to rats induced necrosis whereas a low KA dose of 9 mg/kg induced programmed cell death without apoptotic morphology (Tokuhara *et al.*, 2007). However, without measuring serum and/or brain concentrations of KA it is impossible to know the extent to which variability in absorption and distribution may have contributed to within-dose or inter-animal variability in response. The duration and/or the severity of seizures in response to KA is also not predictive of the subsequent hippocampal cell death or synaptic reorganisation (Vincent and Mulle, 2009). Differences in the duration and/or the severity of seizures can cause variation in the degree of neuronal damage.

Limiting the duration of SE with diazepam standardises the insult and is a common approach in such models. There is no evidence that it has any effect on the subsequent epileptogenesis (Halonen et al., 2001; Aroniadou-Anderjaska et al., 2008). It has been shown that diazepam given after 2 hours of generalised seizure does not reduce brain damage despite blocking seizure discharges induced by KA in the hippocampus induced by KA (Ben-Ari et al., 1980). Most investigators allow 90 to 120 minutes of acute seizure activity prior to pharmacological termination with drugs such as diazepam as this allows

sufficient duration of the initial insult to induce the later development of epilepsy, standardises the duration of insult, and limits mortality (Löscher, 2002).

The reason for using this model was to ensure that all animals experienced a generalised seizure and to minimise the mortality associated with KA administration. SE is characterised by prolonged seizure activity and some published papers have established criteria to assess when animals are in SE and when they are simply experiencing repeated single acute seizures (Hellier et al., 1998; Hellier and Dudek, 1999; Buckmaster, 2004; Hellier and Dudek, 2005). Different laboratories use different criteria to define SE, but generally it is reported to be consistent with convulsive motor seizures at a Racine score of ≥3 for more than 2 hours (Hellier et al., 1998; Buckmaster, 2004; Hellier and Dudek, 2005). As such, not all mice used in this study can be considered to have achieved SE. There were many variations in the response to KA in this model, but there is strength in the fact that all animals were allowed 2 hours of seizure activity after the onset of the first generalised convulsive seizure prior to termination with diazepam. This standardised the initial seizure duration and eliminated the major confounding effects of differing seizure durations on the long-term outcome (Löscher and Brandt, 2010). Variations between animals in terms of seizure induction, duration and severity are difficult to avoid despite refinement of protocols. Reduced variability between batches of animals might be achievable using animals bred in-house to minimise genetic variation. However, producing a homogeneous, reproducible model that behaves in the same way every time is unrealistic and arguably not representative of the clinical condition. Nevertheless, experimental design needs to be carefully considered to control the inherent variability associated with the KA model of epileptogenesis.

Chapter 4
Spike frequency and coastline: algorithms for electrographic spikes in intracranial EEG recordings

4.1. Introduction

EEG is the recording of spontaneous electrical activity of the brain over a period of time (Niedermeyer and de Silva, 2005). EEG is often used in encephalopathies to indicate a CNS disorder, a focal process or ongoing seizure activity without motor manifestations (Brenner, 2009). Clinically, EEG can be used to confirm an established diagnosis or rule out a diagnosis (Brenner, 2009), and is the most useful diagnostic tool for epilepsy (Noachtar and Rémi, 2009). EEG is also used in animal models to study the development of epilepsy (Lehmkuhle et al., 2009).

There are two types of EEG electrode placement for animals, epicranial and intracranial (Galanopoulou et al., 2013). Epicranial surface recording of the brain involves placing electrodes on the skull surface and does not require opening the skull, hence minimising the risk of brain damage. It is easier to implant the electrodes for epicranial than intracranial recordings (Galanopoulou et al., 2013). Intracranial (subdural or extra-dural) and depth electrode implantation require opening the skull and inserting the EEG electrode through a burr hole to record electrical activity from the brain. Intracranial or depth electrode implantation can detect recordings from focal seizures arising from deeper structures within the brain, and in general provides a better signal-to-noise ratio and is more reliable than epicranial electrode implantation (Galanopoulou et al., 2013). Extra-dural electrode implantation involves placing the electrodes on the surface of the *dura mater* without penetrating through it (Galanopoulou et al., 2013). On the other hand, intracranial subdural or depth electrode implantation involves inserting the electrodes into the brain by penetrating the *dura mater* and can directly record activity precisely from the seizure onset zone, but the placement of the electrode is difficult to confirm and can cause additional injury within the brain (Galanopoulou et al., 2013). Methods of receiving data from the electrodes can be either tethered or remote. Tethered systems tend to cause some distress to the animals and cause more movement artefacts than remote systems. Remote systems are overall better systems with all the electrodes and the transmitter implanted within an animal's body so that the animal can move freely within its cage, providing more comfort for long-term monitoring (Chang et al., 2011).

The measurement of EEG has the benefits of applying an objective measure to support the subjective behavioural observations that could differ between experimenters. Behavioural observation of animals to assess seizure severity is an easy method to set up with minimal equipment needed. However, the behavioural method is not standardised between experimenters and can cause inconsistent reports of seizure severity (Benkovic et al., 2004). Additionally, EEG monitoring enables experimenters to quantitatively measure brain activity and to define what pattern of electrographic activity is indicative of a seizure in experimental animals (Galanopoulou et al., 2013). Seizures are transient symptoms with a complex manifestation of underlying aberrant synchronous electrical activity in the brain but the correlation between seizure severity and neuropathology is unclear, hence the use of electrical recording of neuronal activity may give a better representation of seizure severity (Benkovic et al., 2004; Chang et al., 2011).

Furthermore, there is evidence that electrographic brain activity can precede the first observable behavioural seizure (Williams et al., 2007; 2009; Dudek and Staley, 2011). Studies have used KA to induce acute seizures and showed that EEG spikes occurred a few days before the first spontaneous convulsive motor seizure was observed (Bertram and Cornett, 1993; Williams et al., 2009; White et al., 2010). It was accordingly proposed that EEG spikes may be used as a predictive experimental biomarker for the development of chronic epilepsy (White et al., 2010). The duration of epileptogenesis has been shown to be variable and differed substantially between animals that were video-monitored and those with EEG recordings (Lévesque and Avoli, 2013), demonstrating discrepancies between behavioural and electrographic seizure assessments. By measuring electrical activity in the hippocampus of experimental animals, EEG patterns indicative of SE are observed without any significant behavioural seizure activity suggesting that electrographic activity may not be reflected in behaviour (Benkovic et al., 2004). This may partly explain the discrepancies between behavioural and electrographic seizure reports from the literature. Given these examples, using EEG to monitor seizure activity would be more reliable than

behavioural assessment alone. Using EEG to continuously monitor electrographic signals is now a common method in experimental epilepsy research (Galanopoulou et al., 2013) and can be used to explore the efficacy of potential antiepileptogenic drugs, with EEG generally recorded immediately after a brain insult and before SRS occur (Löscher, 2011).

Two types of method to identify seizure-like events have been used for EEG analysis. This can be achieved by visual pattern recognition or computer-based algorithms (Galanopoulou et al., 2013). Computer-based algorithms are generally more efficient and objective than visually reviewing EEG traces (Galanopoulou et al., 2013). Several different algorithms for detecting seizures have been investigated, including spike frequency (White et al., 2010), coastline (White et al., 2010), power spectral density (White et al., 2010; Tsuchiya and Kogure, 2011), range autocorrelation (White et al., 2006), wave area/spike amplitude ratio (Huneau et al., 2013), wavelet transformation (Bergstrom et al., 2013), logistic regression (Subasi and Erçelebi, 2005) and spike sorting (Lewicki, 1998). Their accuracies in seizure detection from EEG in experimental animals vary and the algorithms relying on spike frequency, coastline or power spectral density have been shown to have lower sensitivity to detect subtle non-convulsive seizures than range autocorrelation due to the impact of noise and artefact on these algorithms (White et al., 2006). Nevertheless, there is currently no reported study demonstrating the correlation between any seizure-detecting algorithms with behavioural seizure severity in experimental animals.

The objective of the work described in this chapter is to investigate the use of spike frequency and coastline algorithms to analyse the EEG data recorded from C57BL/6J mice with electrodes implanted extra-durally prior to KA administration. The correlation of the two algorithms with behavioural seizure severity (as described in section 3.2.3) after the first onset of generalised seizures was also investigated. Additionally, the effects on EEG activity of the potential anti-epileptogenic drug interventions, PSD95BP and PSD95BP plus 1400W, as described in section 1.5, were also investigated when administered after KA-induced seizures.

4.2. Materials and methods

4.2.1. Animals

All experimental procedures were completed in accordance with the Animal (Scientific Procedures) Act, 1986 (UK). All methodological details regarding the source of animals, their housing conditions, surgical implantation of telemetry electrodes, KA-induced seizures, EEG equipment set-up, video monitoring for behavioural analysis and EEG data analyses are provided in sections 2.1 and 2.2. The method for the behavioural seizure severity quantification is provided in section 3.2.3. Prior to the start of baseline recordings, all animals were housed individually and were therefore all treated the same way before the induction of acute seizures. Each cage was placed on top of a DSI receiver pad with a maximum of 6 animals being recorded simultaneously. Implanted transmitters were turned on by placing a magnet next to the animal until the 'carrier' light on the receiver pad was illuminated. This light indicated the transmitter was detected. Video recording also began from the start of baseline recordings until the end of the experiment.

4.2.2. Study design

All mice were given KA treatment with 5 mice allocated per treatment group. As this was a pilot study, the expected effect size, power and standard deviation for each treatment group for each EEG algorithm were not known, therefore the sample size was not calculated. A sample size of n=5 per treatment group was chosen based on the n numbers used in previous experiments demonstrating changes in epileptiform activity during the early phases of epileptogenesis following the administration of PSD95BP and 1400W (Beamer et al, 2013). There were 3 treatment groups for the study in this chapter, one group served as control and received KA alone, another group was treated with PSD95BP alone and the remaining group was treated with a combination of PSD95BP and 1400W. PSD95BP (courtesy of Professors Tymianski and Salt, University of Toronto) was prepared in saline and administered as a single bolus dose of 7.6mg/kg via intravenous injection to mice one hour after diazepam

administration. 1400W dihydrochloride (Tocris Bioscience, Bristol, UK) was formulated to 4mg/ml with distilled water and mice were given an initial dose of 20mg/kg via i.p. injection one hour after diazepam administration, followed by a further two doses administered 1 and 3 days after the first onset of Stage 5 seizures. Seizure severity data from one control animal were lost, meaning that analysis was based on a total of 14 animals, with n=4 in the control group.

4.2.3. Data analysis

EEG analyses for spike frequency and coastline are described in section 2.2.5. Spike frequency is the number of spikes with amplitudes greater than the threshold determined from baseline EEG recordings (before KA was administered), per minute. Coastline is the sum of distances between consecutive data points over a specified time interval. Coastline was normalised to each animal's mean baseline coastline value (before KA was administered) by determining the difference between the coastline of each mouse from the first dose of KA and their respective baseline values. Another method to illustrate normalised coastline was by separating the coastline data into 30 second epochs. The coastline per epoch in normal baseline EEG recording remains generally constant, while an epileptiform spike would transiently increase the coastline. Therefore, the absolute number of post-KA epochs that were out-with 3 x SD of the mean baseline epoch.

The correlation of spike frequency and normalised coastline against behavioural seizure severity in the KA model of epileptogenesis was performed using Pearson's product-moment correlation approach. The mean spike frequency and the mean normalised coastline during the 2-hour behavioural assessment period between first onset of generalised seizures and diazepam administration were correlated with the quantified behavioural seizure severity (as described in section 3.2.3).

4.2.4. Video monitoring of animals' behaviour

Video recordings were carried out concurrently with EEG recordings in order to correlate behaviour with EEG activity. The video set up is described in section

2.2.4. The assessment of animals' behaviour from the videos was carried out during the 24 hours after diazepam administration, and again for 24 hours on the 7th day and on the 14th day after KA-induced seizures. The raw EEG data from animals with observed behavioural seizures from the video recordings were traced back to the approximate time to when the seizure occurred. Raw EEG data were then visually reviewed to identify any seizure-like events that may have occurred approximately when seizures may have occurred for confirmation.

4.2.5. Statistical analysis

Statistical comparisons of seizure severity, spike frequency and coastline between treatment groups (control vs. PSD95BP and control vs. combination treatment of PSD95BP and 1400W dihydrochloride) were performed by one-way Analysis of Variance (ANOVA) using SPSS version 21 (IBM). Statistical comparisons of specific spike frequencies on days 7 and 14 after KA-induced seizures between treatment groups was also performed by two-sample t-test using SPSS. Area under the curve (AUC) from the start of KA administration to 28 days after KA-induced seizures for all treatment groups was calculated using the trapezium rule. The AUC was most accurately determined by calculating the sum of the area between every consecutive data point within a 1-hour interval using the following equation.

$$\sum_{t=1}^{t=\infty} \frac{t(s_{n+1} + s_n)}{2}$$

s indicates spike frequency or coastline value of the data point; *n* indicates the hour of the data point; *t* indicates the time interval which is 1-hour. Statistical analysis comparing AUC between treatment groups was performed by two-sample t-test using SPSS. Raw p-values are reported throughout, without correction for occasional multiple testing.

4.3. Results

4.3.1. Kainic acid sensitivity

A total of 15 mice implanted with an EEG transmitter were dosed with KA. The range of KA doses required to induce Stage 5 generalised seizures in these animals was between 5-30mg/kg i.p. (Figure 4.1).

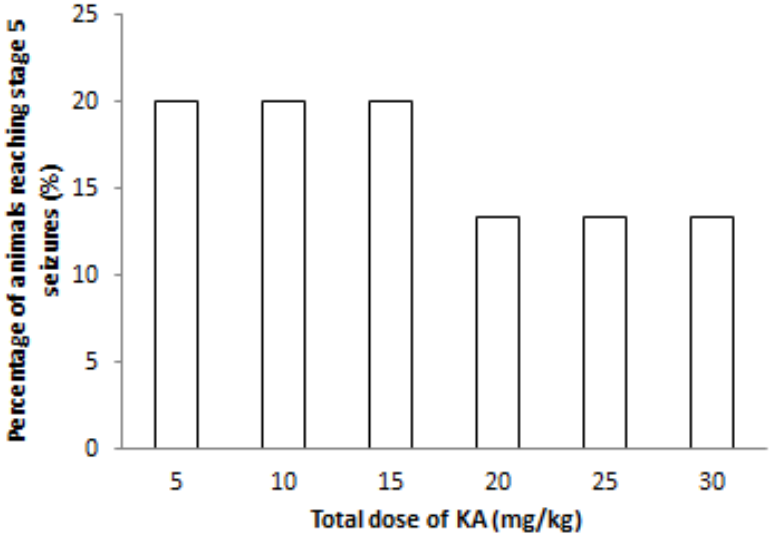

Figure 4.1. Total dose of kainic acid (KA), when given in repeated doses of 5 mg/kg per dose via intraperitoneal injection, required to reach Stage 5 seizures in C57BL/6J mice implanted with a Data Scientific International TA10ETA-F20 Physiotel® transmitter. Data are expressed as the percentage of all mice implanted with EEG transmitter (n=15).

4.3.2. Seizure severity between treatment groups

The seizure severity induced by KA after the first onset of generalised seizure for the control group had a cumulative score of 30 (± 6.99), which was significantly lower when compared to the group that received a combination of PSD95BP plus 1400W that had a cumulative score of 100.6 (± 4.37) ($p<0.01$) (Figure 4.2). The group that received PSD95BP alone had a cumulative score of 55.6 (± 14.18), which was also significantly lower than compared to the PSD95BP plus 1400W group ($p<0.05$) (Figure 4.2).

4.3.3. Behavioural vs. electrographic seizure severity

Correlation analyses were undertaken to explore the relationship, if any, between spike frequency and normalised coastline, as recorded by EEG, and behavioural

seizures, during the 2-hour behavioural assessment between the first onset of Stage 5 seizures induced by KA administration and the administration of diazepam. There was a clear correlation between mean spike frequency during the 2-hour assessment period and the severity of behavioural seizures based on the modified Racine scale, which showed a correlation coefficient (R^2) of 0.5857 (Figure 4.3). The correlation between normalised coastline and behavioural seizure severity was less robust, with an R^2 of 0.1438 (Figure 4.4).

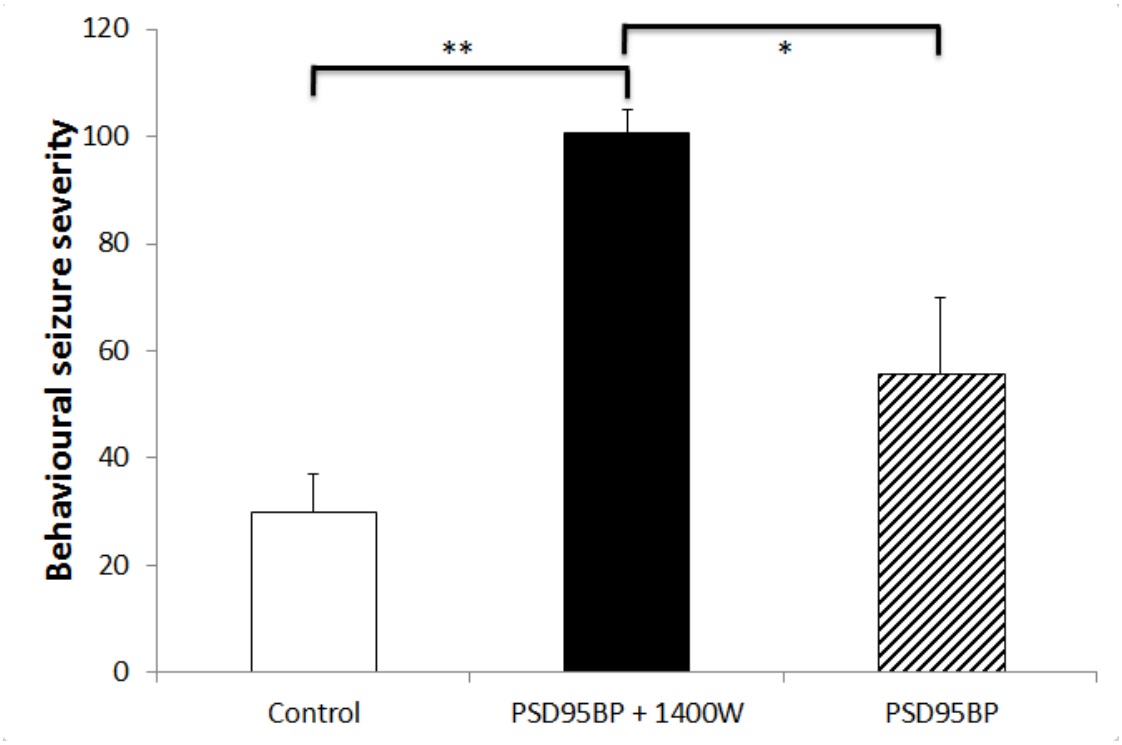

Figure 4.2. The behavioural seizure severity for C57BL/6J mice in each treatment group (n=4 for the control group, n=5 for the drug intervention treatment groups), determined using the cumulative Racine score from the first onset of generalised seizures induced by kainic acid (KA) administration to the administration of diazepam 2 hours after. Repeated administration of KA was given via intraperitoneal injection every 30 minutes until the first onset of generalised seizures. Behavioural assessment on the highest seizure score observed in each 5-minute epoch was recorded based on the Racine scale and summed over the 2-hour period. Data are expressed as the cumulative Racine score (± SEM) and was compared statistically using one-way Analysis of Variance (*$p<0.05$; **$p<0.01$).

4.3.4. Effect of drug interventions on spike frequency

Spike frequency increased for all animals when KA was administered and reached a maximum of 248.6 (± 53.5) spikes per minute when the first onset of Stage 5 generalised seizures occurred (Figures 4.5 and 4.6). After diazepam was administered, the spike frequency for all animals decreased and reached 4.1 (± 2.1) spikes per minute (Figures 4.5 and 4.6). PSD95BP was given 1 hour after diazepam and 1400W was given over 3 days after diazepam.

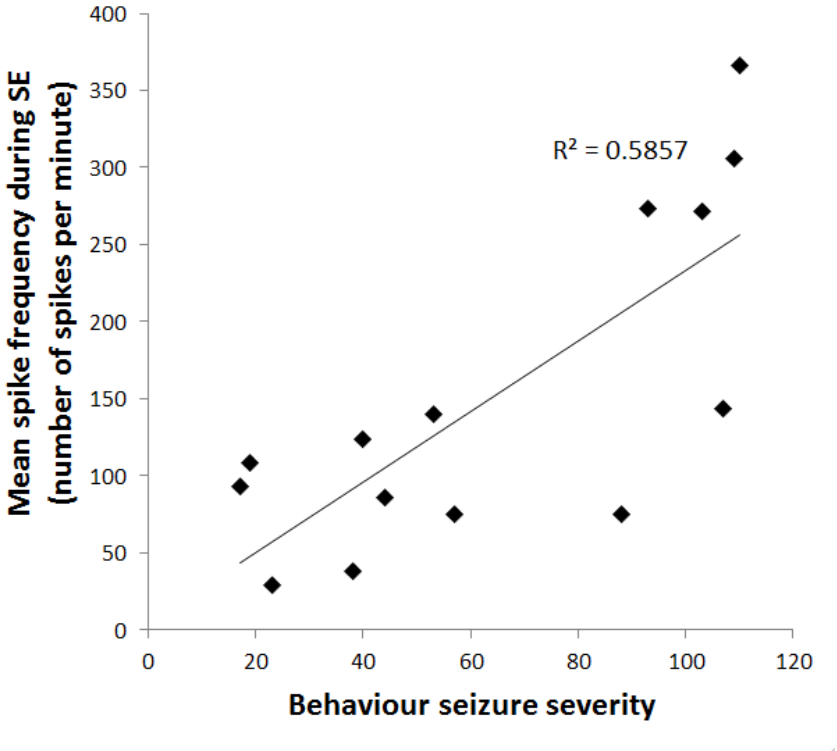

Figure 4.3. Correlation between mean spike frequency recorded by extra-dural EEG and behavioural seizure severity quantification during the 2-hour period following onset of the first Stage 5 seizure induced by kainic acid in C57BL/6J mice. Spike frequency data are expressed as the mean number of spikes per minute recorded in 5-minute epochs and averaged across the 2-hour period. Seizure severity quantification is reported as the Racine scale score observed in each 5-minute epoch and summed over the 2-hour period. Each data point represents a single animal (n=14). Pearson's product-moment correlation is represented by the solid line, with the corresponding correlation co-efficient (R^2) reported.

There were no differences in spike frequencies from days 1 to 5 after KA-induced seizures between the control group and the drug intervention groups (Figures 4.5, 4.6 and 4.7). The control group had a mean spike frequency of 31.0 (± 23.1)

spikes per minute, the PSD95BP plus 1400W combined group had a mean of 29.5 (± 13.8) spikes per minute, and PSD95BP group had a mean of 21.3 (± 14.5) spikes per minute (Figures 4.5, 4.6 and 4.7). From days 6 to 10, the spike frequencies of the control group and the drug intervention groups started to diverge, with the spike frequency of the control group gradually increasing from 42.6 (± 35.9) to 83.7 (± 78.4) spikes per minute whilst the PSD95BP plus 1400W combined treatment group had a mean spike frequency of 15.7 (± 6.1) spikes per minute, and the PSD95BP group had a mean of 16.6 (± 8.8) spikes per minute (Figures 4.5, 4.6 and 4.7).

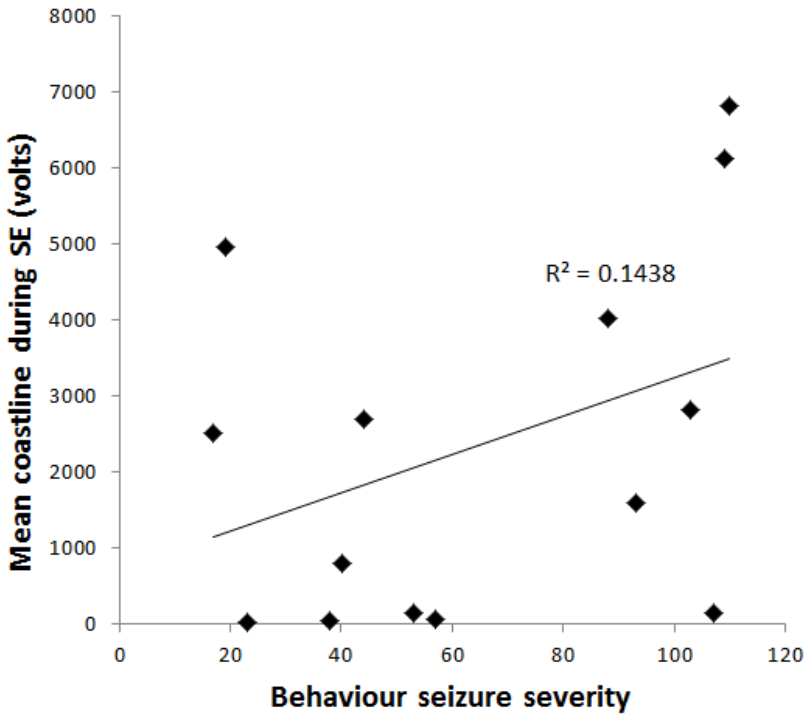

Figure 4.4. Correlation between mean normalised coastline recorded by extra-dural EEG and behavioural seizure severity quantification during the 2-hour period following onset of the first Stage 5 seizure induced by kainic acid in C57BL/6J mice. Coastline data are expressed as the mean sum of distances between consecutive data points in 5-minute epochs averaged across the 2-hour period. The coastline data were normalised to the baseline coastline value of each mouse before KA was administered. Seizure severity quantification is reported as the Racine scale score observed in each 5-minute epoch and summed over the 2-hour period. Each data point represents a single animal (n=14). Pearson's product-moment correlation is represented by the solid line, with the corresponding correlation co-efficient (R^2) reported.

At day 10 after KA-induced seizures, the spike frequency for the control group levelled out at 96.8 (± 77.2) spikes per minute up to 28 days after KA-induced seizures (Figures 4.5, 4.6 and 4.7). The PSD95BP plus 1400W combined treatment group had a mean spike frequency of 23.0 (± 11.8) spikes per minute from day 10 up to day 28 after KA-induced seizures (Figures 4.5 and 4.7). The PSD95BP treatment group had a mean spike frequency of 10.2 (± 3.1) spikes per minute from day 10 up to day 28 after KA-induced seizures (Figures 4.6 and 4.7). There appears to be some regular oscillations in the spike frequency profiles from day 9 in all treatment groups (Figures 4.5 and 4.6) which correlates with a 24h cycle, suggests that spike frequency may be able to detect the circadian rhythm using EEG.

Assessing the statistical significance using ANOVA for spike frequency by day did not show significant differences between the control group and either of the drug-intervention groups (Figure 4.7). A two-sample t-test was then used to compare the differences in spike frequency between the control group and the drug intervention groups on days 7, 14 and 26. The spike frequency of the PSD95BP plus 1400W combined treatment group was significantly lower than that of the control group on days 7 and 14 ($p<0.05$) (Figures 4.8 and 4.9). The spike frequency of the PSD95BP plus 1400W combined treatment group on day 7 was 14.7 (± 6.2) spikes per minute and on day 14 was 14.6 (± 7.1) spikes per minute, compared to the spike frequency of the control group on day 7 with 58.3 (± 53.3) spikes per minute, and on day 14 with 84.6 (± 77.3) spikes per minute (Figures 4.8 and 4.9). There were no significant differences in spike frequency between control group and the combined treatment group on day 26, with 109.9 (± 76.9) spikes per minute and 41.2 (± 18.9) spikes per minute, respectively (Figure 4.10). For PSD95BP treatment alone, no significant difference was observed on day 7 after KA-induced seizures, with a spike frequency of 20.0 (± 12.9) spikes per minute compared to the control group of 58.3 (± 53.3) spikes per minute (Figure 4.8). The spike frequency of the PSD95BP treatment group on day 14 was 9.2 (± 2.0) spikes per minute and on day 26 was 10.1 (± 3.5) spikes per minute, which were significantly lower than that of the control group, with 84.6

(± 77.3) spikes per minute on day 14 and 109.9 (± 76.9) spikes per minute on day 26 ($p<0.05$) (Figures 4.9 and 4.10).

AUC was used to measure the spike frequency over a 28-day profile for all animals and to compare the control group with drug-intervention groups using a two-sample t-test. The overall AUC of the PSD95BP treatment group was 8962 (± 3281) spikes.hour/min, which was significantly lower than the control group with the overall AUC of 54261 (± 43280) spikes.hour/min ($p<0.05$) (Figure 4.11). The overall AUC of the PSD95BP plus 1400W treatment group was 15414 (± 4648) spikes.hour/min, which was also significantly lower than the control group ($p<0.05$) (Figure 4.11).

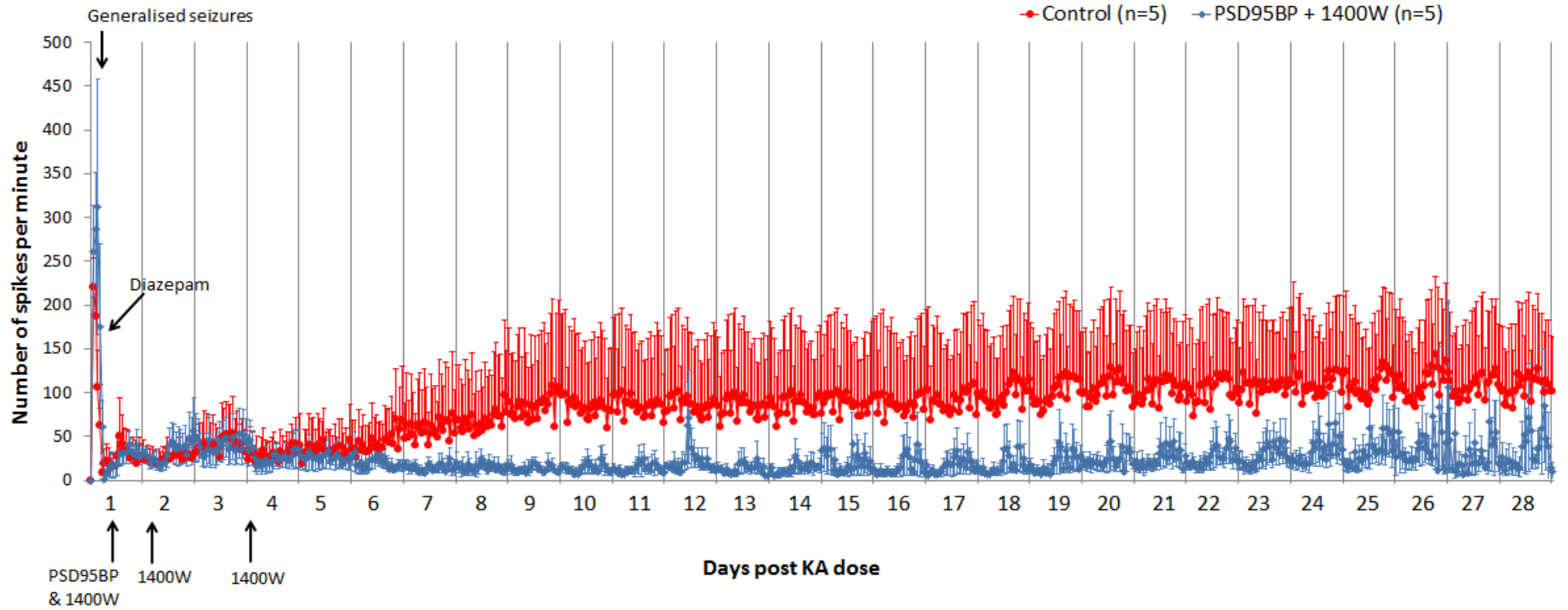

Figure 4.5. Spike frequency over 28 days post-kainic acid (KA), comparing animals from the control group (red data points) and those treated with a combination of post-synaptic density 95 blocking peptide (PSD95BP) and 1400W (blue data points). KA was administered to groups of C57BL/6J mice until the first onset of generalised seizures and diazepam was administered 2 hours thereafter. Intravenous injection of PSD95BP at 7.6 mg/kg and the first intraperitoneal dose of 1400W at 20mg/kg were administered 1 hour after diazepam administration. Two further doses of 1400W at 20mg/kg were administered 1 and 3 days after generalised seizure. Spike frequency is reported as the mean number of spikes per minute (± SEM) over one hour epochs (n=5).

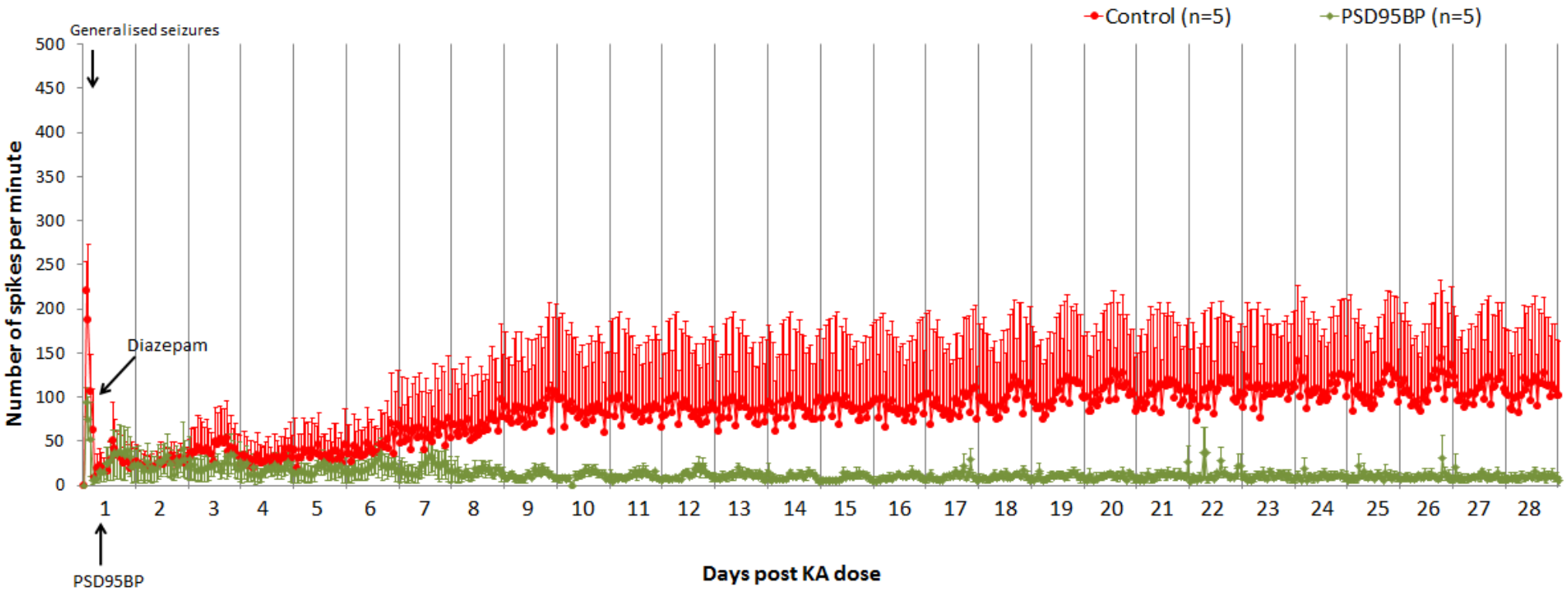

Figure 4.6. Spike frequency over 28 days post-kainic acid (KA), comparing animals from the control group (red data points) and those treated with post-synaptic density 95 blocking peptide (PSD95BP) (green data points). KA was administered to groups of C57BL/6J mice until the first onset of generalised seizures and diazepam was administered 2 hours thereafter. Intravenous injection of PSD95BP at 7.6mg/kg was administered 1 hour after diazepam administration. Spike frequency is reported as the mean number of spikes per minute (± SEM) over one hour epochs (n=5).

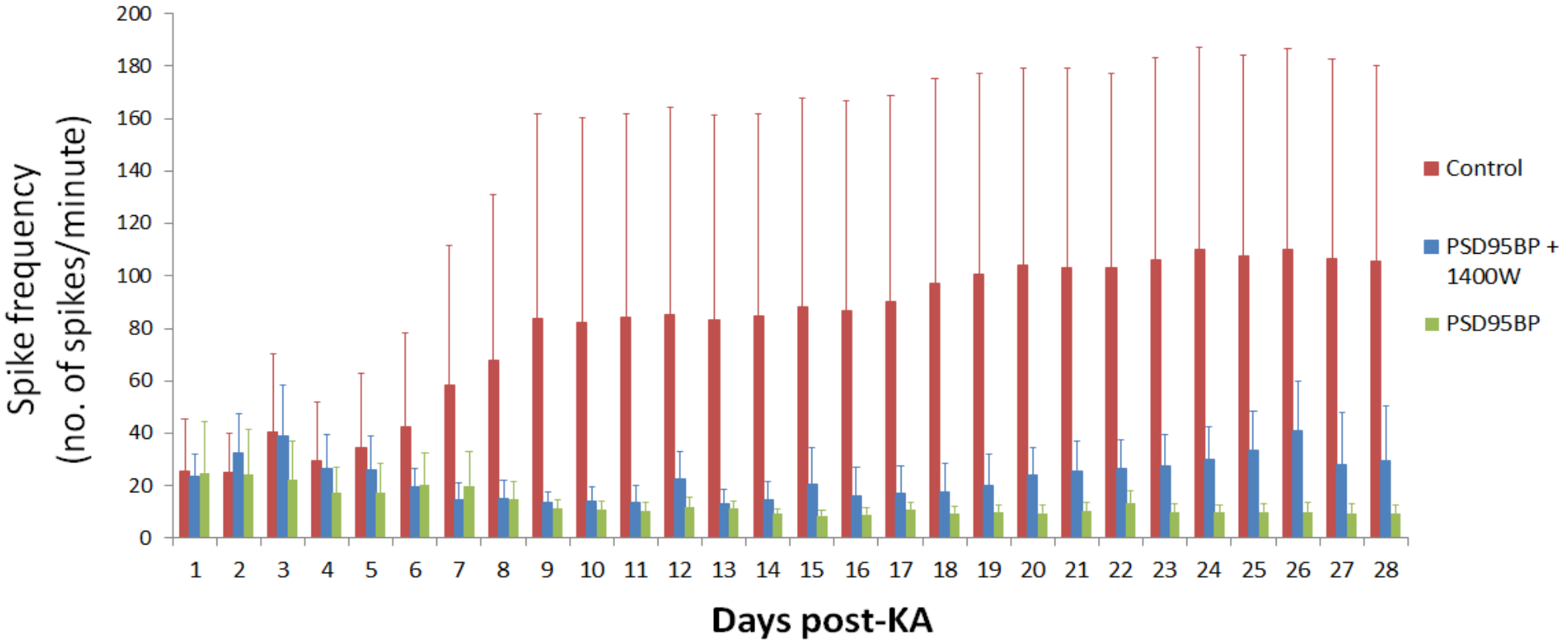

Figure 4.7. Daily spike frequency over 28 days post-kainic acid (KA), comparing animals from the control group (red bars), those treated with a combination of post-synaptic density 95 blocking peptide (PSD95BP) and 1400W (blue bars), and those treated with PSD95BP alone (green bars). KA was administered to groups of C57BL/6J mice until the first onset of generalised seizures and diazepam was administered 2 hours thereafter. Intravenous injection of PSD95BP at 7.6mg/kg and the first intraperitoneal dose of 1400W at 20mg/kg were administered 1 hour after diazepam administration. Two further doses of 1400W at 20mg/kg were administered 1 and 3 days after generalised seizure. Spike frequency is reported as the mean number of spikes per minute (± SEM) over 24 hour epochs (n=5).

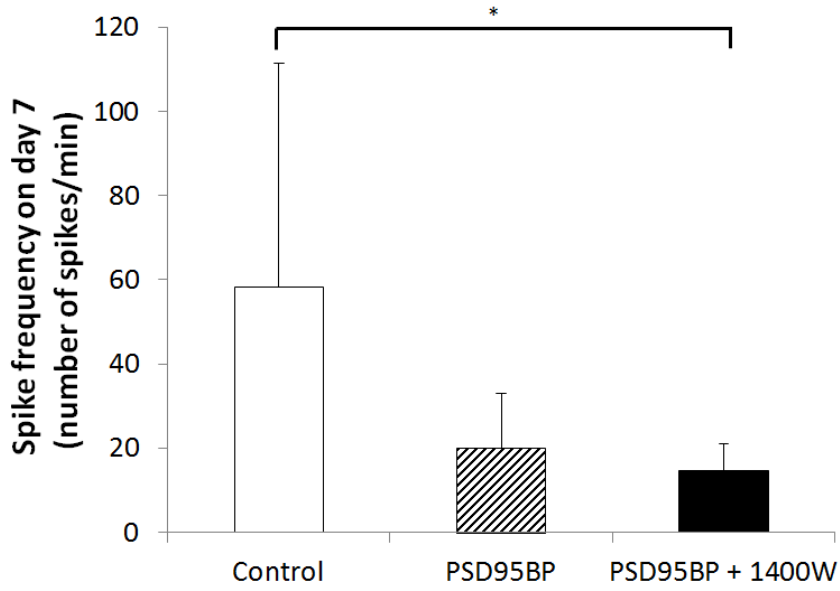

Figure 4.8. Mean spike frequency recorded by extra-dural EEG on day 7 after acute seizures induced by kainic acid in C57BL/6J mice (n=5 per group) treated with post-synaptic density 95 blocking peptide (PSD95BP) and a combination of PSD95BP plus 1400W, in comparison to vehicle-treated animals (control). Data are expressed as mean (± SEM) number of spikes per minute recorded in one-hour epochs and averaged across the full day and was compared statistically using a two-sample t-test (*p<0.05).

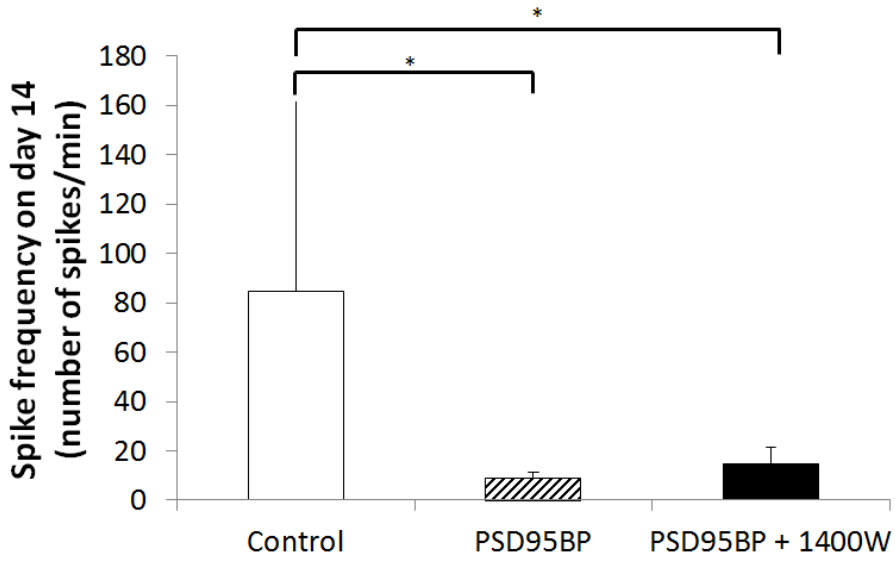

Figure 4.9. Mean spike frequency recorded by extra-dural EEG on day 14 after acute seizures induced by kainic acid in C57BL/6J mice (n=5 per group) treated with post-synaptic density 95 blocking peptide (PSD95BP), and a combination of PSD95BP plus 1400W, in comparison to vehicle-treated animals (control). Data are expressed as the mean (± SEM) number of spikes per minute recorded in one-hour epochs and averaged across the full day and was compared statistically using a two-sample t-test (*p<0.05).

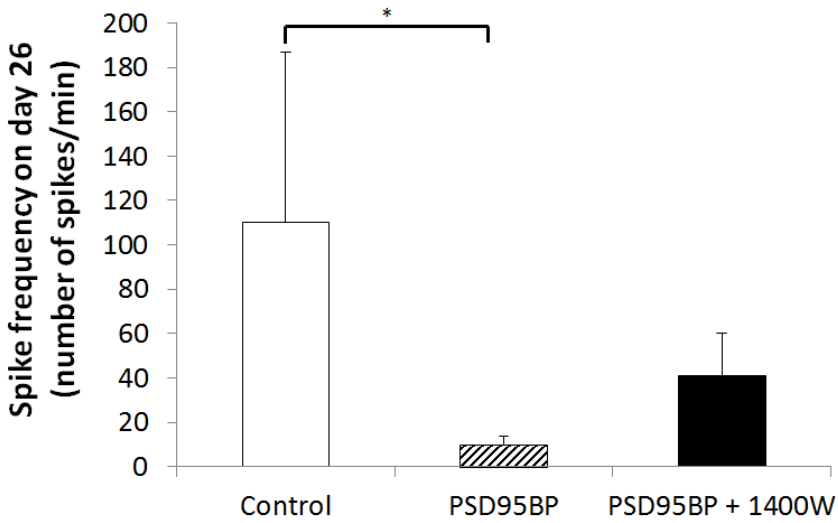

Figure 4.10. Mean spike frequency recorded by extra-dural EEG on day 26 after acute seizures induced by kainic acid in C57BL/6J mice (n=5 per group) treated with post-synaptic density 95 blocking peptide (PSD95BP) and a combination of PSD95BP plus 1400W, in comparison to vehicle-treated animals (control). Data are expressed as the mean (± SEM) number of spikes per minute recorded in one-hour epochs and averaged across the full day and was compared statistically using a two-sample t-test (*p<0.05).

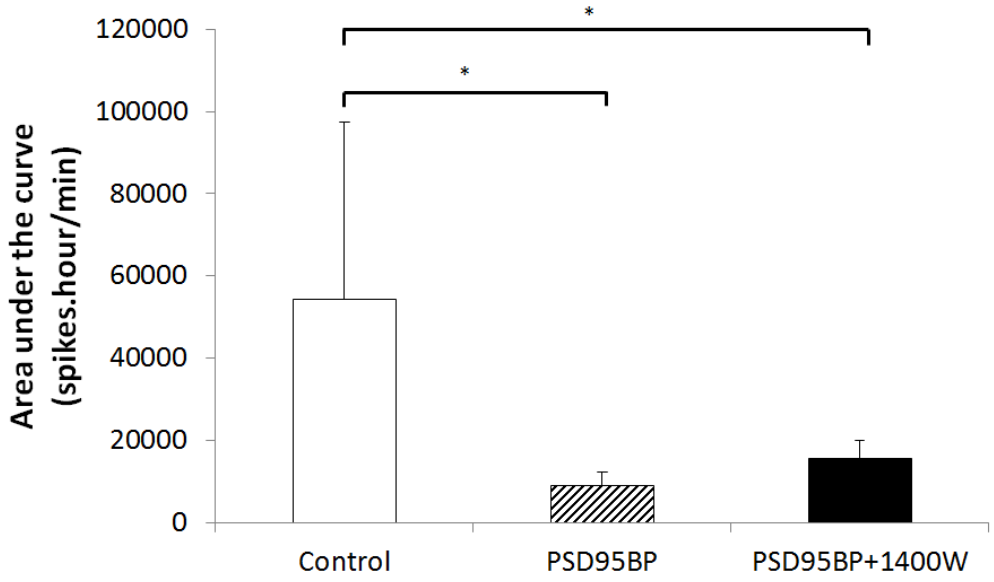

Figure 4.11. Mean area under the curve recorded by extra-dural EEG over 28 days after acute seizures induced by kainic acid in C57BL/6J mice (n=5 per group) treated with post-synaptic density 95 blocking peptide (PSD95BP) and a combination of PSD95BP plus 1400W, in comparison to vehicle-treated (control). Data are expressed as the mean (± SEM) area under the curve determined from the sum of the area between every consecutive data point within an-hour interval, averaged across the 28 days and compared statistically using a two-sample t-test (*p<0.05).

4.3.5. Effect of drug interventions on coastline

The change in normalised coastline profile over 28 days following KA-induced seizures did not show any significant differences between control and the drug intervention groups (Figures 4.11-4.13). The coastline data were then analysed in 30-second epochs and reported as the absolute number of post-KA epochs each day that had lengths more than 3 SDs from the mean baseline (Figure 4.15). From the epoch calculation method, there were significantly fewer numbers of extended post-KA epochs on day 7 in the PSD95BP treatment group, with 92.2 (± 42.23) epochs, compared to the control group, with 919.6 (± 581.64) epochs ($p<0.01$) (Figure 4.16). On day 14, there were significantly fewer numbers of extended post-KA epochs in the PSD95BP plus 1400W combined group, with 122.2 (± 105.3) epochs, compared to the control group, with 850.2 (± 552.93) epochs ($p<0.05$) (Figure 4.17). Calculating AUC for the epoch calculated data over a 28-day profile did not show any significant differences between control and the drug intervention groups (Figure 4.18).

4.3.6. Video monitoring of animals' behaviour

A maximum of four animals per treatment group could, in theory, be video-monitored using the available hardware. However, due to various technical difficulties, unexpected mortality, and animal housing issues, videos were only available for 4 control animals, 3 PSD95BP animals, and just 1 animal from the combined treatment group.

In order to confirm that diazepam administration had terminated SE in all animals and that subsequent seizure onset was spontaneous, behavioural assessment was performed for a 24-hour period after diazepam administration. One out of four control mice recovered from the sedative effects of diazepam within 1 hour post-dose and the remaining three mice recovered 4 hours post-diazepam with no abnormal behaviour thereafter.

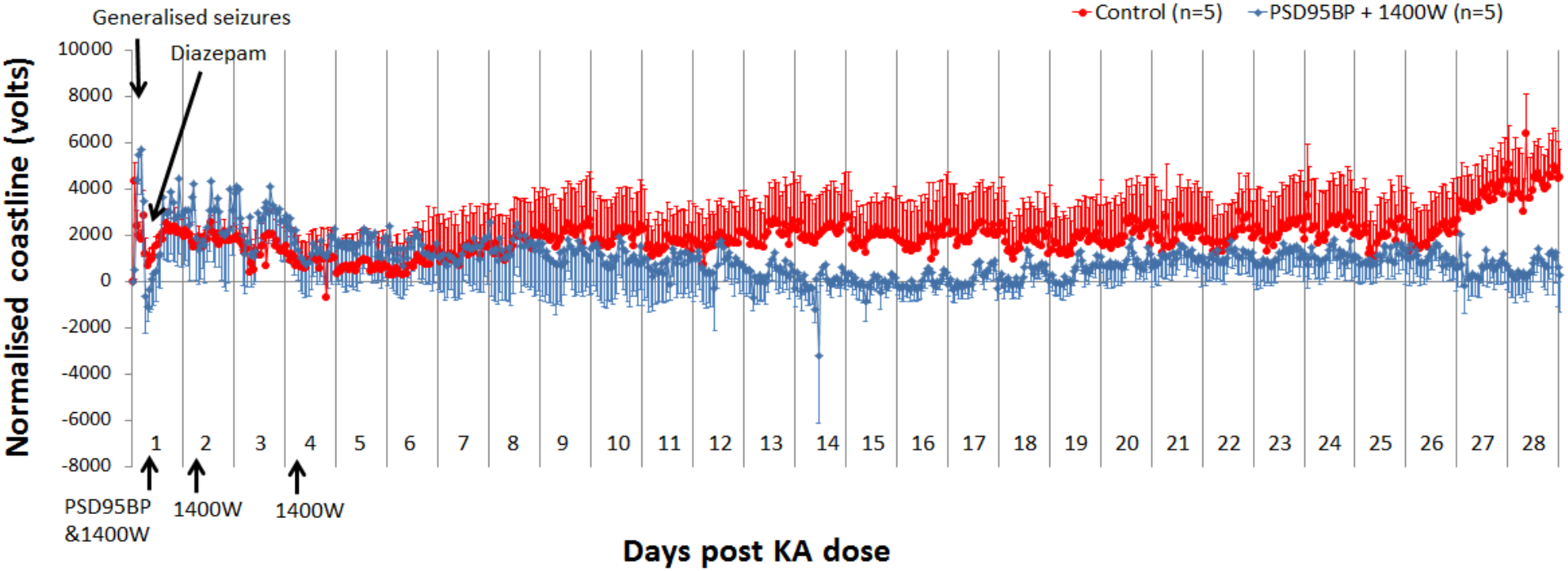

Figure 4.12. Normalised coastline over 28 days post-kainic acid (KA), comparing animals from the control group (red data points) and those treated with a combination of post-synaptic density 95 blocking peptide (PSD95BP) and 1400W (blue data points). KA was administered to groups of C57BL/6J mice until the first onset of generalised seizures and diazepam was administered 2 hours thereafter. Intravenous injection of PSD95BP at 7.6mg/kg and the first intraperitoneal dose of 1400W at 20mg/kg were administered 1 hour after diazepam administration. Two further doses of 1400W at 20mg/kg were administered 1 and 3 days after generalised seizure. Normalised coastline is reported as the mean sum of distances (± SEM) between consecutive data points normalised to the baseline coastline value before KA insult over one hour epochs (n=5).

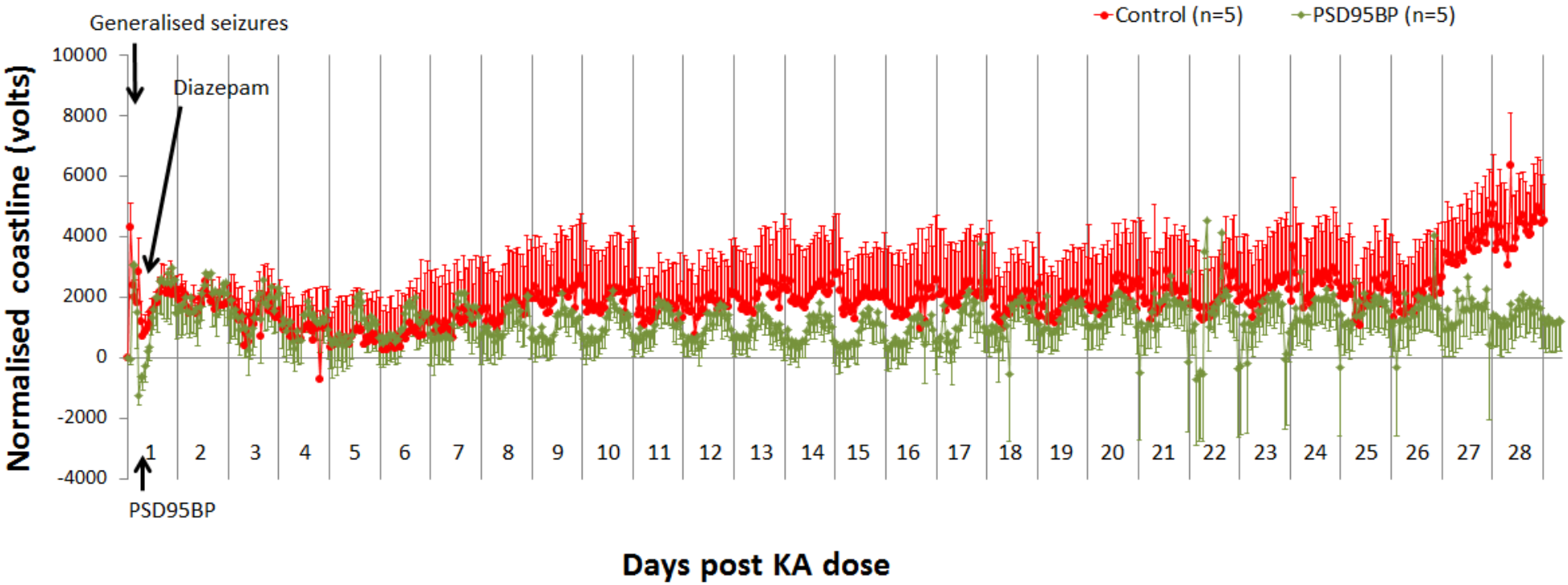

Figure 4.13. Normalised coastline over 28 days post-kainic acid (KA), comparing animals from the control group (red data points) and those treated with post-synaptic density 95 blocking peptide (PSD95BP) only (green data points). KA was administered to groups of C57BL/6J mice until the first onset of generalised seizures and diazepam was administered 2 hours thereafter. Intravenous injection of PSD95BP at 7.6mg/kg was administered 1 hour after diazepam administration. Normalised coastline is reported as the mean sum of distances (± SEM) between consecutive data points normalised to the baseline coastline value before KA insult over one hour epochs (n=5).

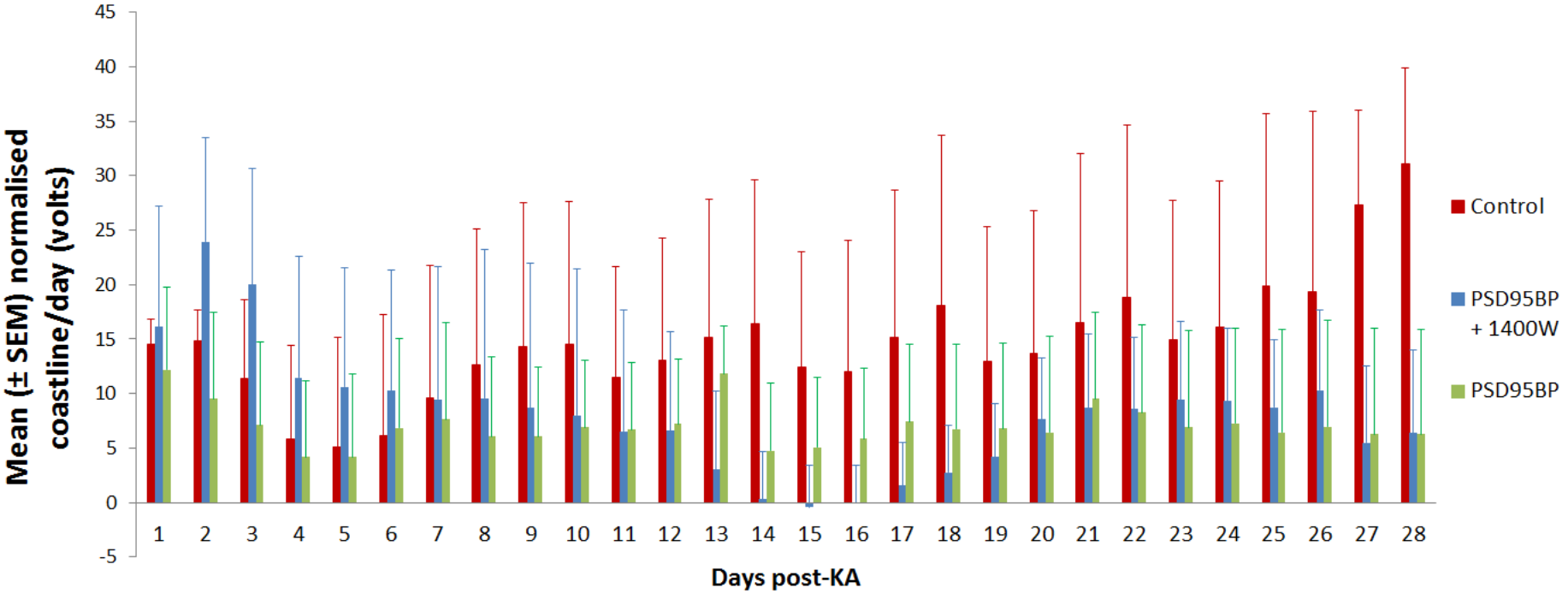

Figure 4.14. Daily normalised coastline over 28 days post-kainic acid (KA), comparing animals from the control group (red bars), those treated with a combination of post-synaptic density 95 blocking peptide (PSD95BP) and 1400W (blue bars), and those treated with PSD95BP alone (green bars). KA was administered to groups of C57BL/6J mice until the first onset of generalised seizures and diazepam was administered 2 hours thereafter. Intravenous injection of PSD95BP at 7.6mg/kg and the first intraperitoneal dose of 1400W at 20mg/kg were administered 1 hour after diazepam administration. Two further doses of 1400W at 20mg/kg were administered 1 and 3 days after generalised seizure. Normalised coastline is reported as the mean sum of distances (± SEM) between consecutive data points normalised to the baseline coastline value before KA insult over one hour epochs (n=5).

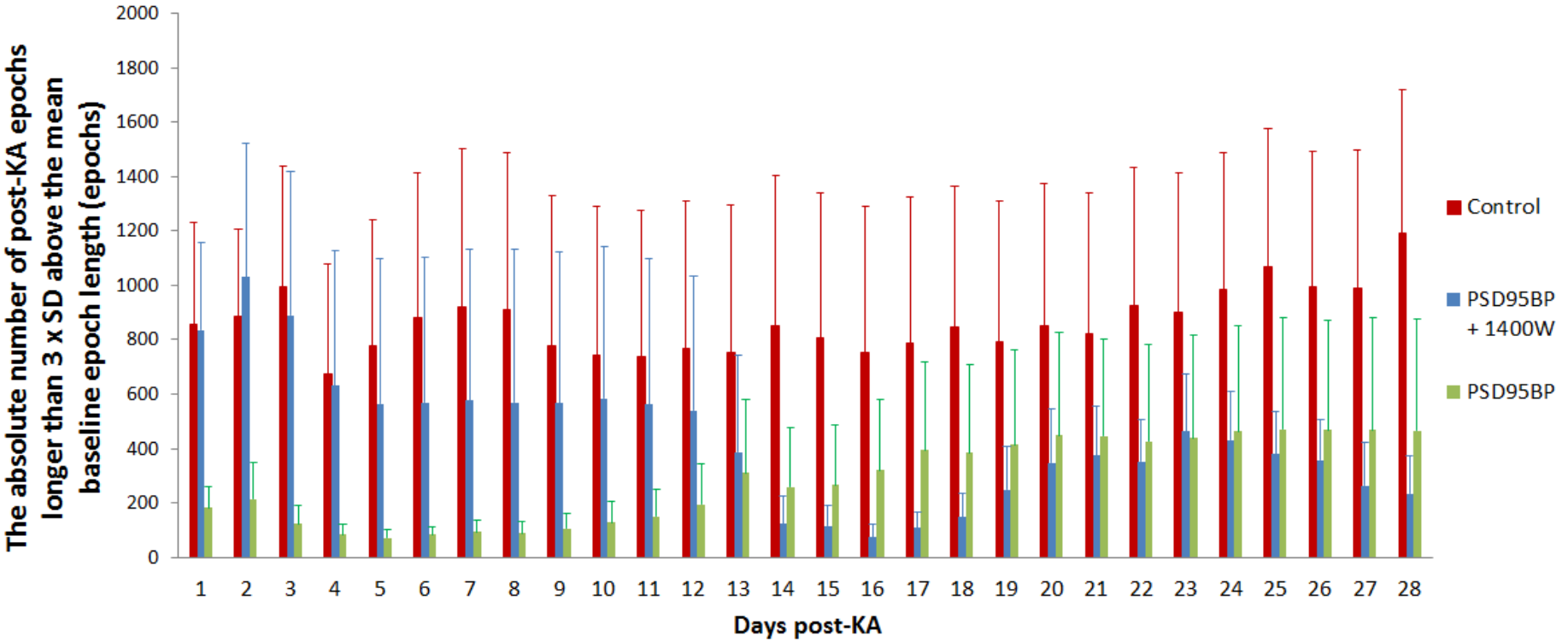

Figure 4.15. The absolute number of post-kainic acid (KA) epochs with coastline that was more than 3 standard deviations (SDs) from the mean baseline (pre-KA) epoch length per day. The data compare animals from the control group (red bars), those treated with a combination of the post-synaptic density 95 blocking peptide (PSD95BP) and 1400W (blue bars), and those treated with PSD95BP alone (green bars). The coastline data for all animals were separated into 30-second epochs and the SD in each 30-second epoch during baseline for each animal was determined. The absolute number of post-KA epochs (± SEM) each day wth coastline lengths out-with 3 SDs of the mean baseline (n=5).

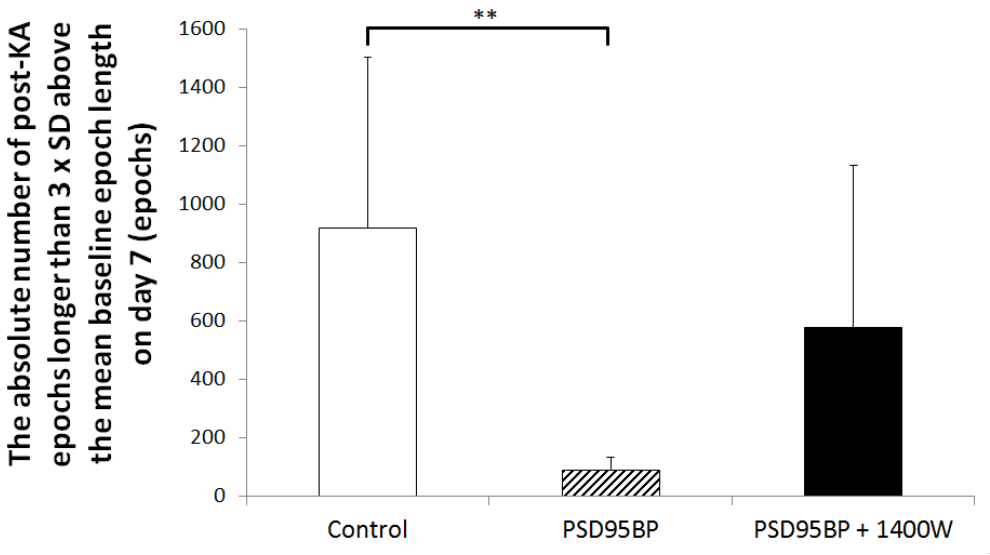

Figure 4.16. The absolute number of post-kainic acid (KA) epochs with coastline that was more than 3 standard deviations (SD) from the mean baseline (pre-KA) epoch length on day 7 after acute seizures induced by KA in C57BL/6J mice (n=5 per group). The data compare animals from the control group, those treated with post-synaptic density 95 blocking peptide (PSD95BP) alone, and those treated with a combination of the PSD95BP and 1400W. The coastline data for all animals were separated into 30-second epoch and the SD in each 30-second epochs during baseline for each animal was determined. Data are expressed as the absolute number of post-KA epochs each day (± SEM) that had lengths more than 3 SDs from the mean baseline length, and was compared statistically using two-sample t-test (**$p<0.01$).

All three mice given PSD95BP returned to normal behaviour 3 hours post-diazepam and the mouse given PSD95BP and 1400W combined treatment returned to normal behaviour 12 hours after diazepam administration.

On day 7, one control mouse had one occurrence of Stage 4 seizures that lasted less than 1 minute. Raw EEG traces for this mouse at the corresponding time revealed higher amplitude discharges than the baseline EEG trace that lasted 34 seconds (Figure 4.19). All mice treated with PSD95BP, and the mouse treated with PSD95BP and 1400W combined had normal behaviour throughout the 24-hour monitoring, with no evident behavioural seizures. On day 14, two other control mice had convulsive seizures, one experienced a single occurrence of a Stage 3 seizure that lasted less than 1 minute and another experienced a single occurrence of a Stage 5 seizure that also lasted less than 1 minute.

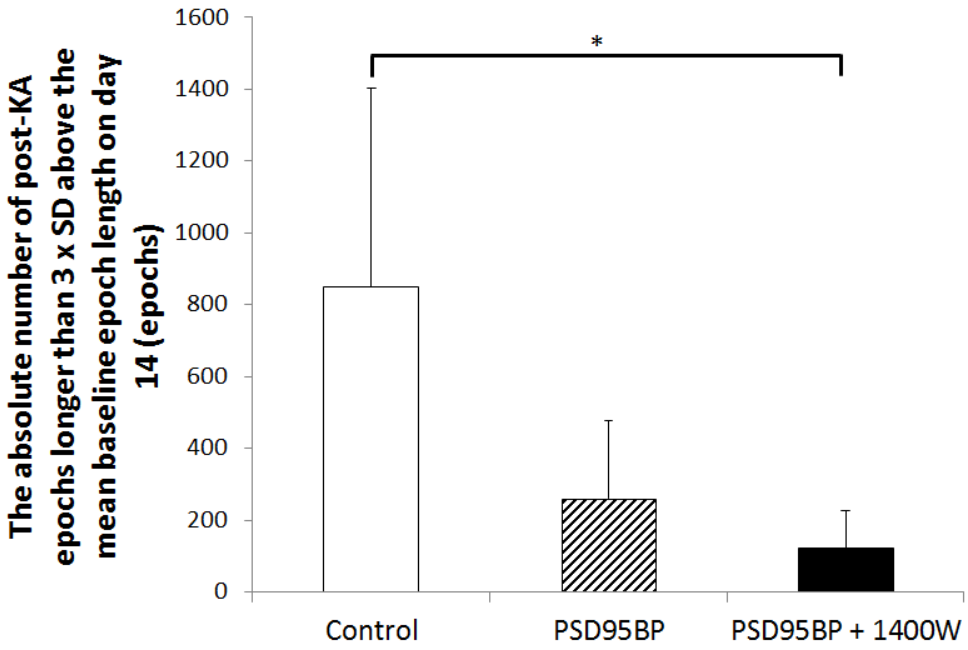

Figure 4.17. The absolute number of post-kainic acid (KA) epochs with coastline that was more than 3 standard deviations (SDs) from the mean baseline (pre-KA) epoch length on day 14 after acute seizures induced by KA in C57BL/6J mice (n=5 per group). The data compare animals from the control group, those treated with post-synaptic density 95 blocking peptide (PSD95BP) alone, and those treated with a combination of the PSD95BP and 1400W. The coastline data for all animals were separated into 30-second epoch and the SD in each 30-second epochs during baseline for each animal was determined. Data are expressed as the absolute number of post-KA epochs each day (± SEM) that had lengths more than 3 SDs from the mean baseline length, and was compared statistically using two-sample t-test (*$p<0.05$).

Raw EEG traces for the mouse that experienced the Stage 3 seizure at the corresponding time to the behavioural seizure also revealed higher amplitude discharges than the baseline EEG trace that lasted 28 seconds (Figure 4.30A & B). For the mouse that experienced the Stage 5 seizure, raw EEG traces at the corresponding time to the behavioural seizure also revealed higher amplitude discharges than baseline EEG trace that lasted 49 seconds (Figure 4.30C & D). All mice treated with PSD95BP and the mouse treated with PSD95BP and 1400W combined had normal behaviour throughout the 24-hour monitoring, with no evident behavioural seizures. All seizures observed in control animals only occurred in the light phase.

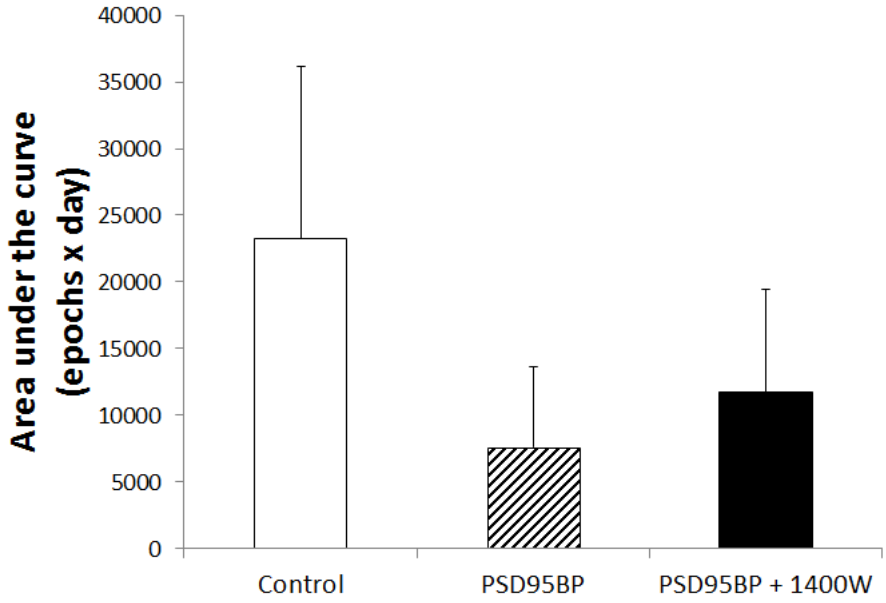

Figure 4.18. Mean area under the curve recorded by extra-dural EEG over 28 days after acute seizures induced by kainic acid in C57BL/6J mice (n=5 per group) treated with post-synaptic density 95 blocking peptide (PSD95BP) and a combination of PSD95BP plus 1400W, in comparison to vehicle-treated (control). Data are expressed as the mean (± SEM) area under the curve determined from the absolute number of post-KA epochs each day that had lengths more than 3 SDs from the mean baseline length averaged across the 28 days and compared statistically using a two-sample t-test.

4.4. Discussion

The purpose of the study in this chapter was to investigate the use of spike frequency and coastline for analysing extra-dural EEG recordings from C57BL/6J mice in a KA model of epileptogenesis. The effects of PSD95BP alone and the combination of PSD95BP plus 1400W, with potential anti-epileptogenic effects were also evaluated. There was a variable range of KA doses required to induce Stage 5 generalised seizures in mice implanted with EEG transmitter (Figure 4.1). The inherent variation may be partly due to subtle genetic variations between breeding lines, as described in chapter 3, or due to the surgical implantation of EEG transmitter that may have affected the KA sensitivity of the mice, or possibly both. Spike frequency and coastline analyses have been previously studied to detect seizures in rat EEG recordings in order to determine their sensitivity and specificity to subtle behavioural seizures (White et al., 2006).

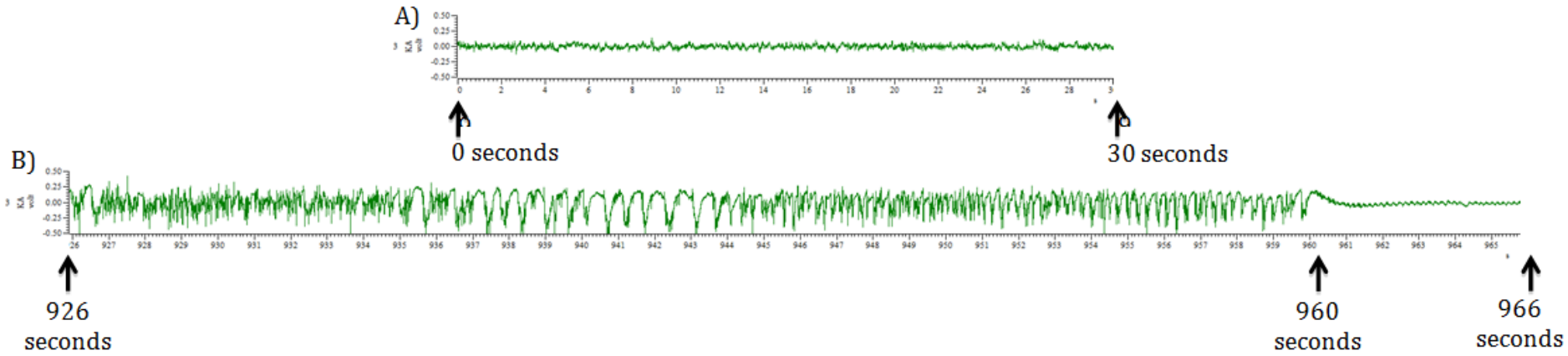

Figure 4.19. Electroencephalography (EEG) traces of one C57BL/6J mouse implanted with a DSI TA10ETA-F20 Physiotel® transmitter that experienced an isolated Stage 4 seizure 7 days after being subject to kainic acid (KA)-induced acute seizures. Repeated intraperitoneal administration of KA at 5 mg/kg was given every 30 minutes until the first onset of generalised seizures. Diazepam was administered intramuscularly 2 hours after the first onset of generalised seizures. (A) A normal EEG trace over 30 seconds of the animal during baseline recording. (B) An EEG trace over 40 seconds of the same animal on day 7 after KA-induced seizures. The EEG trace showing epileptiform discharges that occurred at a similar timing to when Stage 4 seizures occurred, confirmed using video monitoring. EEG was recorded at an output sample rate of 100Hz using Spike2 version 5 and is expressed as volts.

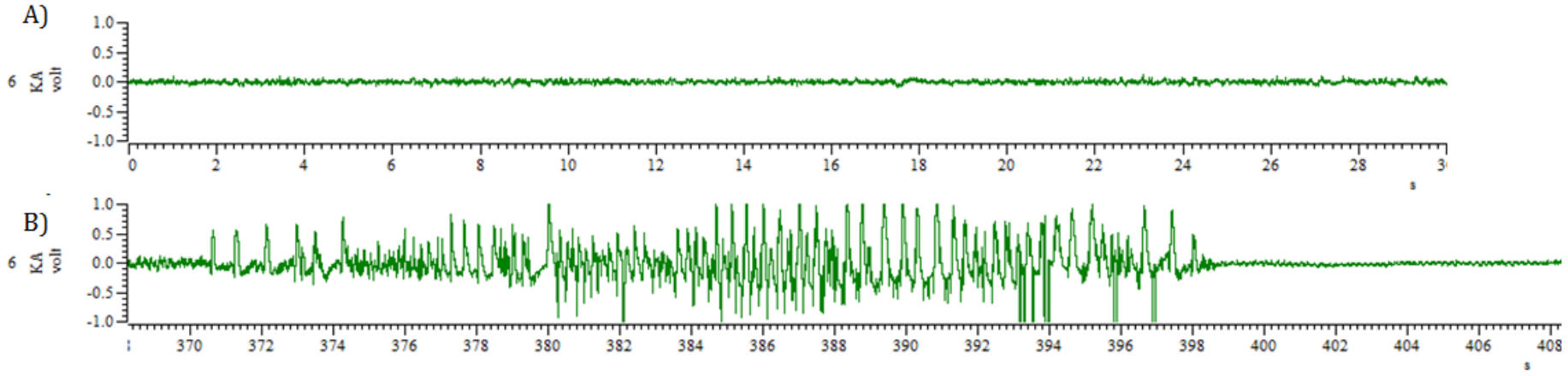

Figure 4.20. Electroencephalography (EEG) traces of one C57BL/6J mouse implanted with a DSI TA10ETA-F20 Physiotel® transmitter that experienced an isolated Stage 3 seizure 7 days after being subject to kainic acid (KA)-induced acute seizures. Repeated intraperitoneal administration of KA at 5 mg/kg was given every 30 minutes until the first onset of generalised seizures. Diazepam was administered intramuscularly 2 hours after the first onset of generalised seizures. (A) A normal EEG trace over 30 seconds of the animal during baseline recording. (B) An EEG trace over 40 seconds of the same animal on day 14 after KA-induced seizures. The EEG trace showing epileptiform discharges that occurred at a similar timing to when Stage 3 seizures occurred, confirmed using video monitoring. EEG was recorded at an output sample rate of 100Hz using Spike2 version 5 and is expressed as volts.

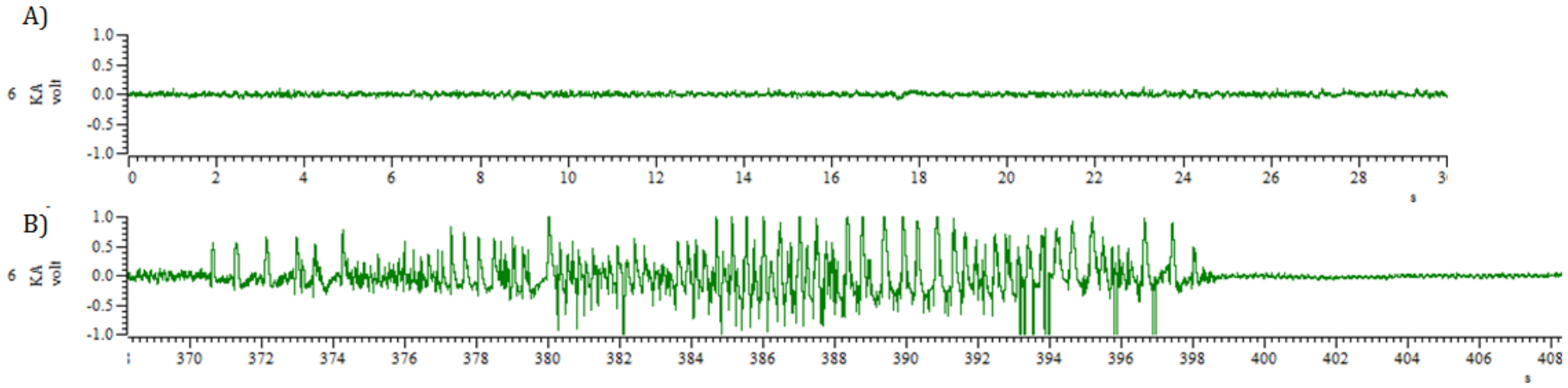

Figure 4.21. Electroencephalography (EEG) traces of one C57BL/6J mouse implanted with a DSI TA10ETA-F20 Physiotel® transmitter that experienced an isolated Stage 5 seizure 7 days after being subject to kainic acid (KA)-induced acute seizures. Repeated intraperitoneal administration of KA at 5 mg/kg was given every 30 minutes until the first onset of generalised seizures. Diazepam was administered intramuscularly 2 hours after the first onset of generalised seizures. (A) A normal EEG trace over 30 seconds of the animal during baseline recording. (B) An EEG trace over 58 seconds of the same animal (number 4) on day 14 after KA-induced seizures. The EEG trace showing epileptiform discharges that occurred at a similar timing to when Stage 5 seizures occurred, confirmed using video monitoring. EEG was recorded at an output sample rate of 100Hz using Spike2 version 5 and is expressed as volts.

Both algorithms were shown to be insensitive to non-convulsive seizure activities (White et al., 2006). In this study, the correlation between behavioural seizure severity using the cumulative Racine score in the 2-hour assessment period and the two algorithms were investigated. Spike frequency (Figure 4.3) appeared to show a better correlation to behavioural seizure severity than normalised coastline (Figure 4.4), suggesting that spike frequency is the better algorithm of the two for analysing the EEG data recorded in this study.

The spike frequency profiles of the control group, PSD95BP plus 1400W combined, and PSD95BP alone diverged from 6 days after the acute seizures (Figures 4.4, 4.5 and 4.6). On day 7, the spike frequency of PSD95BP plus 1400W combined treatment group is significantly lower than the control group (Figure 4.8), however PSD95BP treatment alone did not show any significant differences (Figure 4.8). On day 14, the spike frequencies of both treatment groups, PSD95BP plus 1400W combined and PSD95BP alone, were significantly lower than the control group (Figure 4.9). On day 26, the spike frequency of PSD95BP alone treatment was significantly lower than the control group, however the combined PSD95BP plus 1400W treatment group did not show any significant differences (Figure 4.10). These results suggest that PSD95BP alone and PSD95BP plus 1400W combined treatments were both able to reduce the spike frequency after KA-induced seizures. The significant reduction in spike frequency of the PSD95BP plus 1400W combined treatment group did not persist until 28 days after KA-induced seizures. On the other hand, the significant reduction seen with PSD95BP treatment alone continued up to 28 days after KA-induced seizures. Using AUC, the spike frequency profiles in the PSD95BP group and in the combined treatment group were significantly lower than in the control group (Figure 4.11), with PSD95BP appearing to be more effective than the combined treatment of PSD95BP and 1400W. It is possible that 1400W limited the efficacy of PSD95BP in a combined treatment or the differences in initial severity of SE affected the efficacy of the combined treatment group (Figure 4.2).

No significant differences in normalised coastline profile were observed between the control and the drug-intervention groups, when data were plotted for every hour (Figures 4.11 and 4.12) or in mean normalised coastline per day (Figure 4.14). This was possibly due to the transient changes in coastline being swamped by overall EEG coastline in each one hour epoch. Normal physiological relevant EEG frequency in a mouse brain band from 0-25Hz (Bergstrom et al, 2013), which is lower than the frequency signal of 100Hz used in this study. High frequency noise may have disguised the high amplitude discharges that were observed when animals experienced convulsive seizures. This may explain why coastline has a poorer correlation with behavioural seizure severity than spike frequency. The noise detected may also have suppressed the differences in normalised coastline between control and drug-intervention groups that could explain the non-significant differences between treatment groups. Apart from recording at a lower frequency, this could be resolved by applying more aggressive signal filtering to further reduce the high frequency noise. Alternatively, splitting the coastline profile into smaller 30-second epochs and profiling the number of epochs with an extended coastline (more than 3 SDs from the mean baseline epoch length) may be another method to differentiate the coastline changes during high amplitude discharges and high frequency noise. The number of extended epochs showed significant differences between the control and drug-treated groups (Figure 4.15). PSD95BP treated group had significantly fewer numbers of extended epochs than the control group on day 7 (Figure 4.16) and PSD95BP plus 1400W combined group had significantly fewer numbers of extended epochs than the control group on day 14 (Figure 4.17). However, AUC for extended epochs per day over 28-day profile did not show any overall significant changes (Figure 4.18).

The EEG profiles for all 3 treatment groups were continuously monitored from the time of KA-induced acute insult to the end of the experiment with no breaks in the period of recording, meaning that seizure clusters did not obscure the progressive nature of acquired epileptogenesis (Dudek and Staley, 2011; Galanopoulou et al., 2013). Based on the animals' behaviour from video monitoring, no apparent seizure activity was observed in any animals within 24 hours after the administration of diazepam. This suggests that the diazepam administered was

able to suppress SE induced by KA for up to 24 hours post-dose and therefore any subsequent seizure occurrence is likely to be spontaneous and not continued from the initial insult. One control mouse had a spontaneous seizure on day 7 and two other control mice had spontaneous seizures on day 14. None of the mice treated with PSD95BP or combined treatment of PSD95BP and 1400W showed any evidence of spontaneous seizures on days 7 and 14. The changes in EEG traces for the control mice at a time corresponding to the behavioural seizures showed higher amplitude discharges than the baseline traces. The duration of these higher amplitude traces appeared to correlate with the severity of the behavioural seizure observed, as the longest trace was observed for the Stage 5 seizure and the Stage 3 seizure showed the shortest trace (Figures 4.19-4.21). However, this would require confirmation with software that is able to record EEG traces and video monitoring simultaneously in real-time in order to accurately assess the relationship between the duration of epileptiform discharges and behavioural seizure severity.

The mean seizure severity during the 2-hour behavioural assessment period was different between treatment groups. The control group had the lowest seizure severity score and the combined PSD95BP plus 1400W group had the highest severity score (Figure 4.2). Given that the control group had significantly higher spike frequency and higher number of extended coastline epochs than the drug-treated groups during the 28 day follow-up period, this would suggest that a low seizure severity in the initial behavioural assessment period did not hinder the subsequent changes in spike frequency or coastline epochs.

The spike frequency and coastline for the control group after KA-induced seizures were variable, with a greater degree of variability in the control group than in the drug-treated groups. Variability in the latency to the first spontaneous motor seizure after the initial insult between rats was reported in an epilepsy model where KA was administered in a repeated low dose regimen (Hellier et al., 1998; Bauer and Norwood, 2013). Greater degree of variability seen in the control group could be due to the different latency in the onset of spontaneous seizures between the mice. Statistical significance was not achieved by comparing the spike

frequency and coastline between the control and the drug intervention groups during the 28 day follow-up period using ANOVA. A post hoc power analysis (Cohen, 2013) for spike frequency showed that the sample size required to give sufficient statistical power to yield significant differences between control and drug intervention groups is n=35 to 40 per treatment group (Figure 4.22). This suggests that the EEG algorithms investigated in this chapter are so variable that robust conclusions could not be drawn about the differences between treatment groups without resorting to a study with unreasonably large number of animals.

Current spike detection techniques are known to have flaws due to disagreement amongst experts with regard to what constitutes an EEG spike (White et al., 2006). The criteria of a spike used in the spike frequency analysis of this study focused on those with amplitudes that were higher than baseline, before the induction of KA insult. It is unknown whether all high amplitude spikes detected were directly related to seizures, although more high amplitude spikes appeared during seizure activity. Although it is unsure whether spike frequency algorithm can be used to predict seizure activities, it has been reported that a significant increase in spike frequency is seen in rodents that developed chronic epilepsy compared to those that did not (White et al., 2010).

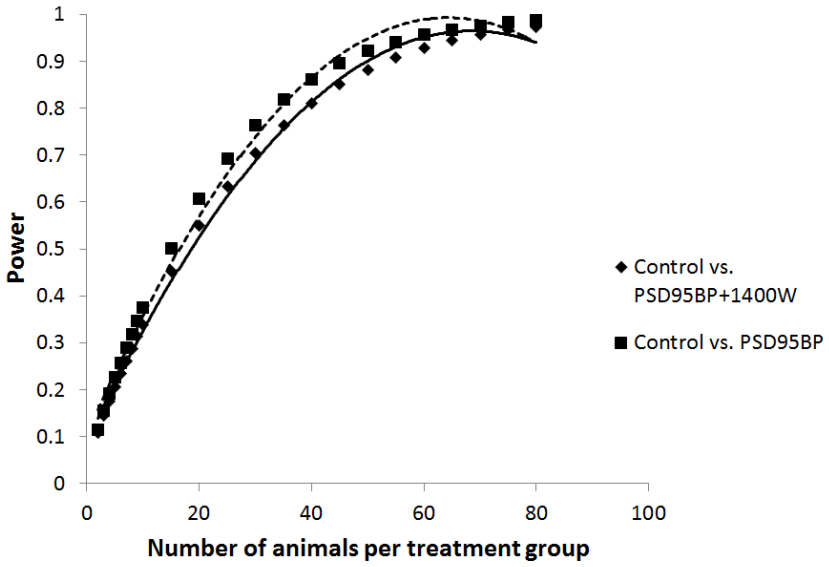

Figure 4.22. Post hoc power analysis for spike frequency on day 14 after KA-induced seizures comparing control with post-synaptic density 95 blocking peptide (PSD95BP) and the combined treatment of PSD95BP and 1400W. Power is (1- β error probability when the null hypothesis is false) a function of effect size and sample size. One-tailed independent t-test was used to compare the difference between two independent means of the control and the combined group, or the control and the PSD95BP group. The effect size d was 0.570477 for control vs. PSD95BP and 1400W combined treatment group and d was 0.616882 for control vs. PSD95BP. The allocation ratio N2/N1 was 1 and the significance level (α error probability when the null hypothesis is true but rejected) was 0.05.

In this study, spontaneous seizures were observed in some mice from the control group when there was a higher spike frequency. Nevertheless, an increase in spike frequency would not be able to reliably predict the occurrence of subsequent spontaneous seizures due to the lack of sensitivity of this analysis. Further investigation will be required to refine the spike frequency algorithm to improve on its specificity.

Chapter 5

Proteomic profile of the hippocampus: acute insult vs. potential anti-epileptogenic drug interventions

5.1. Introduction

Proteins are the most multi-purpose macromolecules in the living system and are crucial to the various cellular events that govern the function of biological systems (Berg et al., 2002; Kumar and Mann, 2009). Altered protein expressions are implicated in several disease states, therefore the understanding of proteins and their interactions is fundamental for biomedical research (Hondermarck, 2004; Kumar and Mann, 2009). Proteomics is a large-scale study of proteins that determines the entire complement of proteins expressed in a particular cell or tissue at a single point in time. Their interactions with other molecules are also determined in order to characterise their roles in biological processes, disease progression and therapeutic drug effects (Anderson and Anderson, 1998; Morrison et al., 2002; Hondermarck, 2004).

5.1.1. Principles and instrumentation

A proteomics assay is typically a two-stage process: large-scale protein separation, followed by characterisation of the separated proteins by MS analysis (Molloy and Witzmann, 2002; Morrison et al., 2002). Multi-dimensional capillary liquid chromatography (LC) separation of protein digests is normally used to minimise the number of peptides being introduced to the mass spectrometer, thus increasing the overall dynamic range of the MS measurements and optimising the detection of low abundance peptides (Morrison et al., 2002). The sensitivity of the proteomics assay required to identify low abundance proteins is ultimately dependent on the MS instrumentation (Morrison et al., 2002). MS is a well-established protein identification tool and has become a powerful technology for the large-scale study of proteins (Ong et al., 2003; Kumar and Mann, 2009). It enables rapid identification and characterisation of proteins in a global study of cellular proteomes in tissues or cells (James, 1997; Molloy and Witzmann, 2002; Kumar and Mann, 2009). Two commonly used forms of MS in proteomics are: matrix-assisted laser desorption ionisation time-of-flight (MALDI-TOF) spectrometry and MS/MS (Hondermarck, 2004). MALDI-TOF makes use of a single mass analyser and is normally used to analyse simple peptide mixtures, whereas MS/MS integrated with LC is used for the analysis of more complex samples

(Aebersold and Mann, 2003). MS/MS was the method of choice for the protein identification described in this chapter due to the level of information it can provide (Hondermarck, 2004).

5.1.2. Protein identification and quantification

Protein identification is based on peptide ion analysis, where the peptide ion data obtained for each sample is queried against a peptide database in an effort to correlate the measured peptide ions with known peptide ions derived from theoretical digests of unique proteins (Molloy and Witzmann, 2002). A popular approach to identification with raw MS/MS data is to search databases of known genomes and proteomes with un-interpreted data using Mascot (http://www.matrixscience.com) (James, 1997; Perkins et al., 1999; Ma et al., 2003). Protein quantification mostly involves the use of isotope labelling to compare samples that were labelled via MS (Elrick et al., 2006). However, for proteins that were not isotopically labelled, such as from animal tissues, samples are typically analysed by label-free quantification (Kumar and Mann, 2009). Label-free quantification measures and compares the MS signal intensity of the peptide ions to determine the relative amount of proteins in the biological samples of interest (Bantscheff et al., 2007). A variety of analytical methods have been applied to interpret quantified proteomics datasets, such as multivariate statistics (Tarroux, 1983; Anderson et al., 1984; Vilain et al., 2004), relative quantitation or expression (Blackstock and Weir, 1999; Ong et al., 2003; Bantscheff et al., 2007), quantitative trait loci mapping (Damerval et al., 1994; Picotti et al., 2013) and cluster correlation (Weinstein et al., 1997; Carlson et al., 2007). Another approach for protein quantification is using PEAKS (Bioinformatics Solutions Inc.; http://www.bioinfor.com), which calculates the peptide ratios from raw MS/MS data based on peak areas of the top-3 unique peptides identified for the protein in order to visualise the quantification results in a 2D heat map (Ma et al., 2003; Bin Ma and Johnson, 2012).

5.1.3. Protein profiling and interactions

The most simple and common way to present large-scale proteomics data is to list the expression of proteins as a function of the tissue condition, to help identify any

changes in protein expressions associated with its biological function (Aebersold and Mann, 2003). Relative quantitative analysis can provide a list of proteins that are different between each sample in order to compare the level of protein expression between different conditions or treatments (Bantscheff et al., 2007). It has been suggested that listing the affected proteins based on magnitude of change does not necessarily facilitate the identification of biomarkers of disease because changes in protein expression of small magnitude may be just as likely to initiate the disease process as changes of large magnitude (Drabik et al., 2007). The prediction of cellular processes from relative quantitative data alone is also known to be inadequate, especially when aiming to identify a biomarker for a specific disease (Aebersold and Mann, 2003; Drabik et al., 2007). The study of protein function and its interactions within the organism is helpful in identifying disease-associated protein markers (Drabik et al., 2007). Cellular processes are typically carried out by stable or transiently assembled protein complexes and so identifying protein-protein interactions can allude to cellular function (Kumar and Mann, 2009). Functional analysis of the quantitative expression mapping can emerge from proteomic comparisons between treatment groups (Kumar and Mann, 2009). On a functional level, proteins can be mapped to network and pathway databases to visualise those proteins in their modular functional contexts, which may be important in the disease process or in the mechanism of action of drug interventions (Banks et al., 2000; Kumar and Mann, 2009). Search Tool for the Retrieval of Interacting Genes/Proteins (STRING; http://string-db.org) is a database containing information from numerous sources about known and predicted protein interactions, including direct (physical) and indirect (functional) associations (Mering et al., 2003; 2005; Szklarczyk et al., 2011; Franceschini et al., 2013). These associations are derived from genomic context, high throughput experiments, co-expression and previous knowledge from published literature. Protein-protein interaction networks can also be used to predict interaction networks that can lead to hypotheses for follow up experimental research and interaction mapping (Schwartz et al., 2009).

5.1.4. Proteomics in neurosciences

Proteomic technology provides the opportunity to integrate information about the expression of proteins and their cellular localisation (Jain, 2002). It has been used to study the mechanisms of several neurological and neurodegenerative disorders and has facilitated the development of diagnostic biomarkers and potential therapeutic targets (Jain, 2002; Morrison et al., 2002; Kim and Sheng, 2004). These disorders include Alzheimer's disease (Fountoulakis, 2001; Jain, 2002; Johnson et al., 2005; Drabik et al., 2007), Parkinson's disease (Johnson et al., 2005; Drabik et al., 2007), Huntington's disease (Drabik et al., 2007), Down's syndrome (Fountoulakis, 2001; Jain, 2002; Johnson et al., 2005), schizophrenia (Jain, 2002), prion disease (Banks et al., 2000; Drabik et al., 2007), polyglutamine disease (Johnson et al., 2005), injury-induced neurodegeneration (Johnson et al., 2005), motor neuron disease (Johnson et al., 2005) and epilepsy (Krapfenbauer et al., 2001a; 2001b; Liu et al., 2008; Li et al., 2010; Löscher and Brandt, 2010; Kan et al., 2012; Persike et al., 2012). A proteomic approach can help dissect the molecular pathways involved in both physiological and pathological neurological states. In epilepsy, protein expression profiles in brains from patients (Kan et al., 2012; Persike et al., 2012) and mouse models have been investigated (Krapfenbauer et al., 2001a; 2001b; Liu et al., 2008; Li et al., 2010; Löscher and Brandt, 2010), in order to gain insight into the mechanisms of epileptogenesis and to identify potential targets for treatment. The use of proteomic technology to characterise the cellular effects of potential anti-epileptogenic drugs has not been reported. The abundance or structure of proteins that are regulated by drugs can provide important insight into their mechanisms of action (Anderson and Anderson, 1998). The objective of the research described in this chapter was therefore to investigate the proteomic profile of the hippocampus of C57BL/6J mice following KA-induced seizures and the subsequent effect of pharmacological interventions that target NO signalling pathway. Details of the KA model and the respective drugs, PSD95BP and 1400W, are provided in previous chapters. Changes in the proteomic profile were investigated using relative protein quantitation, heat map visualisation and predicted protein-protein interaction mapping.

5.2. Materials and methods

5.2.1. Animals

All experimental procedures were completed in accordance with the Animal (Scientific Procedures) Act, 1986 (UK). All methodological details regarding the source of animals, their housing conditions, and administration of KA to induce seizures are provided in section 2.1. There were six treatment groups in this study (n=4 per group), three of which received KA followed by either PSD95BP, 1400W or distilled water (as a treatment control) and three that received distilled water (to control for KA administration) and then either PSD95BP, 1400W or additional distilled water (again as a treatment control). The preparation and dosing regimens of PSD95BP and 1400W are outlined in section 4.2.2. Seven days after KA-administration (or appropriate control), all mice were euthanised, as described in section 2.1.4. This timepoint was chosen based on the spike frequency EEG algorithm that appeared to diverge between the control animals and the drug-intervention groups from 7 days after KA-induced acute seizures in chapter 4. The divergence may be indicative of the start of spontaneous seizures in the control animals. The brains were removed and the hippocampi were dissected and stored in cryovials prior to being snap-frozen in liquid nitrogen. All samples were stored in -80^{o}C until required for proteomic analysis.

5.2.2. Proteomics protocol

All hippocampi were thawed on ice before homogenisation. Protocols for tissue homogenisation, digestion and LC-MS are outlined in section 2.4. Tryptic digests of hippocampal homogenates were analysed by nanoflow reversed-phase LC-MS on the Q Exactive™ (Thermo Fisher, UK) at 2h LC gradients with an Orbitrap analyser. Each MS cycle had a full range scan at high resolution followed by sequential fragmentation of the 10 most abundant peptide ions. The fragments were then measured at high mass resolution in the Orbitrap.

5.2.3. Data collection

Raw data files were searched against the Universal Protein Resource (UniProt; http://www.uniprot.org) mouse database using Proteome Discoverer 3.1 and

between 1,650 and 1,800 proteins were identified with a false discovery rate of 0.1-0.5%. Label-free LC-MS analysis was performed using Progenesis LC-MS version 4.0 (Nonlinear Dynamics Ltd, UK) with protein identifications from the Mascot search engine based on the mouse UniProt database.

5.2.4. Statistical analysis

The MS peak list produced in Progenesis and searched in Mascot against the UniProt mouse database returned 2,426 protein hits. Statistical analysis for the proteomics data was performed by one-way ANOVA using a built-in tool within the Progenesis software. All identified proteins were short-listed based on statistical significance with a cut off p-value of 0.0125, which incorporates a Bonferroni correction to account for multiple comparisons (n=4).

5.2.5. Protein quantification and interaction analysis

The outcome of comparisons between treatment groups was represented by the total number of proteins showing significant changes, separated into those that were down-regulated or up-regulated, and was also expressed as the percentage of the total number of proteins identified (n=2,426). Relative protein quantitative analysis was carried out by listing all proteins with significant changes between treatment groups in the order of statistical significance, from lowest p-value to highest. The percentage change in relative abundance between the treatment groups was also shown. Heat maps were generated using PEAKS Studio 7.0 (Bioinformatics Solutions Inc., Canada). The raw MS/MS data were filtered to a retention time range of 0-270s for each sample and the cut-off value for statistical significance was $p<0.01$. Predicted protein-protein interactions were mapped for each of the three most significantly changed proteins between treatment groups using STRING version 9.1. The known or predicted functional partner(s) with the strongest evidence for association, indicated by the number of connectors in the network map, was selected for further scrutiny.

5.3. Results

5.3.1. Overall changes in protein expression between treatment groups

KA administration resulted in SE in all animals, which was followed by treatment with either PSD95BP, 1400W or vehicle alone. Interventions were applied after KA-induced seizures to ensure that they did not exert their effects by modulating the initial insult. In the 7 days between KA-induced SE and harvesting of tissue, there were no obvious signs of seizure activity in any of the animals and no notable behavioural sequelae of the interventions. The overall effects of KA-administration, and/or treatment with PSD95BP or 1400W, on protein expression in the hippocampus are outlined in Table 5.1.

The administration of KA resulted in a significant change in the expression of 30 proteins (1.2% of total; 27 up-regulated, 3 down-regulated) in the hippocampus 7 days thereafter when compared to animals that had initially received vehicle alone. Treatment with either PSD95BP or 1400W alone was associated with modest numbers of affected proteins; the expression of 16 proteins (0.7% of total; 6 up-regulated, 10 down-regulated) was altered by PSD95BP administration and just 8 proteins (0.3% of total; 6 up-regulated, 2 down-regulated) were altered by 1400W. Animals that received KA followed by PSD95BP showed 38 affected proteins (1.6% of total; 26 up-regulated, 12 down-regulated) when compared to those that received PSD95BP alone, while those that were treated with KA plus 1400W showed a difference in expression of 41 proteins (1.7% of total; 22 up-regulated, 19 down-regulated) in the hippocampus compared to mice that received 1400W alone. Finally, animals that received KA followed by PSD95BP showed 31 affected proteins (1.3% of total; 12 up-regulated, 19 down-regulated) when compared to those that received KA alone. In contrast, animals that were treated with KA plus 1400W showed a difference in expression of 36 proteins (1.5% of total; 21 up-regulated, 15 down-regulated) in the hippocampus compared to mice that received KA alone.

5.3.2. Relative quantitative analysis

Proteins whose expression patterns were significantly changed in the treatment group comparisons described above were sorted by p-value and are listed in Tables 5.2-5.8. The three proteins with lowest p-values in each of the comparisons were shortlisted for further investigation of their protein-protein interactions mapping, as reported in section 5.3.4.

Treatment group comparisons	Up-regulated (n)	Down-regulated (n)	Total significant	% significant of all proteins identified
Vehicle alone vs KA alone	27	3	30	1.2%
Vehicle alone vs PSD95BP alone	6	10	16	0.7%
Vehicle alone vs 1400W alone	6	2	8	0.3%
PSD95BP alone vs KA+PSD95BP	26	12	38	1.6%
1400W alone vs KA+1400W	22	19	41	1.7%
KA alone vs KA+PSD95BP	12	19	31	1.3%
KA alone vs KA+1400W	21	15	36	1.5%

Table 5.1. The number of proteins significantly altered in the hippocampus of C57BL/6J mice at 7 days after kainic acid (KA) administration followed by treatment with either PSD95BP, 1400W or vehicle alone (n=4 per group). Results are expressed as the number of proteins up-regulated, the number down-regulated, the total number of proteins changed, and also as percentage of the total protein identified (n=2,426). Statistical significance ($p<0.05$) was determined by one-way Analysis of Variance with Bonferroni correction for multiple comparisons.

The effect of kainic acid alone

A total of 30 proteins showed significantly altered expression in the hippocampus between mice that received KA and those that received vehicle alone. P-values for those proteins ranged from 9.56×10^{-6} to 3.35×10^{-2} (Table 5.2).

The effect of drug interventions alone

A total of 16 proteins showed significantly altered expression in the hippocampus when comparing mice that received PSD95BP and those that received vehicle alone. P-values for those proteins ranged from 3.31×10^{-3} to 3.99×10^{-2} (Table 5.3). A total of 8 proteins showed significantly altered expression in the hippocampus when comparing mice that received 1400W and those that received vehicle alone. P-values for those proteins ranged from 5.0×10^{-3} to 3.34×10^{-2} (Table 5.4).

Rank	Protein	P-value	% change
1	Complement C1q subcomponent subunit B	9.56×10^{-6}	66%
2	Galectin-1	3.57×10^{-4}	93%
3	Moesin	5.08×10^{-4}	83%
4	CD44 antigen	1.72×10^{-3}	213%
5	Cystatin C	2.33×10^{-3}	30%
6	Glial Fibrillary Acidic Protein	2.37×10^{-3}	162%
7	Complement C1q subcomponent subunit C	3.47×10^{-3}	49%
8	Protein kinase C and casein kinase substrate in neurons 2, isoform CRA_a	3.68×10^{-3}	22%
9	Hspb1 protein	3.88×10^{-3}	177%
10	Vimentin	4.96×10^{-3}	150%
11	Protein-glutamine gamma-glutamyltransferase 2	7.20×10^{-3}	73%
12	Murinoglobulin-1	7.48×10^{-3}	-46%
13	Metallothionein-2	7.72×10^{-3}	87%
14	Complement C1q subcomponent subunit A	9.92×10^{-3}	109%
15	MCG142467	1.21×10^{-2}	61%
16	Cytosolic 10-formyltetrahydrofolate dehydrogenase	1.24×10^{-2}	24%
17	Translational activator of cytochrome c oxidase 1	1.32×10^{-2}	31%
18	MCG18019	1.36×10^{-2}	56%
19	Lysosomal membrane glycoprotein 1, isoform CRA_c	1.49×10^{-2}	38%
20	Rho-related GTP-binding protein RhoC	1.76×10^{-2}	21%
21	DNA topoisomerase 2-beta	2.01×10^{-2}	69%
22	Secretogranin-2	2.31×10^{-2}	53%
23	Heme oxygenase (Decycling) 2	2.46×10^{-2}	11%
24	Bleomycin hydrolase	2.57×10^{-2}	-18%
25	Annexin	2.62×10^{-2}	82%
26	Filamin, alpha	2.74×10^{-2}	71%
27	Calbindin	2.75×10^{-2}	-36%
28	Dehydrogenase/reductase SDR family member 1	2.82×10^{-2}	90%
29	Transgelin	3.02×10^{-2}	84%
30	Proenkephalin-A	3.35×10^{-2}	53%

Table 5.2. Proteins (n=30) whose expression was significantly changed in the hippocampus of C57BL/6J mice 7 days after kainic acid-induced seizures, when compared to hippocampi of mice that received vehicle (distilled water) alone (n=4 per group). Homogenised hippocampal tissues were analysed using liquid chromatography mass spectrometry, and proteins identified based on the peptide sequences detected and queried through Mascot. Results are ranked in the order of p-value (lowest to highest), with percentage change in expression indicated (a negative percentage change represents a down-regulation). Statistical significance ($p<0.05$) was determined by one-way Analysis of Variance with Bonferroni correction for multiple comparisons.

Rank	Protein	P-value	% change
1	Rho guanine nucleotide exchange factor 2	3.31×10^{-3}	-24%
2	Protein farnesyltransferase subunit beta	5.72×10^{-3}	-38%
3	DNA topoisomerase 2-beta	1.68×10^{-2}	72%
4	Adenosine kinase	1.75×10^{-2}	-10%
5	ADP-ribosylation factor guanine nucleotide-exchange factor 2 (Brefeldin A-inhibited)	1.78×10^{-2}	-16%
6	Filamin, alpha	2.26×10^{-2}	41%
7	Signal transducing adaptor molecule (SH3 domain and ITAM motif) 1	2.32×10^{-2}	-12%
8	Cacna2d1 protein	2.44×10^{-2}	-19%
9	Syntaxin-2	2.58×10^{-2}	30%
10	Microsomal glutathione S-transferase 3	2.80×10^{-2}	-30%
11	Ubiquitin-fold modifier-conjugating enzyme 1	2.93×10^{-2}	-25%
12	Huntingtin-associated protein 1	3.08×10^{-2}	192%
13	Calumenin, isoform CRA_a	3.09×10^{-2}	8%
14	Collagen, type IV, alpha 2	3.51×10^{-2}	21%
15	Cullin-4B	3.77×10^{-2}	-23%
16	Dihydropyrimidinase-related protein 3	3.99×10^{-2}	-19%

Table 5.3. Proteins (n=16) whose expression was significantly changed in the hippocampus of C57BL/6J mice 7 days after administration of vehicle (distilled water) followed by PSD95BP, when compared to hippocampi of mice that received distilled water alone (n=4 per group). Homogenised hippocampal tissues were analysed using liquid chromatography mass spectrometry, and proteins identified based on the peptide sequences detected and queried through Mascot. Results are ranked in the order of p-value (lowest to highest), with percentage change in expression indicated (a negative percentage change represents a down-regulation). Statistical significance ($p<0.05$) was determined by one-way Analysis of Variance with Bonferroni correction for multiple comparisons.

Rank	Protein	P-value	% change
1	3'-phosphoadenosine 5'-phosphosulphate synthase 1, isoform CRA_b	5.0×10^{-3}	18%
2	Protein kinase C and casein kinase substrate in neurons 2, isoform CRA_a	1.0×10^{-2}	12%
3	Glycine cleavage system H protein, mitochondrial	1.03×10^{-2}	16%
4	MCG1395	1.27×10^{-2}	-22%
5	2410002F23Rik protein	1.46×10^{-2}	184%
6	Dihydropyrimidinase-related protein 3	2.69×10^{-2}	-19%
7	Delta-1-pyrroline-5-carboxylate dehydrogenase, mitochondrial	2.79×10^{-2}	22%
8	Quinone oxidoreductase-like protein 2	3.34×10^{-2}	115%

Table 5.4. Proteins (n=8) whose expression was significantly changed in the hippocampus of C57BL/6J mice 7 days after administration of vehicle (distilled water) followed by 1400W, when compared to hippocampi of mice that received distilled water alone (n=4 per group). Homogenised hippocampal tissues were analysed using liquid chromatography mass spectrometry, and proteins identified based on the peptide sequences detected and queried through Mascot. Results are ranked in the order of p-value (lowest to highest), with percentage change in expression indicated (a negative percentage change represents a down-regulation). Statistical significance ($p<0.05$) was determined by one-way Analysis of Variance with Bonferroni correction for multiple comparisons.

The effect of kainic acid in drug treated mice

A total of 38 proteins showed significantly altered expression in the hippocampus when comparing mice that received KA plus PSD95BP and those that received PSD95BP alone. P-values for those proteins ranged from 1.65×10^{-4} to 3.91×10^{-2} (Table 5.5). A total of 41 proteins showed significantly altered expression in the hippocampus when comparing mice that received KA plus 1400W and those that received 1400W alone. P-values for those proteins ranged from 2.33×10^{-5} to 3.86×10^{-2} (Table 5.6).

The effect of drug interventions in kainic acid treated mice

A total of 31 proteins showed significantly altered expression in the hippocampus when comparing mice that received KA plus PSD95BP and those that received KA alone. P-values for those proteins ranged from 1.70×10^{-3} to 3.78×10^{-2} (Table 5.7). A total of 36 proteins showed significantly altered expression in the hippocampus when comparing mice that received KA plus 1400W and those that received KA alone. P-values for those proteins ranged from 1.94×10^{-5} to 3.88×10^{-2} (Table 5.8).

5.3.3. Heatmap visualisation

Protein quantification using heat map visualisation was based on the detected peak areas of the top three unique peptide ratios calculated from the raw MS/MS data. The peak area is illustrated in a spectrum from red to black to green. Average peak areas are shown in black, whilst smaller peak areas are shown in green and larger peak areas are shown in red. The gradation of the change in peak areas is indicated by the intensity of the green or red colour.

Rank	Protein	P-value	% change
1	Glutathione S-transferase Mu 5 (Fragment)	1.65×10^{-4}	-17%
2	Glutamine synthetase	9.64×10^{-4}	-16%
3	Vimentin	9.68×10^{-4}	100%
4	Angiotensin 1 converting enzyme (Peptidyl-dipeptidase(A) 1	2.02×10^{-3}	62%
5	Phospholemman	2.42×10^{-3}	31%
6	Reticulon-4 (RTN4)	2.83×10^{-3}	-25%
7	Nucleoside diphosphate kinase A	4.52×10^{-3}	14%
8	DEAH (Asp-Glu-Ala-His) box polypeptide 15, isoform CRA_a	4.68×10^{-3}	28%
9	Protein Spnb1 (Beta-I spectrin)	5.60×10^{-3}	-15%
10	Glial fibrillary acidic protein	8.80×10^{-3}	105%
11	Delta-1-pyrroline-5-carboxylate dehydrogenase, mitochondrial	9.72×10^{-3}	27%
12	Rbp1 protein	1.34×10^{-2}	37%
13	Heat shock 70kD protein 5 (Glucose-regulated protein)	1.35×10^{-2}	14%
14	Sodium- and chloride-dependent GABA transporter 1	1.43×10^{-2}	-12%
15	Gamma-aminobutyric acid receptor subunit beta-1	1.55×10^{-2}	-21%
16	Keratin, type II cytoskeletal 5	1.76×10^{-2}	-66%
17	Dehydrogenase/reductase SDR family member 1	2.41×10^{-2}	43%
18	Podoplanin	2.47×10^{-2}	77%
19	Calponin-3	2.50×10^{-2}	53%
20	Heat shock protein HSP 90-beta	2.54×10^{-2}	14%
21	Barrier-to-autointegration factor	2.54×10^{-2}	16%
22	S100 calcium binding protein A13	2.58×10^{-2}	29%
23	CaM kinase-like vesicle-associated protein	2.61×10^{-2}	-12.43
24	Eukaryotic translation initiation factor 2, subunit 3, structural gene X-linked	2.74×10^{-2}	10%
25	Peripheral plasma membrane protein CASK	2.76×10^{-2}	-10%
26	Ribonuclease inhibitor	2.81×10^{-2}	28%
27	S100 protein, beta polypeptide, neural, isoform CRA_b	2.83×10^{-2}	36%
28	Uncharacterised protein (Fragment) F6QH50	2.85×10^{-2}	-20%
29	Complement C1q subcomponent subunit B	2.86×10^{-2}	38%
30	Moesin	2.87×10^{-2}	52%
31	Uncharacterised protein (Fragment) F8WHU8	2.87×10^{-2}	17%
32	Probable cationic amino acid transporter	3.00×10^{-2}	11%
33	Hspb1 protein	3.16×10^{-2}	140%
34	Short coiled-coil protein	3.36×10^{-2}	40%
35	Small nuclear ribonucleoprotein Sm D3	3.38×10^{-2}	7%
36	NADH dehydrogenase [ubiquinone] 1 beta subcomplex subunit 7	3.70×10^{-2}	-7%
37	Clusterin	3.76×10^{-2}	40%
38	Potassium inwardly-rectifying channel J3	3.91×10^{-2}	-16%

Table 5.5. Proteins (n=38) whose expression was significantly changed in the hippocampus of C57BL/6J mice 7 days after administration of kainic acid followed by PSD95BP, when compared to hippocampi of mice that received PSD95BP alone (n=4 per group). Homogenised hippocampal tissues were analysed using liquid chromatography mass spectrometry, and proteins identified based on the peptide sequences detected and queried through Mascot. Results are ranked in the order of p-value (lowest to highest), with percentage change in expression indicated (a negative percentage change represents a down-regulation). Statistical significance ($p<0.05$) was determined by one-way Analysis of Variance with Bonferroni correction for multiple comparisons.

Rank	Protein	P-value	% change
1	Cystatin C	2.33×10^{-5}	28%
2	Moesin	1.82×10^{-3}	91%
3	Rbp1 protein	1.98×10^{-3}	41%
4	Glutamine synthetase	2.04×10^{-3}	-15%
5	BolA-like protein 1	2.13×10^{-3}	-18%
6	Corticosteroid 11-beta-dehydrogenase isozyme 1 (Fragment)	2.51×10^{-3}	-66%
7	Glial fibrillary acidic protein	2.70×10^{-3}	116%
8	Complement C1q subcomponent subunit C	4.68×10^{-3}	46%
9	Peroxisomal acyl-coenzyme A oxidase 1	4.76×10^{-3}	66%
10	Complement C1q subcomponent subunit B	5.08×10^{-3}	42%
11	NADH dehydrogenase [ubiquinone] flavoprotein 1, mitochondrial	5.52×10^{-3}	10%
12	Cytosolic 10-formyltetrahydrofolate dehydrogenase	6.20×10^{-3}	26%
13	Alanine aminotransferase 1	6.88×10^{-3}	-32%
14	Uncharacterised protein putative	8.44×10^{-3}	-16%
15	Heterogeneous nuclear ribonucleoprotein A1	8.76×10^{-3}	17%
16	Glycoprotein m6a, isoform CRA_b	9.52×10^{-3}	-13%
17	Vimentin	1.02×10^{-2}	114%
18	Peroxisomal multifunctional enzyme type 2	1.06×10^{-2}	20%
19	Galectin-1	1.16×10^{-2}	77%
20	Phytanoyl-CoA hydroxylase-interacting protein	1.24×10^{-2}	-17%
21	CD44 antigen	1.28×10^{-2}	211%
22	Ras-related protein Rab-8B	1.30×10^{-2}	-15%
23	Uncharacterised protein E9PWP6	1.50×10^{-2}	-212%
24	Ribosomal protein	1.56×10^{-2}	6%
25	Acetyl-CoA acetyltransferase, cytosolic	1.71×10^{-2}	30%
26	UPF0160 protein MYG1, mitochondrial (Fragment)	1.77×10^{-2}	173%
27	CaM kinase-like vesicle-associated protein	1.93×10^{-2}	-17%
28	Calmodulin	1.95×10^{-2}	-9%
29	Uncharacterised -protein Yjefn3 (Fragment)	2.16×10^{-2}	-51%
30	Microtubule-associated serine/threonine-protein kinase 3	2.18×10^{-2}	-13%
31	Catalase	2.24×10^{-2}	24%
32	Cannabinoid receptor 1 (Brain)	2.30×10^{-2}	-30%
33	S100 calcium binding protein A13	2.34×10^{-2}	19%
34	Dgkh protein	2.35×10^{-2}	-32%
35	Alpha globin 1	2.76×10^{-2}	33%
36	G protein-regulated inducer of neurite outgrowth 1	3.17×10^{-2}	-11%
37	Acidic leucine-rich nuclear phosphoprotein 32 family member B	3.51×10^{-2}	47%
38	RTN4	3.59×10^{-2}	-27%
39	Tial1 cytotoxic granule-associated RNA binding protein-like 1, isoform CRA_c	3.60×10^{-2}	13%
40	Neuroligin-2	3.64×10^{-2}	-22%
41	Kalirin	3.86×10^{-2}	-44%

Table 5.6. Proteins (n=41) whose expression was significantly changed in the hippocampus of C57BL/6J mice 7 days after administration of kainic acid followed by 1400W, when compared to hippocampi of mice that received 1400W alone (n=4 per group). Homogenised hippocampal tissues were analysed using liquid chromatography mass spectrometry, and proteins identified based on the peptide sequences detected and queried through Mascot. Results are ranked in the order of p-value (lowest to highest), with percentage change in expression indicated (a negative percentage change represents a down-regulation). Statistical significance ($p<0.05$) was determined by one-way Analysis of Variance with Bonferroni correction for multiple comparisons.

Rank	Protein	P-value	% change
1	Phosphatidate cytidylyltransferase 1	1.70×10^{-3}	-38%
2	Gene model 1604B, (NCBI)	2.66×10^{-3}	235%
3	Basigin	3.73×10^{-3}	-18%
4	Angiotensin 1 converting enzyme (Peptidyl-dipeptidase(A) 1	4.36×10^{-3}	146%
5	Putative ATP-dependent Clp protease proteolytic subunit, mitochondrial	4.88×10^{-3}	17%
6	Glycylpeptide N-tetradecanoyltransferase	7.12×10^{-3}	-15%
7	Synaptic vesicle membrane protein VAT-1 homolog-like	8.32×10^{-3}	94%
8	Nitric oxide synthase, brain	8.92×10^{-3}	43%
9	Potassium inwardly-rectifying channel J3	9.76×10^{-3}	-22%
10	Mammalian ependymin-related protein 1	1.42×10^{-2}	22%
11	Proline-rich AKT1 substrate 1 (Fragment)	1.49×10^{-2}	-18%
12	Sideroflexin-5	1.50×10^{-2}	-12%
13	CAP-Gly domain-containing linker protein 2	1.56×10^{-2}	-47%
14	Ataxin-2-like protein	1.64×10^{-2}	-37%
15	Proprotein convertase subtilisin/kexin type 1 inhibitor	1.64×10^{-2}	44%
16	Alpha-adducin	1.68×10^{-2}	-24%
17	Protein kinase C beta type	1.80×10^{-2}	-17%
18	Calbindin-28K	1.84×10^{-2}	52%
19	Integral membrane protein 2B	2.07×10^{-2}	-21%
20	Acyl-CoA thioesterase 11	2.10×10^{-2}	-26%
21	Small nuclear ribonucleoprotein-associated protein	2.30×10^{-2}	-19%
22	BTB/POZ domain-containing protein 17	2.62×10^{-2}	-18%
23	Putative uncharacterised protein	2.63×10^{-2}	-20%
24	Somatostatin	2.66×10^{-2}	72%
25	Protein Dos	2.67×10^{-2}	50%
26	Cytochrome b-c1 complex subunit 10	2.96×10^{-2}	-17%
27	Neural visinin-like type 1 protein	3.00×10^{-2}	-12%
28	Long-chain-fatty-acid--CoA ligase 3	3.08×10^{-2}	-13%
29	Copine-2	3.28×10^{-2}	119%
30	Plasma membrane calcium-transporting ATPase 2	3.59×10^{-2}	-14%
31	Nuclear protein localisation protein 4 homolog	3.78×10^{-2}	38%

Table 5.7. Proteins (n=31) whose expression was significantly changed in the hippocampus of C57BL/6J mice 7 days after administration of kainic acid followed by PSD95BP, when compared to hippocampi of mice that received KA alone (n=4 per group). Homogenised hippocampal tissues were analysed using liquid chromatography mass spectrometry, and proteins identified based on the peptide sequences detected and queried through Mascot. Results are ranked in the order of p-value (lowest to highest), with percentage change in expression indicated (a negative percentage change represents a down-regulation). Statistical significance ($p<0.05$) was determined by one-way Analysis of Variance with Bonferroni correction for multiple comparisons.

Rank	Protein	P-value	% change
1	Src substrate cortactin	1.94×10^{-5}	-12%
2	Sideroflexin-1	2.33×10^{-3}	15%
3	Acid ceramidase	2.99×10^{-3}	63%
4	Ataxin-10	5.20×10^{-3}	39%
5	Basigin	6.32×10^{-3}	-17%
6	CAP-Gly domain containing linker protein 2	6.60×10^{-3}	-47%
7	Albumin 1	6.68×10^{-3}	69%
8	Prosaposin, isoform CRA_e	7.72×10^{-3}	79%
9	Ferritin heavy chain	9.40×10^{-3}	17%
10	G protein-regulated inducer of neurite outgrowth 1	1.26×10^{-2}	-14%
11	Myosin-11	1.35×10^{-2}	85%
12	Tubulointerstitial nephritis antigen-like 1	1.39×10^{-2}	29%
13	Quinone oxidoreductase-like protein 2	1.46×10^{-2}	90%
14	Protein kinase, cAMP dependent regulatory, type II alpha	1.49×10^{-2}	16%
15	MCG5603	1.72×10^{-2}	-31%
16	Protein Gm8994	1.72×10^{-2}	33%
17	Peroxisomal acyl-coenzyme A oxidase 1	1.82×10^{-2}	24%
18	Uncharacterised protein (putative)	1.96×10^{-2}	-21%
19	Protein SOGA3	1.98×10^{-2}	-11%
20	D-dopachrome tautomerase	1.99×10^{-2}	-33%
21	Signal peptidase complex subunit 2	2.06×10^{-2}	-30%
22	NADH-ubiquinone oxidoreductase chain 1	2.18×10^{-2}	33%
23	Acetyl-CoA acetyltransferase, cytosolic	2.33×10^{-2}	29%
24	Glutamate [NMDA] receptor subunit epsilon-1	2.56×10^{-2}	-23$%
25	Integral membrane protein 2B	2.59×10^{-2}	-13%
26	Folh1 protein	2.70×10^{-2}	23%
27	Echinoderm microtubule-associated protein-like 2	2.81×10^{-2}	36%
28	MCG5232	3.00×10^{-2}	83%
29	Immunity-related GTPase family Q protein	3.14×10^{-2}	-27%
30	Presequence protease, mitochondrial	3.14×10^{-2}	18%
31	Synaptic vesicle membrane protein VAT-1 homolog-like	3.21×10^{-2}	95%
32	Metallothionein	3.29×10^{-2}	-16%
33	Phospholipase D3	3.36×10^{-2}	-18%
34	Small ubiquitin-related modifier 2	3.44×10^{-2}	-14%
35	Alpha globin 1	3.72×10^{-2}	63%
36	Protein Pzp	3.88×10^{-2}	123%

Table 5.8. Proteins (n=36) whose expression was significantly changed in the hippocampus of C57BL/6J mice 7 days after administration of kainic acid followed by 1400W, when compared to hippocampi of mice that received KA alone (n=4 per group). Homogenised hippocampal tissues were analysed using liquid chromatography mass spectrometry, and proteins identified based on the peptide sequences detected and queried through Mascot. Results are ranked in the order of p-value (lowest to highest), with percentage change in expression indicated (a negative percentage change represents a down-regulation). Statistical significance ($p<0.05$) was determined by one-way Analysis of Variance with Bonferroni correction for multiple comparisons.

In the PSD95BP analysis, a total of 20 proteins were shortlisted using heat map visualisation. The peak areas of the majority of these proteins were increased following KA-induced seizures, whereas those that received vehicle rather than KA had peak areas that were typically lower than average (Figure 5.1). Administration of PSD95BP led to an increase in peak area for a number of proteins, in comparison to controls that received vehicle alone (Figure 5.1). When PSD95BP was given to animals that had previously experienced KA-induced seizures, the increase in peak areas was compounded and was consistent with an additive effect of the two compounds given alone (Figure 5.1).

In the 1400W analysis, a total of 22 proteins were shortlisted using heat map visualisation. As in the PSD95BP analysis, KA administration increased peak areas of the majority of proteins, while the corresponding vehicle treatment had the opposite effect (Figure 5.2). Likewise, treatment with 1400W increased the peak areas of several proteins when compared to vehicle-only controls and had an additive effective, in terms of numbers of proteins with increased peak area, when given to animals that had previously received KA (Figure 5.2).

5.3.4. Protein-protein interactions mapping

The first 3 proteins with the most significant changes between treatment groups, based on the relative quantitative analysis shown in section 5.3.2, were used for the protein-protein interactions mapping.

The effect of kainic acid alone

The three proteins with the lowest p-values in the analysis of hippocampal proteomes between KA and corresponding vehicle-treated animals were complement C1q subcomponent subunit B, galectin-1 and moesin (Table 5.2). Complement component 1 q subcomponent β subunit largely interacts with other complement component 1 subcomponents (Figure 5.3A). Galectin-1 has greatest interaction with neuroblastoma ras oncogene compared to the other functional partners (Figure 5.3B). Moesin has the greatest interaction with rho-associated coiled-coil containing protein kinase 2 compared to the other functional partners (Figure 5.3C).

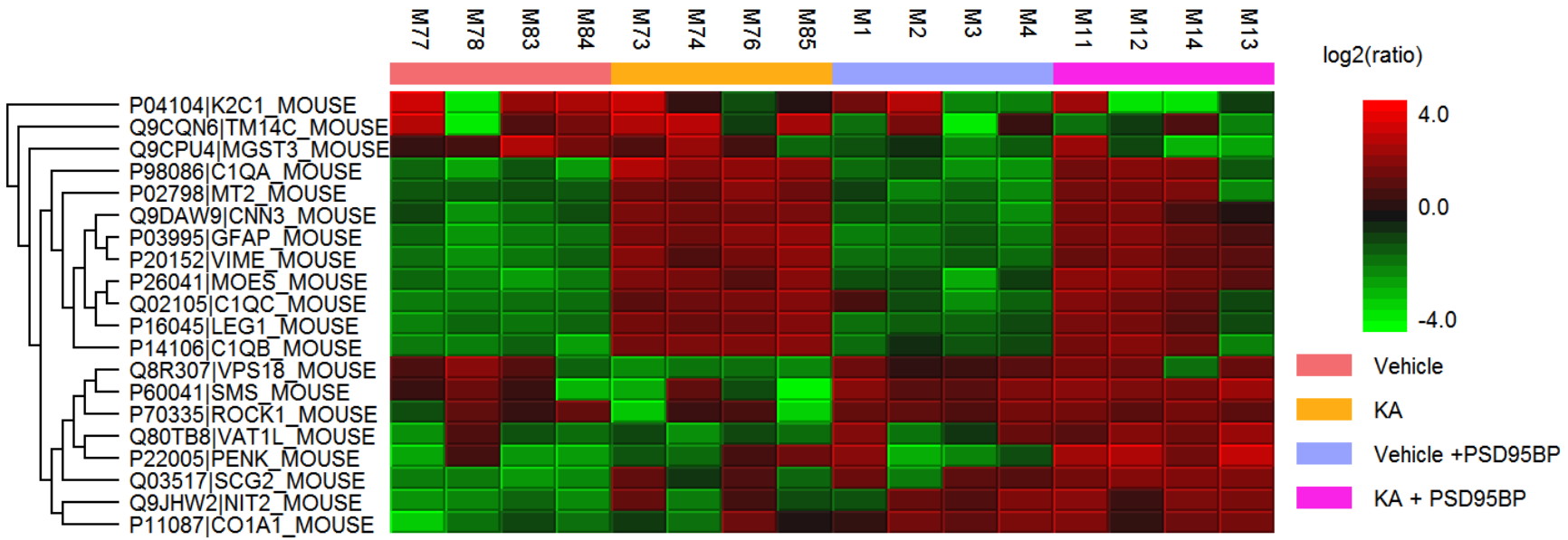

Figure 5.1. A heat map display comparing the difference in protein quantification between the hippocampi of vehicle and kainic acid (KA)-treated C57BL/6J mice at 7 days, with or without the subsequent administration of post-synaptic density 95 blocking peptide (PSD95BP) (n=4). Homogenised hippocampal tissues were analysed using liquid chromatography mass spectrometry and protein quantification was based on the detected peak areas of the top-3 unique peptide ratios calculated from raw tandem mass spectrometry data. The horizontal axis shows the sample names per treatment group (vehicle samples: M77, M78, M83 and M84; KA samples: M73, M74, M76 and M85; vehicle + PSD95BP samples: M1, M2, M3 and M4; KA + PSD95BP samples: M11, M12, M14 and M13). The vertical axis shows the peaks of the protein with unique peptides identified. The raw data were filtered to a retention time range of 0-270s for each sample and the cut-off value for the peptide feature statistical significance was $p<0.01$. Average peak areas are shown in black, peak areas lower than the average are shown in green and those larger than average are shown in red.

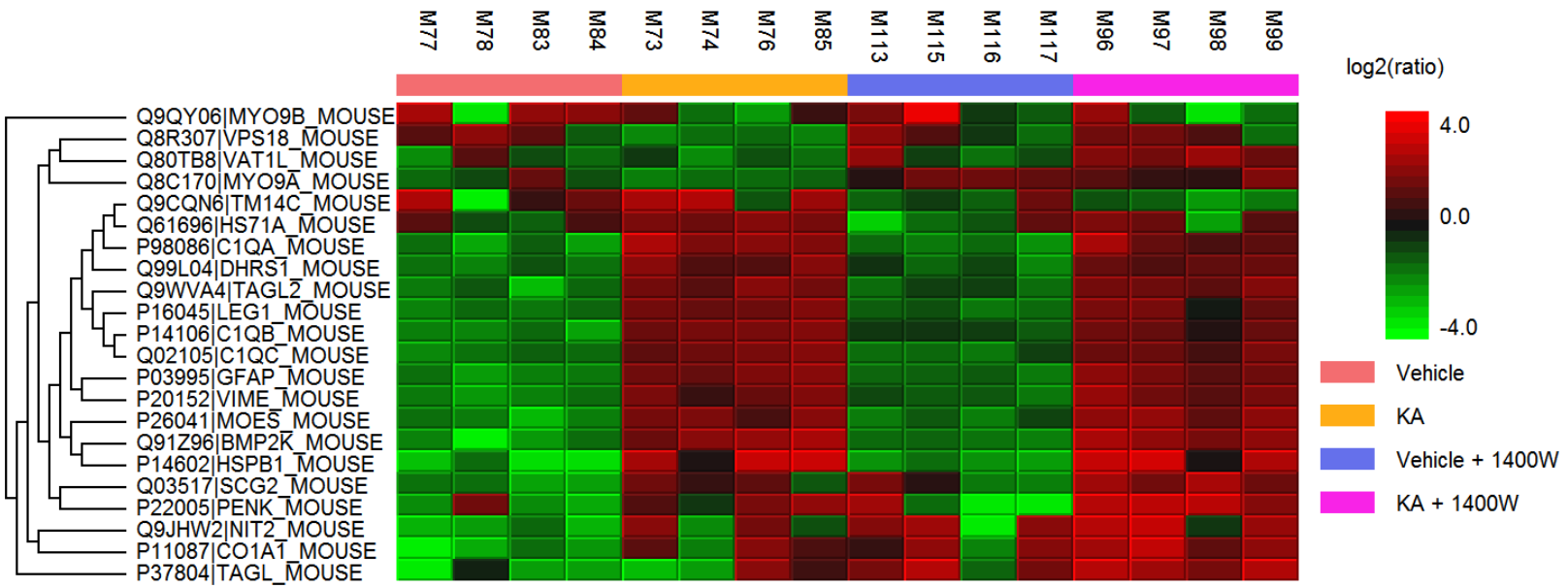

Figure 5.2. A heat map display comparing the difference in protein quantification between the hippocampi of vehicle and kainic acid (KA)-treated C57BL/6J mice at 7 days, with or without the subsequent administration of 1400W (n=4). Homogenised hippocampal tissues were analysed using liquid chromatography mass spectrometry and protein quantification was based on the detected peak areas of the top-3 unique peptide ratios calculated from raw tandem mass spectrometry data. The horizontal axis shows the sample names per treatment group (vehicle samples: M77, M78, M83 and M84; KA samples: M73, M74, M76 and M85; vehicle + 1400W samples: M113, M115, M116 and M117; KA + 1400W samples: M96, M97, M98 and M99). The vertical axis shows the peaks of the protein with unique peptides identified. The raw data were filtered to a retention time range of 0-270s for each sample and the cut-off value for the peptide feature statistical significance was $p<0.01$. Average peak areas are shown in black, peak areas lower than the average are shown in green and those larger than average are shown in red.

The effect of PSD95BP alone

The three most significantly changed proteins in the analysis of hippocampal proteomes between PSD95BP and corresponding vehicle-treated animals were Ras homologous (Rho) guanine nucleotide exchange factor 2, protein farnesyltransferase subunit β and DNA topoisomerase 2-β (Table 5.3). Rho guanine nucleotide exchange factor 2 has more evident interactions with RAS-related C3 botulinum substrate 1, Rho gene family member B and cell division cycle 42 homolog compared to the other functional partners (Figure 5.4A). Protein farnestyltransferase subunit B has the greatest interaction with protein farnestyltransferase subunit A (Figure 5.4B). DNA topoisomerase II β and all its functional partners, except for DNA topoisomerase II α, interact closely with one another (Figure 5.4C). The functional partners for DNA topoisomerase II β include bromodomain adjacent to zinc finger 1B, SWI/SNF related, matrix associated, actin dependent regulator of chromatin, subfamily c, member 1; subfamily a, member 2; subfamily d, member 3; subfamily a, member 4, AT rich interactive domain 1A; 1B, actin-like 6A, PHD finger protein 10 (Figure 5.4C).

The effect of 1400W alone

The three proteins with the lowest p-values in the analysis of hippocampal proteomes between 1400W and corresponding vehicle-treated animals were 3'-phosphoadenosine 5'-phosphosulphate synthase 1, protein kinase C/casein kinase substrate in neurons 2 and glycine cleavage system H protein (Table 5.4). 3'-phosphoadenosine 5'-phosphosulphate synthase 1 has the greatest interaction with 3'-phosphoadenosine 5'-phosphosulphate synthase 2 (Figure 5.5A). Protein kinase C and casein kinase substrate in neurons 2 has the most evident interactions with 3'-phosphoadenosine 5'-phosphosulphate synthase 1 and dynamin 2 (Figure 5.5B). Glycine cleavage system protein H interacts mostly with glycine decarboxylase, aminomethyltransferase, serine hydroxymethyltransferase 1, sarcosine dehydrogenase and dimethylglycine dehydrogenase (Figure 5.5C).

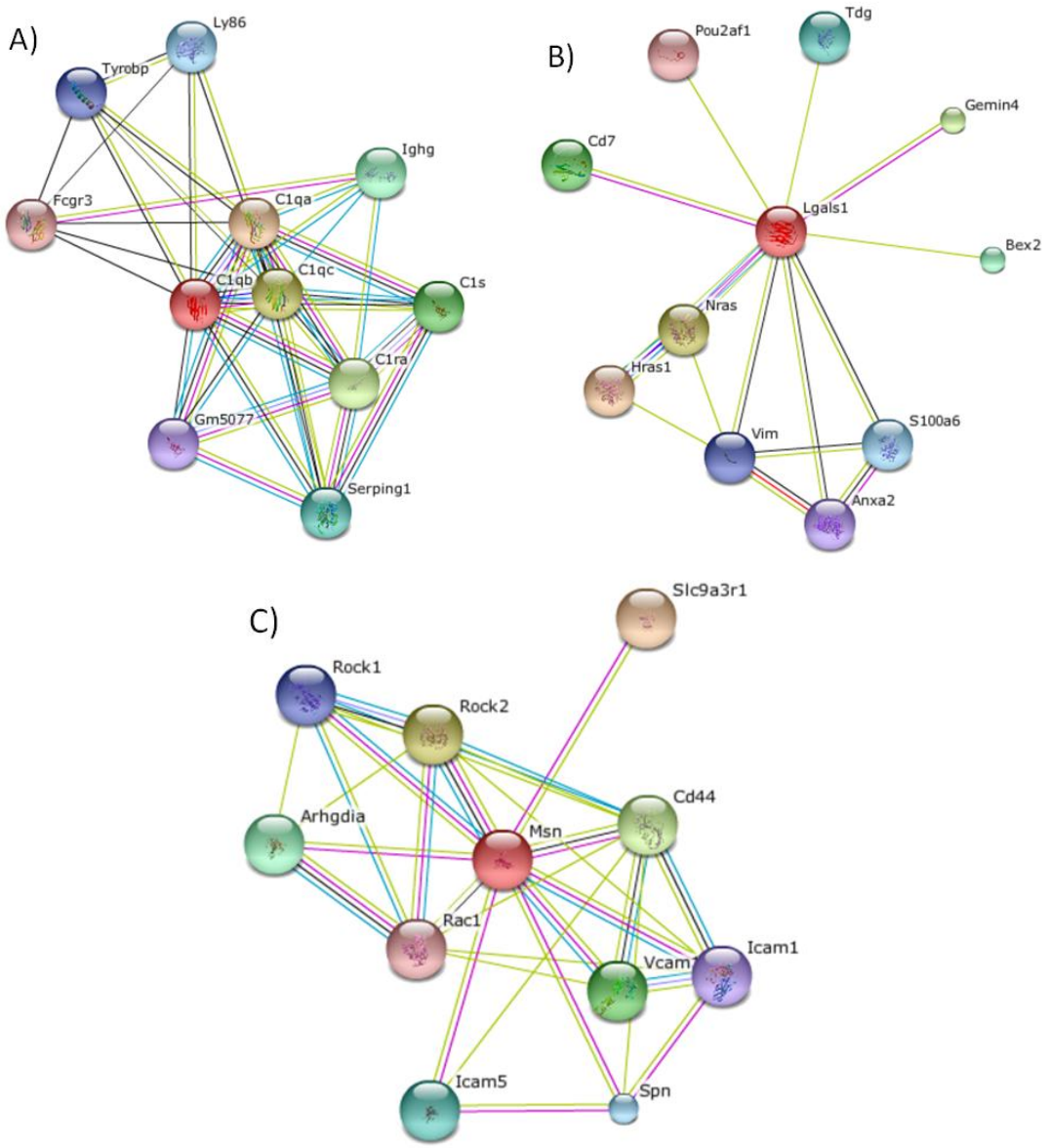

Figure 5.3. Network representations of the top 3 most significantly affected proteins in the hippocampus of C57BL/6J mice following administration of kainic acid or corresponding vehicle, with known or predicted protein interactions with other functional partners plotted by Search Tool for the Retrieval of Interacting Genes/Proteins (STRING). In this view, the number of different coloured lines represents the number of different types of evidence for the association.(A) Complement component 1 q subcomponent, beta subunit (C1qb) with functional partners including complement component 1, q subcomponent, α polypeptide (C1qa); C chain (C1qc); r subcomponent A (C1ra); s subcomponent (C1s), immunoglobulin heavy chain, γ polypeptide (Ighg), serine (or cysteine) peptidase inhibitor, clade G, member 1 (Serping1), lymphocyte antigen 86 (Ly86), TYRO protein tyrosine kinase binding protein (Tyrobp); predicted gene 5077 (Gm5077) and Fc receptor, IgG, low affinity III (Fcgr3). (B) Galectin-1 (Lgals1) with functional partners including Harvey rat sarcoma virus oncogene 1 (Hras1), neuroblastoma ras oncogene (Nras), gem (nuclear organelle) associated protein 4 (Gemin4), CD7 antigen (Cd7), brain expressed X-linked 2 (Bex2), thymine DNA glycosylase (Tdg), S100 calcium binding protein A6 (calcyclin) (S100a6), vimentin (Vim), annexin A2 (Anxa2) and POU domain, class 2, associating factor 1 (Pou2af1). (C) Moesin (Msn) with functional partners including solute carrier 9 (sodium/hydrogen exchanger), member 3 regulator 1 (Slc9a3r1), Rho-associated coiled-coil containing protein kinase 2 (Rock2), CD44 antigen (Cd44), vascular cell adhesion molecule 1 (Vcam1), Rho GDP dissociation inhibitor (GDI) alpha (Arhgdia), intercellular adhesion molecule 5 (Icam5), sialophorin (Spn), Rho-associated coiled-coil containing protein kinase 1 (Rock1), intercellular adhesion molecule 1 (Icam1) and RAS-related C3 botulinum substrate 1 (Rac1).

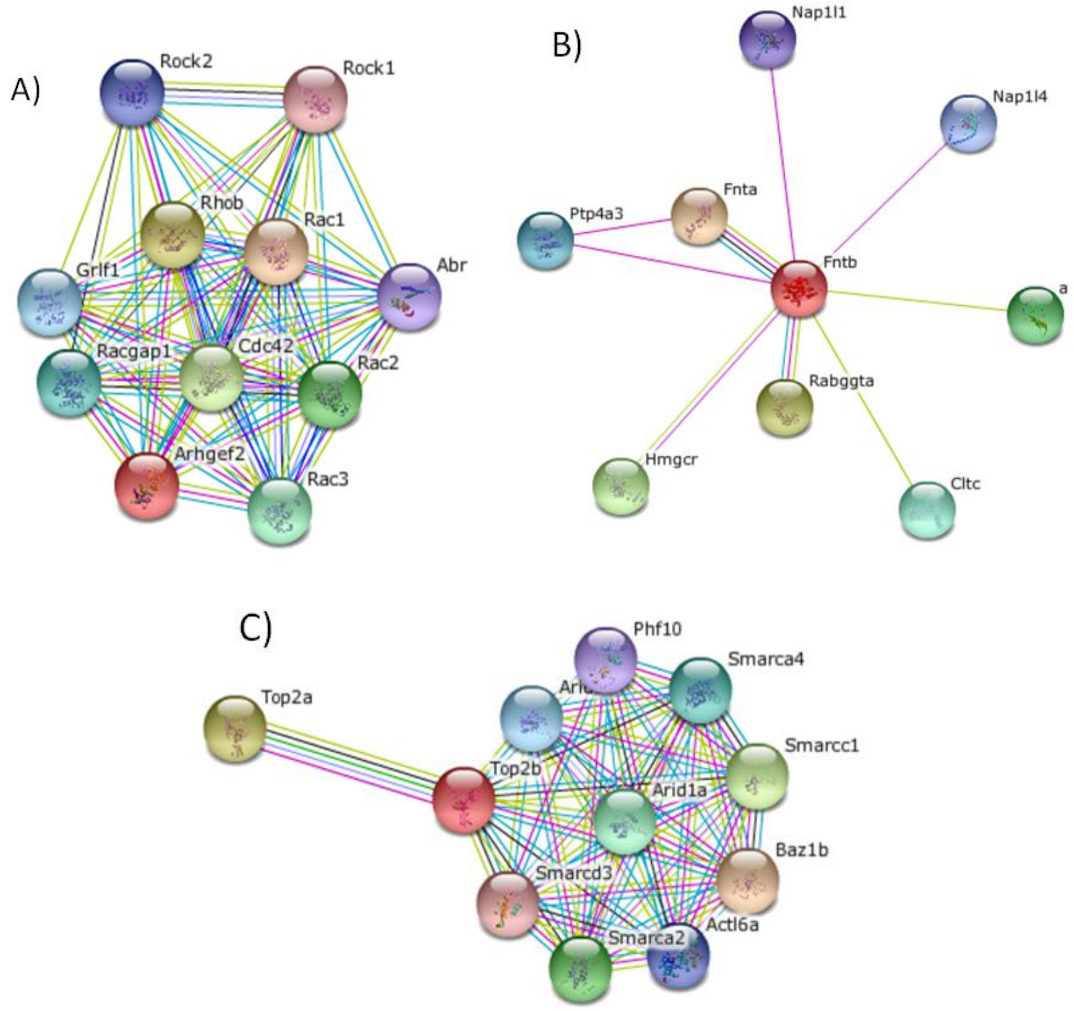

Figure 5.4. Network representations of the top 3 most significantly affected proteins in the hippocampus of C57BL/6J mice following the administration of post-synaptic density 95 blocking peptide or corresponding vehicle, with known or predicted protein interactions with other functional partners plotted by Search Tool for the Retrieval of Interacting Genes/Proteins (STRING). In this view, the number of different coloured lines represents the number of different types of evidence for the association.(A) Rho guanine nucleotide exchange factor 2 (Arhgef2) with functional partners: RAS-related C3 botulinum substrate 1 (Rac1); 2 (Rac2); 3 (Rac3), ras homolog, member B (Rhob), cell division cycle 42 (Cdc42), Rac GTPase-activating protein 1 (Racgap1), glucocorticoid receptor DNA binding factor 1 (Grlf1), Rho-associated coiled-coil containing protein kinase 2 (Rock2); 1 (Rock1), active BCR-related gene (Abr). (B) Protein farnesyltransferase subunit beta (Fntb) with functional partners: protein farnesyltransferase subunit a (Fnta), Rab geranylgeranyl transferase a subunit (Rabggta), 3-hydroxy-3-methylglutaryl-Coenzyme A reductase (Hmgcr), nonagouti (a), clathrin (Cltc), protein tyrosine phosphatase 4a3 (Ptp4a3), nucleosome assembly protein 1-like 4 (Nap1l4); 1 (Nap1l1). (C) DNA topoisomerase II beta (Top2b) with functional partners: bromodomain adjacent to zinc finger 1B (Baz1b), topoisomerase (DNA) II alpha (Top2a), SWI/SNF related, matrix associated, actin dependent regulator of chromatin, subfamily c, member 1 (Smarcc1); subfamily a, member 2 (Smarca2); subfamily d, member 3 (Smarcd3); subfamily a, member 4 (Smarca4), AT rich interactive domain 1A (Arid1a); 1B (Arid1b), actin-like 6A (Actl6a), PHD finger protein 10 (Phf10).

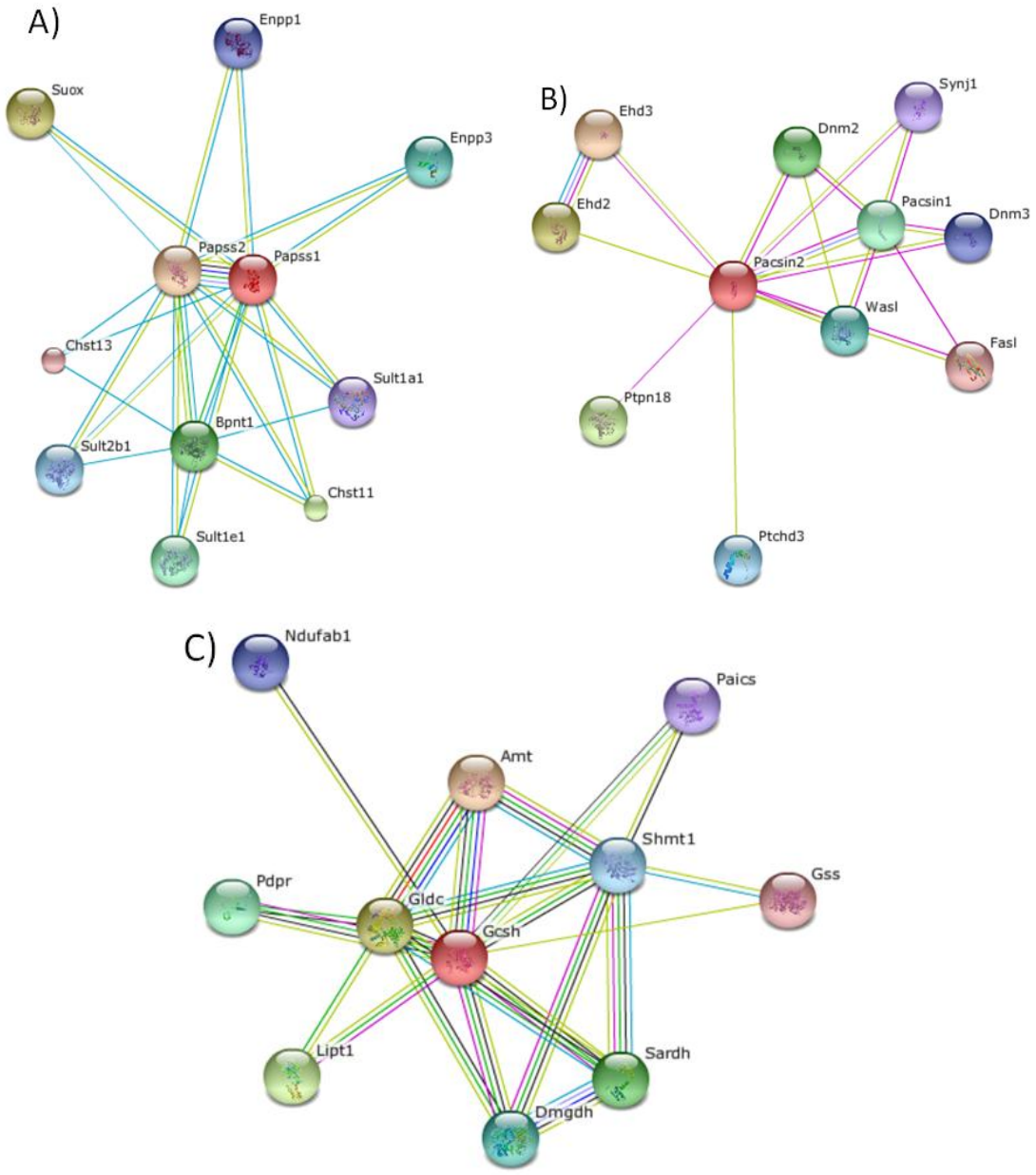

Figure 5.5. Network representations of the top 3 most significantly affected proteins in the hippocampus of C57BL/6J mice following the administration of 1400W or corresponding vehicle, with known or predicted protein interactions with other functional partners plotted by Search Tool for the Retrieval of Interacting Genes/Proteins (STRING). In this view, the number of different coloured lines represents the number of different types of evidence for the association.(A) 3'-phosphoadenosine 5'-phosphosulphate synthase 1 (Papss1) with functional partners: 3'-phosphoadenosine 5'-phosphosulphate synthase 2 (Papss2), Sulfite oxidase (Suox), carbohydrate sulfotransferase 11 (Chst11); 13 (Chst13), biphosphate 3'-nucleotidase 1 (Bpnt1), sulfotransferase family 1E member 1 (Sult1e1); 2B member 1 (Sult2b1); 1A member 1 (Sult1a1), ectonucleotide pyrophosphatase/phosphodiesterase 1 (Enpp1); 3 (Enpp3).(B) protein kinase C and casein kinase substrate in neurons 2 (Pacsin2) with functional partners: EH-domain containing 2 (Ehd2); 3 (Ehd3), protein tyrosine phosphatase non-receptor type 18 (Ptpn18), dynamin 2 (Dnm2); 3 (Dnm3), protein kinase C and casein kinase substrate in neurons 1 (Pacsin1), Wiskott-Aldrich syndrome-like (Wasl), patched domain containing 3 (Ptchd3), synaptojanin 1 (Synj1), Fas ligand (TNF family, member 6) (Fasl).(C) Glycine cleavage system protein H (Gcsh) with functional partners: aminomethyltransferase (Amt), glycine decarboxylase (Gldc), lipoyltransferase 1 (Lipt1), sarcosine dehydrogenase (Sardh), RIKEN cDNA (Pdpr), dimethylglycine dehydrogenase (Dmgdh), serine hydroxymethyltransferase 1 (Shmt1), NADH dehydrogenase 1 alpha/beta subcomplex 1 (Ndufab1), phosphoribosyl-aminoimidazole carboxylase, phosphoribosylaminoribosyl-aminoimidazole, succinocarboxamide synthetase (Paics), glutathione synthetase (Gss).

The effect of kainic acid in PSD95BP-treated mice

The three most significantly changed proteins in the analysis of hippocampal proteomes between PSD95BP-treated animals that had previously received KA or its corresponding vehicle were glutathione S-transferase, glutamine synthetase and vimentin (Table 5.5). Glutathione S-transferase mu 5 largely interacts with other glutathione S-transferase isoforms (Figure 5.6A). Glutamine synthetase has more interactions with glutaminase and glutaminase 2 than other functional partners (Figure 5.6B). Vimentin has the most evident interactions with caspase 6 and 8 (Figure 5.6C).

The effect of kainic acid in 1400W-treated mice

The three proteins with the lowest p-values in the analysis of hippocampal proteomes between 1400W-treated animals that had previously received KA or its corresponding vehicle were cystatin C, moesin and retinol binding protein 1 (rbp1) protein (Table 5.6). Cystatin C interacts closely with all its functional partners and each partner interacts with one another (Figure 5.7A). The functional partners for cystatin C include transthyretin, integral membrane protein 2B, amyloid β (A4) precursor protein, gelsolin, β-2 microglobulin, apolipoprotein A-I, calcitonin/calcitonin-related polypeptide α, milk fat globule-EGF factor 8 protein, lactotransferrin, prolactin (Figure 5.7A). Moesin has the greatest interaction with rho-associated coiled-coil containing protein kinase 2 compared to the other functional partners (Figure 5.7B). Rbp1 has more interactions with lecithin-retinol acyltransferase, EIA binding protein p300 and retinoic acid receptor α than other functional partners (Figure 5.7C).

The effect of PSD95BP in kainic acid treated mice

The three most significantly changed proteins in the analysis of hippocampal proteomes between KA-treated animals that subsequently received PSD95BP or its corresponding vehicle were phosphotidate cytidylyltransferase 1, gene model 1604B, and basigin (Table 5.7). Phosphatidate cytidylyltransferase 1 interacts with all its functional partners equally (Figure 5.8A). Gene model 1604B also interacts with all its functional partners equally (Figure 5.8B). These functional partners include gene model 1381, REV1 homolog and secretory carrier membrane protein

4 (Figure 5.8B). Basigin has the most evident interaction with solute carrier family 16 (Figure 5.8C).

The effect of 1400W in kainic acid treated mice

The three proteins with the lowest p-values in the analysis of hippocampal proteomes between KA-treated animals that subsequently received 1400W or its corresponding vehicle were src substrate cortactin, sideroflexin-1 and acid ceramidase (Table 5.8). Substrate cortactin has the greatest interactions with dynamin 1 compared to the other functional partners (Figure 5.9A). Sideroflexin 1 is only functionally interacting with solute carrier family 25 (Figure 5.9B). Acid cerimidase TBC1 domain family member 10c has the greatest interactions with DENN/mitogen-activated-protein-kinase activating death domain (MADD) domain containing 1C compared to the other functional partners (Figure 5.9C).

5.4. Discussion

A proteomic approach was used to investigate the effects of KA in the hippocampus of C57BL/6J mice and the effects of drug interventions, PSD95BP or 1400W, when administered after KA-induced seizures. The results from the overall percentage of proteins affected between treatment groups and the heat map visualisation showed that the greatest changes in protein expression in the hippocampus occurred after KA (Table 5.1, Figures 5.1 and 5.2). Previous proteomics studies using 2D gel quantification have shown that KA-induced seizures significantly affect the expression of 19 proteins in the rat brain (Krapfenbauer et al., 2001b). PSD95BP or 1400W alone caused changes to only a small number of proteins in the hippocampus, although the number of proteins affected was increased when the drug interventions were given after mice had KA-induced seizures (Table 5.1). The fewer number of proteins significantly affected in vehicle pre-treated mice suggest that the drug interventions have lesser impact on protein levels in normal hippocampus compared to one that has been challenged with KA. The proteins that were selectively affected by drug treatment in animals that had previously been treated with KA might represent those are activated in an effort to protect against the brain insult.

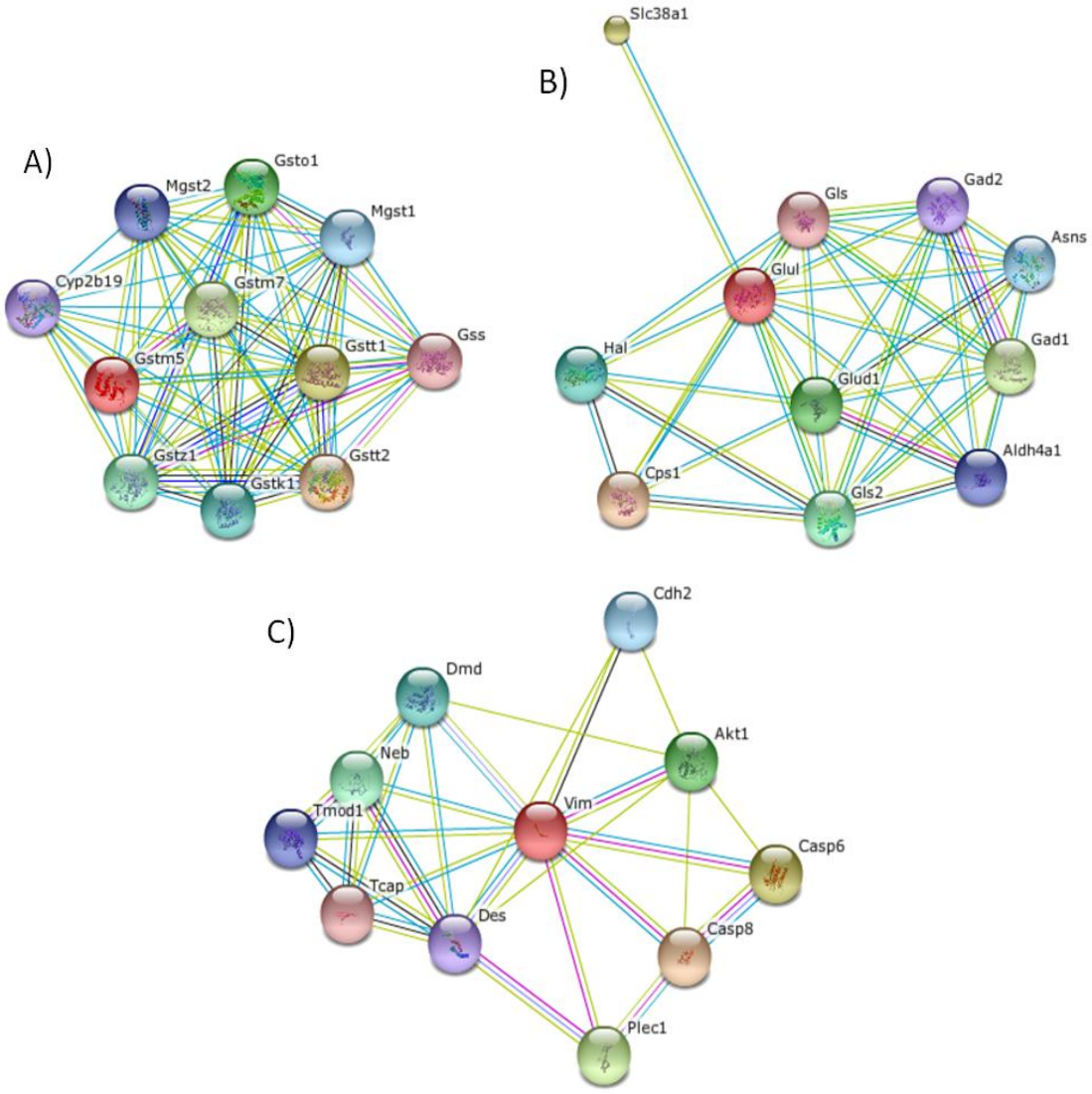

Figure 5.6. Network representations of the top 3 most significantly affected proteins in the hippocampus of post-synaptic density 95 blocking peptide treated C57BL/6J mice treated, comparing those that had previously received kainic acid or its corresponding vehicle, with known or predicted protein interactions with other functional partners plotted by Search Tool for the Retrieval of Interacting Genes/Proteins (STRING). In this view, the number of different coloured lines represents the number of different types of evidence for the association.(A) Glutathione S-transferase Mu 5 (Gstm5) with functional partners: glutathione S-transferase theta 2 (Gstt2); theta 1 (Gstt1); Mu 7 (Gstm7); omega 1 (Gsto1); zeta 1 (Gstz1); kappa 1 (Gstk1), microsomal glutathione S-transferase 1 (Mgst1); 2 (Mgst2), glutathione synthetase (Gss), cytochrome P450 family 2 subfamily b polypeptide 19 (Cyp2b19). (B) Glutamine synthetase (Glul) with functional partners: carbamoyl-phosphate synthetase 1 (Cps1), solute carrier family 38 member 1 (Slc38a1), glutamic acid decarboxylase 1 (Gad1); 2 (Gad2), glutamate dehydrogenase 1 (Glud1), glutaminase (Gls); 2 (Gls2), histidine ammonia lyase (Hal), asparagine synthetase (Asns), aldehyde dehydrogenase 4 family member A1 (Aldh4a1).(C) Vimentin (Vim) with functional partners: caspase 6 (Casp6); 8 (Casp8), plectin 1 (Plec1), thymoma viral proto-oncogene 1 (Akt1), nebulin (Neb), dystrophin muscular dystrophy (Dmd), cadherin 2 (Cdh2), tropomodulin 1 (Tmod1), desmin (Des), titin-cap (Tcap).

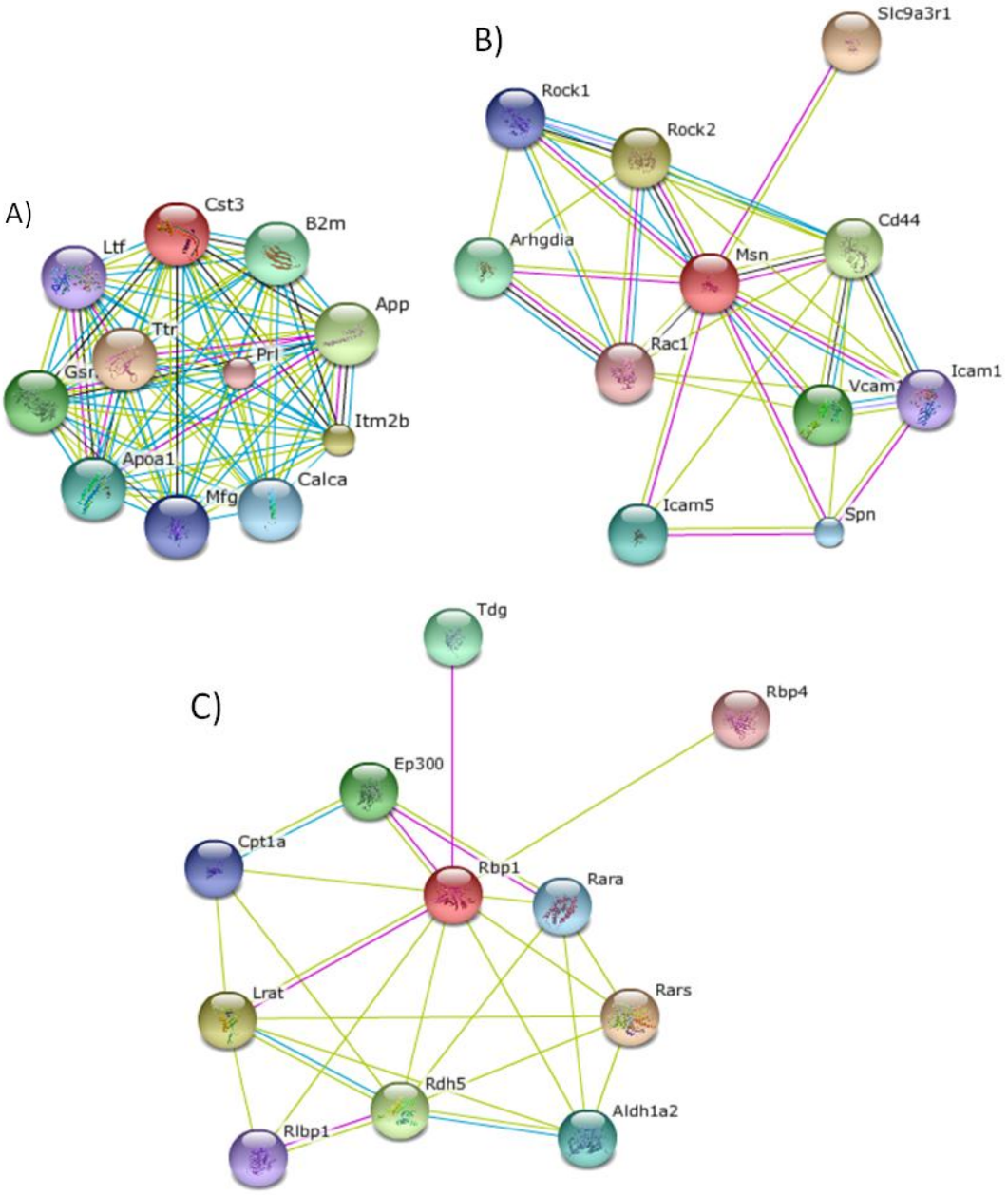

Figure 5.7. Network representations of the top 3 most significantly affected proteins in the hippocampus of 1400W treated C57BL/6J mice treated, comparing those that had previously received kainic acid or its corresponding vehicle, with known or predicted protein interactions with other functional partners plotted by Search Tool for the Retrieval of Interacting Genes/Proteins (STRING). In this view, the number of different coloured lines represents the number of different types of evidence for the association.(A) Cystatin C (Cst3) with functional partners: transthyretin (Ttr), integral membrane protein 2B (Itm2b), amyloid beta (A4) precursor protein (App), gelsolin (Gsn), beta-2 microglobulin (B2m), apolipoprotein A-I (Apoa1), calcitonin/calcitonin-related polypeptide, alpha (Calca), milk fat globule-EGF factor 8 protein (Mfge8), lactotransferrin (Ltf), prolactin (Prl).(B) Moesin (Msn) with functional partners: solute carrier 9 (sodium/hydrogen exchanger), member 3 regulator 1 (Slc9a3r1), Rho-associated coiled-coil containing protein kinase 2 (Rock2); CD44 antigen (Cd44); vascular cell adhesion molecule 1 (Vcam1); Rho GDP dissociation inhibitor (GDI) alpha (Arhgdia); intercellular adhesion molecule 5 (Icam5); sialophorin (Spn); Rho-associated coiled-coil containing protein kinase 1 (Rock1); intercellular adhesion molecule 1 (Icam1); RAS-related C3 botulinum substrate 1 (Rac1). (C) Retinol binding protein 1 (Rbp1) with functional partners: arginyl-tRNA synthetase (Rars), lecithin-retinol acyltransferase (Lrat), biogenesis of lysosome-related organelles complex-1 (Rdh5), E1A binding protein p300 (Ep300), thymine DNA glycosylase (Tdg), aldehyde dehydrogenase family 1 subfamily A2 (Aldh1a2), retinoic acid receptor alpha (Rara), carnitine palmitoyltransferase 1a (Cpt1a), retinaldehyde binding protein 1 (Rlbp1), retinol binding protein 4 (Rbp4).

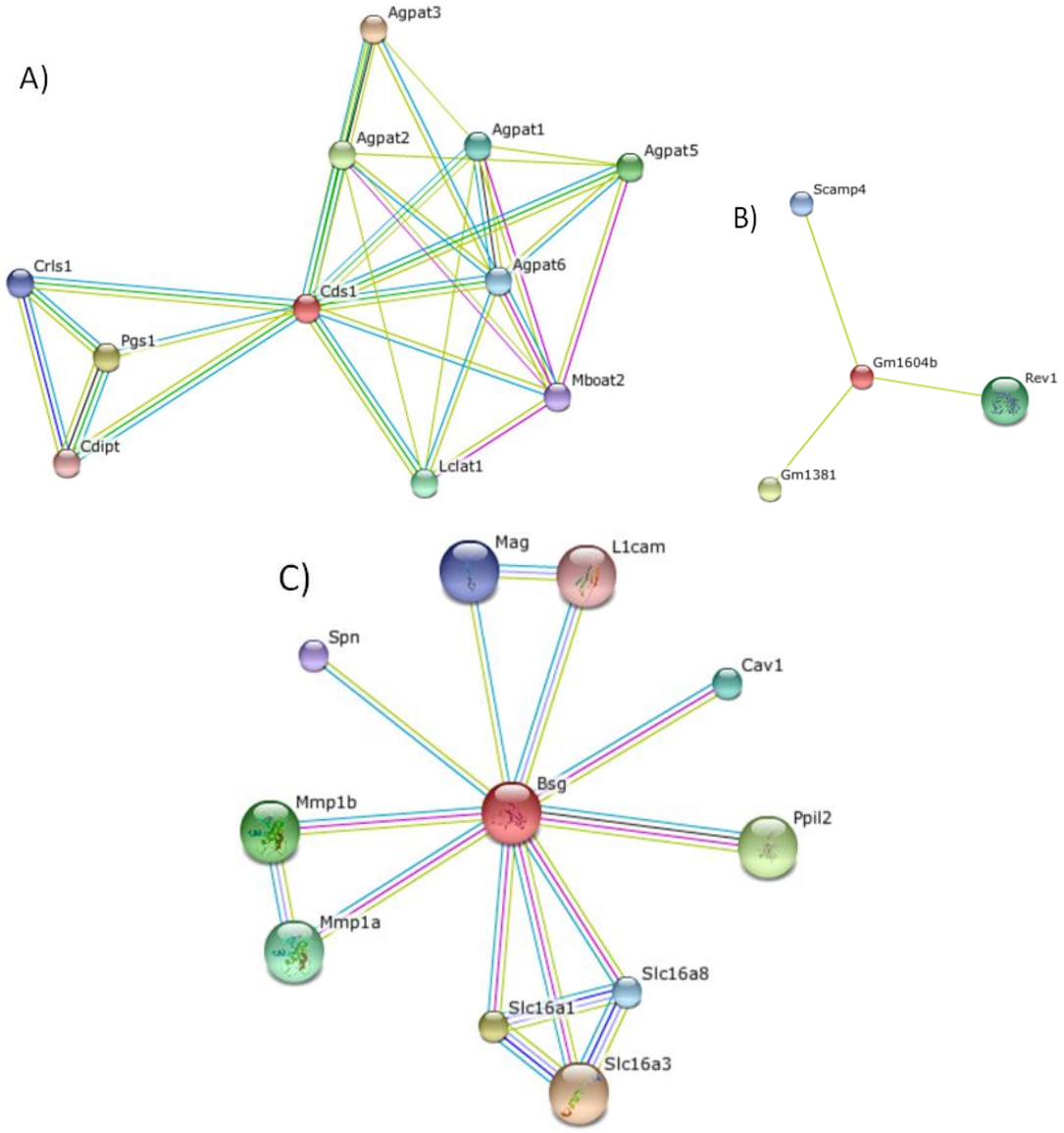

Figure 5.8. Network representations of the top 3 most significantly affected proteins in the hippocampus of kainic acid treated C57BL/6J mice treated, comparing those that subsequently received post-synaptic density 95 blocking peptide or its corresponding vehicle, with known or predicted protein interactions with other functional partners plotted by Search Tool for the Retrieval of Interacting Genes/Proteins (STRING). In this view, the number of different coloured lines represents the number of different types of evidence for the association.(A) Phosphatidate cytidylyltransferase 1 (Cds1) with functional partners: 1-acylglycerol-3-phosphate O-acyltransferase 1 (Agpat1); 2 (Agpat2); 3 (Agpat3); 5 (Agpat5); 6 (Agpat6), phosphatidylglycerophosphate synthase 1 (Pgs1), lysocardiolipin acyltransferase 1 (Lclat1), cardiolipin synthase 1 (Crls1), membrane bound O-acyltransferase domain containing 2 (Mboat2), CDP-diacylglycerol—inositol 3-phosphatidyltransferase (Cdipt). (B) Gene model 1604B (Gm1604b) with functional partners: Gene model 1381 (Gm1381), REV1 homolog (Rev1), secretory carrier membrane protein 4 (Scamp4). (C) Basigin (Bsg) with functional partners: solute carrier family 16 member 1 (Slc16a1); member 3 (Slc16a3); member 8 (Slc16a8), peptidylprlyl isomerase-like 2 (Ppil2), matrix metallopeptidase 1a (Mmp1a); 1b (Mmp1b), caveolin 1 (Cav1), myelin-associated glycoprotein (Mag), sialophorin (Spn), L1 cell adhesion molecule (L1cam).

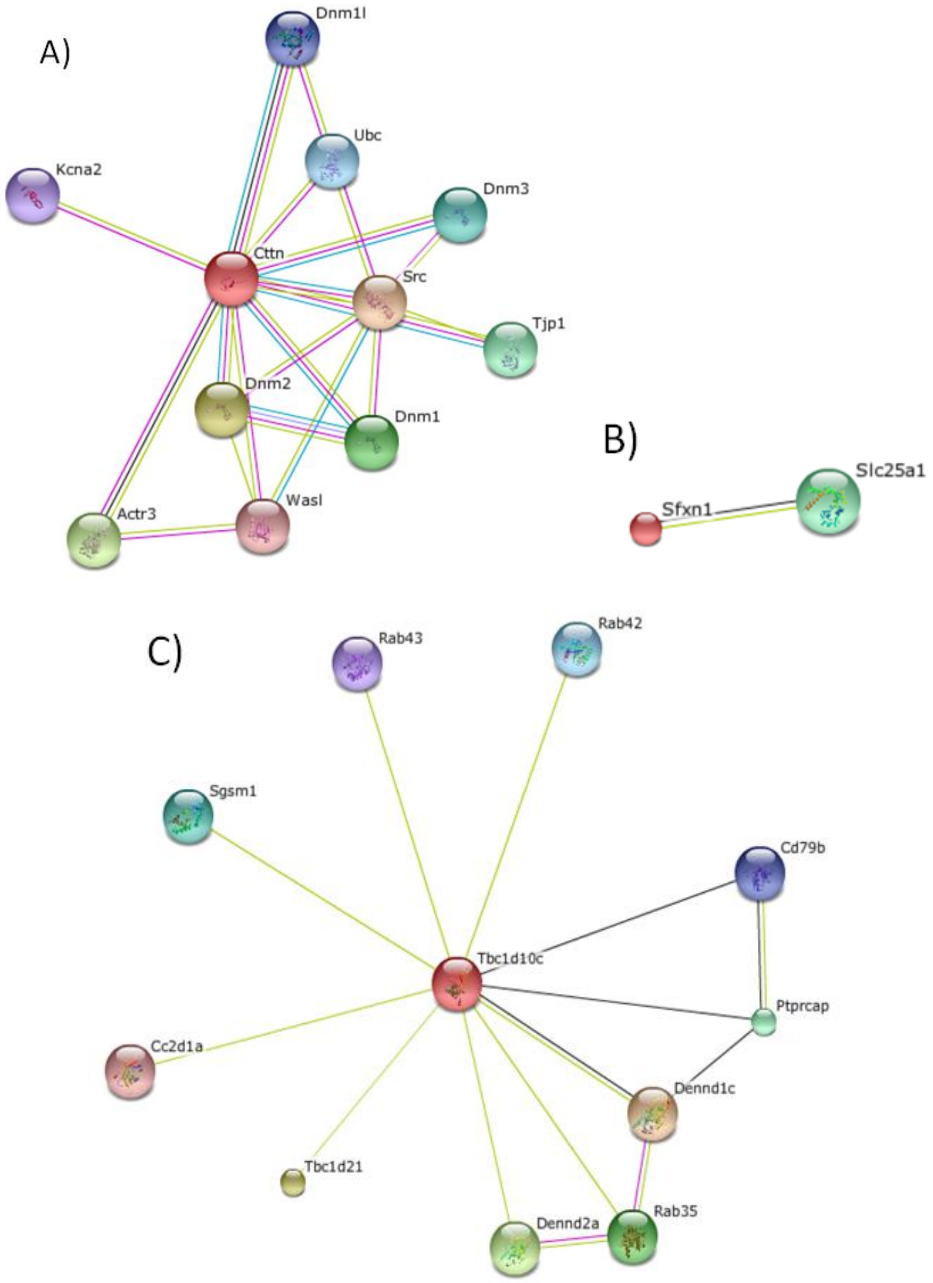

Figure 5.9. Network representations of the top 3 most significantly affected proteins in the hippocampus of kainic acid treated C57BL/6J mice treated, comparing those that subsequently received 1400W or its corresponding vehicle, with known or predicted protein interactions with other functional partners plotted by Search Tool for the Retrieval of Interacting Genes/Proteins (STRING). In this view, the number of different coloured lines represents the number of different types of evidence for the association.(A) Substrate cortactin (Cttn) with functional partners: Rous sarcoma oncogene (Src), dynamin 1 (Dnm1); 2 (Dnm2); 3 (Dnm3); 1-like (Dnm1l), ARP3 actin-related protein 3 (Actr3), tight junction protein 1 (Tjp1), predicted gene 4802 (Ubc), potassium voltage-gated channel shaker-related subfamily member 2 (Kcna2), Wiskott-Aldrich syndrome-like (Wasl). (B) Sideroflexin 1 (Sfxn1) with functional partners: solute carrier family 25 member 1 (Slc25a1). (C) Acid ceramidase TBC1 domain family member 10c (Tbc1d10c). Functional partners: DENN/MADD domain containing 1C (Dennd1c); 2a (Dennd2a), TBC1 domain family member 21 (Tbc1d21), RAB35 member RAS oncogene (Rab35), protein tyrosine phosphatase receptor type C polypeptide-associated protein (Ptprcap), small G protein signalling modulator 1 (Sgsm1), RAB42 member RAS oncogene (Rab42); RAB43 member RAS oncogene (Rab43), CD79B antigen (Cd79b), coiled-coil and C2 domain containing 1A (Cc2d1a).

Protein-protein interaction mapping was used to estimate the impact on cellular function of changes in protein expression for each of the top 3 proteins in each analysis using published functional information. Following KA administration, complement component 1q subunit b (C1qb), galectin-1 and moesin were the top 3 proteins, all of which were up-regulated (Table 5.2 and Figure 5.3). Complement component 1q (C1q) interacts closely with other complement component 1 subcomponents (Figure 5.3A). C1q plays a key role in the recognition of immune complexes (Kishore and Reid, 2000) and the complement system has a role in the pathogenesis of neurological disorders (Griffiths et al., 2009; Amor et al., 2010). Up-regulation of C1q and other complement subcomponents have been proposed to be associated with synaptic remodelling and neuronal loss after the generation of an epileptic focus (Ivens et al., 2007). Galectin-1 and its closest functional partner, neuroblastoma ras oncogene (Figure 5.3B) regulate cell adhesion, proliferation and survival (Bar-Sagi and Feramisco, 1985; Perillo et al., 1998). Moesin is a protein that links actin cytoskeleton to the plasma membrane (Ben-Aissa et al, 2012), and is closely associated with Rho-associated coiled-coil containing protein kinase 2 (Rock2) (Figure 5.3C) that is important for cell-cell recognition, signalling and cell movement (Wilgenbus et al., 1994). Rock2 is one of two key regulators of actin organisation that regulates cell migration (Riento and Ridley, 2003). From the interaction mapping, it is hypothesised that KA-induced seizures can cause synaptic remodelling, neuronal loss, and may also affect the immune/inflammatory pathways, actin organisation and various biological processes, such as cell adhesion, proliferation and survival.

Following PSD95BP administration, Rho guanine nucleotide exchange factor 2 and protein farnestyltransferase subunit B were significantly down-regulated and DNA topoisomerase II β was up-regulated (Table 5.3 and Figure 5.4). Rho guanine nucleotide exchange factor 2 is associated with Ras-related C3 botulinum substrate 1 (Rac1), rho homolog gene family member B (Rhob) and cell division cycle 42 homolog (Cdc42) (Figure 5.4A). Guanine nucleotide exchange factors (GEFs) are responsible for the activation of rho-family guanosine triphosphate (GTP) hydrolase enzymes, GTPases, to regulate cell proliferation, differentiation and

migration (Rossman et al., 2005). The functional partners Rac1, Rhob and Cdc42 are groups within the rho family (Rossman et al., 2005). Protein farnestyltransferase subunit B has a close interaction with its subunit A (Figure 5.4B). The enzymes target members of the Ras superfamily of small GTP-binding proteins for cell cycle progression and have roles in signal transduction and intracellular trafficking pathways (Casey and Seabra, 1996). DNA topoisomerase II β and its functional partners closely interact with one another, except for its α isozyme. Both DNA topoisomerase II isozymes can alter DNA topology by introducing transient double strand break (Nitiss, 2009). The α isozyme is essential for separating replicated chromosomes for all cells, and the β isozyme is required for normal development, but dispensable in some cell types (Nitiss, 2009). The β isozyme is also important in transcriptional regulation and has a key role in the survival of some neural cells. From the interaction mapping, it is hypothesised that PSD95BP administration can affect various biological processes such as cell proliferation, differentiation, division and migration. It can also affect signal transduction, intracellular trafficking pathways and neural cell survival.

Following 1400W administration, 3'-phosphoadenosine 5-'phosphosulphate synthase 1 (Papss1), protein kinase C and casein kinase substrate in neurons 2, glycine cleavage system protein H were significantly up-regulated (Table 5.4 and Figure 5.5). Papss1 is associated with Papss2 (Figure 5.5A). 3'-phosphoadenosine 5'-phosphosulphate (Paps) is a sulphate donor for the catalytic reaction of sulphotransferase (Xu et al., 2000). Sulphate conjugation is an important pathway in the metabolism of exogenous and endogenous compounds, including drugs and xenobiotics (Xu et al., 2000). Protein kinase C and casein kinase substrate in neurons 2 (PACSIN2) have close interactions with Papss1 and dynamin 2 (Figure 5.5B). PACSIN2 is a negative regulator of epidermal growth factor receptor activation and signalling (de Kreuk et al., 2012), therefore its up-regulation would be expected to suppress these processes. Dynamin 2 is a GTPase responsible for endocytosis in most cell types (Diatloff-Zito et al., 1995; Altschuler et al., 1998). Glycine cleavage system protein H and many of its functional partners are members of the glycine cleavage system (Figure 5.5C). The glycine cleavage system, also called the glycine decarboxylase complex, is a series of enzymes that

respond to high concentrations of glycine (Kikuchi, 1973; Kikuchi et al., 2008). The functional partners, aminomethyltransferase and glycine decarboxylase are proteins within the system and are involved in glycine decarboxylation (Kikuchi, 1973; Douce et al., 2001; Kikuchi et al., 2008). The remaining functional partners are involved in glycine production (Porter et al., 1985; Stover and Schirch, 1990). From the interaction mapping, it is hypothesised that 1400W may exert its effects in the hippocampus by modulating the metabolism of exogenous and endogenous compounds, epidermal growth factor activation, endocytosis and regulation of glycine.

.

When PSD95BP was administered to KA-treated animals, phosphotidate cytidylyltransferase 1 (Cds1) and basigin were down-regulated, and gene model 1604B was significantly up-regulated in comparison to control (Table 5.7 and Figure 5.8). Cds1 interacts with all of its functional partners equally (Figure 5.8A) and is involved in the regeneration of the signalling molecule phosphatidylinositol-4,5-bisphosphate from phosphatidic acid to regulate phosphoinositide-mediated signalling cascade (Wu et al., 1995). Gene model 1604b closely interacts with gene model 1381, REV1 homolog and secretory carrier membrane protein 4 (Figure 5.8B). The functions of gene models 1604b and 1381 are not reported in the literature. REV1 is a DNA repair protein that recruits DNA polymerases to damaged DNA (Lawrence, 2002) and secretory carrier membrane protein 4 is an integral membrane protein found in mammals that is implicated in membrane trafficking (Hubbard et al., 2000). Basigin is associated with solute carrier family 16 (Figure 5.8C) and is a receptor for a parasite ligand that is essential for blood stage growth (Crosnier et al., 2011). Solute carrier family 16 is a family of monocarboxylate transporters that carries molecules with one carboxylate group across biological membranes (Halestrap and Meredith, 2004). From the interaction mapping, it is hypothesised that PSD95BP affects KA-induced seizures by regulating the phosphoinositide-mediated signalling cascade, DNA repair, membrane trafficking, blood stage growth and amino acid/acidic drug transport.

When 1400W was administered to KA-treated animals, substrate cortactin was down-regulated; sideroflexin 1 and acid cerimidase were up-regulated in

comparison to control (Table 5.8 and Figure 5.9). Substrate cortactin is a cortical actin binding protein that promotes cell migration and endocytosis (Cosen-Binker and Kapus, 2006; Ammer and Weed, 2008). Its down-regulation suggests suppression in cellular development. Its functional partner, dynamin 1 is a GTPase responsible for endocytosis in neurons and neuroendocrine cells (Altschuler et al., 1998). Sideroflexin 1 is associated with solute carrier family 25 (Figure 5.9B) but its function is unknown (Li et al., 2010). Solute carrier family 25 is a large family of mitochondrial nuclear-encoded transporters that transport an extensive range of solutes (Palmieri, 2013). Acid cerimidase is associated with DENN/MADD domain containing 1C (Figure 5.9C) and is a lipid hydrolase that plays a central role in sphingolipid metabolism, particularly in regulating the levels of ceramide and sphingosine in cells (Park and Schuchman, 2006). DENN/MADD domain containing 1C functions as a GEF for activating the Rab GTPases to regulate cell proliferation, differentiation and migration (Marat et al., 2011). From the interaction mapping, it is hypothesised that 1400W affects KA-induced seizures by suppressing cell division, endocytosis of neurons and neuroendocrine cells, mitochondrial nuclear-encoded transport and sphingolipid metabolism.

The effect of KA significantly down-regulated glutathione S-transferase and glutamine synthetase but up-regulated vimentin in PSD95BP treated mice (Table 5.5). Glutathione S-transferases are a family of detoxification enzymes that catalyse the conjugation of glutathione to a variety of endogenous and exogenous compounds (Hayes and Pulford, 1995; Townsend and Tew, 2003). These enzymes have key roles in the metabolism of leukotrienes/prostaglandins, and regulate mitogen-activated protein (MAP) kinase pathway responsible for cellular survival and death signals (Townsend and Tew, 2003). Glutamine synthetase plays an essential role in catabolising glutamate into glutamine (Norenberg and Martinez-Hernandez, 1979) and is closely associated with glutaminase (Figure 5.6B), which generates glutamate from glutamine (Yudkoff et al., 1988). Vimentin is a major constituent of the intermediate filament family of proteins and is known to maintain cellular integrity and resistance against stress (Satelli and Li, 2011). Increased vimentin expression has been reported in various injuries, including the brain (Lewis and Fisher, 2003; Bryant et al., 2006; Satelli and Li, 2011). From the

interaction mapping, it is hypothesised that KA affects PSD95BP treated mice by decreasing detoxification, glutamate/glutamine regulation and increase resistance to stress.

The effect of KA significantly up-regulated cystatin C, moesin and retinol binding protein 1 in 1400W treated mice (Table 5.6). Cystatin C is an endogenous cysteine protease inhibitor and has been recently shown to have endogenous neuroprotective properties in neuronal cells (Watanabe et al., 2014). Elevation of cystatin C is shown to be associated with neuronal death in Alzheimer's disease (Deng et al., 2001). Moesin, as previously mentioned, is closely associated with Rock2 (Figure 5.3) and are both involved with actin organisation (Wilgenbus et al., 1994) (Riento and Ridley, 2003; Ben-Aissa et al., 2012). Retinol binding protein 1 is involved in vitamin A metabolism (Lepreux et al., 2004) and is present within the endothelial cells of the BBB (MacDonald et al., 1990). Increased levels of retinol binding protein have been reported in brains of Alzheimer's disease patients (Maury and Teppo, 1987). From the interaction mapping, it is hypothesised that KA affects 1400W treated mice by increasing neuronal death, affect actin organisation and vitamin A metabolism.

Moesin is modulated in more than one analysis described in this chapter, lending weight to its involvement in the generation of experimental seizures and its attenuation by novel NO pathway targeted agents. Moesin is up-regulated by the effects of KA in vehicle-treated mice and in 1400W-treated mice. Moesin and its closest functional partner, Rock2, regulate actin organisation. It is therefore hypothesised that KA affects actin organisation in mice and the administration of 1400W does not protect against this. Interaction mapping is unable to hypothesise further on the regulation of functional partners, therefore, the effects of KA on the expression of Rock2 in the hippocampus will require further investigation.

Using several methods for analysing proteomics data, theoretical conclusions can be drawn from changes in the protein profile between treatment groups and from protein-protein interaction mapping. Using qualitative analysis, basic information on protein-protein interactions can be integrated with previously published

functional information to build hypotheses on the role of proteins within the complex biological mechanisms and pathophysiological processes of a disease. With the progression of bioinformatics technology, it may be beneficial to use more sophisticated bioinformatics tools and databases to analyse the large amount of data generated in this chapter. The use of large-scale technologies for protein analysis can contribute to the volume and complexity of the data (Hondermarck, 2004). With only a small sample size used in this study, this introduces greater variability to the list of proteins expressed in animals within each treatment group. Nevertheless, this experiment was conducted as a pilot study to provide insights into the changes in hippocampal proteins after the induction of seizures and when potential anti-epileptogenic agents were administered. A follow-up study will be required to investigate potential cellular mechanisms that are associated with the effects of PSD95BP or 1400W.

Chapter 6

Effects of nitric oxide signalling pathway on albumin-mediated transforming growth factor β signalling pathways during epileptogenesis

6.1. Introduction

Albumin is the most abundant protein in the blood, constituting 50% of the total human plasma protein content (Peters, 1995; Farrugia, 2010). It is synthesised peripherally by the liver and does not readily diffuse across an intact BBB because of its size (Blyth et al., 2009; Farrugia, 2010). The purpose of the BBB is to limit the penetration of a variety of substances from the blood into the brain as a defence mechanism (Van Vliet et al., 2007). In pathological conditions, chemical mediators are released that increase BBB permeability and therefore the barrier becomes dysfunctional (Ballabh et al., 2004). BBB dysfunction is a hallmark of brain insults and has been found to be associated with several neurological disorders, including epilepsy (Roch et al., 2002; Seiffert et al., 2004). BBB dysfunction usually occurs around the lesion (Heinemann et al., 2012) with epilepsy patients showing increased BBB permeability localised within the presumed epileptic focus (Tomkins et al., 2008; 2011). Albumin is used as a biomarker for BBB damage in several models of neuropathological conditions, including epilepsy (Bolwig et al., 1977; Seiffert et al., 2004; Van Vliet et al., 2007). Although it has not yet been shown whether the extent of BBB dysfunction can predict the development of epilepsy in patients (Seiffert et al., 2004; Heinemann et al., 2012), animal studies have shown positive correlation between the extent of BBB opening and epileptogenesis (Ivens et al., 2007; Tomkins et al., 2007; Van Vliet et al., 2007). It is still unclear, however, whether the increased BBB permeability is a result of the disease process, or is a contributor to the pathogenesis of the disease (Seiffert et al., 2004; Friedman, 2011).

Several animal models of acute seizures have shown a transient increase in BBB permeability after an initial insult (Nitsch and Klatzo, 1983; Pont et al., 1995; Uva et al., 2008; Williams et al., 2009). A number of blood-borne proteins and antibodies can enter the brain through the dysfunctional BBB and affect the seizure threshold in animals (Van Vliet et al., 2007; Maggio et al., 2008; Blyth et al., 2009; Vincent et al., 2010). Of these, extravasation of albumin into brain has been the most extensively investigated (Nadal et al., 1995; Ivens et al., 2007; Cacheaux et al., 2009; Farrugia, 2010), with studies showing increased brain albumin level in

epileptic patients (Mihály and Bozóky, 1984) and in experimental epilepsy models (Lassmann et al., 1984; Sokrab et al., 1989). This chapter focuses on albumin and its role in epileptogenesis.

6.1.1. Albumin-mediated effects in the brain

Extravasation of albumin into the brain activates the TGFβ signalling cascade and alters the function of astrocytes (Ivens et al., 2007; Cacheaux et al., 2009; Heinemann et al., 2012). TGFβ is a pleiotropic cytokine that regulates cellular proliferation and differentiation, embryonic development, wound healing, immune response and apoptosis in a variety of cells (Blobe et al., 2000; Heinemann et al., 2012). Changes in production of TGFβ have been linked to the pathogenesis of numerous diseases, as well as the altered expression of its receptors and associated intracellular signalling molecules (Blobe et al., 2000). Elevated TGFβ levels have been observed in models associated with BBB dysfunction, such as in injured neurons from animals that experienced acute brain insult and in astrocytes present in the hippocampus of animals that experienced SE (Aronica et al., 2000; Zhu et al., 2000; Dohgu et al., 2005).

The effect of albumin on the brain appears to be receptor-mediated (Nadal et al., 1995). In the brains of animals with BBB dysfunction, albumin binds to the TGFβ receptor (TGFβR) in order to activate TGFβ signalling (Ivens et al., 2007; Cacheaux et al., 2009). There are two types of TGFβRs, TGFβRI and TGFβRII (Heinemann et al., 2012); albumin appears to mediate its effects in the brain via uptake into astrocytes by TGFβRI (Ivens et al., 2007) and thereafter by altering potassium homeostasis. During periods of neuronal activity, extracellular potassium increases are buffered by astroglial uptake (Binder and Steinhäuser, 2006). However, under pathological conditions, potassium regulation fails and high extracellular potassium concentrations are able to initiate and propagate seizures (Wallraff et al., 2006). Seizure activity has been shown to increase extracellular potassium concentrations *in vivo* (Hinterkeuser et al., 2000; Binder and Steinhäuser, 2006; Jabs et al., 2008). Impaired potassium buffering has also been reported in the hippocampus of people with TLE (Gabriel et al., 1998; Schröder et al., 2000) and in epileptic rodents (Wallraff et al., 2006; Xu et al., 2009).

Uptake of albumin into astrocytes via TGFβRI results in down-regulation of the inward rectifying potassium channel 4.1 ($K_{ir}4.1$) and impaired potassium buffering (Perillan et al., 2002; Ivens et al., 2007; Heinemann et al., 2012). $K_{ir}4.1$ has been extensively investigated in the brain, where its expression is essentially limited to astrocytic membranes (Higashi et al., 2001; Binder and Steinhäuser, 2006). Down-regulation of this channel affects potassium homeostasis, leading to depolarisation of astrocytes, and enhanced neuronal excitotoxicity that can lead to epileptiform discharges (Ivens et al., 2007).

6.1.2. The regulation of TGFβ activity

TGFβ exists in 5 isoforms, 3 of which, namely TGFβ1, TGFβ2 and TGFβ3, are expressed in mammals (Khalil, 1999). All 3 mammalian isoforms are synthesised as precursor proteins (Khalil, 1999). TGFβ undergoes a number of intracellular processing steps prior to its secretion by cells. One such step is the proteolytic digestion of the precursor protein, which has a relative molecular mass of 44kDa (Lyons et al., 1990), to yield two products that assemble into a dimer with a relative molecular mass of 30kDa (Khalil, 1999). This dimer form is also referred to as the 'latent form' (Khalil, 1999; Taylor, 2009). One of the two products formed by proteolytic digestion of the precursor form is termed the latency-associated peptide (LAP), and the other is the homodimer, also referred to as 'mature' or 'active' TGFβ and which has a relative molecular mass of 25kDa (Lyons et al., 1990; Khalil, 1999). LAP binds TGFβ, which prevents TGFβ binding to TGFβR and therefore makes it biologically inactive (Khalil, 1999). However, LAP can facilitate the transport of active TGFβ from the cell by binding to another protein called latency binding protein (LTBP)(Khalil, 1999). TGFβ is secreted in the latent dimer form, with LTBP aiding secretion of this form into the extracellular matrix (Khalil, 1999). The regulation of TGFβ activity is based on controlling the mechanism that converts this important cytokine from its precursor to its biologically active form (Khalil, 1999; Taylor, 2009).

Pathways of activation of latent TGFβ1 have been extensively studied, as it is believed that this form predominates over the other two TGFβ isoforms and many

endogenous substances, including enzymes and proteins, have been shown to be able to activate the latent TGFβ1 dimer (Vodovotz, 1997; Khalil, 1999). ROS can activate TGFβ1 by affecting the amino acid residues of LAP that are susceptible to oxidation (Khalil, 1999). The oxidation process results in altered stability of LAP, resulting in the loss of its association with active TGFβ1 or a change to its structure that exposes the TGFβR binding domain (Khalil, 1999). Increased ROS production can occur from a brain insult and can lead to an increase in TGFβ1 activation (Khalil, 1999). TGFβ1 expression has been shown to be elevated in the brains of patients with neurodegenerative diseases (Heinemann et al., 2012). The role of TGFβ1 in neuronal injury is contradictory, with some claims that the production of TGFβ1 is protective against cell damage, and other results showing that increased production of TGFβ1 exacerbates excitotoxicity (Heinemann et al., 2012). These contrasting findings are believed to be dependent on the cell type and disease state (Heinemann et al., 2012).

Recent studies on the regulation of albumin-mediated TGFβ signalling and astrocytic transformation during epileptogenesis have aimed to investigate whether BBB dysfunction can be used as a potential early biomarker for the prediction of the development of epilepsy in the clinic (Heinemann et al., 2012). At present, it is unknown whether albumin mediates its effects on epileptogenesis by increasing the level of TGFβ1 or only from binding to TGFβRI (Ivens et al., 2007). The angiotensin receptor antagonist, losartan, has recently shown anti-epileptogenic effects in a model of epilepsy associated with vascular injury by blocking albumin-induced TGFβ activation in the brain and thereby preventing the development of SRS (Bar-Klein et al, 2014). This confirms that anti-epileptogenesis can impact on albumin-mediated TGFβ signalling. The objective of research described in this chapter was therefore to explore the contribution of the albumin-mediated TGFβ signalling pathway to epileptogenesis following pharmacological modulation of nitric oxide pathway in the aftermath of an acute brain insult. The abundance of albumin, TGFβ1, TGFβRI and $K_{ir}4.1$ in the hippocampus of C57BL/6J mice following repeated doses of KA to induce acute seizures was assessed. The effect of drug interventions (PSD95BP, 1400W and

PSD95BP plus 1400W combined) on expression of these proteins was also investigated.

6.2. Materials and methods

6.2.1. Animals

All experimental procedures were completed in accordance with the Animal (Scientific Procedures) Act, 1986 (UK). The methodological details regarding the source of the animals, their housing conditions, KA-induced seizures are described in section 2.1. The preparation and dosing regimens of PSD95BP and 1400W are described in section 4.2.2. For western blot, animals were euthanised 7 or 14 days after KA-induced seizures as described in section 2.1.4. A separate cohort of animals was used for IHC; these animals were anaesthetised and their brains perfused 7 or 14 days after KA-induced seizures as described in section 2.7.2. These timepoints were chosen based on the results from the EEG chapter (chapter 4) that showed a difference in the EEG algorithms used between control and drug-intervention groups. The divergence on day 7 may be indicative of the start of spontaneous seizures in the control animals and day 14 might be when the control animals have developed epilepsy. All control animals in this chapter refers to KA-treated animals without drug-interventions to compare to drug-intervention effects after KA-induced seizures.

6.2.2. Sample collection for western blot

Terminal blood samples were collected by cardiac puncture and stored in lithium heparin tubes that were placed on ice prior to centrifugation. The heparin blood tubes were then centrifuged at 2,000 × *g* for 20 minutes at 4°C and the plasma was isolated. Plasma samples were aliquoted into microcentrifuge tubes and stored at -20°C. Hippocampi were dissected from whole brains and placed in cryovials before being snap frozen in liquid nitrogen. Hippocampal samples were stored at -80°C until required.

6.2.3. Sample preparation for western blot

Plasma samples were diluted to 1:100 with 25mM ammonium bicarbonate and 1µl of the diluted plasma was used for western blot. Hippocampal tissues were prepared as described in section 2.5.2. Bradford protein assay was performed to determine the protein concentration of all resulting supernatants and to establish the volume required for each assay. The total amount of protein per assay was as follows: albumin 10µg, TGFβ1 20µg, TGFβRI 30µg and K_{ir}4.1 30µg. Supernatant samples were reduced and denatured prior to loading onto the gel, as described in section 2.5.3.

6.2.4. Western blot

Anti-albumin mouse polyclonal antibody (Abcam, UK) was diluted to 1:1000 and anti-mouse secondary antibody conjugated with HRP (Abcam, UK) was diluted to 1:5000 with 5% skim milk in TBST. The formulation of TBST is described in section 2.5.1. Anti-TGFβ1 rabbit polyclonal antibody (Abcam, UK) was diluted to 1:200 and anti-rabbit secondary antibody conjugated with HRP (Santa Cruz Biotechnology Inc., UK) was diluted to 1:1000 with 5% skim milk in TBST. Anti-TGFβRI rabbit polyclonal antibody (Abcam, UK) was diluted to 1:50 and anti-rabbit secondary antibody conjugated with HRP was diluted to 1:1000 with 5% skim milk in TBST. Anti-K_{ir}4.1 rabbit polyclonal antibody (Millipore, UK) was diluted to 1:40 and anti-rabbit polyclonal antibody was diluted to 1:1000 with 5% skim milk in TBST.

6.2.5. Densitometric analysis

The relative intensity of the bands was measured as described in section 2.5.4. The optical density ratio between the bands of each protein and their corresponding GAPDH bands was normalised and expressed using arbitrary units.

6.2.6. Immunohistochemistry

All brains for IHC were prepared as described in section 2.7.2. Immunostaining was carried out as described in section 2.7.3. In order to determine the optimum concentration for each antibody, serial dilutions were carried out for each antibody on spare brain sections and the antibody concentrations that produced

the best visualisation using a fluorescence microscope was chosen. The anti-albumin mouse polyclonal (Abcam, UK) primary antibody was tested at 1:1000, 1:500 and 1:200 dilutions, and the anti-mouse secondary antibody conjugated with CY3 fluorophore was tested at 1:500, 1:250 and 1:150 dilutions. The anti-TGFβ rabbit polyclonal (Abcam, UK) primary antibody was tested at 1:20, 1:10 and 1:5 dilutions, and the anti-rabbit secondary antibody conjugated with CY3 fluorophore was tested at 1:300 and 1:150 dilutions. The anti-TGFβRI rabbit polyclonal (Abcam, UK) primary antibody was tested at 1:20, 1:10 and 1:5 dilutions, and the anti-rabbit secondary antibody conjugated with CY3 fluorophore was tested at 1:300 and 1:150 dilutions. The anti-K_{ir}4.1 guinea pig polyclonal (Alomone Labs, Israel) primary antibody was tested at 1:300 and 1:150 dilutions, and the anti-guinea pig secondary antibody conjugated with CY3 fluorophore (Abcam, UK) was tested at 1:300 and 1:150 dilutions. All antibodies were diluted in antibody diluting fluid, as described in section 2.7.1. All brain slices were counterstained with DAPI (as described in section 2.7.3.). DAPI is a DNA-specific stain that forms a fluorescent complex by binding to the adenine-thymine rich sequences of DNA (Kapuscinski, 1995). Therefore, this stain can be used to identify the presence of living cells in the tissue.

6.2.7. Cell area measurement and cell counting in the hippocampal formation

IHC analyses were carried out by measuring the area of stained cells and by determining the percentage of stained cells against counterstained DAPI-stained cells, as described in section 2.7.5. The hippocampal structure was separated into specific anatomical sub-fields, comprising DG, CA3, CA2, CA1 and subiculum (Sb) (Figure 6.1). IHC analyses were carried out within each sub-field separately, and as a mean of all the sub-fields in the hippocampal formation. No comparisons were made between the sub-fields in the hippocampal formation.

6.2.8. Statistical analysis

Statistical analysis to compare the abundance of proteins between vehicle control and KA-treated animals at 7 and 14 days after KA-induced seizures, and between control animals and those that received drug interventions, again at 7 and 14 days

after KA-induced seizures, were performed by one way ANOVA with Tukey correction using SPSS version 21.

6.3. Results

6.3.1. Albumin

Changes in albumin levels induced by KA administration

When KA was administered to mice, there were no significant differences in the abundance of albumin in the hippocampus or in the plasma at either 7 or 14 days after KA-induced seizures, when compared to vehicle-treated mice that received distilled water alone (Figure 6.2 and 6.3).

Images and figures resulting from western blot are included for representative purposes, even where negative. For all subsequent results, only those showing statistically significant data are included in the interests of space.

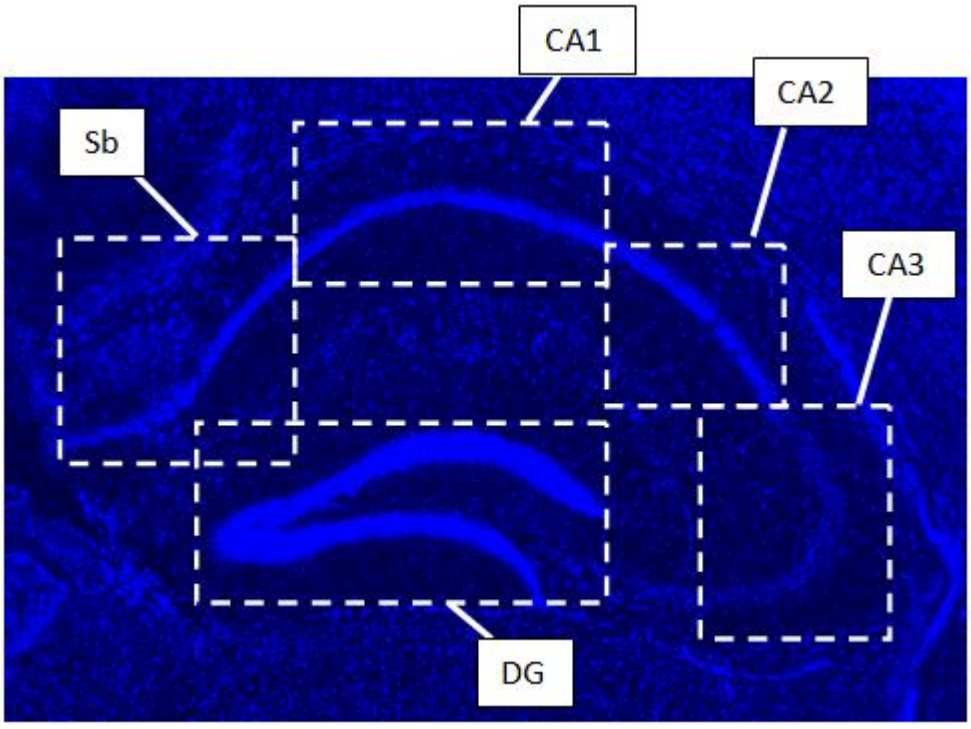

Figure 6.1. Diagram illustrating the anatomical regions of the hippocampal formation used in IHC analysis. Paraformaldehyde-fixed gelatin-embedded mouse hippocampus tissue was sectioned coronally. Tissue was stained with 4',6-diamidino-2-phenylindole (DAPI) to show the cellular structure of the hippocampal formation. For the purposes of analysis, the following regions were

used - dentate gyrus (DG), *Cornu Ammonis* 3 (CA3), *Cornu Ammonis* 2 (CA2), *Cornu Ammonis* 1 (CA1) and subiculum (Sb). Magnification, 2.5X.

Changes in albumin levels induced by 1400W administration

When 1400W was administered following KA-induced seizures, there were no changes in the abundance of plasma albumin at either 7 or 14 days thereafter (Figure 6.4). A significant increase in hippocampal albumin, measured by western blot, and in the overall percentage of albumin stained cells within the entire hippocampal formation, measured by DAPI-adjusted IHC, was however observed at day 7 (Figures 6.4 and 6.5). The mean normalised albumin to GAPDH ratio increased from 1.2 ± 0.29 arbitrary units in control mice to 5.63 (± 1.55) arbitrary units in 1400W-treated mice ($p<0.05$) (Figure 6.4). In addition, the percentage of albumin to DAPI-stained cells in the hippocampal formation as a whole increased from 2.37% (± 0.12) in control mice to 6.10% (± 0.09) in 1400W-treated mice ($p<0.01$) (Figure 6.5). There were no other changes in the abundance of albumin in relation to area, GAPDH or DAPI staining in the hippocampal subfields or in the hippocampal formation as a whole (data not shown).

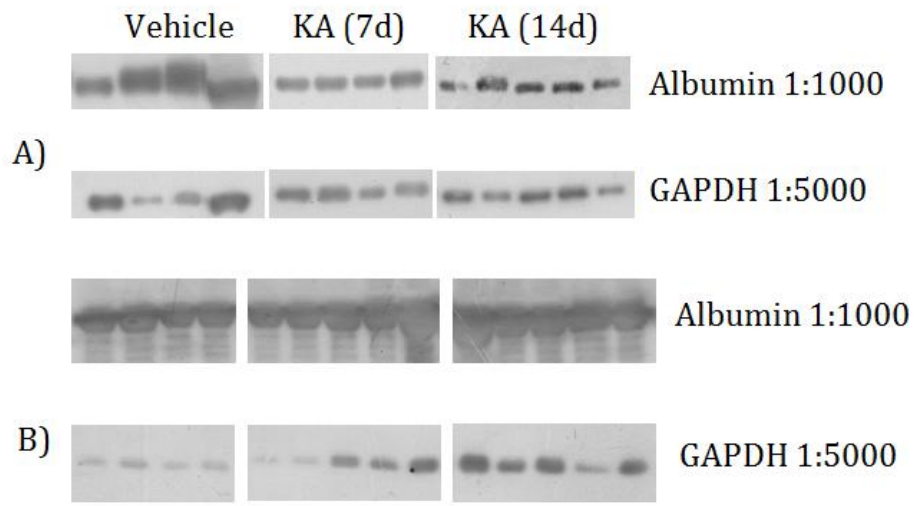

Figure 6.2. Representative western blots for albumin and glyceraldehyde 3-phosphate dehydrogenase (GAPDH) in (A) hippocampal homogenates and (B) plasma for vehicle-treated animals 7 days post-administration and for kainic acid (KA)-treated animals 7 and 14 days after KA-induced seizures in C57BL/6J mice. An equal amount of protein was used for all homogenates and all plasma samples were diluted to 1:100. All samples were analysed by western blot using polyclonal antibodies directed against albumin at 1:1000 and GAPDH at 1:5000 dilutions.

Changes in albumin levels induced by PSD95BP administration

When PSD95BP was administered 1 hour after KA-induced seizures, there were no significant changes in hippocampal albumin levels compared to vehicle-treated controls (Figures 6.6 and 6.7; data for IHC not shown). There was however a significant decrease in plasma albumin levels at day 14, from 3.32 (± 0.59) arbitrary units in the vehicle-treated control mice to 1.28 (± 0.34) arbitrary units in PSD95BP treated mice ($p<0.05$) (Figure 6.7).

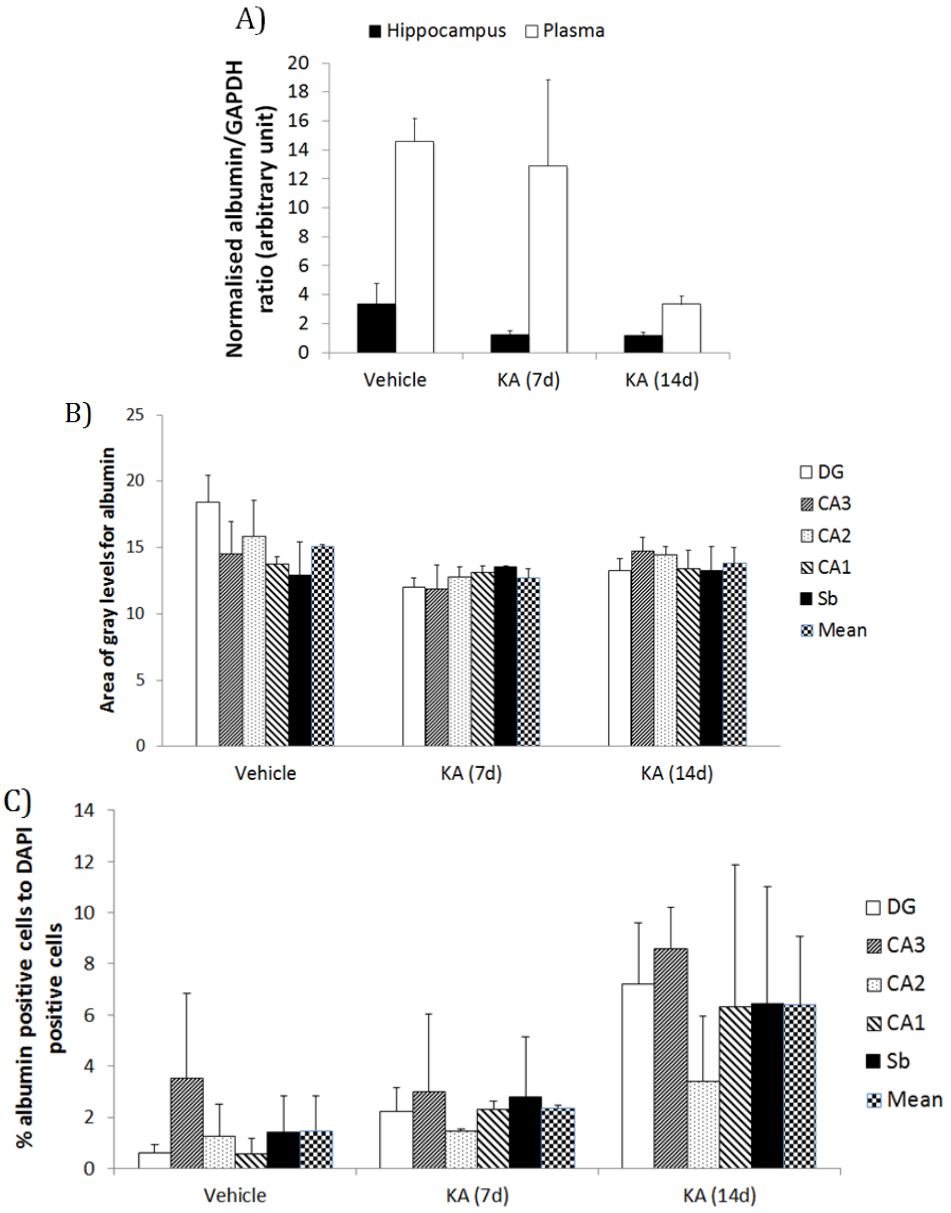

Figure 6.3. The effect of kainic acid (KA) on abundance of albumin in the hippocampus and plasma at 7 and 14 days after KA-induced seizures in C57BL/6J mice. Vehicle-treated control animals received distilled water alone, with plasma and hippocampal samples harvested 7 days thereafter. (A) Densitometric analysis of western blots for albumin in hippocampal homogenates and plasma of vehicle-treated (n=4) and KA-exposed mice (n=4-5) mice. Data are expressed as mean (± SEM) normalised albumin to glyceraldehyde 3-phosphate dehydrogenase (GAPDH) ratio in arbitrary units. (B) Immunohistochemical analysis of albumin stained cells in the dentate gyrus (DG), *Cornu Ammonis 3* (CA3), *Cornu Ammonis 2* (CA2), *Cornu Ammonis 1* (CA1) and subiculum (Sb) sub-fields of the hippocampus and the hippocampal formation as a whole in vehicle-treated and KA-exposed mice (n=2 per group), with pixel intensity adjusted to a set threshold in order to standardise gray level for all images. Data are expressed as mean (± SEM) area of gray levels. (C) Immunohistochemical analysis of albumin stained cells in relation to 4',6-diamidino-2-phenylindole (DAPI) stained cells in the DG, CA3, CA2, CA1 and Sb regions of the hippocampus and the hippocampal formation as a whole in vehicle-treated and KA-exposed mice (n=2 per group). Data are expressed as mean (± SEM) percentage of albumin to DAPI-stained cells.

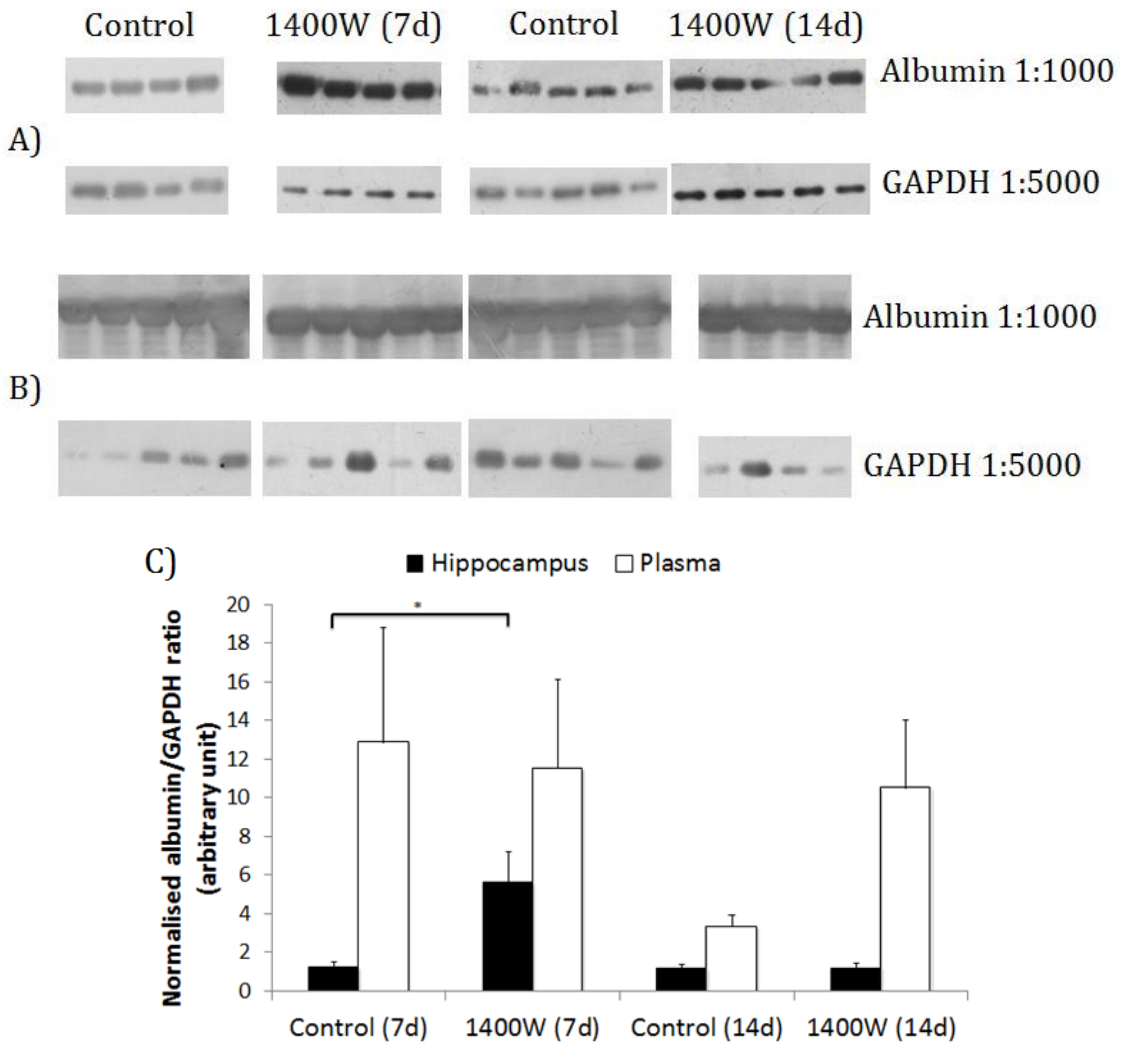

Figure 6.4. Representative western blots for albumin and glyceraldehyde 3-phosphate dehydrogenase (GAPDH) in (A) hippocampal homogenates and (B) plasma for control and 1400W-treated animals 7 and 14 days after kainic acid-induced seizures in C57BL/6J mice. An equal amount of protein was used for all homogenates and all plasma samples were diluted to 1:100. All samples were analysed by western blot using polyclonal antibodies directed against albumin at 1:1000 and GAPDH at 1:5000 dilutions. (C) Densitometric analysis of western blots for albumin in hippocampal homogenates and plasma of control and 1400W-treated mice (n=4-5 for all groups). Data are expressed as mean (± SEM) normalised albumin to glyceraldehyde 3-phosphate dehydrogenase (GAPDH) ratio in arbitrary units and was compared statistically using a one way Analysis of Variance with Tukey correction (*$p<0.05$).

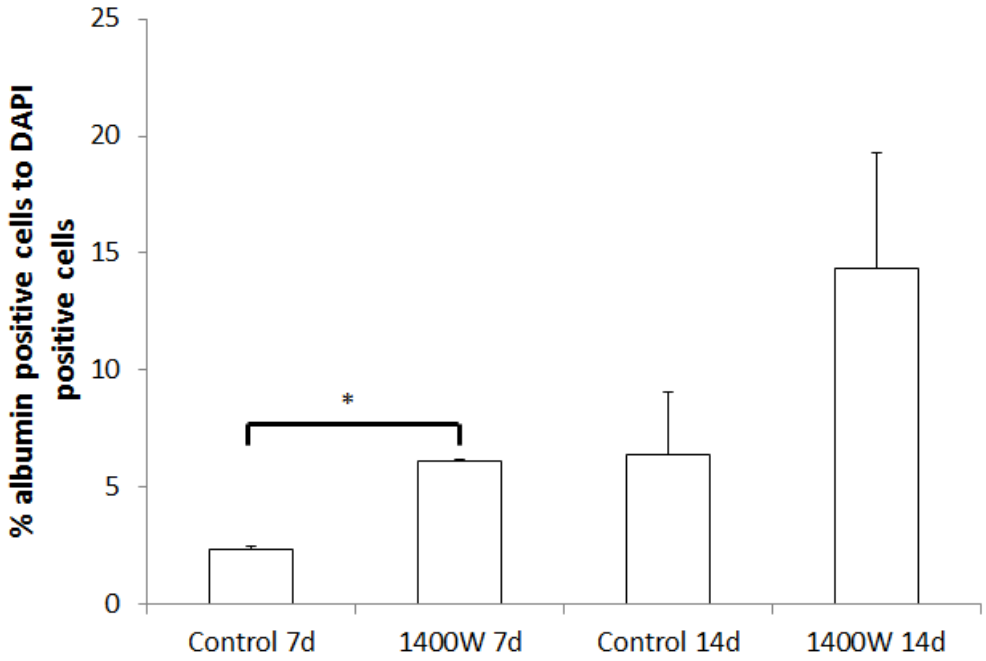

Figure 6.5. The effect of 1400W treatment on the abundance of albumin in the hippocampus at 7 and 14 days after kainic acid (KA)-induced seizures in C57BL/6J mice using immunohistochemical analysis of albumin stained cells in relation to 4',6-diamidino-2-phenylindole (DAPI) stained cells in the hippocampal formation as a whole (n=2 per group). Data are expressed as mean (± SEM) percentage of albumin to DAPI-stained cells and was compared statistically using a one way Analysis of Variance with Tukey correction (*p<0.01).

Changes in albumin levels induced by combined administration of PSD95BP and 1400W

When PSD95BP plus 1400W were co-administered after KA-induced seizures, no changes were observed in plasma or hippocampal albumin levels using western blot or IHC at either day 7 or day 14 (data not shown).

6.3.2. Transforming growth factor β1

Changes in TGFβ1 levels induced by KA administration

There was an increase in TGFβ1 precursor form in hippocampus after KA-induced seizures (Figure 6.8 and 6.9). The TGFβ1 precursor form increased from 0.25 (± 0.09) arbitrary units in vehicle-treated control mice to 0.82 (± 0.47) arbitrary units at 7 days after KA exposure and 2.49 (± 0.76) arbitrary units at 14 days after KA

(Figure 6.8 and 6.9), although this was only statistically significant ($p<0.05$) at 14 days. For the dimer form of TGFβ1, there were no differences between vehicle-treated control mice and those that received KA, but there was a significant reduction in hippocampal expression between 7 and 14 days after KA, dropping from 1.54 (± 0.37) arbitrary units at day 7 to 0.18 (± 0.05) arbitrary units at day 14 ($p<0.05$). The active form of TGFβ1 showed a marginal increase in hippocampal expression after KA administration increasing from 0.05 (± 0.03) arbitrary units in vehicle-treated control mice to 0.18 (± 0.05) arbitrary units at 7 days after KA and 0.23 (± 0.04) arbitrary units at 14 days (Figure 6.8 and 6.9). This effect was statistically significant ($p<0.05$) at 14 days alone.

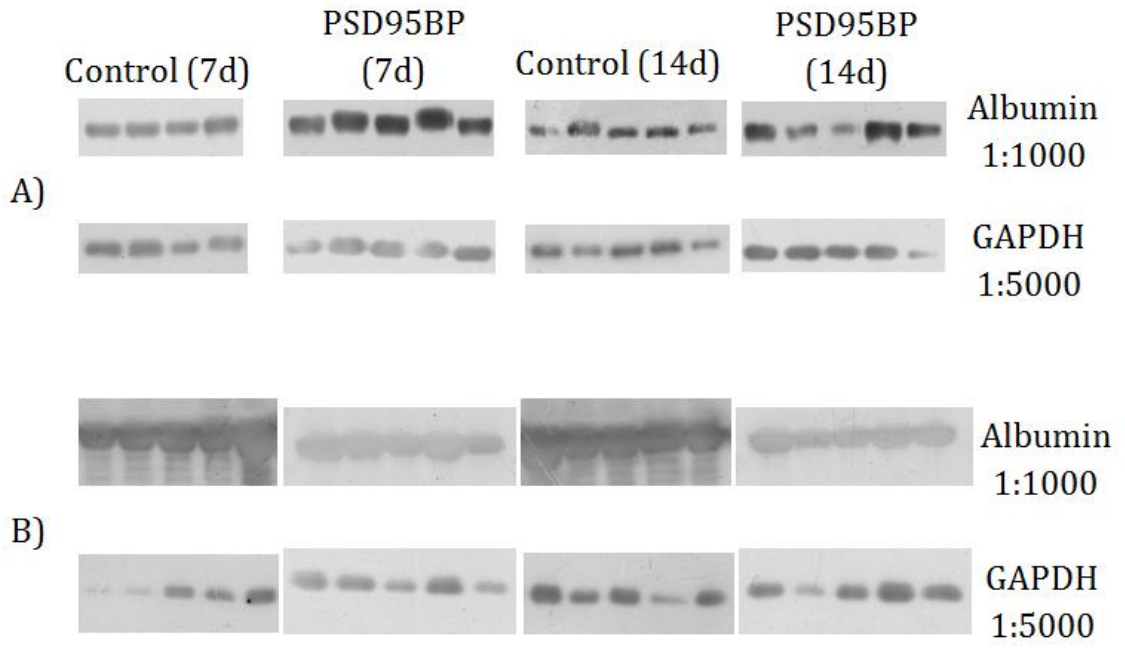

Figure 6.6. Representative western blots for albumin and glyceraldehyde 3-phosphate dehydrogenase (GAPDH) in (A) hippocampal homogenates and (B) plasma for control and post-synaptic density 95 blocking peptide (PSD95BP) treated animals at 7 and 14 days after kainic acid-induced seizures. An equal amount of protein was used for all homogenates and all plasma samples were diluted to 1:100. All samples were analysed by western blot using polyclonal antibodies directed against albumin at 1:1000 and GAPDH at 1:5000 dilutions.

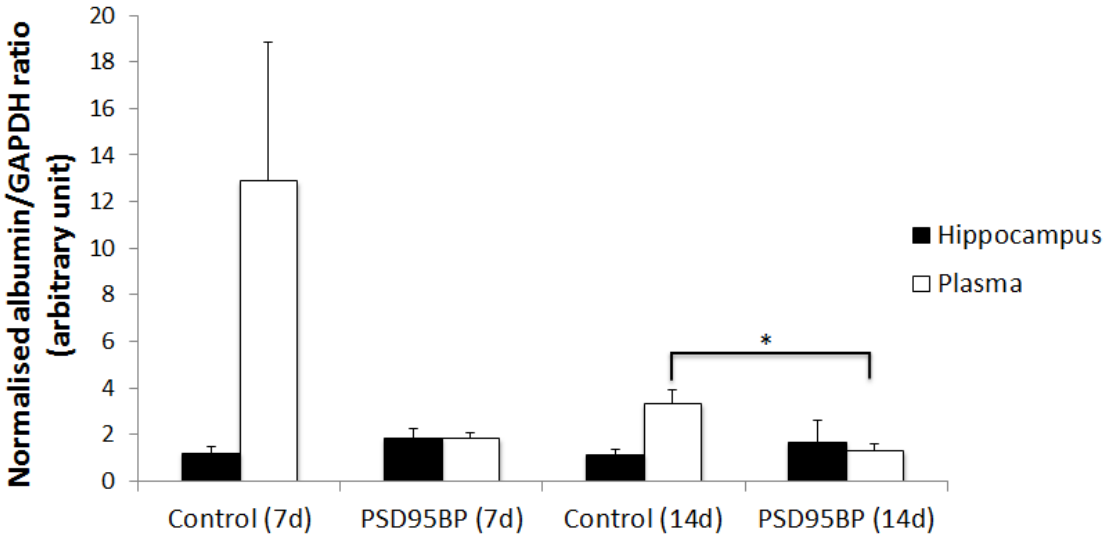

Figure 6.7. The effect of post-synaptic density 95 blocking peptide (PSD95BP) treatment on albumin levels at 7 and 14 days following kainic acid-induced seizures in C57BL/6J mice. Densitometric analysis of western blot for albumin in hippocampal homogenates and plasma of the control and PSD95BP-treated mice (n=5 per group). Data are expressed as mean (± SEM) normalised albumin to glyceraldehyde 3-phosphate dehydrogenase (GAPDH) ratio in arbitrary units and was compared statistically using one way Analysis of Variance with Tukey correction (*$p<0.05$).

In IHC analysis, no difference in the area of TGFβ1-stained cells was observed (data not shown). The percentage of TGFβ1 to DAPI-stained cells in the DG increased from 1.82% ± 0.38 in vehicle-treated control mice to 6.93% (± 0.95) in KA-exposed mice at 7 days ($p<0.05$) but then decreased to 2.58% (± 0.23) on day 14 ($p<0.05$; compared to 7 days) (Figure 6.9). There were no significant changes in other hippocampal sub-fields. The percentage of TGFβ1 to DAPI-stained cells in the entire hippocampal formation also showed no difference following KA-induced seizures (data not shown).

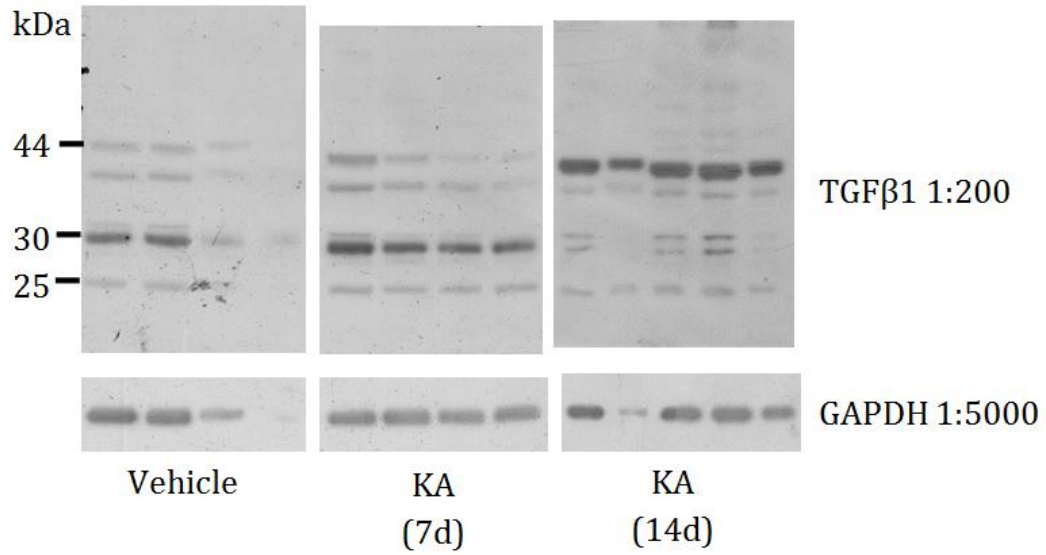

Figure 6.8. Representative western blots for transforming growth factor β1 (TGFβ1) and glyceraldehyde 3-phosphate dehydrogenase (GAPDH) in hippocampal homogenates from C57BL/6J mice at 7 days after treatment with vehicle (distilled water) and at 7 and 14 days after kainic acid (KA)-induced seizures. An equal amount of protein was used for all homogenates and all samples were analysed by western blot using polyclonal antibodies directed against TGFβ1 at 1:200 and GAPDH at 1:5000 dilutions.

Changes in TGFβ1 levels induced by 1400W administration

When 1400W was administered from 1 hour up to 3 days after KA-induced seizures, a significant decrease in the precursor form of TGFβ1 was observed at day 14, from 2.49 (± 0.76) arbitrary units in the control group that also experienced KA-induced seizures, to 0.08 (± 0.01) arbitrary units in the 1400W-treated group (*$p<0.05$) (Figures 6.11 and 6.12). There was also a significant decrease in the dimer form of TGFβ1 at day 7, from 1.54 (± 0.37) arbitrary units in the control group to 0.35 (± 0.01) arbitrary units in the 1400W-treated group ($p<0.05$) (Figures 6.11 and 6.12). In contrast, at 14 days after 1400W treatment there was a significant increase in the expression of the dimer form of TGFβ1 in the hippocampus, from 0.18 ± 0.05 arbitrary units in the control group to 0.56 (± 0.03) arbitrary units in the 1400W-treated group ($p<0.001$) (Figures 6.11 and 6.12). Finally, 1400W treatment reduced the hippocampal expression of the active form of TGFβ1, from 0.18 (± 0.05) arbitrary units (day 7 control) and 0.23 (± 0.04) arbitrary units (day 14 control) to below detectable limits in both cases (both $p<0.01$) (Figure 6.12).

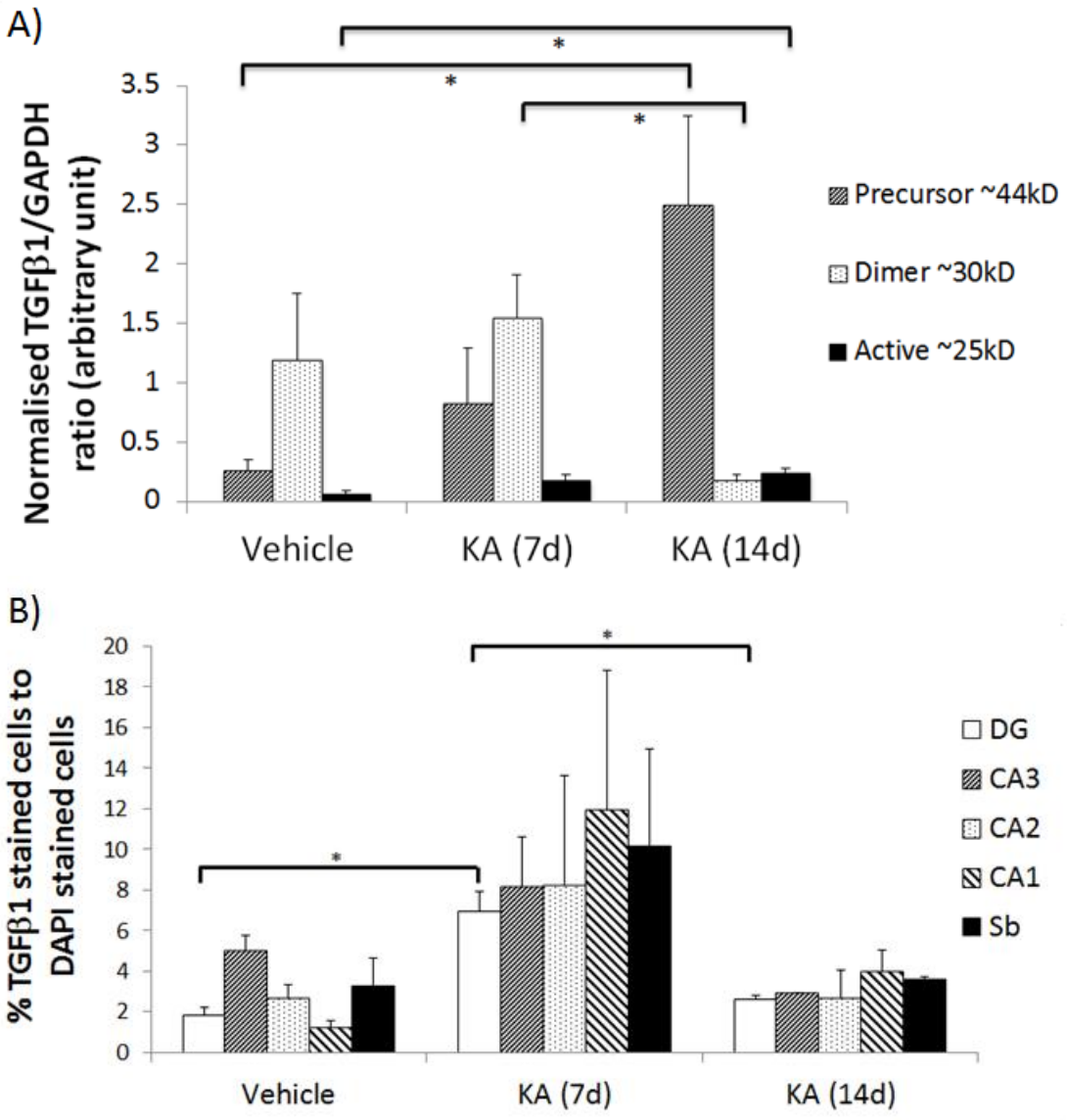

Figure 6.9. The effect of kainic acid (KA) on the abundance of transforming growth factor β1 (TGFβ1) in the hippocampus at 7 and 14 days after KA-induced seizures in C57BL/6J mice. Vehicle-treated control mice received distilled water alone, with hippocampal samples harvested 7 days thereafter. (A) Densitometric analysis was performed on the western blots for the precursor, dimer and active forms of TGFβ1 (n=4-5 per group), and normalised to corresponding glyceraldehyde 3-phosphate dehydrogenase (GAPDH) bands. Data are expressed as the mean (± SEM) TGFβ1 to GAPDH ratio in arbitrary units and was compared statistically using one way Analysis of Variance (ANOVA) with Tukey correction (*p<0.05). (B) Immunohistochemical analysis of TGFβ1 stained cells in relation to 4',6-diamidino-2-phenylindole (DAPI) stained cells in the dentate gyrus (DG), *Cornu Ammonis 3* (CA3), *Cornu Ammonis 2* (CA2), *Cornu Ammonis 1* (CA1) and subiculum (Sb) sub-fields of the hippocampus in mice (n=2 per group). Data are expressed as mean (± SEM) percentage of TGFβ1 to DAPI-stained cells and was compared statistically using one way ANOVA with Tukey correction (*p<0.05).

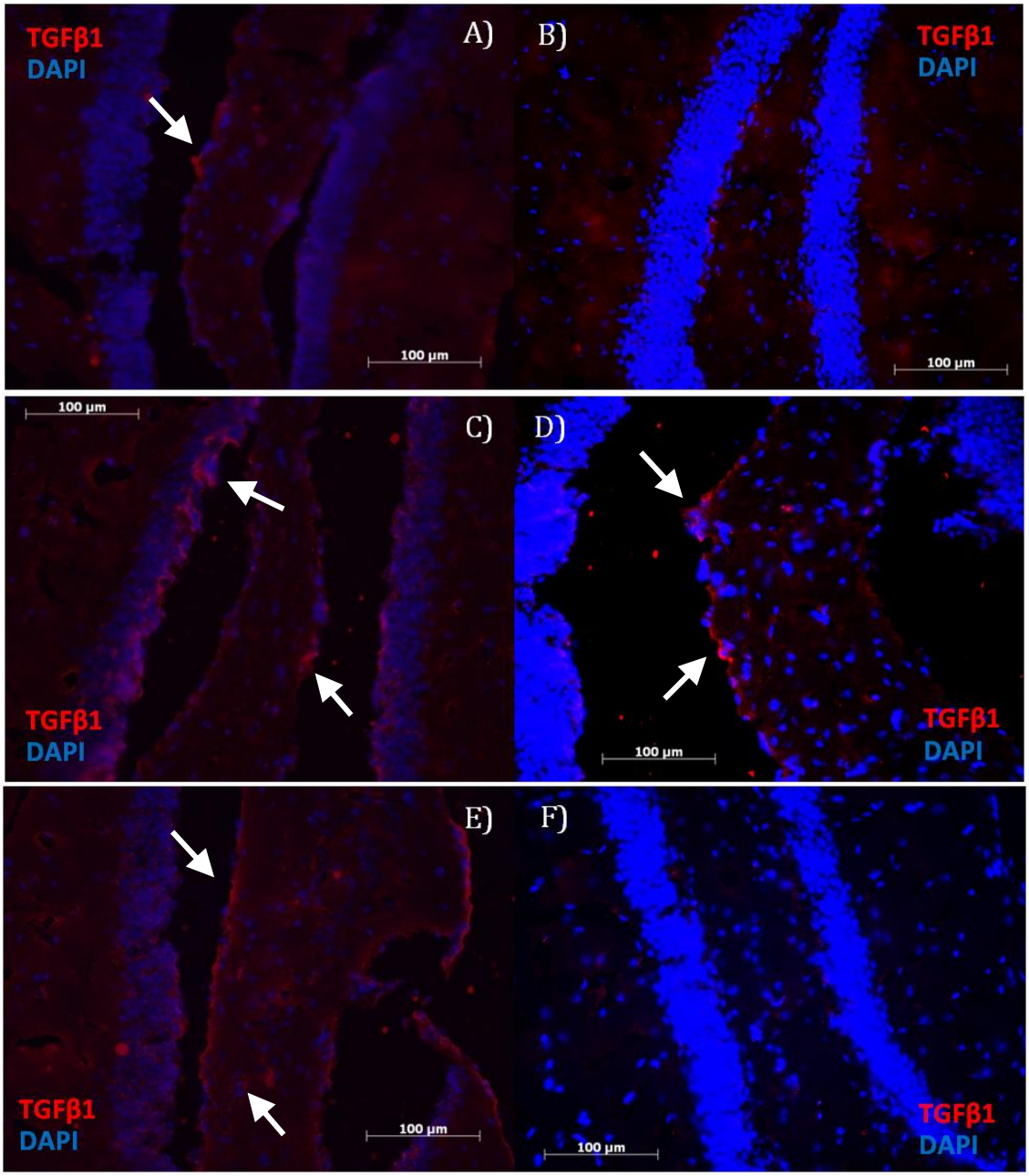

Figure 6.10. The effect of kainic acid on the number of transforming growth factor β1 (TGFβ1) stained cells in the hippocampus at 7 or 14 days after treatment in C57BL/6J mice. Paraformaldehyde-fixed gelatin-embedded mouse hippocampus tissue was cut coronally and the dentate gyrus region of two vehicle-treated control mice (A+B) and two KA-treated mice 7 days (C+D) and 14 days (E+F) after treatment was stained with TGFβ1 antibody conjugated with cyanine fluorescent dye (red). Tissue was counterstained with 4',6-diamidino-2-phenylindole (blue). Magnification, 20X. Scale bar, 100µm.

For IHC analyses, there were no changes in the area of TGFβ1 stained cells after 1400W treatment (data not shown). There was a significant decrease in the percentage of TGFβ1 to DAPI-stained cells in the DG on day 7, from 6.93% (± 0.95) in the control mice to 0.42% (± 0.02) in the 1400W-treated mice ($p<0.05$) (Figure 6.12), but no changes in other hippocampal sub-fields or at day 14 (Figure 6.12). Similarly, there was no effect of 1400W treatment on the percentage of TGFβ1 to DAPI-stained cells across the hippocampal formation as a whole (data not shown).

Changes in TGFβ1 levels induced by PSD95BP administration

Administration of PSD95BP 1 hour after KA-induced seizures resulted in a reduction in the hippocampal expression of TGFβ1 precursor and dimer forms, from 0.82 (± 0.47) arbitrary units (precursor) and 1.54 (± 0.37) arbitrary units (dimer) to below detectable limits at 7 days thereafter (precursor, not significant; dimer $p<0.01$) (Figures 6.13 and 6.14). A similar effect was observed at 14 days, with reductions from 2.49 (± 0.76) arbitrary units (precursor) and 0.18 (± 0.05) arbitrary units (dimer), to below detectable limits of the assay (precursor, $p<0.05$; dimer $p<0.01$) (Figures 6.13 and 6.14). In contrast, hippocampal expression of the active form of TGFβ1 increased significantly from 0.18 (± 0.05) arbitrary units in the control group to 0.49 (± 0.06) arbitrary units in the PSD95BP-treated group on day 7 ($p<0.01$) (Figure 6.14) and again from 0.23 (± 0.04) arbitrary units in the control group to 1.13 (± 0.18) arbitrary units in the PSD95BP-treated group on day 14 ($p<0.01$) (Figure 6.14). No changes were observed in albumin levels using IHC at either day 7 or day 14 (data not shown).

Changes in TGFβ1 induced by combined administration of PSD95BP and 1400W

When PSD95BP and 1400W were administered together after KA-induced seizures, a significant increase in the dimer form of TGFβ1 on day 14 was observed, rising from 0.18 ± 0.05 arbitrary units in the hippocampus of control mice to 1.89 ± 0.24 arbitrary units in that of drug-treated animals ($p<0.001$) (Figures 6.15 and 6.16). There were no treatment-related differences in the expression of the different isoforms of TGFβ1 in the hippocampus at 7 days and no change in the abundance of the precursor and active forms at day 14 (Figure 6.16).

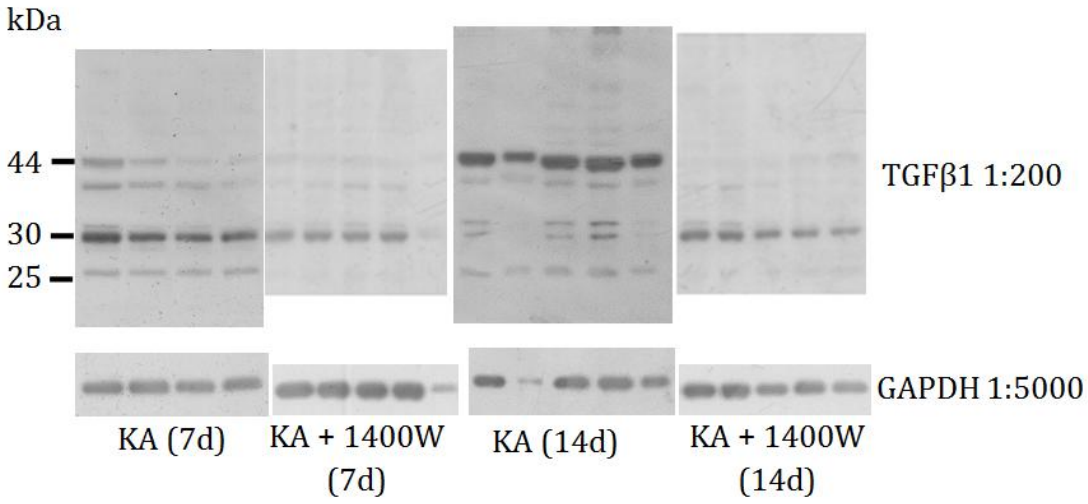

Figure 6.11. Representative western blots for transforming growth factor β1 (TGFβ1) and glyceraldehyde 3-phosphate dehydrogenase (GAPDH) in hippocampal homogenates from 1400W-treated C57BL/6J mice at 7 and 14 days after kainic acid (KA)-induced seizures. An equal amount of protein was used for all homogenates and all samples were analysed by western blot using polyclonal antibodies directed against TGFβ1 at 1:200 and GAPDH at 1:5000 dilutions.

In IHC analysis, there was an increase in the area of TGFβ1 stained cells in the Sb on day 7, rising from 9.06μm^2 ± 1.97 in control animals to 21.36μm^2 ± 0.31 in mice treated with a combination of PSD95BP and 1400W ($p<0.05$) (Figure 6.16 and 6.17), but this did not influence the total area of TGFβ1 stained cells in the hippocampal formation as a whole (data not shown). Likewise, there were no significant differences in the percentage of TGFβ1 to DAPI-stained cells in any of the hippocampal sub-fields, or in the hippocampal formation as a whole, following the combined treatments (data not shown).

6.3.3. Transforming growth factor β receptor 1

The antibodies used for TGFβRI were not detectable using western blot despite increasing the hippocampal supernatant volume to the maximum capacity for each loading well (equivalent to 30μg of protein), and increasing the primary antibody dilution to 1:50. As a result, only IHC was used to quantify TGFβRI expression.

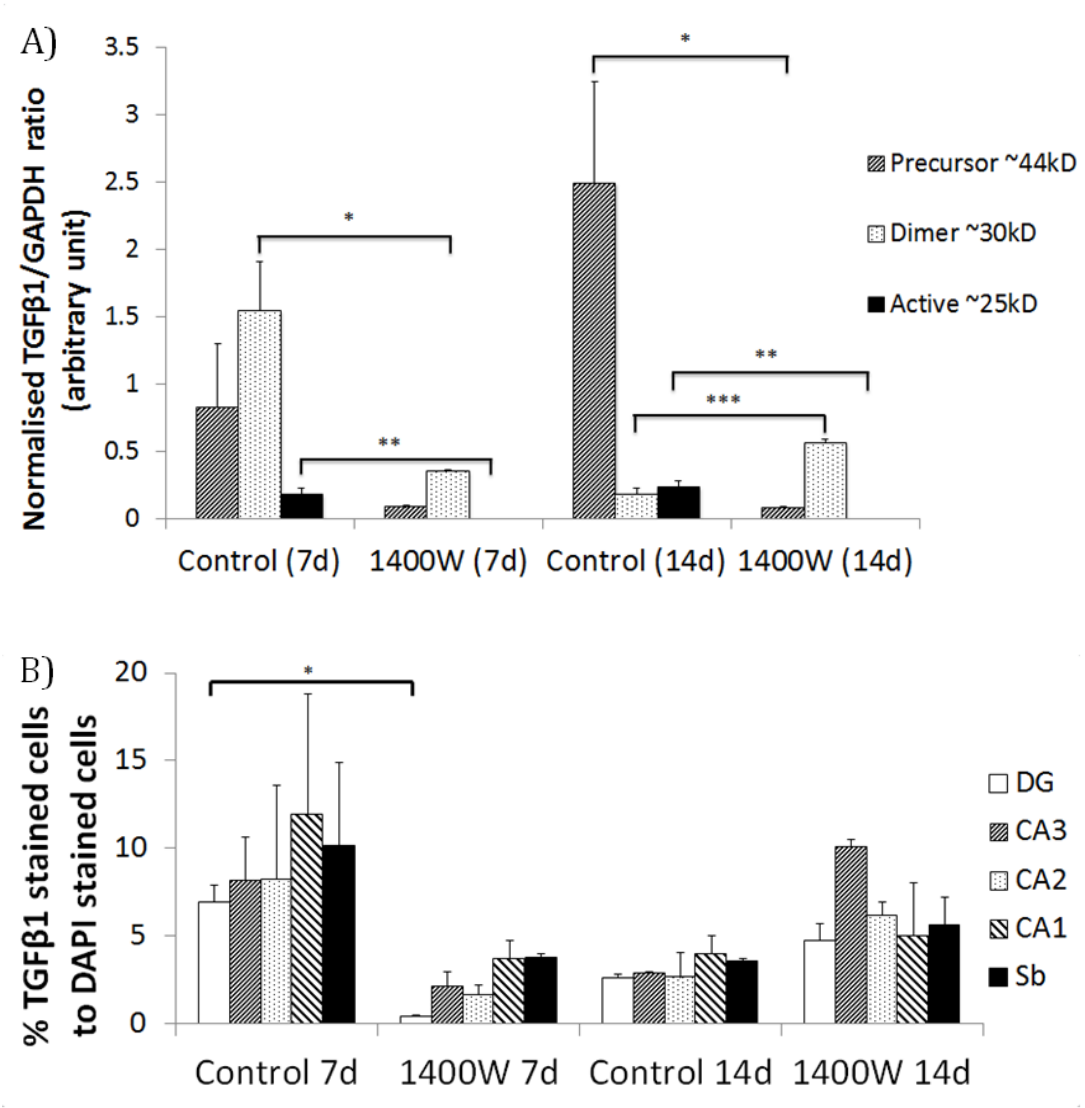

Figure 6.12. The effect of 1400W treatment on the abundance of transforming growth factor β1 (TGFβ1) in the hippocampus at 7 and 14 days after kainic acid-induced seizures in C57BL/6J mice. (A) Densitometric analysis was performed on the western blots for the precursor, dimer and active forms of TGFβ1 (n=4-5 per group), and normalised to their corresponding glyceraldehyde 3-phosphate dehydrogenase (GAPDH) bands. Data are expressed as mean (± SEM) TGFβ1 to GAPDH ratio in arbitrary units and was compared statistically using a one way Analysis of Variance (ANOVA) with Tukey correction (*p<0.05; **p<0.01; ***p<0.001). (B) Immunohistochemical analysis of TGFβ1 stained cells in relation to 4',6-diamidino-2-phenylindole (DAPI) stained cells in the dentate gyrus (DG), *Cornu Ammonis 3* (CA3), *Cornu Ammonis 2* (CA2), *Cornu Ammonis 1* (CA1) and subiculum (Sb) sub-fields of the hippocampus in mice (n=2 per group). Data are expressed as mean (± SEM) percentage of TGFβ1 to DAPI-stained cells and was compared statistically using one way ANOVA with Tukey correction (*p<0.05).

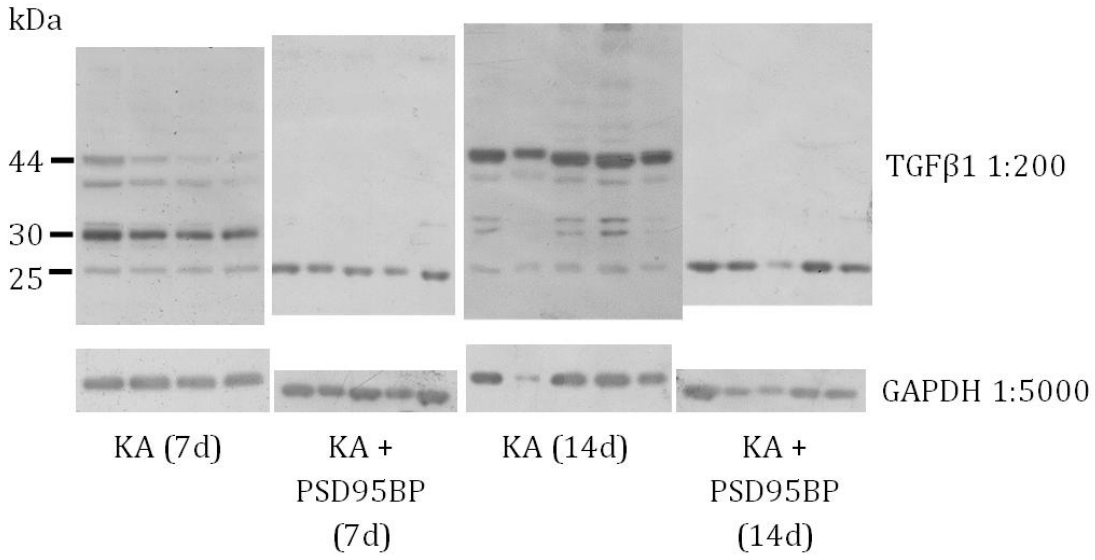

Figure 6.13. Representative western blots for transforming growth factor β1 (TGFβ1) and glyceraldehyde 3-phosphate dehydrogenase (GAPDH) in hippocampal homogenates from post-synaptic density 95 blocking peptide (PSD95BP) treated animals at 7 and 14 days after kainic acid (KA)-induced seizures in C57BL/6J mice. An equal amount of protein was used for all homogenates by western blot using polyclonal antibodies directed against TGFβ1 at 1:200 and GAPDH at 1:5000 dilutions.

Changes in TGFβRI levels induced by KA administration

Following administration of KA to mice, there were no changes in the area of TGFβRI stained cells in the hippocampus or the percentage of TGFβRI to DAPI-stained cells in the hippocampus at either 7 or 14 days after KA-exposure (data not shown). This lack of effect applied equally to all hippocampal sub-fields and the hippocampal formation as a whole.

Changes in TGFβRI levels induced by 1400W administration

Following the administration of 1400W to mice after KA-induced seizures there were no changes in the area of TGFβRI stained cells in the hippocampus on days 7 and 14 (data not shown). The percentage of TGFβRI to DAPI-stained cells in the various hippocampal sub-fields was unchanged following treatment with 1400W (data not shown), but there was a significant reduction in the percentage of TGFβRI to DAPI-stained cells in the hippocampal formation as a whole at day 7, decreasing from 3.50% ± 0.13 in control animals to 1.95% ± 0.16 in the 1400W-treated mice ($p<0.05$) (Figure 6.18).

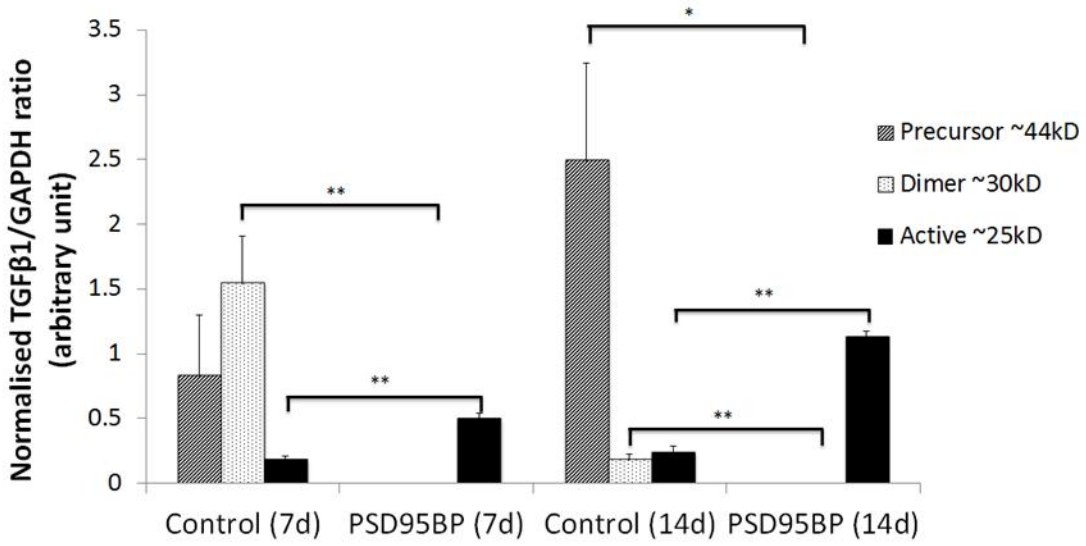

Figure 6.14. The effect of post-synaptic density 95 blocking peptide (PSD95BP) on the abundance of transforming growth factor β1 (TGFβ1) in the hippocampus at 7 and 14 days after kainic acid-induced seizures in C57BL/6J mice. Densitometric analysis was performed on the western blots for the precursor, dimer and active forms of TGFβ1 (n=5 per group) and normalised to the corresponding glyceraldehyde 3-phosphate dehydrogenase (GAPDH) bands. Data are expressed as the mean (± SEM) TGFβ1 to GAPDH ratio in arbitrary units and was compared statistically using one way Analysis of Variance with Tukey correction (*p<0.05; **p<0.01).

Changes in TGFβRI levels induced by PSD95BP administration

Following the administration of PSD95BP administration to mice after KA-induced seizures, there were no changes in the area of TGFβRI stained cells in the hippocampus or the percentage of TGFβRI to DAPI-stained cells in the hippocampus at either 7 or 14 days after KA exposure (data not shown).

Changes in TGFβRI levels induced by combined administration of PSD95BP and 1400W

Combined treatment with PSD95BP and 1400W in C57BL/6J mice following KA-induced seizures had no significant effect on the expression of TGFβRI in any hippocampal sub-field or in the hippocampal formation as a whole when measured by either TGFβRI staining area or as a percentage of DAPI-stained cells and at either 7 or 14 days after KA-exposure (data not shown).

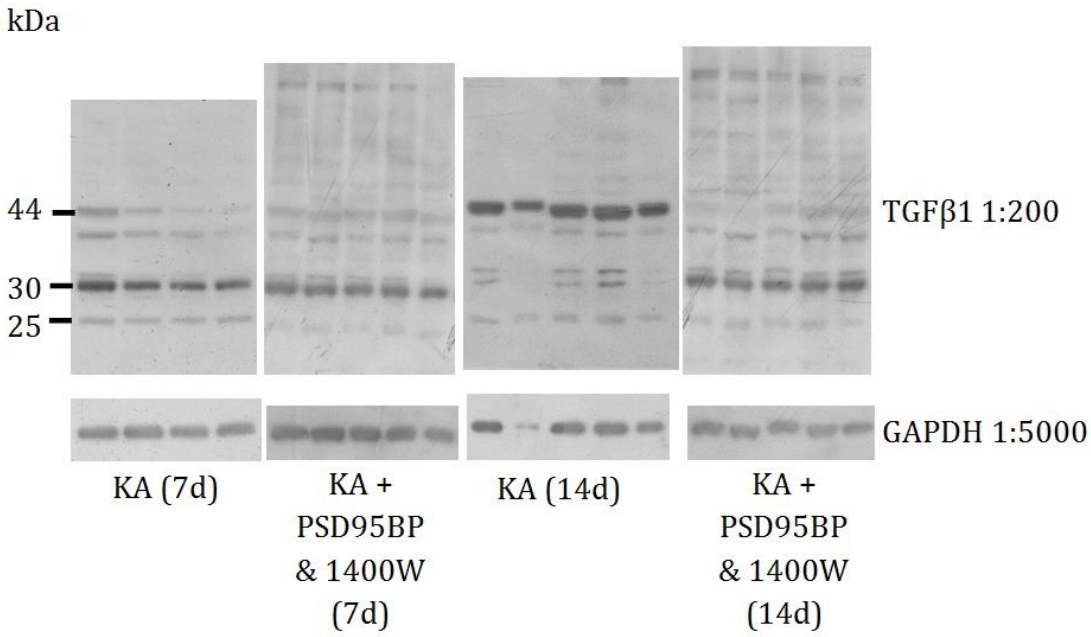

Figure 6.15. Representative western blots for transforming growth factor β1 (TGFβ1) and glyceraldehyde 3-phosphate dehydrogenase (GAPDH) in hippocampal homogenates from C57BL/6J mice treated with a combination of post-synaptic density 95 blocking peptide (PSD95BP) and 1400W at 7 and 14 days after kainic acid (KA)-induced seizures. An equal amount of protein for all homogenates were analysed by western blotting using polyclonal antibodies directed against TGFβ1 at 1:200 and GAPDH at 1:5000 dilutions.

6.3.4. Inwardly-rectifying potassium channel 4.1

Changes in K_{ir}4.1 levels induced by KA administration

Following KA administration to mice, there were no significant changes in K_{ir}4.1 expression, as determined by western blot and by the area of K_{ir}4.1 stained cells in hippocampal sub-fields and in the hippocampal formation as a whole (data not shown). However, a significant reduction in the percentage of K_{ir}4.1 to DAPI-stained cells was observed in the CA3 region at day 7, decreasing from 11.5% (± 2.53) in vehicle-treated control animals to 1.71% (± 0.03) in mice that experienced KA-induced seizures ($p<0.05$) (Figure 6.19). This effect was mirrored by a significant decrease in the percentage of K_{ir}4.1 to DAPI-stained cells, from 5.14% (± 0.29) in the vehicle-treated mice to 2.07% (± 0.58) in the KA-treated mice, in the hippocampal formation as a whole ($p<0.05$) (Figure 6.19). There were no significant changes in the percentage of K_{ir}4.1 to DAPI-stained cells in hippocampal

sub-fields other than CA3 at 7 days (Figure 6.19) and no changes in any measure of $K_{ir}4.1$ expression at 14 days after KA-exposure (data not shown).

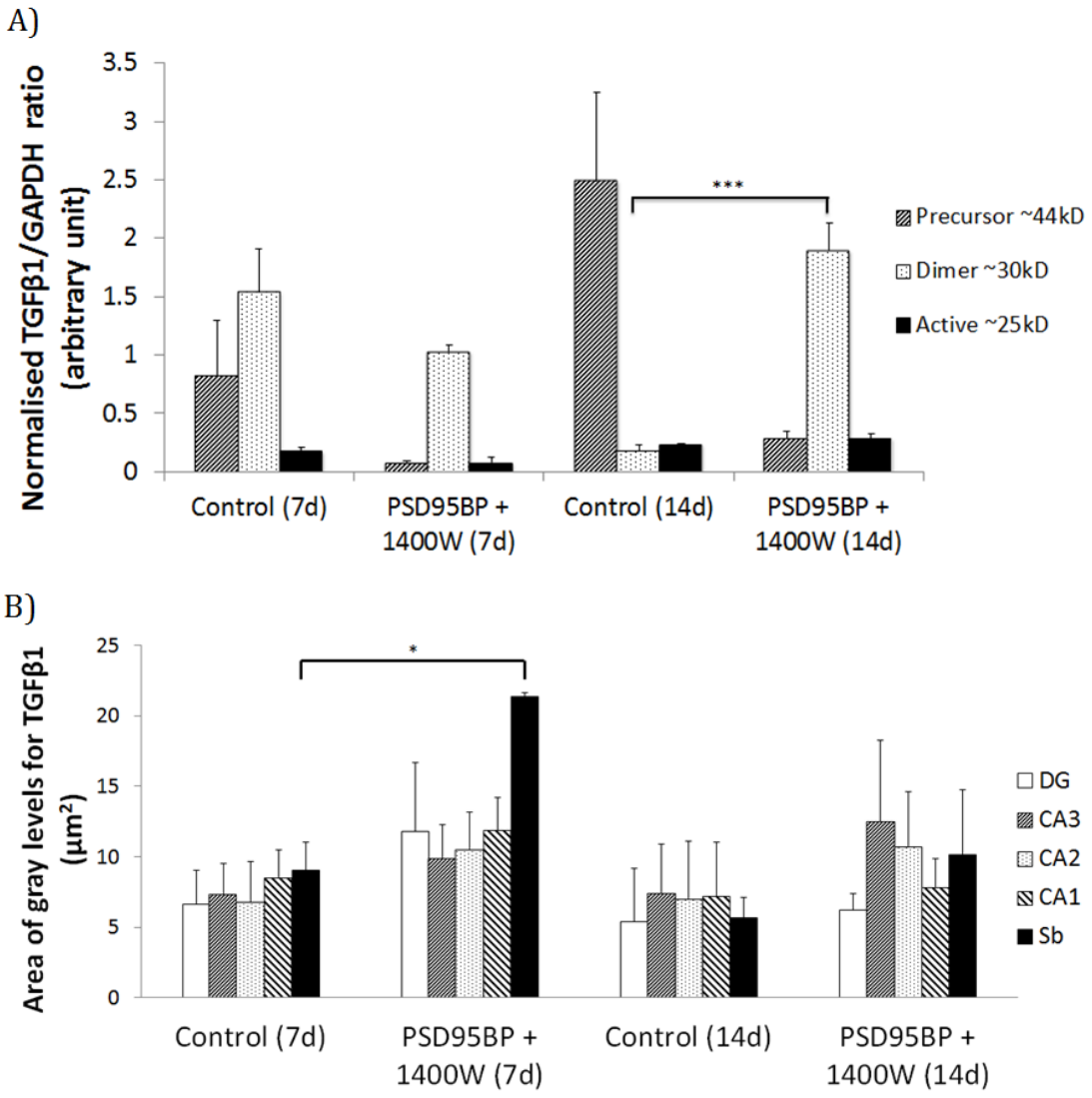

Figure 6.16. The effect of combined treatment with post-synaptic density 95 blocking peptide (PSD95BP) and 1400W on the abundance of transforming growth factor β1 (TGFβ1) in the hippocampus at 7 and 14 days after kainic acid-induced seizures in C57BL/6J mice. (A) Densitometric analysis was performed on the western blots for the precursor, dimer and active forms of TGFβ1 (n=5 per group) and normalised to the corresponding glyceraldehyde 3-phosphate dehydrogenase (GAPDH) bands. Data are expressed as the mean (± SEM) TGFβ1 to GAPDH ratio in arbitrary units and was compared statistically using a one way Analysis of Variance (ANOVA) with Tukey correction (***$p<0.001$). (B) Immunohistochemical analysis of TGFβ1-stained area in the dentate gyrus (DG), *Cornu Ammonis 3* (CA3), *Cornu Ammonis 2* (CA2), *Cornu Ammonis 1* (CA1) and subiculum (Sb) sub-fields of the hippocampus (n=2 per group), with pixel intensity adjusted to a set threshold, in order to standardise gray level for all images. Data are expressed as the mean (± SEM) area of gray levels and was compared statistically using a one way ANOVA with Tukey correction (*$p<0.05$).

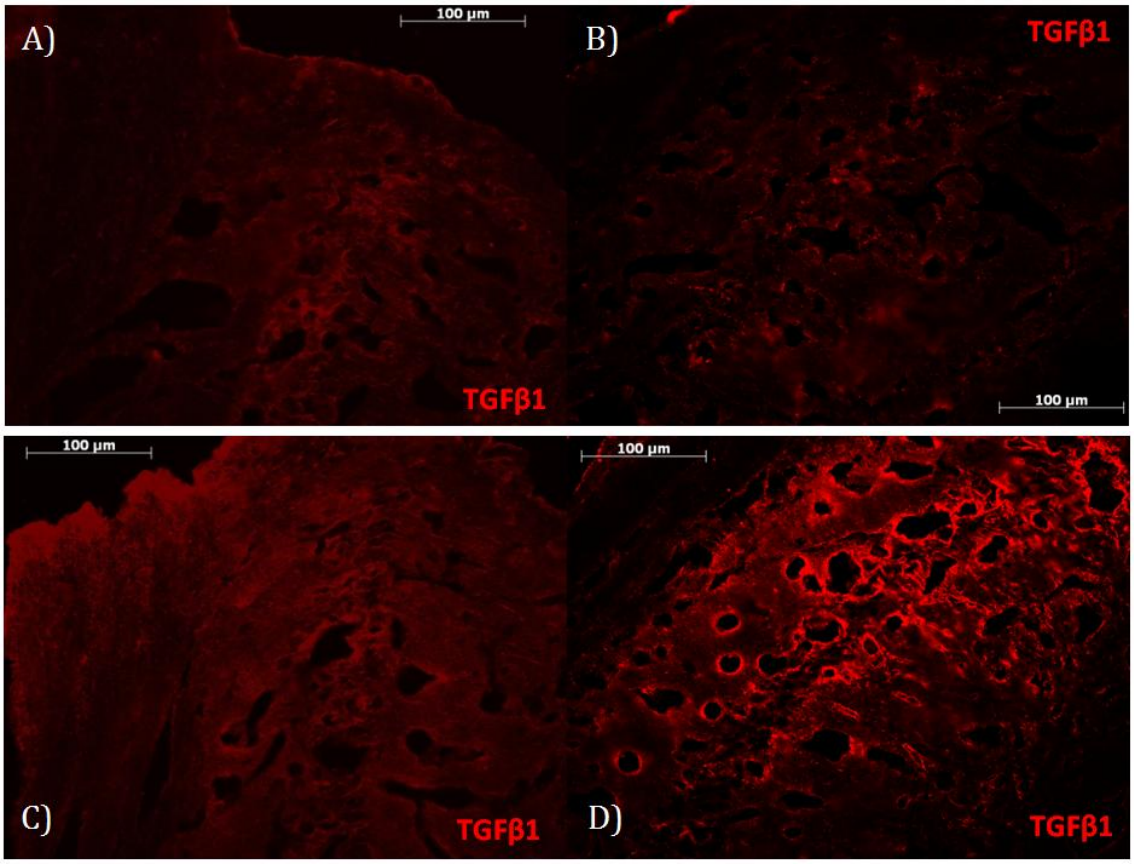

Figure 6.17. The effect of post-synaptic density 95 blocking peptide and 1400W administered together on the area of transforming growth factor β1 (TGFβ1) stained cells in the hippocampus at 7 days after kainic acid (KA)-induced seizures in C57BL/6J mice. Paraformaldehyde-fixed gelatin-embedded mouse hippocampus tissues were cut coronally and the subiculum region of two control mice (A+B) and two drug-treated mice (C+D) were stained with TGFβ1 antibody conjugated with cyanine fluorescent dye (red). Tissue was counterstained with 4',6-diamidino-2-phenylindole (blue). Magnification, 20X. Scale bar, 100µm.

Changes in K_{ir}4.1 levels induced by 1400W administration

Administration of 1400W following KA-induced seizures had no effect on the expression of K_{ir}4.1 levels in the hippocampus or in hippocampal sub-fields, when measured by western blot or when expressed as a percentage of DAPI-stained cells following IHC (data not shown). However, there was an isolated increase in the area of K_{ir}4.1 stained cells in the CA2 sub-field of the hippocampus at day 7, rising from 10.19 (± 0.47) μm^2 in control animals to 14.85 (± 0.51) μm^2 in 1400W-treated mice ($p<0.05$) (Figure 6.20). There were no changes in the area of K_{ir}4.1 staining in other hippocampal sub-fields at day 7, no changes in any sub-fields or in the whole hippocampus on day 14, and the localised increase in K_{ir}4.1 staining in CA2

on day 7 did not impact the area of staining in the hippocampal formation as a whole (data not shown).

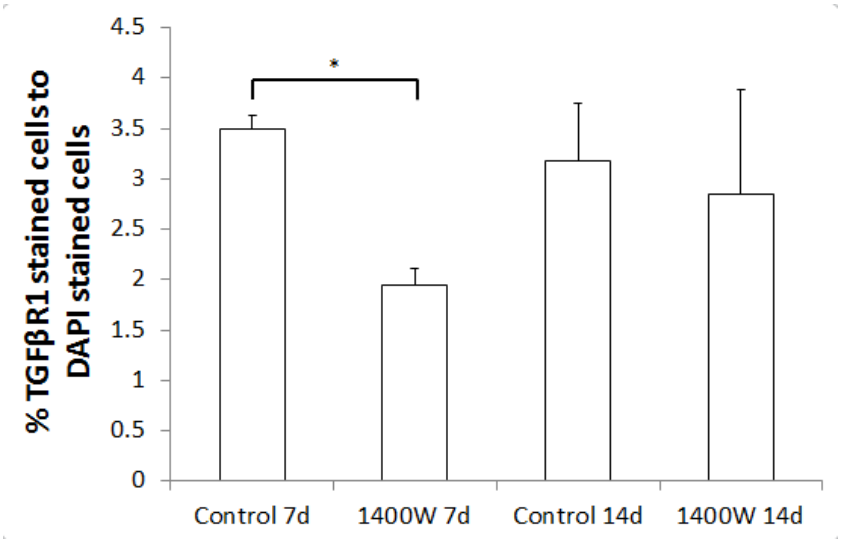

Figure 6.18. The effect of 1400W on the abundance of transforming growth factor β receptor 1 (TGFβRI) in the hippocampus at 7 and 14 days following kainic acid-induced seizures in C57BL/6J mice using immunohistochemical analysis of TGFβRI-stained cells in relation to 4',6-diamidino-2-phenylindole (DAPI)-stained cells in the DG, CA3, CA2, CA1 and Sb sub-fields of the hippocampus (n=2 per group). Data are expressed as the mean (± SEM) percentage of TGFβRI to DAPI-stained cells and was compared statistically using a one way Analysis of Variance with Tukey correction (*p<0.05).

Changes in K_{ir}4.1 levels induced by PSD95BP administration

PSD95BP administration 1 hour after KA-induced seizures was associated with an increase in hippocampal K_{ir}4.1 expression, measured by western blot on day 14, rising from 0.23 (± 0.05) arbitrary units in control animals to 0.65 (± 0.13) arbitrary units in PSD95BP-treated mice ($p<0.05$) (Figures 6.21 and 6.22). No changes in K_{ir}4.1 abundance were noted in any of the IHC analyses (data not shown).

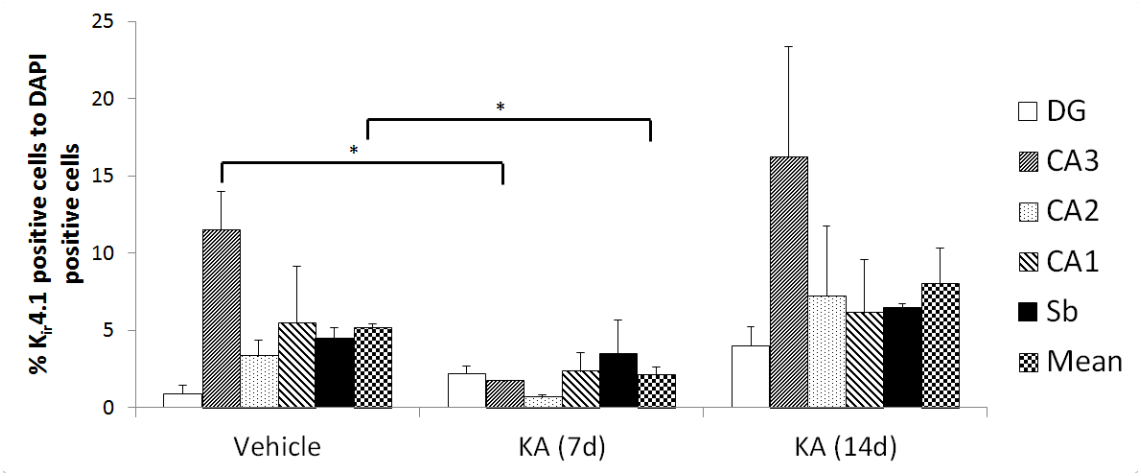

Figure 6.19. The effect of kainic acid (KA) on the abundance of the inwardly-rectifying potassium channel (K_{ir}4.1) in the hippocampus at 7 and 14 days after KA-induced seizures in C57BL/6J mice (n=2 per group). Vehicle-treated control animals received distilled water alone, with hippocampal samples harvested 7 days thereafter. Immunohistochemical analysis for K_{ir}4.1 in relation to 4',6-diamidino-2-phenylindole (DAPI) stained cells in the dentate gyrus (DG), *Cornu Ammonis 3* (CA3), *Cornu Ammonis 2* (CA2), *Cornu Ammonis 1* (CA1) and subiculum (Sb) sub-fields of the hippocampus, and the hippocampal formation as a whole. Data are expressed as the mean (± SEM) percentage of K_{ir}4.1 to DAPI-stained cells and was compared statistically using one way Analysis of Variance with Tukey correction (*p<0.05).

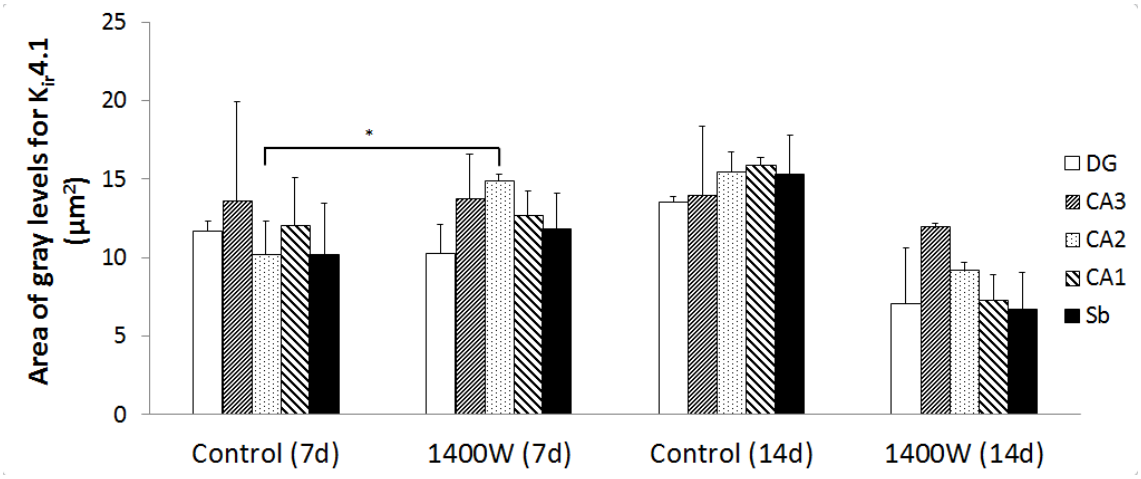

Figure 6.20. The effect of 1400W on the abundance of the inwardly-rectifying potassium channel (K_{ir}4.1) stained cells in the hippocampus at 7 and 14 days following kainic acid-induced seizures in C57BL/6J mice (n=2 per group). Immunohistochemical analysis of the K_{ir}4.1-stained area was undertaken in the dentate gyrus (DG), *Cornu Ammonis 3* (CA3), *Cornu Ammonis 2* (CA2), *Cornu Ammonis 1* (CA1) and subiculum (Sb) sub-fields of the hippocampus, with pixel intensity adjusted to a set threshold in order to standardise gray levels for all images. Data are expressed as the mean (± SEM) area of gray levels and was compared statistically using a one way Analysis of Variance with Tukey correction (*p<0.05).

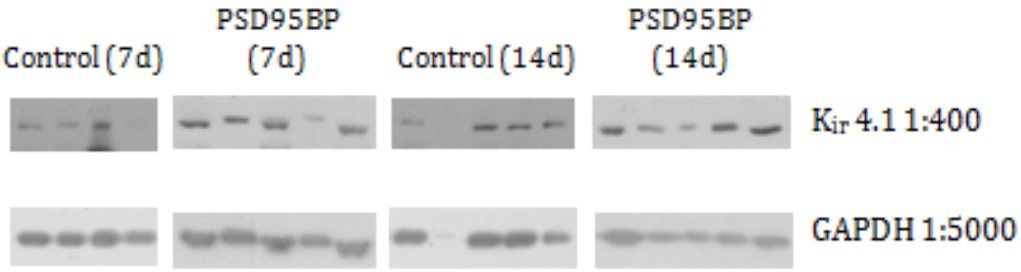

Figure 6.21. Representative western blots for inwardly-rectifying potassium channel (K_{ir}4.1) and glyceraldehyde 3-phosphate dehydrogenase (GAPDH) in hippocampal homogenates from vehicle-treated control and post-synaptic density 95 blocking peptide (PSD95BP) treated animals at 7 and 14 days after kainic acid-induced seizures in C57BL/6J mice (n=4-5 per group). An equal amount of protein for all homogenates were analysed by western blotting using polyclonal antibodies directed against K_{ir}4.1 at 1:400 and GAPDH at 1:5000 dilutions.

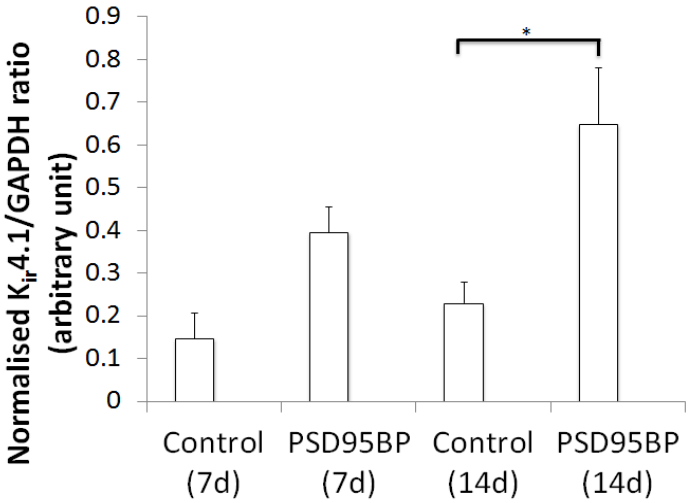

Figure 6.22. The effect of post-synaptic density 95 blocking peptide (PSD95BP) treatment on the abundance of the inwardly-rectifying potassium channel (K_{ir}4.1) in the hippocampus at 7 and 14 days after kainic acid-induced seizures in C57BL/6J mice. Densitometric analysis of the western blot for K_{ir}4.1 in hippocampal homogenates from vehicle-treated control and PSD95BP-treated mice (n=4-5 per group) were normalised to glyceraldehyde 3-phosphate dehydrogenase (GAPDH) bands. Data are expressed as mean (± SEM) K_{ir}4.1 to GAPDH ratio, using arbitrary units, and was compared statistically using a one way Analysis of Variance with Tukey correction (*$p<0.05$).

Changes in K_{ir}4.1 levels induced by combined administration of PSD95BP and 1400W

Combined administration of PSD95BP and 1400W after KA-induced seizures led to a significant elevation in K_{ir}4.1 expression, as measured by western blot, in the

hippocampus on day 14, rising from 0.23 (± 0.05) arbitrary units in control animals to 0.42 (± 0.03) arbitrary units in the drug-treated mice ($p<0.05$) (Figures 6.23 and 6.24). IHC data revealed a significant increase in the area of $K_{ir}4.1$ stained cells in the CA2 region of the hippocampus on day 7, rising from 10.19 (± 0.47) μm^2 in control mice to 13.01 (± 0.4) μm^2 in drug-treated animals ($p<0.05$) (Figure 6.24). There were no changes in the area of Kir4.1 staining in other hippocampal sub-fields on day 7 (Figure 6.24) or in the hippocampal formation as a whole (data not shown). This method similarly failed to find any significant effect of drug-treatment on day 14 (Figure 6.24).

The combined administration of PSD95BP and 1400W after KA-induced seizures resulted in a significant increase in the percentage of $K_{ir}4.1$ to DAPI-stained cells in the CA2, CA1 and Sb sub-fields of the hippocampus on day 7 (Figure 6.24). In CA2, the percentage of $K_{ir}4.1$ to DAPI-stained cells increased from 0.66% (± 0.18) to 16.20% (± 2.05), CA1 increased from 2.32% (± 1.21) to 14.64% (± 2.1), and in the Sb it increased from 3.48% (± 2.17) to 18.41% (± 1.32) (all $p<0.05$) (Figure 6.24). These increases impacted on the overall percentage of $K_{ir}4.1$ to DAPI-stained cells in the hippocampus on day 7, which increased from 2.07% (± 0.58) in control animals to 13.56% (± 2.11) in the drug-treated animals ($p<0.05$) (Figure 6.24).

Further changes were observed at 14 days, at which point the combined treatment was associated with a significant decrease in the percentage of $K_{ir}4.1$ to DAPI-stained cells in the Sb, dropping from 6.48% ± 0.24 in control animals to 1.48% ± 1.29 in drug-treated animals ($p<0.05$) (Figure 6.24). There were no changes in other hippocampal sub-fields on day 14 (Figure 6.24) or in the hippocampal formation as a whole (Figure 6.24).

6.4. Discussion

The purpose of this study was to investigate the effects of KA-induced seizures with or without targeting NO pathway by pharmacological intervention, on albumin-mediated pathways in the brain. Quantification of the expression of albumin, TGFβ1, TGFβRI and $K_{ir}4.1$ in the hippocampus of C57BL/6J mice was

performed using western blot and also IHC, which allowed for more specific regional assessments within the hippocampal formation.

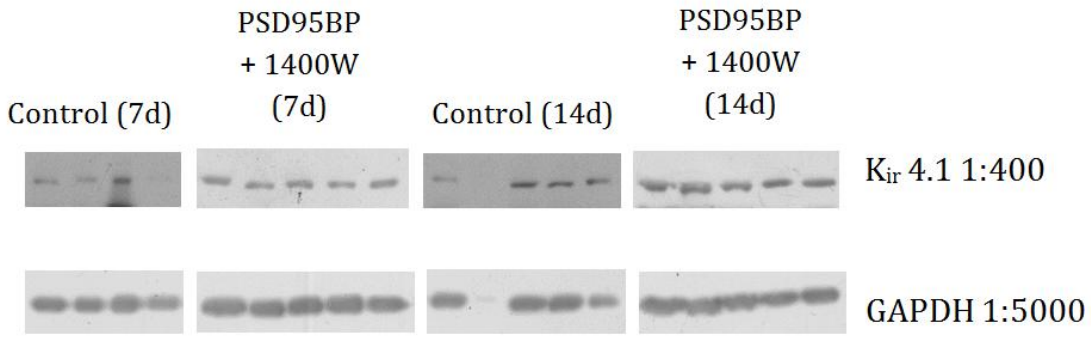

Figure 6.23. Representative western blot for inwardly-rectifying potassium channel ($K_{ir}4.1$) and glyceraldehyde 3-phosphate dehydrogenase (GAPDH) in hippocampal homogenates from control and combined drug treatment (post-synaptic density 95 blocking peptide (PSD95BP) and 1400W) groups at 7 and 14 days after KA-induced seizures in C57BL/6J mice (n=4-5 per group). An equal amount of protein for all homogenates were analysed by western blotting using polyclonal antibodies directed against $K_{ir}4.1$ at 1:400 and GAPDH at 1:5000 dilutions.

6.4.1. Albumin

No significant changes in albumin were observed in the hippocampus at either 7 or 14 days after KA-induced acute insult (Figure 6.3). Given that increased BBB permeability only occurs transiently after the initial insult, it is possible that extravasation of albumin may have occurred before day 7.

When 1400W was administered to mice following KA-induced seizures, the resulting increase in albumin levels in the hippocampus indicates that 1400W has either disrupted BBB permeability or that initial BBB dysfunction after the acute insult was prolonged. There were no changes in plasma albumin levels after 1400W administration, therefore the observed increase in hippocampal albumin is unlikely to be influenced by the peripheral blood. A previous study revealed that NO production is involved in the preservation of BBB function by triggering the release of interleukin-6 (IL-6) (Krizanac-Bengez et al., 2003).

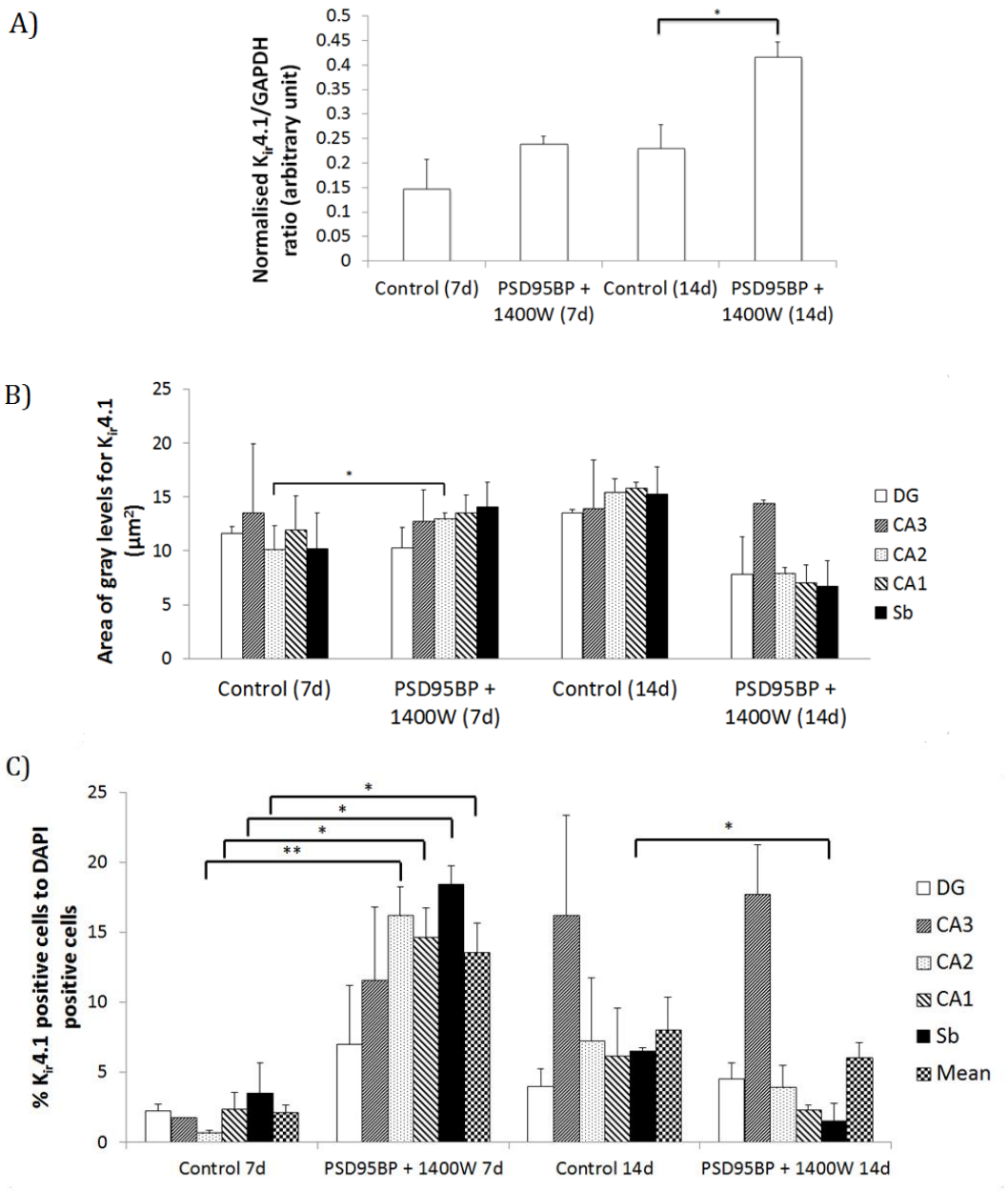

Figure 6.24. The effect of combined treatment with post-synaptic density 95 blocking peptide (PSD95BP) and 1400W on the abundance of the inwardly-rectifying potassium channel (K_{ir}4.1) in the hippocampus at 7 and 14 days after kainic acid-induced seizures in C57BL/6J mice. (A) Densitometric analysis of western blots for K_{ir}4.1 in hippocampal homogenates of control and drug-treated animals (n=4-5 per group). Data are expressed as mean (± SEM) K_{ir}4.1 to glyceraldehyde 3-phosphate dehydrogenase (GAPDH) ratio in arbitrary units and was compared statistically using a one way Analysis of Variance (ANOVA) with Tukey correction (*p<0.05). (B) Immunohistochemical analysis of the K_{ir}4.1-stained area in the dentate gyrus (DG), *Cornu Ammonis 3* (CA3), *Cornu Ammonis 2* (CA2), *Cornu Ammonis 1* (CA1) and subiculum (Sb) sub-fields of the hippocampus (n=2 per group), with pixel intensity adjusted to a set threshold in order to standardise the gray level for all images. Data are expressed as mean (± SEM) area of gray levels and compared statistically using a one way ANOVA with Tukey correction (*p<0.05). C) Immunohistochemical analysis of the K_{ir}4.1-stained cells in relation to 4',6-diamidino-2-phenylindole (DAPI) stained cells in the DG, CA3, CA2, CA1 and Sb sub-fields of the hippocampus, and the hippocampal formation as a whole (n=2 per group). Data are expressed as the mean (± SEM) percentage of K_{ir}4.1 to DAPI-stained cells and was compared statistically using a one way ANOVA with Tukey correction (*p<0.05; **p<0.01).

NO production in astrocytes occurs specifically by iNOS activation through cytokine up-regulation, and blood-borne cytokines such as IL-6 diffuse into the CNS by binding to the BBB endothelial cells (Krizanac-Bengez et al., 2003). Many studies have demonstrated that IL-6 acts as a neuroprotective agent by preserving BBB endothelial cells as part of the ROS defense system (Matsuda et al., 1996; Hayashi et al., 1997; Loddick et al., 1998; Ali et al., 2000; Yamashita et al., 2005; Suzuki et al., 2008; Jung et al., 2011). Inhibition of NOS has been shown to decrease IL-6 production and increase permeability across the endothelial monolayer (Krizanac-Bengez et al., 2003). This may explain, at least partly, the mechanism of 1400W disruption of BBB permeability, leading to an increase in albumin levels in the hippocampus.

When PSD95BP was administered after the KA-induced seizures, no changes in hippocampal albumin levels were observed either 7 or 14 days after treatment. The decrease in plasma albumin levels observed on day 14 is unlikely to have had any impact on epileptogenesis, unless this resulted from extravasation of peripheral albumin into other brain regions that were not measured in this study. PSD95BP and 1400W administered together had no effect in hippocampal albumin levels either 7 or 14 days after treatment.

6.4.2. Transforming growth factor β1

The expression of the precursor and active forms of TGFβ1 showed an upward trend over time following KA exposure. This would suggest that TGFβ1 synthesis and activation increased with time following acute seizures. This result is consistent with reports that showed TGFβ1 up-regulation in the hippocampus of rats that experienced SE (Aronica et al., 2000), and an increase in TGFβ1 activation following a brain insult (Khalil, 1999). The decrease in the dimer form of TGFβ1 from day 7 to day 14 after KA may have been due to the increased demand of TGFβ1 secretion from cells to compensate for the increase in activation at day 14. Using IHC, an increase in TGFβ1 expression in the DG of KA-treated animals was observed at day 7 but was decreased again by day 14. Since the 3 forms of TGFβ1 were not distinguished in the IHC staining, it is not possible to draw any conclusions with regards to the regulation of TGFβ1 activity from this observation.

However, the increase in staining at day 7 was seen only in the DG, which has a role in spatial learning and memory (Amaral et al., 2007; Jonas and Lisman, 2014), and is known to support the neurogenesis of granule cells (Cameron and McKay, 2001; Kempermann, 2002). Seizure-induced neurogenesis has been shown in animal models of epilepsy and was suggested to have a pro-epileptogenic role in the epileptic hippocampus (Parent and Lowenstein, 2002). It is possible that seizure-induced neurogenesis might occur through TGFβ1 since this cytokine can regulate the proliferation and differentiation of cells. Nevertheless, further investigation is required to confirm this hypothesis.

When 1400W was administered after KA-induced seizures, the decrease in the precursor form of TGFβ1 and the failure to detect the active form suggested that 1400W had prevented the increase in TGFβ1 synthesis and activation that were induced by KA exposure. A decrease in the dimer form occurred at day 7, with a rebound increase at day 14 (Figure 6.12). The increase in dimer form at day 14 may have been the result of the reduced activation of TGFβ1 by 1400W, causing a reduced demand for cellular secretion and leading to an accumulation of the dimer form. 1400W also appeared to reverse the increase in TGFβ1 in the DG 7 days after the acute insult (Figure 6.12).

Following administration of PSD95BP, the precursor and dimer forms of TGFβ1 were below detectable limits of the western blot (Figure 6.14). In contrast, an increase in the active form of TGFβ1 occurred with PSD95BP, suggesting that it may have induced the activation of TGFβ1 but not its synthesis.

When PSD95BP and 1400W were co-administered, there was an increase in the dimer form observed at day 14 (Figure 6.16). There were no changes in expression of the precursor and active form of TGFβ1 after the combined treatments, suggesting that increased synthesis and activation caused by KA was not altered by the combined treatment. The increased expression of the dimer form observed after combined treatments may have been related to increased cellular secretion to compensate for TGFβ1 activation. Using IHC, an increase in the area of TGFβ1 staining was observed at day 7 in the Sb sub-field of the

hippocampus (Figure 6.16). The Sb is also responsible for memory retrieval and spatial encoding and plays an important role in the initiation and maintenance of epileptic discharges in TLE (Stafstrom, 2013). Acute overproduction of TGFβ1 in the brain is thought to organise the repair processes and protect neurons from degeneration, whereas chronic overproduction resulted in degeneration (Wyss-Coray et al., 2001). The increase in TGFβ1 in the Sb only occurred at day 7 with no difference in TGFβ1 levels on day 14 compared to vehicle. This transient increase suggests that there is a possibility that the combined treatments contributed to the promotion of repair and protection from TGFβ1 in response to the acute insult in the hippocampal region.

Overall, TGFβ1 synthesis and activation were up-regulated after KA-induced seizures. PSD95BP and 1400W inhibited the increase in TGFβ1 synthesis. 1400W also inhibited the increase in TGFβ1 activation seen following seizures, whereas PSD95BP increased its activation and the combined treatment was without effect. Some hypotheses can be drawn from the regional expressions of TGFβ1 in the hippocampus regarding its contribution towards epileptogenesis. However, because TGFβ1 has multiple functions with complex interactions between different cell types in the brain, further investigation is required to further characterise the mechanism of TGFβ1 regulation in epileptogenesis and the impact of PSD95BP and 1400W, both independently and in combination.

6.4.3. Transforming growth factor β receptor I

Albumin effects in the brain derive from binding to TGFβRI to activate TGFβ signalling (Ivens et al., 2007; Cacheaux et al., 2009). There were no changes in TGFβRI expression after KA-induced seizures. When 1400W was administered, there was an overall decrease in the percentage of TGFβRI stained cells in the hippocampal formation as a whole. When PSD95BP alone or in combination with 1400W were administered after KA-induced seizures, there were no effects on TGFβRI level.

6.4.4. Inwardly-rectifying potassium channel 4.1

The uptake of albumin into astrocytes can result in down-regulation of K_{ir}4.1, with evidence of K_{ir} currents being down-regulated in the CA1 region of the sclerotic hippocampus from epilepsy patients (Hinterkeuser et al., 2000). In the current study, the expression of K_{ir}4.1 was decreased in the hippocampus 7 days after KA-induced seizures, and most prominently in the CA3 region. This is consistent with reported literature showing that K_{ir}4.1 is down-regulated in response to brain insult (Seifert et al., 2006; Wetherington et al., 2008; Heinemann et al., 2012). The CA3 pyramidal cells are the most susceptible hippocampal cell type to the epileptogenic effects of KA (as discussed in chapter 3) and the selective reduction in the expression of K_{ir}4.1 in CA3 may be a marker of KA-induced pyramidal cell loss in this area.

When 1400W was administered following KA exposure, there was an increase in K_{ir}4.1 expression in the CA2 region of the hippocampus at 7 days. The CA2 region is essential for social memory and is known to be damaged in patients with TLE (Helmstaedter et al., 2003; Hitti and Siegelbaum, 2014). The effects of PSD95BP administration were less discrete with an increase in K_{ir}4.1 levels throughout the hippocampus 14 days after KA-induced seizures. When PSD95BP and 1400W were administered together, there was a widespread increase in K_{ir}4.1 abundance throughout the hippocampus and which was most pronounced on day 7. There was sufficient overlap to suggest that day 7 results with combination treatment were largely mediated by 1400W (i.e. effects on CA2) and day 14 results mediated by PSD95BP. However, the combination therapy also led to an increase in K_{ir}4.1 expression in the CA1 and Sb sub-fields of the hippocampus, which are regions that are also affected in epilepsy patients (Lehmann et al., 2000; Stafstrom, 2013).

In summary, it is well-documented that down-regulation of K_{ir}4.1 occurs following BBB dysfunction and that when the brain is exposed to albumin, it triggers the uptake of albumin into astrocytes by TGFβRI, activating TGFβ1 signalling, thereby affecting potassium buffering that can, in turn, affect neuronal excitability leading to epileptiform activity (Perillan et al., 2002; Ivens et al., 2007; Cacheaux et al., 2009; David et al., 2009). From the results reported in this chapter, it would

appear that KA-induced seizures do not affect hippocampal albumin levels, possibly because this is a transient effect that has subsided by 7 days. The seizure-induced reduction in K_{ir}4.1 expression levels may reflect the selective vulnerability of CA3 pyramidal cells to KA neurotoxicity. For the most part, PSD95BP and 1400W reduced or reversed the effects of the seizures. It is important to note that all treatments were given after KA-induced seizures, meaning that their effects are not mediated simply by modulation of the initial insult. Other notable effects were observed including (1) an increase in hippocampal albumin following 1400W treatment that may be explained by iNOS inhibition leading to reduced IL-6 release and preservation of BBB endothelial cells, (2) an enhanced activation of TGFβ1 mediated by PSD95BP but inhibition of its synthesis and secretion, and (3) a possible synergistic effect of PSD95BP and 1400W on K_{ir}4.1, which was characterised by widespread increase in K_{ir}4.1 abundance in the hippocampus that was more extensive than the effects of either drug given alone.

It remains unclear whether albumin mediates its effects in the brain by increasing the level of TGFβ1 since there was no increase in albumin observed after acute seizures in this study. However, KA did up-regulate TGFβ1 synthesis and increased the level of the active form of TGFβ1 that binds to TGFβRI. Further investigations are required to confirm whether these effects may have been the aftermath of a transient increase in albumin that was missed by waiting until 7 days before taking brain specimens. Nevertheless, the therapeutic approach used here, i.e. target NO pathway, has for the first time been shown to moderate and in some cases reverse the cellular effects of KA-induced seizures on TGFβ signalling pathways that are believed to contribute to the development of epilepsy. This represents a positive signal for anti-epileptogenesis.

Chapter 7

The influence of intracranial surgical implantation of electrodes in a kainic acid model of epileptogenesis

7.1. Introduction

The incidence of seizures following intracranial surgery in the clinic is estimated to be 15-20% (Pulman et al., 1996; Manaka et al., 2003). Post-operative seizures are most likely to occur in patients within the first month of surgery and in acute cases, seizures can occur within the first 7 to 10 days (Pulman et al., 1996; Koh et al., 2004). The risk of experiencing a seizure varies greatly depending on the severity of the surgically induced brain insult and the patient's pre-existing neurological conditions (Pulman et al., 1996; Manaka et al., 2003). Seizures after intracranial surgery typically occur as a result of haemorrhage or when the brain tissue becomes ischemic or hypoxic (Manaka et al., 2003). These post-operative seizures may develop into epilepsy (Pulman et al., 1996).

7.1.1. Intracranial surgery in animal models of epilepsy

In some animal models of epilepsy, intracranial surgery is used to implant electrodes for EEG recordings (Galanopoulou et al., 2013) or for electrical kindling (Löscher et al., 1993; 1995; Niespodziany et al., 1999). Surgery can also be used to implant cannulae for intracerebral administration of chemoconvulsants to induce seizures (Ben-Ari et al., 1980; Schwob et al., 1980; Cavalheiro et al., 1982; Rattka et al., 2013). Post-operative seizures in animal models do not commonly occur. However, several studies have reported an alteration in seizure threshold and severity in epilepsy models in which intracranial surgery took place prior to the initial insult (Boast et al., 1976; Löscher et al., 1993; 1995; Ebert and Koch, 1996; Niespodziany et al., 1999). These models typically employed the kindling process to induce seizures. Kindling refers to a phenomenon where daily application of an initially sub-convulsive, behaviourally inert stimulus leads to a progressive increase in seizure sensitivity that manifests initially as focal seizures, then generalised seizures and results in the occurrence of spontaneous seizures (Löscher et al., 1993; Löscher and Brandt, 2010). Implantation of the kindling electrodes causes focal neuronal damage that has been proposed to resemble a penetrating brain injury in humans (Löscher et al., 1993; 1995; Niespodziany et al., 1999; Löscher, 2002) and is thought to play a role in the kindling process (Löscher and Brandt, 2010).

In a study where electrodes had previously been implanted into the amygdala of rats, enhanced susceptibility to electrical kindling was demonstrated by the modified epileptiform pattern of the field potential in *ex vivo* hippocampal slices (Niespodziany et al., 1999). It was also demonstrated in another study that prolonged intra-amygdala electrode implantation induced changes in amino acid levels in several brain regions (Löscher et al., 1993). Depth electrode implantation alone without electrical stimulation results in functionally significant haemorrhagic vascular damage and the consequent extravasation of blood into the brain tissue causing iron deposits (Boast et al., 1976). Brain exposure to iron has been shown to induce chronic focal epileptic discharges (Boast et al., 1976; Willmore et al., 1978). These studies therefore suggest that depth electrode implantation itself may contribute to the development of chronic epilepsy (Willmore et al., 1978). Long-term depth electrode implantation in the limbic system has also been reported to lower the seizure threshold and the rate of kindling of the implanted region (Löscher et al., 1993; 1995). Intracranial surgery has also been shown to reduce the seizure threshold and increase the convulsive response to pentylenetetrazole in rats where intra-hippocampal electrodes were implanted prior to chemical kindling (Löscher et al., 1995), although this observation has not been substantiated to date.

7.1.2. Intracranial surgery on neuroinflammation

The implantation of depth or extra-dural electrodes in the brains of patients and rodents has been shown to lead to widespread chronic neuroinflammation that results from the surgical trauma and the prolonged presence of electrodes in the brain (Yuen et al., 1987; Wolf et al., 1993; Hirshler et al., 2010). This can increase cytokine production, which is also associated with the development of epilepsy (Vezzani et al., 2002; Vezzani, 2004; Matsumoto et al., 2005; Vezzani and Granata, 2005; Choi and Koh, 2008; Vezzani et al., 2008). Cytokines are regulators of responses to infection, inflammation, trauma and immune-system challenge (Matsumoto et al., 2005). They are expressed at very low levels under physiological conditions, however overexpression of cytokines or their expression in regions not associated with inflammation can have adverse effects on overall

immune function (Matsumoto et al., 2005). Pro-inflammatory cytokines promote systemic inflammation, whilst anti-inflammatory cytokines reduce inflammation (Dinarello, 2000; Cavaillon, 2001). In the CNS, increased production of cytokines can occur following several pathological processes (Vezzani et al., 2002; Lehtimäki et al., 2003a; 2007; Vezzani et al., 2013). Increased production of cytokines and their secretion into the cerebrospinal fluid and plasma has been reported after epileptic seizures in humans (Peltola et al., 2000; Lehtimäki et al., 2003b; Sinha et al., 2008).

The involvement of inflammation in disease pathogenesis and prognosis varies depending on the individual cytokine (Deverman and Patterson, 2009). Cytokines are recognised to play important roles in the physiology of the CNS and have implications in the pathogenesis of epilepsy (Probert et al., 1995; Peltola et al., 2000; Vezzani, 2004; Rao et al., 2009). Evidence has shown that pro-inflammatory cytokines interact with glutamatergic neurotransmission and therefore have an impact on neuronal excitability during seizures (Vezzani, 2004). Epileptic seizures can also induce the production of cytokines, which in turn can influence the pathogenesis of the disorder (Li et al., 2011). The roles of pro-inflammatory cytokines, such as IL-1β, IL-6 and tumour necrosis factor alpha (TNF-α), and anti-inflammatory cytokines such as IL-10 have been extensively studied in experimental models and clinical epilepsy (Vezzani et al., 1999; Peltola et al., 2000; Vezzani et al., 2002; Vezzani, 2004; Rao et al., 2009).

Protein expression profiles of inflammatory mediators from surgically resected hippocampi of patients with temporal lobe epilepsy and from serum samples of epilepsy patients have previously been investigated using multiplex immunoassays (Sinha et al., 2008; Kan et al., 2012). The measurement of inflammatory cytokines using a multiplex platform is the most convenient and efficient way of measuring the levels of several cytokines in a single experiment and using only small amounts of biological samples. In this chapter, the MSD electro-chemiluminescence V-PLEX assay was used to explore cytokine levels in plasma and homogenates of cerebral cortex from vehicle and KA-treated mice, with or without prior intracranial surgery. The V-PLEX platform quantifies the

levels of 10 inflammatory cytokines - interferon-γ (IFN-γ), IL-10, bioactive IL-12p70 heterodimer, IL-1β, IL-2, IL-4, IL-5, IL-6, keratinocyte-derived cytokine/growth-related oncogene (KC/GRO) and TNF-α - in a customised 96-well plate with 10-spot multi-array configurations (MSD, USA).

Intracranial surgery is commonplace in animal models of epileptogenesis but it risks causing changes to brain biochemistry and to epileptogenicity that might render the respective model pathologically different from those models that do not incorporate surgery and may therefore model a different 'type' of epileptogenesis, i.e. one that follows a penetrating injury to the brain (Löscher and Brandt, 2010). There is evidence that implantation of intra-cerebral electrodes, which penetrate the *dura mater*, leads to a change in seizure threshold (Boast et al., 1976; Löscher et al., 1993; 1995; Ebert and Koch, 1996; Niespodziany et al., 1999) but it remains unknown if extra-dural electrodes have a similar effect on the threshold to seizures induced by subsequent application of electrical or chemical stimuli. Therefore, the aim of the work described in this chapter was to investigate changes in the threshold to KA-induced seizures, when implantation of extra-dural electrodes had occurred one week prior to seizure induction. Analyses of hippocampal proteins using protein expression modifications and 2D heat map visualisation (as previously described in chapter 5), as well as inflammatory cytokine profiling of the cortex and plasma by multiplex technology were additionally performed.

7.2. Material and methods

7.2.1. Animals

All experimental procedures were completed in accordance with the Animal (Scientific Procedures) Act, 1986 (UK). All methodological details regarding the source of animals, housing conditions, surgical implantation of telemetry electrodes and KA-induced seizures are provided in sections 2.1 and 2.2. Determination of the effects of electrode implantation on seizure threshold was undertaken in all mice described in this thesis, comparing KA sensitivity between implanted and non-implanted animals. In addition, a total of 16 mice were used

exclusively in this chapter for proteomics and MSD multiplex assay. Eight of those animals were surgically implanted with telemetry electrodes, while the remaining eight were surgically naïve (non-implanted). Seven days thereafter, four implanted and four non-implanted mice were subject to KA-induced seizures, with the remainder (4 implanted, 4 non-implanted) receiving treatment with distilled water only as vehicle control. After a further seven days, all mice were euthanised as described in section 2.1.4. Terminal blood samples were collected by cardiac puncture into lithium heparin coated tubes, centrifuged at 2,000 × *g* for 20 minutes at 4°C for the isolation of plasma, and stored at -20°C. Brains were removed and the hippocampi and cortices were dissected and stored in cryovials prior to being snap-frozen in liquid nitrogen. Brain samples were stored in -80°C until required.

7.2.2. Proteomics protocol

All methodological details regarding tissue homogenisation, digestion and LC-MS are described in section 2.4. Tryptic digests of hippocampus homogenates were analysed by nanoflow reversed-phase LC-MS on the Orbitrap Velos™ (Thermo Fisher, UK) at 2h LC gradients with an Orbitrap analyser. Each MS cycle had a full range scan at high resolution followed by sequential fragmentation of the 20 most abundant peptide ions. The fragments were then measured at high mass resolution in the Orbitrap.

7.2.3. Data collection and statistical analysis for proteomics

Raw data files were searched against the Universal Protein Resource (UniProt) mouse database, as previously described in section 5.2.3. Label-free LC-MS analysis with protein identifications from the Mascot search engine based on the UniProt mouse database returned 1,747 protein hits. Statistical analysis of the proteomics data was performed by one-way ANOVA using a built-in tool within the Progenesis software, and with subsequent application of the Bonferroni correction, as described in section 5.2.4. Identified proteins were short-listed on the basis of $p \leq 0.05$.

7.2.4. Protein quantification and interaction mapping

The absolute number of proteins (plus % of total) that were down-regulated, up-regulated and the total that had significantly changed between treatment groups were compared. A heat map was generated using PEAKS Studio 7.0 (Bioinformatics Solutions Inc., Canada). The raw tandem MS data were filtered to a retention time range of 0-270s for each sample and the cut-off value for the peptide feature statistical significance was $p<0.01$.

7.2.5. Linearity of dilution for the Meso Scale Discovery V-PLEX kit

The linearity of dilution was performed on 16 wells of the customised 96-well plate using two cortex supernatant samples. One sample was from a mouse in the non-implanted, non-KA group, while the other sample was from a mouse that had been implanted and treated with KA. These samples were predicted to have the least and the greatest amount of inflammatory changes due to the extent of insult applied to the brain. The preparation of the cortical supernatants for the kit is described in section 2.6.2. Supernatant samples were serially diluted to 1:2, 1:4, 1:8 and 1:16 using Diluent 41 (MSD). The observed values were assessed relative to the assay standard curve produced by the standards solution for all 10 inflammatory cytokines. The results were calculated based on the standard curve and the observed concentration was multiplied by the dilution factor. The criteria for acceptable dilutional linearity was for the corrected observed concentrations to vary no more than 80% to 120% of the theoretical concentration between each serial dilution for each analyte (Ray et al., 2005).

7.2.6. Meso Scale Discovery V-PLEX assay

MSD reagent preparation, experimental protocol and procedure for reading the MSD assay plate are described in section 2.6. Frozen plasma samples were thawed on ice, centrifuged at 10,000 × g for 10 minutes and diluted 1:2 using Diluent 41 before being added to the wells of the customised 96-well plate, in accordance with the manufacturer's instructions (MSD kit reference K15048D-1). The cortex supernatants were diluted using Diluent 41 (MSD) before being added to the remaining wells of the plate. The inflammatory cytokine levels were expressed in

pg/ml for plasma and pg/mg of protein detected in 100 mg/ml cortex tissue, determined using the Bradford protein assay.

7.2.7. Statistical analysis

Statistical analysis of the dose of KA required to induce generalised seizures in naïve, non-implanted mice compared to those that underwent intracranial surgery for electrode implantation was performed by two-sample t-test using SPSS version 21 (IBM). Statistical analysis of the proteomics data is described in section 7.2.3. Statistical analysis of the MSD assay data was performed by one-way ANOVA with Tukey's post hoc test using SPSS. The changes in cytokine levels from the MSD assay were only considered based on statistical significance of $p<0.005$, which incorporates a Bonferroni correction to account for multiple comparisons (n=10). For the purposes of this analysis, cytokine concentrations were assumed to be independent variables.

7.3. Results

7.3.1. KA sensitivity between surgical implanted and non-implanted mice

The effects of surgical implantation of telemetry electrodes on sensitivity to KA-induced seizures was assessed in all animals employed in this thesis. The effect on KA sensitivity was compared in this chapter using the implanted mice from chapter 4 and non-implanted mice from chapters 3, 5 and 6. Therefore, the n numbers of the implanted and non-implanted mice were not balanced because the experiments were not designed for this comparison. The mean total KA dose required to induce acute seizures in 187 non-implanted mice was compared to the dose required to produce the same effect in 15 implanted mice. Implanted mice required significantly lower total KA doses (15.78 (± 1.47) mg/kg) than non-implanted mice (27.98 (± 0.6) mg/kg), to induce the onset of generalised seizures ($p<0.01$) (Figure 7.1). The range of total KA doses for implanted mice was 5 - 30 mg/kg and for non-implanted mice, the range was 15 - 55 mg/kg (Figure 7.2). After a single dose of 5 mg/kg KA, 20% of implanted mice experienced generalised seizures, whereas none of the non-implanted mice did (Figures 7.2 and 7.3). At a total dose of 30 mg/kg KA, all implanted mice had experienced generalised

seizures, compared to just 74.4% of non-implanted mice (Figure 7.3). The ED_{50} for the emergence of generalised seizures was 13.1 mg/kg for implanted mice and 24.8 mg/kg for non-implanted mice (Figure 7.3).

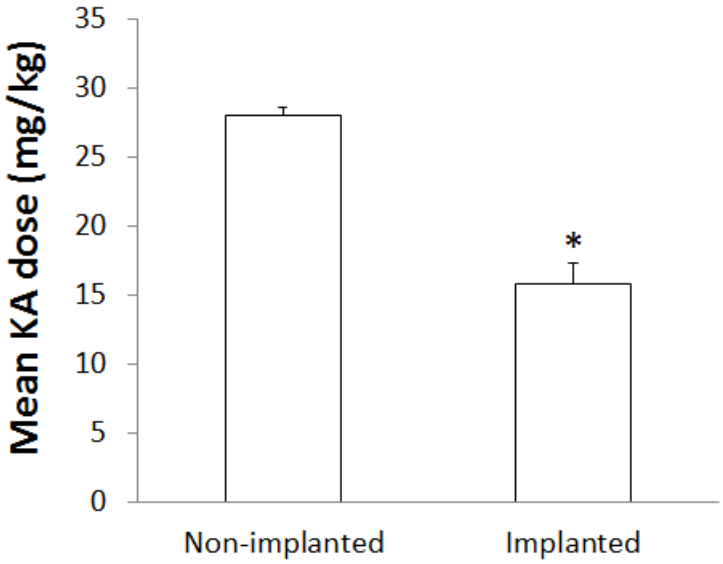

Figure 7.1. The mean kainic acid (KA) dose required to induce generalised convulsive seizures in C57BL/6J mice that were either implanted (n=15) or not implanted (n=187) with extra-dural electrodes one week previously. Data are expressed as the mean (± SEM) KA dose (mg/kg) and compared statistically using two-sample t-test (* $p<0.01$).

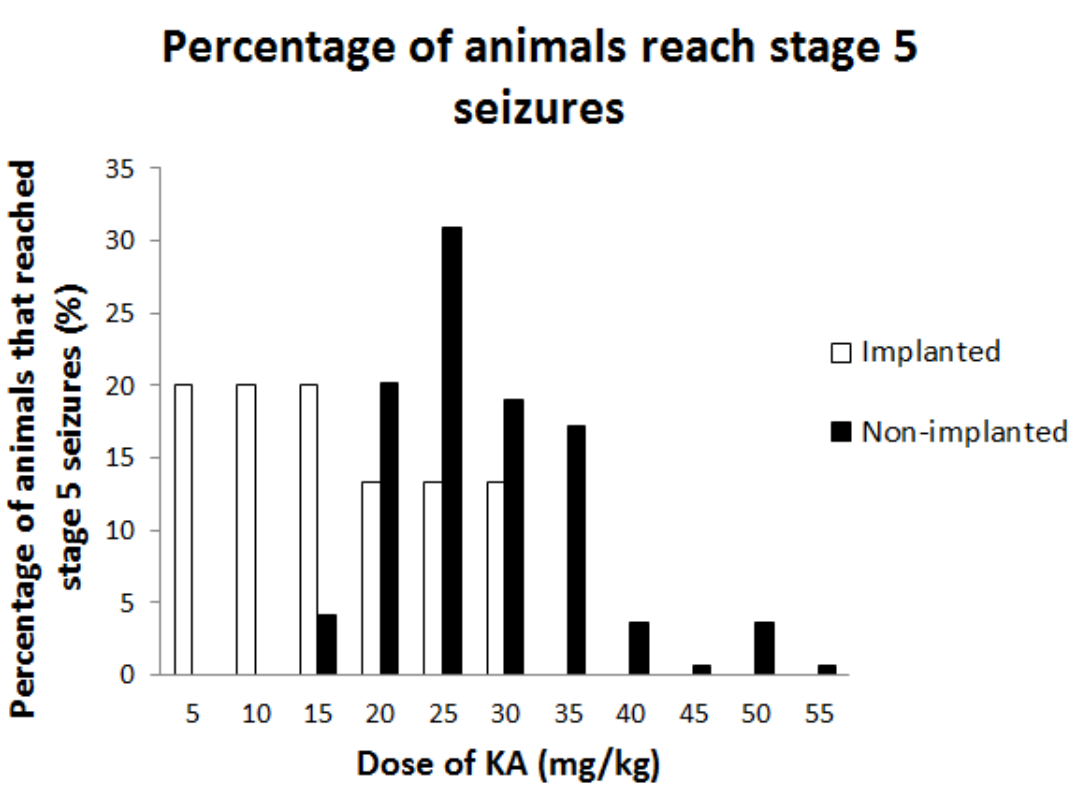

Figure 7.2. Total kainic acid (KA) dose required to induce generalised convulsive seizures in C57BL/6J mice that were either implanted (n=15) or not implanted (n=187) with extra-dural electrodes one week previously. Data are expressed as a percentage of the total number of animals in each group that reached Stage 5 seizures at each dose increment.

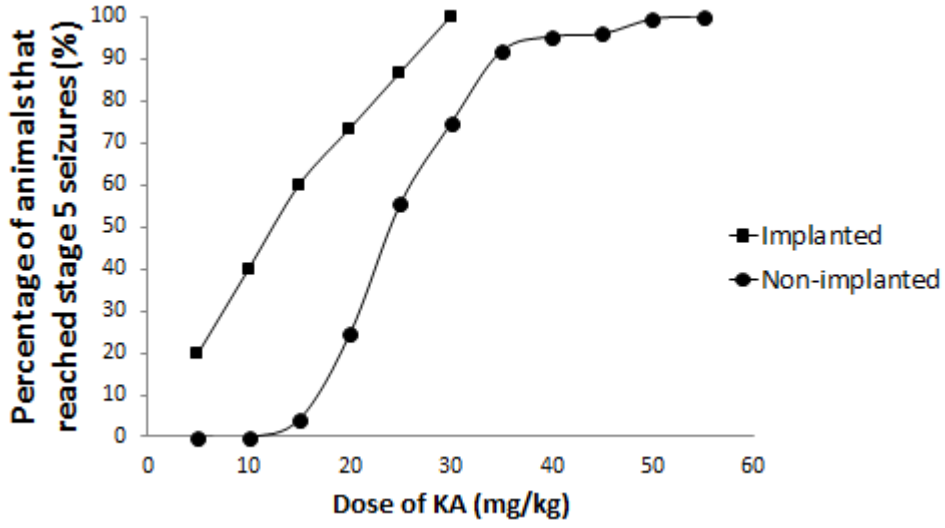

Figure 7.3. Relationship between total kainic acid (KA) dose and emergence of Stage 5 generalised convulsive seizures in C57BL/6J mice that were either implanted (n=15) or not implanted (n=187) with extra-dural electrodes one week previously. Data are expressed as a cumulative percentage of the total number of animals in each group.

7.3.2. Protein expression between non-implanted and implanted mice

Comparisons between treatment groups in terms of proteomic profile were represented as the number of proteins that were significantly down-regulated, the number that was significantly up-regulated, and number that was significantly changed overall as a percentage of the 1,747 proteins identified. The effects of surgical implantation of electrodes and/or KA exposure on hippocampal protein expression are shown in Table 7.1. The impact of surgery was greater than that of KA-induced seizures in terms of the number of proteins with altered expression. KA had a greater effect in non-implanted animals (144 proteins altered; 8% of total) than it had in implanted animals (77 proteins altered; 4% of total) (Table 7.1). Likewise, surgical implantation of electrodes had more impact on hippocampal protein expression in animals that did not subsequently receive KA (474 proteins altered; 27% of total) than in those that did receive KA (354 proteins altered; 20% of total) (Table 7.1).

Treatment group comparisons	Down-regulated (n)	Up-regulated (n)	% significant of all proteins identified
NS+V vs. S+V	266	208	27%
NS+V vs. NS+KA	45	99	8%
S+V vs. S+KA	39	38	4%
NS+KA vs. S+KA	172	182	20%

Table 7.1. Comparison of the change in hippocampal protein expression between treatment groups, reported as absolute numbers and percentage of total identified proteins. Treatment groups (n=4) comprised animals that had undergone surgery (S) for electrode implantation or no surgery (NS) and that subsequently received kainic acid (KA) to induce seizures or vehicle (V) as a control. Data reports proteins with significantly (one-way Analysis of Variance with Bonferroni correction, $p<0.05$) altered expression only, either as an absolute number (n) or as a percentage of all identified proteins (n=1,747).

7.3.3. Heatmap expression

Protein quantification using heat map visualisation was based on the detected peak areas of the top-3 unique peptide ratios calculated from the raw MS/MS data, as described in section 5.3.3. The hippocampi of implanted mice showed increased

peak areas of the majority of proteins in the heat map visualisation compared to non-implanted mice, irrespective of whether animals subsequently received KA or vehicle (Figure 7.4). In contrast, there was much less difference in the effect of KA compared to vehicle in either implanted or non-implanted animals (Figure 7.4).

7.3.4. Meso Scale Discovery V-Plex analysis

Linearity of dilution assessment

According to the manufacturer's instructions, the MSD assay had been validated on mouse serum, plasma and urine samples, but not on mouse brain samples. Therefore, a pre-study validation assessing serial dilutions of mouse cortex supernatant was conducted to determine the extent of the sample dilution required in order that the MSD assay remained in the linear range for each cytokine.

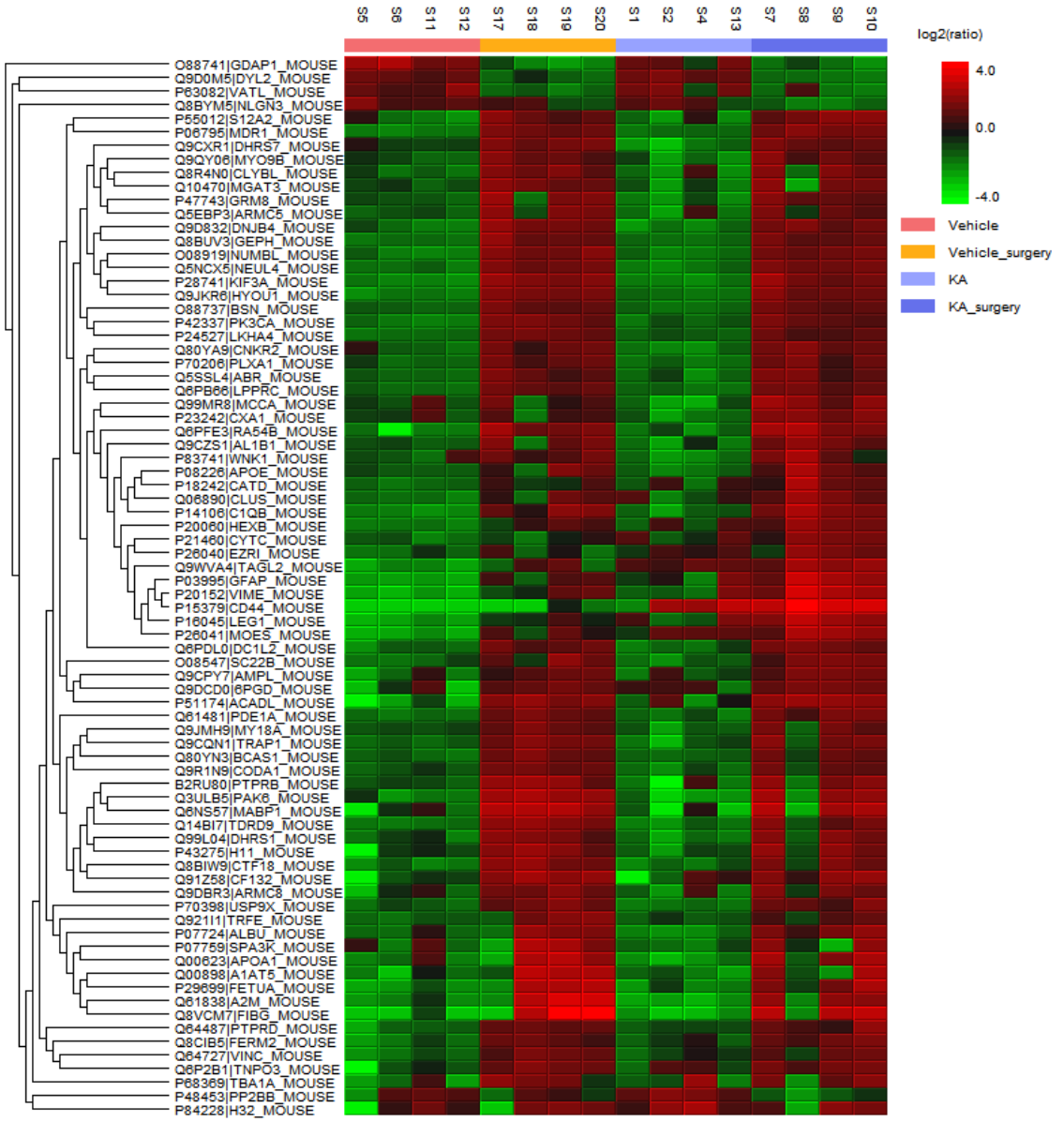

Figure 7.4. Heat map display illustrating the difference in hippocampal protein quantification in groups of animals that had undergone surgery for electrode implantation or no surgery and that subsequently (7 days thereafter) received kainic acid (KA) to induce seizures or vehicle as a control. Protein quantification was based on the detected peak areas of the top-3 unique peptide ratios calculated from raw tandem mass spectrometry data. Each animal in each treatment group is represented by a single column of peak areas, as detailed in the top horizontal bar and corresponding colour key. The vertical axis shows protein peaks with unique peptides identified. Raw data was filtered to a retention time range of 0-270s for each sample and the cut-off value for the peptide feature significance was $p<0.01$. Average peak areas are shown in black, peaks areas smaller than average are shown in green and those larger than average are shown in red.

Two cortical supernatants were used; one from a non-implanted, non-KA mouse that was expected to have the lowest cytokine concentrations and one from an implanted, KA-treated mouse that was expected to have the highest cytokine concentrations. Based on the linearity of dilution results (data not shown), neither

of the serial dilutions showed acceptable dilutional linearity for all 10 analytes, therefore the least diluted sample of 1:2 was considered to be the optimum dilution for the quantification of inflammatory cytokines using the MSD kit.

The detection ranges of all inflammatory cytokines

For the next step, it was necessary to determine whether the cytokine levels in a 1:2 dilution of cortex supernatants lie within the detectable range of the MSD assay.

For IFN-γ, the homogenate samples from the non-implanted mouse (NS+V) and the implanted, KA-treated mouse (S+KA) showed concentrations of 321 and 346 pg/ml, respectively, which lie within the proposed dynamic range (0.0471 to 815 pg/ml) of the MSD kit. For IL-10, supernatants from NS+V and S+KA animals had concentrations of 1016 and 1590 pg/ml, respectively, which lie within the proposed dynamic range (0.742 to 2540 pg/ml) of the MSD kit. For IL-12p70, the NS+V and S+KA animals had concentrations of 429 and 422 pg/ml, respectively, which lie within the proposed dynamic range (7.98 and 22900 pg/ml) of the MSD kit. For IL-1β, the NS+V and S+KA animals had concentrations of 617 and 2367 pg/ml, respectively, and the lower of which lies within the proposed dynamic range (0.123 to 1470 pg/ml) of the MSD kit. For IL-2, the NS+V and S+KA animals had concentrations of 441 and 581 pg/ml, respectively, which lie within the proposed dynamic range (0.259 to 2110 pg/ml) of the MSD kit. For IL-4, the NS+V and S+KA animals had concentrations of 753 and 886 pg/ml, respectively, which lie within the proposed dynamic range (0.120 to 1320 pg/ml) of the MSD kit. For IL-5, the NS+V and S+KA animals had concentrations of 123 and 131 pg/ml, respectively, which lie within the proposed dynamic range (0.0667 to 821 pg/ml) of the MSD kit. For IL-6, the NS+V and S+KA animals had concentrations of 846 and 3838 pg/ml, respectively, the lower of which lies within the detection range of 0.830 to 3490 pg/ml. For KC/GRO, the NS+V and S+KA animals had concentrations of 3032 and 18048 pg/ml, respectively, neither of which lies within the proposed dynamic range (0.208 and 1540 pg/ml). For TNF-α, the NS+V and S+KA animals had concentrations of 866 and 1124 pg/ml, respectively, neither of which lies within the proposed dynamic range (0.127 to 507 pg/ml). For IL-1β and

IL-6, the supernatant from the S+KA mouse, which was expected to have high cytokine concentrations, was above the dynamic range of the assay. For KC/GRO and TNF-α, supernatants from the S+KA mouse and the NS+V mouse, which was expected to have low cytokine concentrations, showed concentrations that were above the dynamic range of the respective assays. This raises a concern that results of these 4 analytes may be unreliable as a result of concentrations being higher than can be accurately measured by the MSD kit at a 1:2 dilution of cortex supernatant. Nevertheless, it was accepted that in an assay with 10 analytes quantified in a single well, some of those analytes would be more reliable than others. Rather than risk diluting the samples further, it was concluded that a 1:2 dilution was preferred and would allow analysis of baseline and moderately elevated concentrations of 8 cytokines from the panel of 10.

Inflammatory cytokine levels in cortex

There were no effects on IFN-γ levels, following surgical implantation of EEG electrodes, irrespective of whether animals receive vehicle or KA, and KA-induced seizures irrespective of whether animals had previously been implanted or not (Figure 7.5A).

There were no effects on IL-10 levels following surgical implantation, irrespective of whether animals subsequently received vehicle or KA, and following KA-induced seizuresirrespective of whether animals had previously been implanted or not (Figure 7.5B).

Surgical implantation of EEG electrodes caused concentrations of IL-12p70 to increase from below detectable limits to 25.87 (± 3.69) pg/mg protein in cerebral cortices of mice that subsequently received vehicle-treatment (NS+V vs. S+V; $p<0.005$). An increase was also seen in implanted versus non-implanted animals that later received KA, with IL-12p70 levels increasing from 8.24 (± 3.21) pg/mg protein to 24.82 (± 1.62) pg/mg protein (NS+KA vs. S+KA, $p<0.005$). There were no effects of KA on IL-12p70 levels, irrespective of whether animals had previously been implanted or not (Figure 7.5C).

There were no effectson IL-1β levels following surgical implantation of EEG electrodes, irrespective of whether animals subsequently received vehicle or KA, and following KA-induced seizures, irrespective of whether animals had previously been implanted or not (Figure 7.5D).

Concentrations of IL-2 in the cerebral cortex were unaffected by surgical implantation of EEG electrodes, irrespective of whether animals subsequently received vehicle or KA, and were also unaffected by KA exposure, irrespective of whether animals had previously undergone surgery (Figure 7.5E).

Concentrations of IL-4 were unaffected by surgical implantation of EEG electrodes, irrespective of whether animals subsequently received vehicle or KA, and were also unaffected by KA exposure, irrespective of whether animals had previously undergone surgery (Figure 7.5F).

Concentrations of IL-5 were unaffected by surgical implantation of EEG electrodes, irrespective of whether animals subsequently received vehicle or KA, and were also unaffected by KA exposure, irrespective of whether animals had previously undergone surgery (Figure 7.5G).

Surgical implantation of EEG electrodes caused concentrations of IL-6 to increase from 16.87 (± 0.53) pg/mg protein to 322.16 (± 80.42) pg/mg protein in cerebral cortices of mice subsequently received vehicle-treatment (NS+V vs. S+V; $p<0.005$). There were no effects of surgery on IL-6 levels in animals that subsequently received KA. Likewise, there was no effect of KA in animals that had not previously been implanted. However, KA exposure did cause a significant decrease in IL-6 levels, from 322.16 (± 80.42) pg/mg protein to 64.01 (± 11.57) pg/mg protein in cerebral cortex of animals that had previously undergone surgery (S+V vs. S+KA; $p<0.005$) (Figure 7.5H).

Concentrations of KC/GRO were unaffected by surgical implantation of EEG electrodes, irrespective of whether animals subsequently received vehicle or KA,

and were also unaffected by KA exposure, irrespective of whether animals had previously undergone surgery (Figure 7.5I).

Surgical implantation of EEG electrodes caused concentrations of TNF-α to increase from 2.08 (± 0.14) pg/mg protein to 5.82 (± 0.4) pg/mg protein in cerebral cortices of mice that subsequently received vehicle-treatment (NS+V vs. S+V; $p<0.005$). An increase was also seen in implanted versus non-implanted animals that later received KA, with TNF-α levels increasing from 2.42 (± 0.12) pg/mg protein to 4.78 (± 0.26) pg/mg protein (NS+KA vs. S+KA; $p<0.005$). There were no effects of KA on TNF-α levels, irrespective of whether animals had previously been implanted or not (Figure 7.5J).

In summary, IL-12p70, IL-6 and TNF-α were significantly increased in cerebral cortex following the surgical implantation of EEG electrodes when animals subsequently received vehicle. IL-12p70 and TNF-α were also significantly increased in cerebral cortex following the surgical implantation of EEG electrodes in those that subsequently received KA. Interestingly, KA treatment had relatively modest effects on the cytokine profile, with no difference from vehicle-treatment in animals that had not previously been implanted, and a decrease in IL-6 and KC/GRO in animals that had previously undergone surgery.

Inflammatory cytokine levels in plasma

The effect of surgical implantation of EEG electrodes and/or KA-induced seizures on the cytokine profile was also explored in plasma samples. There were no significant effects of either surgery or KA exposure on plasma concentrations for all the cytokines (Figure 7.6).

In summary, there were no significant effects of electrode implantation and/or KA-induced seizures on the plasma cytokine profile.

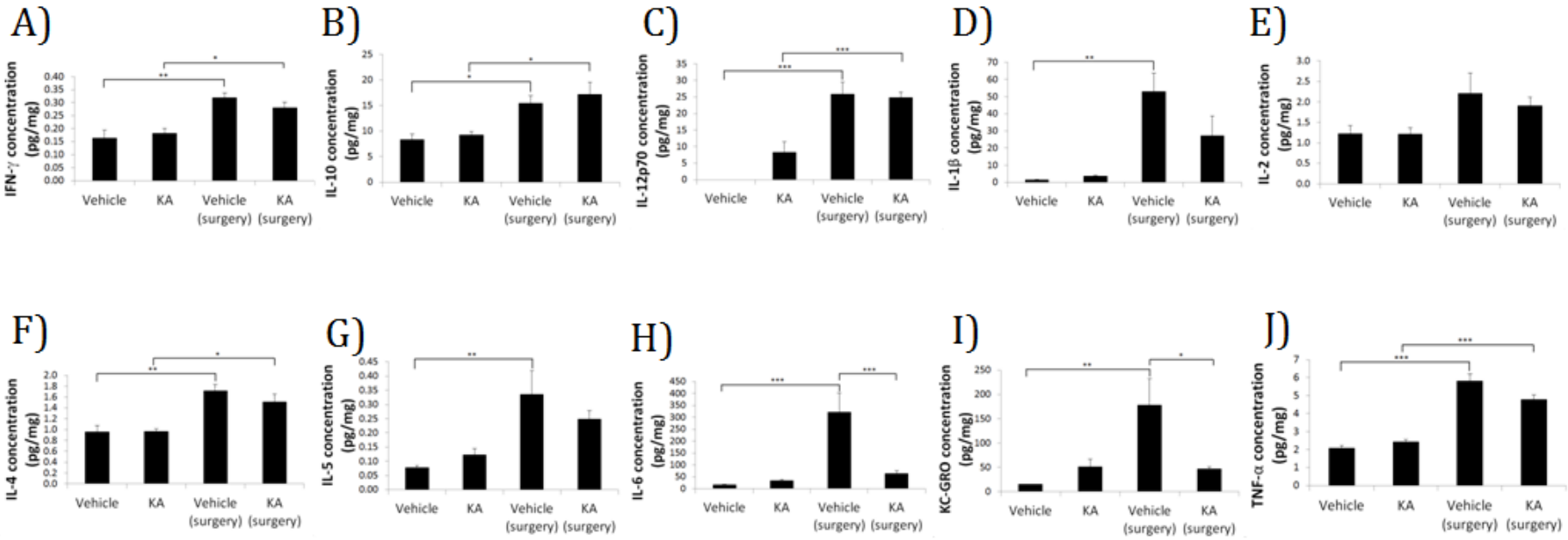

Figure 7.5. The effect of surgical implantation of EEG electrodes and/or kainic acid (KA)-induced seizures on inflammatory cytokine levels in the cerebral cortex of C57BL/6J mice. KA or corresponding vehicle (distilled water) was given 7 days after surgical intervention (where appropriate), with brains samples (n=4) collected 7 days thereafter. The following inflammatory cytokines were measured:(A) interferon-γ (IFN-γ),(B) interleukin-10 (IL-10),(C) interleukin-12p70 (IL-12p70),(D) interleukin-1β (IL-1β),(E) interleukin-2 (IL-2),(F) interleukin-4 (IL-4),(G) interleukin-5 (IL-5),(H) interleukin-6 (IL-6),(I) keratinocyte-derived cytokine/growth-related oncogene (KC-GRO),(J) tumour necrosis factor-α (TNF-α). Data are expressed as the mean (± SEM) cytokine concentration in pg/mg protein was compared statistically using one-way Analysis of Variance with Tukey correction (* $p<0.05$; ** $p<0.01$; ***$p<0.005$).

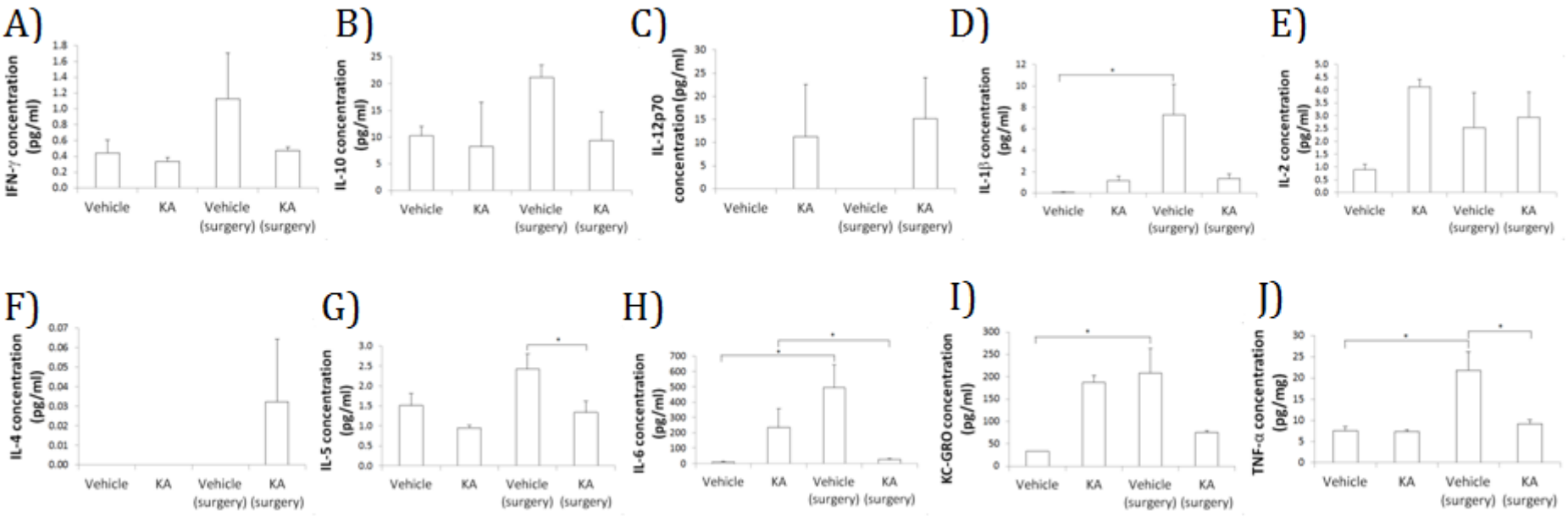

Figure 7.6. The effect of surgical implantation of EEG electrodes and/or kainic acid (KA)-induced seizures on inflammatory cytokine levels in the plasma of C57BL/6J mice. KA or corresponding vehicle (distilled water) was given 7 days after surgical intervention (where appropriate), with plasma samples (n=4) collected a further 7 days thereafter. The following inflammatory cytokines were measured(A) interferon-γ (IFN-γ),(B) interleukin-10 (IL-10),(C) interleukin-12p70 (IL-12p70),(D) interleukin-1β (IL-1β),(E) interleukin-2 (IL-2),(F) interleukin-4 (IL-4),(G) interleukin-5 (IL-5),(H) interleukin-6 (IL-6),(I) keratinocyte-derived cytokine/growth related oncogene (KC-GRO),(J) tumour necrosis factor-α (TNF-α). Data are expressed as the mean (± SEM) cytokine concentration in pg/ml of plasma and was compared statistically using one-way Analysis of Variance with Tukey correction (*$p<0.05$).

7.4. Discussion

The purpose of the work described in this chapter was to assess the impact of intracranial surgery on protein and cytokine profiles in a mouse KA model of epileptogenesis. Extra-dural electrode implantation was performed by drilling burr holes bilaterally and placing the electrode terminals on the surface of the *dura mater*. It was observed from two previous cohorts of mice described in chapter 3 (mice without receiving any surgical procedures) and chapter 4 (mice implanted with EEG transmitters) that the surgical procedure significantly lowered the threshold to generalised seizures induced by KA (Figures 7.1-7.3). This effect may be explained by a localised disruption of the BBB as a result of the surgical procedure, allowing more KA to enter the brain after systemic administration. It is also possible that the surgery causing mechanical or thermal damage to the brain, lowering its tolerance to the neurotoxic effects of KA and rendering the brain more prone to develop acute seizures. Further studies will be required to confirm these hypotheses. The research described in this chapter explored the molecular events occurring in the brain (and plasma) following implantation of EEG electrodes and/or KA-induced seizures using proteomics and cytokine screening in an effort to understand pathways that may have led to altered KA sensitivity.

7.4.1. Proteomics profile and heat map visualisation

A large scale study of proteins was used to compare the neurobiological effects of surgical implantation and/or KA-induced seizures. Comparing the percentage of proteins affected between treatment groups and also the heat map visualisation suggested that the most significant changes in protein expression in the hippocampus occurred as a result of intracranial surgery, irrespective of whether it was followed by administration of vehicle or KA (Table 7.1, Figure 7.4). Overall seizures had a lesser effect on protein expression than surgery and interestingly a more pronounced impact in animals than did not have EEG electrodes implanted than in those that did. This is difficult to understand but may be the result of

adaptive changes in the brain in response to surgical implantation of electrodes that subsequently dampened the proteomic if not epileptogenic effects of KA.

7.4.2. Inflammatory cytokine levels

The results from the multiplex cytokine assay showed that intracranial surgery caused the induction of inflammatory cytokines and that this predominantly occurred centrally rather than peripherally as the majority of cytokines were up-regulated in the brain supernatants and not in the plasma. IL-12p70, IL-6 and TNF-α were up-regulated in the cerebral cortex as a result of the surgical procedure, except for IL-6 in animals that subsequently received KA. All the cytokines investigated here are pro-inflammatory cytokines except for IL-10, that is known to be anti-inflammatory; and IL-5, whose role in inflammation is still unclear (see below). Chronic inflammation has been observed upon histological examination of subdurally implanted brain regions of animals (Yuen et al., 1987; Wolf et al., 1993; Waziri et al., 2009) and extensive neuroinflammation has also been observed using peripheral benzodiazepine receptor labelling in rat brains that were chronically implanted with a transmitter but without any stimulation (Hirshler et al., 2010). However, there are no reported studies showing any effects on individual inflammatory cytokines following extra-dural electrode implantation. The increased expression of 3 pro-inflammatory cytokines in the brain reported in this chapter is consistent with previous findings of intracranial surgery and subdural electrode implantation causing inflammation in the brain.

The roles of the cytokines on inflammation

IFN-γ is a pro-inflammatory cytokine that is produced in inflammatory diseases or by infections and its production is controlled by IL-12 and IL-18, which are also pro-inflammatory (Schroder et al., 2004). Significantly increased levels of IFN-γ have been observed in serum samples from epilepsy patients collected within 24 h of a seizure (Sinha et al., 2008). IL-10 is an anti-inflammatory cytokine that is produced by activated T cells, B cells, keratinocytes and monocytes (Zdanov et al., 1995) and which relays negative feedback signals that dampen the activated

immune system after an inflammatory stimulation (Youn et al., 2013). IL-10 has been shown to be significantly elevated in plasma of patients 48-72 hours after seizure onset (Youn et al., 2013). IL-10 inhibits the production of other inflammatory mediators, including IFN-γ, TNF-α, IL-1, IL-2, IL-6 and IL-12 (Zdanov et al., 1995). It has been suggested that the increase in IL-10 after seizure onset can enhance the inhibition of pro-inflammatory cytokines, therefore IL-10 may have a protective role (Youn et al., 2013). The biological roles of IL-10 and IFN-γ are closely related. These two cytokines have antagonistic effects in several biological assays: IL-10 was found to inhibit IFN-γ production in several immune cells and IFN-γ was found to inhibit IL-10 production in monocytes (Zdanov et al., 1995). IL-10 has also been shown to have anti-convulsant effects against febrile seizures (Ishizaki et al., 2009). An increased production of IL-10 was shown to afford resistance to febrile seizures during infectious disease, especially in predisposed individuals (Ishizaki et al., 2009). Bioactive IL-12p70 is a heterodimer that consists of two subunits: p35 and p40 (Kalinski et al., 2001). IL-12p70 is a pro-inflammatory cytokine produced by dendritic cells, macrophages and B cells in response to microbial pathogens and has a key role in the development of helper T (T_h) cells (Vignali and Kuchroo, 2012). Surgically resected brain tissue from patients with epilepsy has shown a significant increase in IL-12p70 expression alongside marked activation of microglia, astrocytes and diffuse cell death (Choi et al., 2009).

IL-1β is a pro-inflammatory cytokine that exerts pro-convulsant and neurotoxic effects and has been extensively studied in the pathogenesis of epilepsy (Smirnova et al., 2002; Lehtimäki et al., 2003b; Zhu et al., 2006; Balosso et al., 2008). IL-1β mediates an increase in glutamate release, induces phosphorylation of the NR2B subunit of the NMDAR and prevents glutamate uptake by astrocytes (Hu et al., 2000; Balosso et al., 2008; Cacheaux et al., 2009). It has been shown to prolong hippocampal seizures induced by KA by enhancing glutamatergic neurotransmission (Vezzani et al., 1999). TNF-α is a pro-inflammatory, pleiotropic cytokine that is produced primarily by macrophages in response to pathogens

(MacEwan, 2002a; 2002b). TNF-α has been shown to have a direct role in seizure sensitivity (Beattie et al., 2002; Cacheaux et al., 2009; Weinberg et al., 2013). Over-expression of TNF-α causes seizures by promoting the recruitment of AMPA receptors containing the GluR2 subunit to the neuronal membrane, leading to increased calcium influx and enhanced endocytosis of $GABA_A$ receptors (Beattie et al., 2002; Cacheaux et al., 2009). In addition, over-expression of TNF-α increases its pro-inflammatory effects, including leukocyte activation, adherence of neutrophils and monocytes to the endothelium, migration of inflammatory cells into the intercellular matrix, fibroblast proliferation and a locally enhanced production of other pro-inflammatory cytokines (Tracey and Cerami, 1992; Tracey et al., 1994; Probert et al., 1995; Smirnova et al., 2002). Increased levels of TNF-α and IL-1β have been reported to occur after experimental seizures (Lehtimäki et al., 2003b). Significantly increased levels of TNF-α and IL-1β have also been observed in serum samples from epilepsy patients, compared to samples from healthy control individuals when collected within 24 h of a seizure (Sinha et al., 2008).

IL-2, also known as T-cell growth factor, is a pro-inflammatory cytokine that stimulates T-cell proliferation and is essential for the generation and regulation of the immune response (Cantrell and Smith, 1984; Smith, 1988). IL-4 is also a pro-inflammatory cytokine, which induces proliferation and differentiation of T-cells into type 2 T_h cells (Choi and Reiser, 1998; Van Kampen et al., 2005). Significantly increased levels of IL-2 and IL-4 have been observed in serum samples from epilepsy patients collected within 24 h of a seizure (Sinha et al., 2008). IL-5 is another cytokine with a major role in the pathogenesis of asthma and other allergic diseases (Leckie et al., 2000). It is unknown whether IL-5 is a pro- or anti-inflammatory cytokine as its role in inflammation is unclear (Takatsu, 2004). Increased serum levels of IL-5 have been observed in epilepsy patients after treatment with AEDs, including carbamazepine, valproic acid and phenytoin (Andrzejczak, 2011), but there are no reports linking IL-5 levels to the pathogenesis of epilepsy.

IL-6 plays a central role in host defence with pleiotropic activities including immunoglobulin secretion by B cells, maturation of B cells, osteoclast activation and induction of monocyte differentiation into macrophages (Barton, 1996; Smirnova et al., 2002). The biological effects of IL-6 are largely mediated by other cytokines (Peltola et al., 2000), especially IL-1β, which is a potent stimulator of IL-6 production in astrocytes and microglial cells (Erta et al., 2012). IL-6 has a role in adult neurogenesis (Bauer et al., 2007; Deverman and Patterson, 2009) and its levels are transiently increased in response to neuronal injury (Erta et al., 2012). IL-6 concentrations are significantly increased in the cerebrospinal fluid and serum of epilepsy patients within 24 h of a seizure and correlate with seizure severity (Peltola et al., 2000; Lehtimäki et al., 2007; Sinha et al., 2008). This increase in IL-6 is likely to be a consequence of neuronal activity associated with seizures and IL-6 may act as an activation signal for other cytokines in the brain (Peltola et al., 2000). IL-6 has both pro-inflammatory and anti-inflammatory properties, depending on the clinical condition (Jones et al., 2001). Anti-inflammatory IL-6 is capable of limiting neutrophil recruitment and suppresses the activities of pro-inflammatory mediators, such as TNF-α, IFN-γ and IL-8 (Jones et al., 2001). Pro-inflammatory IL-6 binds to IL-6 receptor and forms a complex that has been shown to enhance chemokine and adhesion molecule expression in an *in vivo* model of arthritis (Jones et al., 2001). IL-6 can also afford neuroprotection after an acute seizure insult by preventing the spread of excitation in the rat brain via inhibition of glutamate release (D'arcangelo et al., 2000; Penkowa et al., 2001).

KC/GRO, also known as chemokine C-X-C motif ligand 1 is the IL-8 related protein in rodents (Shiratori et al., 1994). It is a chemoattractant for neutrophils (Shiratori et al., 1994) that directs neutrophils to injured tissues and propagates the inflammatory response by inducing the synthesis of pro-inflammatory cytokines, such as IL-1, IL-6 and TNF-α (Wolpe et al., 1988; Shaftel et al., 2007; Johnson et al., 2011). Chemokines are a family of small proteins involved in the modulation of numerous biological functions, including leukocyte migration and activation, and T

cell activation via G-protein coupled receptors (Cao et al., 2014). Neutrophil infiltration through the BBB is an important step in the development of neuropathology following a seizure insult (Ravizza et al., 2008; Johnson et al., 2011). Significantly increased levels of CXCL-1 in the rat brain have been shown up to 72 hours following SE (Johnson et al., 2011).

Surprisingly, KA failed to have any effects on cytokine expression in animals that had not previously undergone surgery. This contradicts some observations in the literature, including increased expression of IL-1β, IL-6 and TNF-α in rat brains within 24h following KA injection (Lehtimäki et al., 2003b). However, in the current study the hippocampus was dissected 7 days after KA-induced seizures at which point these cytokines may have returned to baseline levels. Looking instead at implanted mice, KA caused a significant decrease in the expressions of IL-6 in the cerebral cortex at 7 days. Reduced expression seems a little strange, especially following electrode implantation and KA-induced seizures, both of which might be expected to elevate cytokine levels, but this may reflect adaptive changes in the brain in the period between surgery and KA exposure.

The effects of intracranial surgery were more pronounced than those of KA. This was particularly evident in animals that subsequently received vehicle treatment to control for the effect of KA exposure. In animals that later received KA, IL-6 levels were unaffected by the impact of surgery Why animals that experienced both surgery and seizures should have lower cytokine levels, or at least a less severe cytokine profile, is unclear but may be the result of the activation of protective mechanisms in the brain following surgery that render it less susceptible to pro-inflammatory insults thereafter.

The role of inflammatory pathways in epileptogenesis is not completely understood (Vezzani et al., 2013), but it is well-documented that some pro-inflammatory cytokines are up-regulated within hours of an acute seizure insult (Vezzani et al., 1999; 2002; Rizzi et al., 2003; Vezzani, 2004; Somera-Molina et al.,

2009). This has led to the hypothesis that inflammation may play a role in seizure-induced brain damage (Rizzi et al., 2003). Three inflammatory cytokines measured in this study showed increased expression in the cortex following surgery but no significant changes after KA exposure in non-implanted animals. This would suggest that intracranial surgery is associated with a greater degree of neuroinflammation in the brain than KA-induced seizures or that neuroinflammation observed following surgery is longer-lasting than that resulting from seizure activity. An additional confounder is the fact that some pro-inflammatory cytokines, such as TNF-α, can have pro-convulsant effects, whereas others, including IL-6 have anti-convulsant effects. A greater increase in anti-convulsant cytokines than in pro-convulsant cytokines following surgery may have moderated the subsequent effects of KA and the consequences of KA-induced seizures.

In conclusion, animals that have undergone surgical implantation of EEG electrodes are more prone to the development of acute seizures following KA-administration than non-implanted animals, even when the electrodes are placed extra-durally and without obvious damage to either the *dura mater* or the cortical surface. The work in this chapter highlights an important issue regarding surgical implantation of electrodes in models of epilepsy, especially when investigating the role of neuroinflammation in epileptogenesis. This is not so important in carefully-controlled studies where all animals receive some form of surgery, with sham-operated animals rather than untreated animals employed as controls. Even then, however, it is possible to over-state or misinterpret the involvement of neuroinflammation. In studies such as this one, where unoperated animals serve as controls, perhaps due to limited resources or limited availability of dummy electrodes and transmitters, a satellite group of implanted animals might be run alongside the main study group, to give an indication of EEG changes in the main group without necessarily recording from all animals. This is not uncommon but it runs the risk of providing false or misleading data regarding the biological changes

that are occurring in the brain and the mechanisms that may be responsible for epileptogenesis.

In this chapter, the total dose of KA required to induce seizures was significantly lower in implanted animals than in those that were not implanted. This is an interesting observation but relatively few animals were implanted and the purpose of the project, as a whole, was not to explore variability *per se* but rather to try to standardise the KA model and use it to investigate the effects of drugs. EEG electrodes were implanted to facilitate that and to look for changes between treatment groups in terms of brain excitability that were not manifest behaviourally. It is important to remember that in the large n number of animals that received KA without previously having undergone surgery, there was still large variability in the dose required to elicit generalised seizures. Likewise, the difference in proteomics and cytokine profiles were observed a small number of animals, and in the case of proteomics, were expressed in relative terms without any real sense of whether the changes were biologically significant.

Nevertheless, the data reported in this chapter suggest that careful considerations are required when comparing results from epilepsy models within and between laboratories, especially where the use of intracranial surgery and/or implantation of electrodes are involved. An epilepsy model with implanted electrodes may not be comparable to the clinical condition as enduring neuroinflammation is not an inevitable characteristic of epilepsy. By optimising surgical techniques, the impact of surgery on the brain might be minimised, however, it is unlikely to be completely eliminated. Opening the skull is always likely to have consequences. The effects of intracranial surgery and depth electrode implantation in epilepsy studies have been explored previously (Boast et al., 1976; Löscher et al., 1993; 1995; Ebert and Koch, 1996; Niespodziany et al., 1999) but the impact may have been underestimated. The findings from this chapter should be considered when choosing an epilepsy model to study and when interpreting data generated from models in which intracranial surgery has been performed.

Chapter 8
General discussion

The overall objective of the work reported in this thesis was to determine whether the effects of PSD95BP and 1400W in a mouse model of epileptogenesis, might represent novel therapeutic strategies for the treatment of TLE. TLE is often resistant to AED therapy and the current alternative approach for drug-resistant TLE is surgical resection to remove specific structural lesions in the hippocampus of patients (Samuel, 2000; Schmidt and Löscher, 2003; Buckmaster, 2004). Several experimental methodologies were employed to explore the effects of potential novel therapeutic drugs in epilepsy.

One of these methodologies involved using an animal model of epileptogenesis to understand the cellular and molecular mechanisms of TLE, and to test potential novel therapies (Herman, 2002; Löscher, 2002; Buckmaster, 2004; Friedman et al., 2009; Bauer and Norwood, 2013). In chapter 3, a KA model of epileptogenesis that employed a repeated dose regimen to administer KA via i.p. injection to C57BL/6J mice was characterised. The hippocampus is susceptible to the epileptogenic effects of KA, which has been shown to elicit patterns of SE-induced neuronal cell loss and astrogliosis in experimental animals that are similar to the neuropathology observed in human TLE. Repeated low dosing of KA was chosen for this model in an attempt to titrate the KA dose according to the animals' behaviour and to ensure that all mice consistently experienced generalised seizures and to limit mortality. Nevertheless, this method introduces variability in the total KA dose that each animal is exposed to. Considerable inter-animal variation in KA sensitivity, acute seizure severity and mortality rate caused by KA-induced seizures was observed. KA has been widely used to induce acute seizures and the variation observed in these experiments was consistent with literature confirming inter-animal variability in response to KA that is difficult to avoid despite refinement of protocols (Lothman et al., 1990; Simonian et al., 1996; Hellier et al., 1998; Kürschner et al., 1998; Hellier and Dudek, 1999; Ben-Ari and Cossart, 2000; Wenzel et al., 2000; Araki et al., 2002; Benkovic et al., 2004; Buckmaster, 2004; Williams et al., 2009; Bauer and Norwood, 2013; Lévesque and Avoli, 2013; Rattka et al., 2013; Carta et al., 2014). Variability might be reduced by

increasing the number of animals used or alternatively by breeding a homogenous colony of mice in-house to reduce batch effects observed in animals from commercial suppliers. However, developing an entirely reproducible model is unrealistic and not representative of the clinical condition.

All mice were single-housed from the start of KA-induced seizures until the end of the experiment when they were then sacrificed. Single-housing animals is thought to induce stress and there is no literature to date that suggests single-housing animals would affect epileptogenesis. However, it has been reported that repeated experimental stress from restraint for 30 minutes accelerated the development of epileptogenesis in a kindling model (Jones et al, 2013). Nevertheless, all animals used in this thesis were single-housed so the effects of the environmental factors would not have affected the epileptogenesis model. In addition to the drugs being explored for their antiepileptogenic potential, animals were exposed to diazepam and pentobarbitone during the course of the various studies. Such drugs have the potential to interfere with the progression of epileptogenesis and to impact results (Aroniadou-Anderjaska et al., 2008; Löscher and Brandt, 2010). However, the administration of GABA agonists after an acute insult has been shown not to prevent epileptogenesis (Halonen et al., 2001; Herman, 2002; Aroniadou-Anderjaska et al., 2008). The use of hypnotic doses of pentobarbitone also did not affect the epileptiform discharges induced by repetitive electrical stimulation of isolated brain tissue (Vazquez et al., 1975). It is therefore unlikely that the administration of diazepam two hours after the onset of KA-induced generalised seizures to standardise the duration of SE, or the overdose of sodium pentobarbitone for euthanasia would have had significant effects on epileptogenesis in this model or on the results reported from this work.

Another method used in this thesis was EEG monitoring of freely-moving mice that allowed an objective and quantitative measure of brain activity in experimental animals to support the subjective behavioural observations that could vary between experimenters. In chapter 4, two EEG algorithms, involving analysis of

spike frequency and EEG coastline, were used to quantify epileptiform activity from extra-dural electrodes. Spike frequency analysis measured the number of electrographic spikes with amplitudes above a pre-specified threshold determined from baseline EEG recordings (prior to acute seizures induced by KA), whereas coastline analysis involved calculating the sum of distances between consecutive data points on the EEG trace over a specified time interval. Both algorithms had previously been shown to have low sensitivity to detect non-convulsive seizures (White et al., 2006). In this chapter, both algorithms were correlated against behavioural seizure severity, which was calculated using modified Racine scores recorded during each 5-minute epoch throughout the 2-hour period of SE. Both algorithms showed changes from baseline after KA-induced seizures. Comparing the two algorithms, spike frequency was shown to correlate better with behavioural seizure severity than coastline analysis. However, neither algorithm could accurately predict the occurrence of spontaneous seizures.

Video monitoring was used concurrently with EEG to confirm the presence of spontaneous seizures following the initial insult. Video monitoring on days 7 and 14 after KA-induced SE showed the occurrence of a spontaneous seizure in 3 mice from the control group, with one mouse experiencing a convulsive seizure on day 7 and the other two experiencing a convulsive seizure each on day 14. No evident seizure behaviour was observed on days 7 or 14 after KA-induced SE in the drug intervention groups that received either PSD95BP plus 1400W combined or 1400W alone. Diazepam administration was used to terminate SE in all mice, with no seizure observed in any animal in the 24 hour period thereafter. This suggests that the seizure behaviour observed in control mice on days 7 and 14 was most likely to be spontaneous seizures arising as a result of an epileptogenic process. Spike frequency and the number of 5-minute epochs with extended EEG coastline per day showed significant differences between the control group and the drug intervention groups. Lower spike frequency and fewer extended coastlines per day in the drug intervention groups is suggestive of potential antiepileptogenic effects by targeting NO pathways using either PSD95BP or 1400W. However, these

EEG effects would require further, extensive review of the video monitoring to confirm the onset of epilepsy and seizure frequency in each animal, which was not possible within the timeframe of this project due to the associated demands on time.

In chapter 5, a large-scale proteomic analysis was used to explore the protein expression profile of the brain and to study alterations in expression that may be linked to seizures and epileptogenesis and that might indicate a potential novel therapeutic target. Tandem MS and label-free quantification was used to measure and compare the relative amount of proteins in hippocampal samples. Another method of quantification was performed using PEAKS to calculate the peptide ratios based on peak areas to visualise the results in a 2D heat map. Protein quantification analyses showed significant changes in the protein profile of the hippocampus following KA-induced seizures. This finding is consistent with a previous study that used 2D gel proteomics quantification and also showed changes in protein expression in the hippocampus following KA-induced seizures (Krapfenbauer et al., 2001b).

Treatment with either PSD95BP or 1400W resulted in fewer affected proteins in control animals than in those previously exposed to KA, suggesting that the effects of drug interventions on protein expression may be selective for brain that has previously undergone a neurological insult. The protein moesin was commonly up-regulated by the effects of KA in vehicle and 1400W-treated mice. This finding suggests that moesin and/or its associated proteins may be direct or indirect targets in KA-induced seizures.

Functional analysis based on protein expression comparisons between treatment groups can be used to map protein-protein interaction networks (Kumar and Mann, 2009). This then allows hypotheses to be made about the role of those proteins within the complex mechanisms underpinning the biological effect using publically available databases (Banks et al., 2000). Follow up studies are obviously

required to confirm these hypotheses. The results from this chapter are novel since there are currently no published reports of proteomics being used to identify the mechanism of potential antiepileptogenic drugs or on interventions targeting NO signalling pathways. A similar approach has however been used to identify proteins that were modified by nitration in the brains of patients with Alzheimer's disease, to provide new insight into potential mechanisms of onset and progression of the disorder (Calabrese et al., 2007).

In order to test the efficacy of the drug interventions on epileptogenesis following an acute brain insult, signalling pathways activated by brain insults and known to contribute to epileptogenesis were investigated. It is commonly known that BBB dysfunction is a hallmark of neurological insults and that albumin can enter the brain via a dysfunctional BBB (Sokrab et al., 1989; Roch et al., 2002; Ballabh et al., 2004; Seiffert et al., 2004; Blyth et al., 2009). The uptake of albumin into astrocytes has been shown to occur via TGFβRI and results in activation of TGFβ1 signalling (Ivens et al., 2007; Cacheaux et al., 2009; Heinemann et al., 2012). This activation can affect potassium buffering via K_{ir}4.1 which can, in turn, cause neuronal excitability leading to epileptiform activity (Ivens et al., 2007; Cacheaux et al., 2009; Heinemann et al., 2012). In chapter 6, the effects of PSD95BP and 1400W on the expression of albumin, TGFβ1, TGFβRI and K_{ir}4.1 were investigated using western blot and IHC. KA-induced seizures increased TGFβ1 activity and reduced K_{ir}4.1 expression in the hippocampus at 7 days, which is consistent with previous reports in the literature (Perillan et al., 2002; Ivens et al., 2007; Cacheaux et al., 2009; David et al., 2009).

Albumin levels increased in the hippocampus when 1400W was administered following KA-induced seizures, indicating that either 1400W caused subsequent damage to the BBB or that 1400W prolonged the increase in BBB permeability induced by the initial insult. This effect is not previously reported in the literature although the induction of iNOS following a brain insult is thought to serve as a defense mechanism by releasing cytokines, such as IL-6, to preserve the BBB

endothelial cells and this mechanism may be crucial to maintaining the integrity of the BBB (Hayashi et al., 1997; Loddick et al., 1998; Krizanac-Bengez et al., 2003; Jung et al., 2011). It has been shown that the release of IL-6 by glia is NO dependent (Krizanac-Bengez et al., 2003). Thus, inhibiting excess NO production that causes neurotoxicity should, in theory, protect the brain against further damage. However, directly inhibiting iNOS activity may also abolish the defense mechanism required to maintain BBB integrity and as a result, may augment the increase in BBB permeability seen after an insult. Since BBB dysfunction has been shown to contribute to epileptogenesis (Ivens et al., 2007; Tomkins et al., 2007; Van Vliet et al., 2007; Tomkins et al., 2008; 2011), direct inhibition of iNOS may not be ideal as a potential antiepileptogenic treatment.

Selective inhibition of the production of NO via iNOS without affecting the release of IL-6 or any other cytokines that may contribute to the defense mechanism in response to the initial insult may be beneficial. 1400W inhibited the increase in TGFβ1 activity following KA and increased K_{ir}4.1 expression after the insult. In contrast, PSD95BP increased TGFβ1 activation but decreased its synthesis and secretion. PSD95BP also increased K_{ir}4.1 expression when administered after KA-induced seizures. Co-administration of PSD95BP and 1400W showed a combination of effects that were consistent with data from experiments in which both drugs were given alone. However, the increase in K_{ir}4.1 expression seen with the combination was more extensive than expected of a simple additive effect, suggesting a possible synergistic effect of the two drug interventions on K_{ir}4.1.

Overall, the drug interventions tended to reverse the effects of KA on TGFβ1 and K_{ir}4.1 expressions in the hippocampus, which may suggest possible restorative effects following KA-induced neurotoxicity. Losaratan, an angiotensin II receptor antagonist approved for the treatment of cardiovascular disorders, has shown antiepileptogenic effects in an experimental model of epilepsy associated with vascular injury by blocking albumin-induced TGFβ activation in the brain and, in turn, the subsequent development of SRS (Bar-Klein et al., 2014). This gives

strength to the suggestion that PSD95BP and/or 1400W can be potential antiepileptogenic agents.

Two distinct groups of mice were used in the research described in this thesis; one group underwent intracranial surgery and the implantation of extra-dural electrodes, while the other group was treatment-naive at the time of KA-induced seizures. To assess the impact of intracranial surgery on epileptogenesis, a comparison between these two groups of mice was undertaken using proteomics and a multiplex cytokine assay (chapter 7). Intracranial surgery lowered the total KA dose required to induce generalised seizures and also caused changes to the neurobiology of the hippocampus and a gross neuroinflammation of the cortex in otherwise naive animals that was more prominent than the effects of KA-induced SE. These findings suggest that the effect of surgery on the brain can potentially compound the initial insult produced by KA.

It is surprising that a surgical technique to implant EEG electrodes in which the *dura mater* remained intact resulted in such a significant change in KA sensitivity. It has previously been reported that intracranial surgery and depth electrode implantation can affect the kindling process used to induce seizures in rodents (Boast et al., 1976; Willmore et al., 1978; Löscher et al., 1993; 1995; Ebert and Koch, 1996; Niespodziany et al., 1999). Depth or subdural electrode implantation has also been shown to lead to widespread chronic neuroinflammation (Yuen et al., 1987; Wolf et al., 1993; Hirshler et al., 2010). The design of epileptogenesis studies comparing naive animals with those that have undergone intracranial surgery requires careful consideration to ensure that the effect of electrode implantation is adequately controlled. Ideally, all animals in any given experiment should either receive EEG electrodes or not; at the very least, a sham-operated control group is required to draw valid conclusions. Fortunately in the work described in this thesis, the effects of the drug interventions were always compared between a control group (that only received KA) and the drug intervention groups (that received drug interventions following KA), except in the analysis of EEG signatures,

where all animals were additionally implanted with EEG electrodes. Thus, all mice in this study had an adequate and corresponding control, meaning that the impact of surgery on epileptogenesis was nullified.

8.1. Review of the current status of glutamate/nitric oxide pathway in epilepsy research

Despite glutamate being one of the more popular targets in the search for new AEDs, only a few glutamate receptor agents have been successful in epilepsy trials. NMDA receptor antagonists have been unsuccessful in clinical trials due to unacceptable adverse effects (Lipton, 2004; Rogawski, 2011). More recently, the focus has been on AMPA receptor as an AED target (Rogawski, 2011). Perampanel is a highly selective non-competitive AMPA receptor antagonist that was recently marketed for the treatment of epilepsy (Hanada et al., 2011; Rogawski, 2011; Ceolin et al., 2012; Löscher and Schmidt, 2012; Krauss et al., 2013). Currently, researchers are exploring KA-type ionotropic glutamate receptors, and specifically the sodium binding site within the channel complex, with the aim of designing an anticonvulsant agent that can prevent sodium flux through the kainate receptor (Dawe et al., 2013). The recent success of PSD95BP in preclinical stroke studies and in phase 2 clinical trials in patients with iatrogenic stroke shows that there may be scope to target NO pathway in the treatment of neurological insults, including epilepsy (Cook et al., 2012; Hill et al., 2012; Savitz and Schäbitz, 2012). 1400W has also been shown to decrease glutamate release and to improve outcome in a rat model of experimental cerebral ischemia (Pérez-Asensio et al., 2005), but there are no reported clinical studies as yet. At this time, there are no other known drug interventions that target the NO signalling pathway and that have shown promise for the treatment of epilepsy.

The influence of NO in epilepsy is still a matter of debate, with studies showing both pro-convulsant and anticonvulsant effects when NO production is inhibited (Del-Bel et al., 1997; Banach et al., 2011). It is likely that the extent to which NO

precipitates seizures is dependent on its brain concentration (Mülsch et al., 1994; Bashkatova et al., 2000; 2003; Gupta and Dettbarn, 2003; Kato et al., 2005; Sumanont et al., 2006), since the balance between neuroprotection and neurotoxicity is dependent on its level of production (Benarroch, 2011). The ability to selectively inhibit the various isoforms of NO synthase is also crucial for a clearer understanding of the physiological and pathological roles of this important signalling molecule.

8.2. Future research

Several further investigations are required to investigate fully whether PSD95BP or 1400W have antiepileptogenic properties and whether these drug interventions might be useful clinically. Although the mouse model used here identified potential antiepileptogenic effects of targeting NO pathway, it is unclear whether this would be translated to humans. If PSD95BP or 1400W can be shown to be at least safe for human use, then it may be possible to test them for their ability to prevent the development of epilepsy following a neurological insult, assuming they can be administered sufficient quickly. Even then, however, this may be unrealistic given the need to treat all individuals with a potentially epileptogenic insult in order to prevent epilepsy in just a few and also given the likely duration of follow-up required. A more realistic approach might be to explore the effects of PSD95BP and/or 1400W in an animal model where drug interventions are not administered until after the onset of SRS. Given that epileptogenesis can continue beyond the first onset of SRS (Williams et al., 2007; 2009), the prevention of the further development of epilepsy by initiating potential antiepileptogenic therapy as soon as an epilepsy diagnosis is made would be a feasible and a potentially beneficial approach. If successful, it would then be useful to investigate how long beyond the insult or first spontaneous seizure the drug interventions remained effective. This would provide information towards the time-window for effective antiepileptogenic therapy in the clinic.

References

Aarts, M., Liu, Y., Liu, L., Besshoh, S., Arundine, M., Gurd, J.W., et al. (2002). Treatment of Ischemic Brain Damage by Perturbing NMDA receptor-PSD-95 protein interactions. Science *298* : 847–850.

Aebersold, R., and Mann, M. (2003). Mass spectrometry-based proteomics. Nature *422*: 198–207.

Alderton, W., Cooper, C.H., and Knowles, R.G. (2001). Nitric oxide synthases: structure, function and inhibition. Biochemical Journal *357*: 1–23.

Ali, C., Nicole, O., Docagne, F., Lesne, S., MacKenzie, E.T., Nouvelot, A., et al. (2000). Ischemia-induced interleukin-6 as a potential endogenous neuroprotective cytokine against NMDA receptor-mediated excitotoxicity in the brain. J. Cereb. Blood Flow Metab. *20*: 956–966.

Altschuler, Y., Barbas, S.M., Terlecky, L.J., Tang, K., Hardy, S., Mostov, K.E., et al. (1998). Redundant and distinct functions for dynamin-1 and dynamin-2 isoforms. The Journal of Cell Biology *143*: 1871–1881.

Amaral, D.G., Scharfman, H.E., and Lavenex, P. (2007). The dentate gyrus: fundamental neuroanatomical organization (dentate gyrus for dummies). Prog. Brain Res.

Ammer, A.G., and Weed, S.A. (2008). Cortactin branches out: Roles in regulating protrusive actin dynamics. Cell Motility and the Cytoskeleton *65*: 687–707.

Amor, S., Puentes, F., Baker, D., and van der Valk, P. (2010). Inflammation in neurodegenerative diseases. Immunology *129*: 154–169.

Anderson, N.L., and Anderson, N.G. (1998). Proteome and proteomics: New technologies, new concepts, and new words. Electrophoresis *19*: 1853–1861.

Anderson, N.L., Hofmann, J.-P., Gemmell, A., and Taylor, J. (1984). Global approaches to quantitative analysis of gene-expression patterns observed by use of two-dimensional gel electrophoresis. Clin. Chem. *30*: 2031–2036.

Andrzejczak, D. (2011). Epilepsy and pro-inflammatory cytokines. Immunomodulating properties of antiepileptic drugs. Neurol. Neurochir. Pol. *45*: 275–285.

Araki, T., Simon, R.P., Taki, W., Lan, J.-Q., and Henshall, D.C. (2002). Characterization of neuronal death induced by focally evoked limbic seizures in the C57BL/6 mouse. J. Neurosci. Res. *69*: 614–621.

Araque, A., Parpura, V., Sanzgiri, R.P., and Haydon, P.G. (1999). Tripartite synapses:

glia, the unacknowledged partner. Trends in Neurosciences *22*: 208–215.

Armengou, A., Hurtado, O., Leira, R., Obón, M., Pascual, C., Moro, M.A., et al. (2003). L-arginine levels in blood as a marker of nitric oxide-mediated brain damage in acute stroke: a clinical and experimental study. J. Cereb. Blood Flow Metab. *23*: 978–984.

Aroniadou-Anderjaska, V., Fritsch, B., Qashu, F., and Braga, M.F.M. (2008). Pathology and pathophysiology of the amygdala in epileptogenesis and epilepsy. Epilepsy Research *78*: 102–116.

Aronica, E., Van Vliet, E.A., Mayboroda, O.A., Troost, D., da Silva, F.H., and Gorter, J.A. (2000). Upregulation of metabotropic glutamate receptor subtype mGluR3 and mGluR5 in reactive astrocytes in a rat model of mesial temporal lobe epilepsy. Eur. J. Neurosci. *12*: 2333–2344.

Baker, G.A., and Jacoby, A. (2013). Quality of Life in Epilepsy (Psychology Press).

Ballabh, P., Braun, A., and Nedergaard, M. (2004). The blood-brain barrier: an overview: structure, regulation, and clinical implications. Neurobiology of Disease *16*: 1–13.

Balosso, S., Maroso, M., Sanchez-Alavez, M., Ravizza, T., Frasca, A., Bartfai, T., et al. (2008). A novel non-transcriptional pathway mediates the proconvulsive effects of interleukin-1beta. Brain *131*: 3256–3265.

Banach, M., Piskorska, B., Czuczwar, S.J., and Borowicz, K.K. (2011). Nitric oxide, epileptic seizures, and action of antiepileptic drugs. CNS & Neurological Disorders - Drug Targets *10*: 808–819.

Banks, R.E., Dunn, M.J., Hochstrasser, D.F., Sanchez, J.-C., Blackstock, W., Pappin, D.J., et al. (2000). Proteomics: new perspectives, new biomedical opportunities. The Lancet *356*: 1749–1756.

Bantscheff, M., Schirle, M., Sweetman, G., Rick, J., and Kuster, B. (2007). Quantitative mass spectrometry in proteomics: a critical review. Anal Bioanal Chem *389*: 1017–1031.

Bar-Klein, G., Cacheaux, L.P., Kamintsky, L., Prager, O., Weissberg, I., Schoknecht, K., et al. (2014). Losartan prevents acquired epilepsy via TGF-β signaling suppression. Ann Neurol. *75*: 864–875.

Bar-Sagi, D., and Feramisco, J.R. (1985). Microinjection of the ras oncogene protein into PC12 cells induces morphological differentiation. Cell *42*: 841–848.

Barton, B.E. (1996). The biological effects of interleukin 6. Med Res Rev *16*: 87–109.

Bashkatova, V., Narkevich, V., Vitskova, G., and Vanin, A. (2003). The influence of

anticonvulsant and antioxidant drugs on nitric oxide level and lipid peroxidation in the rat brain during penthylenetetrazole-induced epileptiform model seizures. Progress in Neuro-Psychopharmacology and Biological Psychiatry *27*: 487–492.

Bashkatova, V., Vitskova, G., Narkevich, V., Vanin, A., Mikoyan, V., and Rayevsky, K. (2000). Nitric Oxide Content Measured by ESR-Spectroscopy in the Rat Brain Is Increased During Pentylenetetrazole-Induced Seizures. Journal of Molecular Neuroscience *14*: 183–190.

Bauer, S., and Norwood, B.A. (2013). What can we learn from animal models of convulsive status epilepticus? Zeitschrift Für Epileptologie *26*: 70–74.

Bauer, S., Kerr, B.J., and Patterson, P.H. (2007). The neuropoietic cytokine family in development, plasticity, disease and injury. Nature Reviews Neuroscience *8*: 221–232.

Beamer, E. (2013). A kainic acid-induced status epilepticus model of epileptogenesis in the C57BL/6J mouse. Interventions targeting nitric oxide and NMDA receptor-mediated pathophysiology (PhD). University of Liverpool.

Beamer, E., Otahal, J., Sills, G.J., and Thippeswamy, T. (2012). N ω-Propyl-l-arginine (L-NPA) reduces status epilepticus and early epileptogenic events in a mouse model of epilepsy: behavioural, EEG and immunohistochemical analyses. European Journal of Neuroscience *36*: 3194–3203.

Beattie, E.C., Stellwagen, D., Morishita, W., Bresnahan, J.C., Ha, B.K., Zastrow, Von, M., et al. (2002). Control of synaptic strength by glial TNFalpha. Science *295*: 2282–2285.

Ben-Aissa, K., Patino-Lopez, G., Belkina, N.V., Maniti, O., Rosales, T., Hao, J.-J., et al. (2012). Activation of moesin, a protein that links actin cytoskeleton to the plasma membrane, occurs by phosphatidylinositol 4,5-bisphosphate (PIP2) binding sequentially to two sites and releasing an autoinhibitory linker. Journal of Biological Chemistry *287*: 16311–16323.

Ben-Ari, Y., and Cossart, R. (2000). Kainate, a double agent that generates seizures: two decades of progress. Trends in Neurosciences *23*: 580–587.

Ben-Ari, Y., Tremblay, E., Ottersen, O.P., and Meldrum, B.S. (1980). The role of epileptic activity in hippocampal and 'remote' cerebral lesions induced by kainic acid. Brain Research *191*: 79–97.

Benarroch, E.E. (2011). Nitric oxide: A pleiotropic signal in the nervous system. Neurology *77*: 1568–1576.

Benkovic, S.A., O'Callaghan, J.P., and Miller, D.B. (2004). Sensitive indicators of injury reveal hippocampal damage in C57BL/6J mice treated with kainic acid in the absence of tonic–clonic seizures. Brain Research *1024*: 59–76.

Berg, J.M., Tymoczko, J.L., and Stryer, L. (2002). Chapter 3, Protein Structure and Function. (New York: W H Freeman).

Bergstrom, R.A., Choi, J.H., Manduca, A., Shin, H.-S., Worrell, G.A., and Howe, C.L. (2013). Automated identification of multiple seizure-related and interictal epileptiform event types in the EEG of mice. Sci. Rep. *3*: 1–8.

Berkovic, S.F., Andermann, F., Olivier, A., Ethier, R.O., Melanson, D., Robitaille, Y., et al. (1991). Hippocampal sclerosis in temporal lobe epilepsy demonstrated by magnetic resonance imaging. Ann Neurol. *29*: 175–182.

Berkovic, S.F., Harkin, L., McMahon, J.M., Pelekanos, J.T., Zuberi, S.M., Wirrell, E.C., et al. (2006). De-novo mutations of the sodium channel gene SCN1A in alleged vaccine encephalopathy: a retrospective study. Lancet Neurol *5*: 488–492.

Bertram, E.H., and Cornett, J. (1993). The ontogeny of seizures in a rat model of limbic epilepsy: evidence for a kindling process in the development of chronic spontaneous seizures. Brain Research *625*: 295–300.

Bin Ma, and Johnson, R. (2012). De novo sequencing and homology searching. Mol. Cell Proteomics *11*: 111–14902.

Binder, D.K., and Steinhäuser, C. (2006). Functional changes in astroglial cells in epilepsy. Glia *54*: 358–368.

Birbeck, G.L. (2010). Epilepsy Care in Developing Countries: Part I of II. Epilepsy Currents *10*: 75–79.

Blackstock, W.P., and Weir, M.P. (1999). Proteomics: quantitative and physical mapping of cellular proteins. Trends in Biotechnology *17*: 121–127.

Blobe, G.C., Schiemann, W.P., and Lodish, H.F. (2000). Role of transforming growth factor beta in human disease. The New England Journal of Medicine *342*: 1350–1358.

Blyth, B.J., Farhavar, A., Gee, C., Hawthorn, B., He, H., Nayak, A., et al. (2009). Validation of Serum Markers for Blood-Brain Barrier Disruption in Traumatic Brain Injury. Journal of Neurotrauma *26*: 1497–1507.

Boast, C.A., Reid, S.A., Johnson, P., and Zornetzer, S.F. (1976). A caution to brain scientists: unsuspected hemorrhagic vascular damage resulting from mere electrode implantation. Brain Research *103*: 527–534.

Bolwig, T.G., Hertz, M.M., and Holm Jensen, J. (1977). Blood—brain barrier permeability during electroshock seizures in the rat. Eur J Clin Invest *7*: 95–100.

Bradford, H.F. (1995). Glutamate, GABA and epilepsy. Progress in Neurobiology *47*: 477–511.

Brandt, C., Potschka, H., Löscher, W., and Ebert, U. (2003). N-Methyl-d-aspartate receptor blockade after status epilepticus protects against limbic brain damage but not against epilepsy in the kainate model of temporal lobe epilepsy. Neuroscience *118*: 727–740.

Brenner, R.P. (2009). How useful is EEG and EEG monitoring in the acutely ill and how to interpret it? Epilepsia *50*: 34–37.

Brodie, M.J. (2010). Antiepileptic drug therapy the story so far. Seizure *19*: 650-655.

Brown, G.C. (2010). Nitric oxide and neuronal death. Nitric Oxide *23*: 153–165.

Bryant, A.E., Bayer, C.R., Huntington, J.D., and Stevens, D.L. (2006). Group A streptococcal myonecrosis: increased vimentin expression after skeletal-muscle injury mediates the binding of Streptococcus pyogenes. J. Infect. Dis. *193*: 1685–1692.

Buckmaster, P.S. (2004). Laboratory animal models of temporal lobe epilepsy. Comparative Medicine *54*: 473–485.

Cacheaux, L.P., Ivens, S., David, Y., Lakhter, A.J., Bar-Klein, G., Shapira, M., et al. (2009). Transcriptome profiling reveals TGF-beta signaling involvement in epileptogenesis. Journal of Neuroscience *29*: 8927–8935.

Calabrese, V., Mancuso, C., Calvani, M., Rizzarelli, E., Butterfield, D.A., and Stella, A.M.G. (2007). Nitric oxide in the central nervous system: neuroprotection versus neurotoxicity. Nature Reviews Neuroscience *8*: 766–775.

Cameron, H.A., and McKay, R.D. (2001). Adult neurogenesis produces a large pool of new granule cells in the dentate gyrus. J. Comp. Neurol. *435*: 406–417.

Cantrell, D.A., and Smith, K.A. (1984). The interleukin-2 T-cell system: a new cell growth model. Science *224*: 1312–1316.

Cao, D.-L., Zhang, Z.-J., Xie, R.-G., Jiang, B.-C., Ji, R.-R., and Gao, Y.-J. (2014). Chemokine CXCL1 enhances inflammatory pain and increases NMDA receptor activity and COX-2 expression in spinal cord neurons via activation of CXCR2. Experimental Neurology *261*: 328–336.

Cao, J., Viholainen, J.I., Dart, C., Warwick, H.K., Leyland, M.L., and Courtney, M.J. (2005). The PSD95-nNOS interface: a target for inhibition of excitotoxic p38 stress-activated protein kinase activation and cell death. The Journal of Cell Biology *168*: 117–126.

Carlson, S.M., Najmi, A., and Cohen, H.J. (2007). Biomarker clustering to address correlations in proteomic data. Proteomics *7*: 1037–1046.

Carta, M., Fièvre, S., Gorlewicz, A., and Hornykiewicz, O. (2014). Kainate receptors

in the hippocampus. European Journal of Neuroscience *39*: 1835–1844.

Casey, P.J., and Seabra, M.C. (1996). Protein prenyltransferases. J. Biol. Chem. *271*: 5289–5292.

Cavaillon, J.M. (2001). Pro- versus anti-inflammatory cytokines: myth or reality. Cell. Mol. Biol. (Noisy-Le-Grand) *47*: 695–702.

Cavalheiro, E.A., Riche, D.A., and Le Gal La Salle, G. (1982). Long-term effects of intrahippocampal kainic acid injection in rats: a method for inducing spontaneous recurrent seizures. Electroencephalography and Clinical Neurophysiology *53*: 581–589.

Ceolin, L., Bortolotto, Z.A., Bannister, N., Collingridge, G.L., Lodge, D., and Volianskis, A. (2012). A novel anti-epileptic agent, perampanel, selectively inhibits AMPA receptor-mediated synaptic transmission in the hippocampus. Neurochem. Int. *61*: 517–522.

Chang, B.S., and Lowenstein, D.H. (2003). Epilepsy. The New England Journal of Medicine *349*: 1257–1266.

Chang, P., Hashemi, K.S., and Walker, M.C. (2011). A novel telemetry system for recording EEG in small animals. Journal of Neuroscience Methods *201*: 106–115.

Chapman, A.G. (2000). Glutamate and Epilepsy. The Journal of Nutrition 1043S–1045S.

Chen, W.-F., Chang, H., Huang, L.-T., Lai, M.-C., Yang, C.-H., Wan, T.-H., et al. (2006). Alterations in long-term seizure susceptibility and the complex of PSD-95 with NMDA receptor from animals previously exposed to perinatal hypoxia. Epilepsia *47*: 288–296.

Chen, Z., Duan, R.-S., Quezada, H.C., Mix, E., Nennesmo, I., Adem, A., et al. (2004). Increased microglial activation and astrogliosis after intranasal administration of kainic acid in C57BL/6 mice. J. Neurobiol. *62*: 207–218.

Chen, Z., Ljunggren, H.-G., Bogdanovic, N., Nennesmo, I., Winblad, B., and Zhu, J. (2002). Excitotoxic neurodegeneration induced by intranasal administration of kainic acid in C57BL/6 mice. Brain Research *931*: 135–145.

Cherian, L., Hlatky, R., and Robertson, C.S. (2006). Nitric Oxide in Traumatic Brain Injury. Brain Pathology *14*: 195–201.

Choi, J., and Koh, S. (2008). Role of Brain Inflammation in Epileptogenesis. Yonsei Med J *49*: 1.

Choi, J., Nordli, D.R., Alden, T.D., DiPatri, A., Laux, L., Kelley, K., et al. (2009). Cellular injury and neuroinflammation in children with chronic intractable epilepsy. J Neuroinflammation *6*: 38–51.

Choi, P., and Reiser, H. (1998). IL-4: role in disease and regulation of production. Clinical & Experimental Immunology *113*: 317–319.

Christopherson, K.S., Hillier, B.J., Lim, W.A., and Bredt, D.S. (1999). PSD-95 assembles a ternary complex with the N-methyl-D-aspartic acid receptor and a bivalent neuronal NO synthase PDZ domain. J. Biol. Chem. *274*: 27467–27473.

Cohen, J. (2013). Statistical Power Analysis for the Behavioral Sciences (Routledge, 2013).

Cook, D.J., Teves, L., and Tymianski, M. (2012). Treatment of stroke with a PSD-95 inhibitor in the gyrencephalic primate brain. Nature *483*: 213–217.

Cosen-Binker, L.I., and Kapus, A. (2006). Cortactin: The Gray Eminence of the Cytoskeleton. Physiology *21*: 352–361.

Crosnier, C., Bustamante, L.Y., Bartholdson, S.J., Bei, A.K., Theron, M., Uchikawa, M., et al. (2011). Basigin is a receptor essential for erythrocyte invasion by Plasmodium falciparum. Nature *480*: 534–537.

Cui, H., Hayashi, A., Sun, H.-S., Belmares, M.P., Cobey, C., Phan, T., et al. (2007). PDZ protein interactions underlying NMDA receptor-mediated excitotoxicity and neuroprotection by PSD-95 inhibitors. Journal of Neuroscience *27*: 9901–9915.

Cull-Candy, S., Brickley, S., and Farrant, M. (2001). NMDA receptor subunits: diversity, development and disease. Curr. Opin. Neurobiol. *11*: 327–335.

Curia, G., Longo, D., Biagini, G., Jones, R.S.G., and Avoli, M. (2008). The pilocarpine model of temporal lobe epilepsy. Journal of Neuroscience Methods *172*: 143–157.

D'arcangelo, G., Tancredi, V., Onofri, F., D'antuono, M., Giovedì, S., and Benfenati, F. (2000). Interleukin-6 inhibits neurotransmitter release and the spread of excitation in the rat cerebral cortex. European Journal of Neuroscience *12*: 1241–1252.

Damerval, C., Maurice, A., Josse, J.M., and de Vienne, D. (1994). Quantitative trait loci underlying gene product variation: a novel perspective for analyzing regulation of genome expression. Genetics *137*: 289–301.

Danysz, W., Parsons, C.G., and Bresink, I. (1995). Glutamate in CNS disorders. Drug News and Perspectives *8*: 261–277.

David, Y., Cacheaux, L.P., Ivens, S., Lapilover, E., Heinemann, U., Kaufer, D., et al. (2009). Astrocytic dysfunction in epileptogenesis: consequence of altered potassium and glutamate homeostasis? Journal of Neuroscience *29*: 10588–10599.

Dawe, G.B., Musgaard, M., Andrews, E.D., Daniels, B.A., Aurousseau, M.R.P., Biggin, P.C., et al. (2013). Defining the structural relationship between kainate-receptor deactivation and desensitization. Nature Publishing Group *20*: 1054–1061.

Dawson, T.M., Dawson, V.L., and Snyder, S.H. (1992). A novel neuronal messenger molecule in brain: The free radical, nitric oxide. Ann Neurol. *32*: 297–311.

Dawson, V.L., and Dawson, T.M. (1996). Nitric oxide neurotoxicity. Journal of Chemical Neuroanatomy *10*: 179–190.

Dawson, V.L., Dawson, T.M., London, E.D., Bredt, D.S., and Snyder, S.H. (1991). Nitric oxide mediates glutamate neurotoxicity in primary cortical cultures. Proc. Natl. Acad. Sci. U.S.a. *88*: 6368–6371.

de Kreuk, B.-J., Anthony, E.C., Geerts, D., and Hordijk, P.L. (2012). The F-BAR protein PACSIN2 regulates epidermal growth factor receptor internalization. Journal of Biological Chemistry *287*: 43438–43453.

De Luca, G., Di Giorgio, R.M., Macaione, S., Calpona, P.R., Di Paola, E.D., Costa, N., et al. (2006). Amino acid levels in some brain areas of inducible nitric oxide synthase knock out mouse (iNOS-/-) before and after pentylenetetrazole kindling. Pharmacol. Biochem. Behav. *85*: 804–812.

Del-Bel, E.A., Oliveira, P.R., Oliveira, J.A.C., Mishra, P.K., Jobe, P.C., and Garcia-Cairasco, N. (1997). Anticonvulsant and proconvulsant roles of nitric oxide in experimental epilepsy models. Brazilian Journal of Medical and Biological Research *30*: 971–979.

Delorme, A., and Makeig, S. (2004). EEGLAB: an open source toolbox for analysis of single-trial EEG dynamics including independent component analysis. Journal of Neuroscience Methods *134*: 9–21.

Deng, A., Irizarry, M.C., Nitsch, R.M., Growdon, J.H., and Rebeck, G.W. (2001). Elevation of Cystatin C in Susceptible Neurons in Alzheimer's Disease. The American Journal of Pathology *159*: 1061–1068.

Deverman, B.E., and Patterson, P.H. (2009). Cytokines and CNS development. Neuron *64*: 61–78.

Devor, M. (2006). Sodium Channels and Mechanisms of Neuropathic Pain. The Journal of Pain *7*: S3–S12.

Diatloff-Zito, C., Gordon, A.J.E., Duchaud, E., and Merlin, G. (1995). Isolation of an ubiquitously expressed cDNA encoding human dynamin II, a member of the large GTP-binding protein family. Gene *163*: 301–306.

Dinarello, C.A. (2000). Proinflammatory cytokines. Chest *118*: 503–508.

Dingledine, R., and McBain, C.J. (1999). Excessive Glutamate Receptor Activation and Neurological Disorders (Philadelphia: Lippincott-Raven).

Dingledine, R., Borges, K., Bowie, D., and Traynelis, S.F. (1999). The glutamate receptor ion channels. Pharmacological Reviews *51*: 7–61.

Dingledine, R., McBain, C.J., and McNamara, J.O. (1990). Excitatory amino acid receptors in epilepsy. Trends in Pharmacological Sciences *11*: 334–338.

Dohgu, S., Takata, F., Yamauchi, A., Nakagawa, S., Egawa, T., Naito, M., et al. (2005). Brain pericytes contribute to the induction and up-regulation of blood-brain barrier functions through transforming growth factor-beta production. Brain Research *1038*: 208–215.

Douce, R., Bourguignon, J., Neuburger, M., and Rébeillé, F. (2001). The glycine decarboxylase system: a fascinating complex. Trends in Plant Science *6*: 167–176.

Drabik, A., Bierczynska Krzysik, A., Bodzon Kulakowska, A., Suder, P., Kotlinska, J., and Silberring, J. (2007). Proteomics in neurosciences. Mass Spectrometry Reviews *26*: 432–450.

Dudek, F.E., and Staley, K.J. (2011). Seizure probability in animal models of acquired epilepsy: A perspective on the concept of the preictal state. Epilepsy Research *97*: 324–331.

Ebert, U., and Koch, M. (1996). Amygdala kindling does not change emotional responding as measured by the acoustic startle response in the rat. Brain Research *733*: 193–202.

Elrick, M.M., Walgren, J.L., Mitchell, M.D., and Thompson, D.C. (2006). Proteomics: recent applications and new technologies. Basic Clin. Pharmacol. Toxicol. *98*: 432–441.

Erta, M., Quintana, A., and Hidalgo, J. (2012). Interleukin-6, a major cytokine in the central nervous system. Int. J. Biol. Sci. *8*: 1254–1266.

Farrugia, A. (2010). Albumin Usage in Clinical Medicine: Tradition or Therapeutic? Transfusion Medicine Reviews *24*: 53–63.

Ferraro, T.N., Golden, G.T., Smith, G.G., and Berrettini, W.H. (1995). Differential Susceptibility to Seizures Induced by Systemic Kainic Acid Treatment in Mature DBA/2J and C57BLl6J Mice. Epilepsia *36*: 301–307.

Forder, J.P., and Tymianski, M. (2009). Postsynaptic mechanisms of excitotoxicity: Involvement of postsynaptic density proteins, radicals, and oxidant molecules. Neuroscience *158*: 293–300.

Förstermann, U., and Sessa, W.C. (2011). Nitric oxide synthases: regulation and function. Eur Heart J *33*: 829–837d.

Fountoulakis, M. (2001). Proteomics: current technologies and applications in neurological disorders and toxicology. Amino Acids *21*: 363–381.

Franceschini, A., Szklarczyk, D., Frankild, S., Kuhn, M., Simonovic, M., Roth, A., et al. (2013). STRING v9.1: protein-protein interaction networks, with increased

coverage and integration. Nucleic Acids Research *41*: D808–15.

French, J.A., Williamson, P.D., Thadani, V.M., Darcey, T.M., Mattson, R.H., Spencer, S.S., et al. (1993). Characteristics of medial temporal lobe epilepsy: I. Results of history and physical examination. Ann Neurol. *34*: 774–780.

Friedman, A. (2011). Blood-brain barrier dysfunction, status epilepticus, seizures, and epilepsy: a puzzle of a chicken and egg? Epilepsia *52 Suppl 8*: 19–20.

Friedman, A., Kaufer, D., and Heinemann, U. (2009). Blood–brain barrier breakdown-inducing astrocytic transformation: Novel targets for the prevention of epilepsy. Epilepsy Research *85*: 142–149.

Gabriel, S., Kivi, A., Kovacs, R., Lehmann, T.N., Lanksch, W.R., Meencke, H.J., et al. (1998). Effects of barium on stimulus-induced changes in [K+]o and field potentials in dentate gyrus and area CA1 of human epileptic hippocampus. Neuroscience Letters *249*: 91–94.

Galanopoulou, A.S., Kokaia, M., Loeb, J.A., Nehlig, A., Pitkänen, A., Rogawski, M.A., et al. (2013). Epilepsy therapy development: technical and methodologic issues in studies with animal models. Epilepsia *54 Suppl 4*: 13–23.

Garvey, E.P., Oplinger, J.A., Furfine, E.S., Kiff, R.J., Laszlo, F., Whittle, B.J., et al. (1997). 1400W is a slow, tight binding, and highly selective inhibitor of inducible nitric-oxide synthase in vitro and in vivo. J. Biol. Chem. *272*: 4959–4963.

Gilioli, I., Vignoli, A., Visani, E., Casazza, M., Canafoglia, L., Chiesa, V., et al. (2012). Focal epilepsies in adult patients attending two epilepsy centers: classification of drug-resistance, assessment of risk factors, and usefulness of 'new' antiepileptic drugs. Epilepsia *53*: 733–740.

Giorgi, F.S., Malhotra, S., Hasson, H., Velíšková, J., and Trimbos, J.B.M.Z. (2005). Effects of status epilepticus early in life on susceptibility to ischemic injury in adulthood. Epilepsia *46*: 490–498.

Glien, M., Brandt, C., Potschka, H., Voigt, H., Ebert, U., and Löscher, W. (2001). Repeated low-dose treatment of rats with pilocarpine: low mortality but high proportion of rats developing epilepsy. Epilepsy Research *46*: 111–119.

González-Hernández, T., García-Marín, V., Pérez-Delgado, M.M., González-González, M.L., Rancel-Torres, N., and González-Feria, L. (2000). Nitric oxide synthase expression in the cerebral cortex of patients with epilepsy. Epilepsia *41*: 1259–1268.

Green, R.C., and Seyfried, T.N. (1991). Kindling Susceptibility and Genetic Seizure Predisposition in Inbred Mice. Epilepsia *32*: 22–26.

Griffiths, M.R., Gasque, P., and Neal, J.W. (2009). The Multiple Roles of the Innate

Immune System in the Regulation of Apoptosis and Inflammation in the Brain. Journal of Neuropathology and Experimental Neurology *68*: 217–226.

Gupta, R.C., and Dettbarn, W.-D. (2003). Prevention of kainic acid seizures-induced changes in levels of nitric oxide and high-energy phosphates by 7-nitroindazole in rat brain regions. Brain Research *981*: 184–192.

Halestrap, A.P., and Meredith, D. (2004). The SLC16 gene family—from monocarboxylate transporters (MCTs) to aromatic amino acid transporters and beyond. Pflugers Arch - Eur J Physiol *447*: 619–628.

Halonen, T., Nissinen, J., and Pitkänen, A. (2001). Chronic elevation of brain GABA levels beginning two days after status epilepticus does not prevent epileptogenesis in rats. Neuropharmacology *40*: 536–550.

Hanada, T., Hashizume, Y., Tokuhara, N., Takenaka, O., Kohmura, N., Ogasawara, A., et al. (2011). Perampanel: A novel, orally active, noncompetitive AMPA-receptor antagonist that reduces seizure activity in rodent models of epilepsy. Epilepsia *52*: 1331–1340.

Hayashi, Y., Nomura, M., Yamagishi, S.-I., Harada, S.-I., Yamashita, J., and Yamamoto, H. (1997). Induction of various blood-brain barrier properties in non-neural endothelial cells by close apposition to co-cultured astrocytes. Glia *19*: 13–26.

Hayes, J.D., and Pulford, D.J. (1995). The Glutathione S-Transferase Supergene Family: Regulation of GST and the Contribution of the lsoenzymes to Cancer Chemoprotection and Drug Resistance Part I. Crit Rev in Biochem and Mol Biol *30*: 445–520.

Heinemann, U., Kaufer, D., and Friedman, A. (2012). Blood-brain barrier dysfunction, TGFβ signaling, and astrocyte dysfunction in epilepsy. Glia *60*: 1251–1257.

Hellier, J.L., and Dudek, F.E. (1999). Spontaneous motor seizures of rats with kainate-induced epilepsy: effect of time of day and activity state. Epilepsy Research *35*: 47–57.

Hellier, J.L., and Dudek, F.E. (2005). Chemoconvulsant Model of Chronic Spontaneous Seizures. Curr Protoc Neurosci *31*: 9.19.1–9.19.12.

Hellier, J.L., Patrylo, P.R., Buckmaster, P.S., and Dudek, F.E. (1998). Recurrent spontaneous motor seizures after repeated low-dose systemic treatment with kainate: assessment of a rat model of temporal lobe epilepsy. Epilepsy Research *31*: 73–84.

Helmstaedter, C., Kurthen, M., Lux, S., Reuber, M., and Elger, C.E. (2003). Chronic epilepsy and cognition: a longitudinal study in temporal lobe epilepsy. Ann Neurol. *54*: 425–432.

Herman, S. (2010). Intractable epilepsy: relapsing, remitting, or progressive? Epilepsy Currents *10*: 146–148.

Herman, S.T. (2002). Epilepsy after brain insult: Targeting epileptogenesis. Neurology *59*: S21–S26.

Higashi, K., Fujita, A., Inanobe, A., Tanemoto, M., Doi, K., Kubo, T., et al. (2001). An inwardly rectifying K(+) channel, Kir4.1, expressed in astrocytes surrounds synapses and blood vessels in brain. Am. J. Physiol., Cell Physiol. *281*: C922–31.

Hill, M.D., Martin, R.H., Mikulis, D., Wong, J.H., Silver, F.L., terBrugge, K.G., et al. (2012). Safety and efficacy of NA-1 in patients with iatrogenic stroke after endovascular aneurysm repair (ENACT): a phase 2, randomised, double-blind, placebo-controlled trial. Lancet Neurol *11*: 942–950.

Hinterkeuser, S., Schröder, W., Hager, G., Seifert, G., Blümcke, I., Elger, C.E., et al. (2000). Astrocytes in the hippocampus of patients with temporal lobe epilepsy display changes in potassium conductances. Eur. J. Neurosci. *12*: 2087–2096.

Hirshler, Y.K., Polat, U., and Biegon, A. (2010). Intracranial electrode implantation produces regional neuroinflammation and memory deficits in rats. Experimental Neurology *222*: 42–50.

Hitti, F.L., and Siegelbaum, S.A. (2014). The hippocampal CA2 region is essential for social memory. Nature *508*: 88–92.

Hondermarck, H. (2004). Proteomics: Biomedical and Pharmaceutical Applications (Kluwer Academic Publishers).

Hopper, R.A., and Garthwaite, J. (2006). Tonic and phasic nitric oxide signals in hippocampal long-term potentiation. Journal of Neuroscience *26*: 11513–11521.

Hu, S., Sheng, W.S., Ehrlich, L.C., Peterson, P.K., and Chao, C.C. (2000). Cytokine effects on glutamate uptake by human astrocytes. Neuroimmunomodulation *7*: 153–159.

Huang, Z., Huang, P.L., Ma, J., Meng, W., Ayata, C., Fishman, M.C., et al. (1996). Enlarged infarcts in endothelial nitric oxide synthase knockout mice are attenuated by nitro-L-arginine. J. Cereb. Blood Flow Metab. *16*: 981–987.

Hubbard, C., Singleton, D., Rauch, M., Jayasinghe, S., Cafiso, D., and Castle, D. (2000). The secretory carrier membrane protein family: structure and membrane topology. Mol. Biol. Cell *11*: 2933–2947.

Huneau, C., Benquet, P., Dieuset, G., Biraben, A., Martin, B., and Wendling, F. (2013). Shape features of epileptic spikes are a marker of epileptogenesis in mice. Epilepsia *54*: 2219–2227.

Imhof, A., Megens, M., Engelberts, J.J., de Lang, D.T.N., Sprik, R., and Vos, W.L.

(1999). Spectroscopy of Fluorescein (FITC) Dyed Colloidal Silica Spheres. J. Phys. Chem. B *103*: 1408–1415.

Ishizaki, Y., Kira, R., Fukuda, M., Torisu, H., Sakai, Y., Sanefuji, M., et al. (2009). Interleukin-10 is associated with resistance to febrile seizures: Genetic association and experimental animal studies. Epilepsia *50*: 761–767.

Ivens, S., Kaufer, D., Flores, L.P., Bechmann, I., Zumsteg, D., Tomkins, O., et al. (2007). TGF-beta receptor-mediated albumin uptake into astrocytes is involved in neocortical epileptogenesis. Brain *130*: 535–547.

Jabs, R., Seifert, G., and Steinhäuser, C. (2008). Astrocytic function and its alteration in the epileptic brain. Epilepsia *49 Suppl 2*: 3–12.

Jafarian-Tehrani, M., Louin, G., Royo, N.C., and Besson, V.C. (2005). 1400W, a potent selective inducible NOS inhibitor, improves histopathological outcome following traumatic brain injury in rats. Nitric Oxide *12*: 61–69.

Jain, K.K. (2002). Role of neuroproteomics in CNS drug discovery. Targets *1*: 95–101.

James, P. (1997). Protein identification in the post-genome era: the rapid rise of proteomics. Q. Rev. Biophys. *30*: 279–331.

Jefferys, J.G.R. (2014). Do Seizures in the Pilocarpine Model Start in the Hippocampal Formation? Epilepsy Currents *14*: 206–207.

Johnson, E.A., Dao, T.L., Guignet, M.A., Geddes, C.E., Koemeter-Cox, A.I., and Kan, R.K. (2011). Increased expression of the chemokines CXCL1 and MIP-1α by resident brain cells precedes neutrophil infiltration in the brain following prolonged soman-induced status epilepticus in rats. J Neuroinflammation *8*: 41.

Johnson, M.D., Yu, L.-R., Conrads, T.P., Kinoshita, Y., Uo, T., McBee, J.K., et al. (2005). The proteomics of neurodegeneration. American Journal of Pharmacogenomics *5*: 259–270.

Jonas, P., and Lisman, J. (2014). Structure, function, and plasticity of hippocampal dentate gyrus microcircuits. Frontiers of Neural Circuits *8*:.

Jones, N.C., Lee, H.E., Yang, M., Rees, S.M., Morris, M.J., O'Brien, T.J., et al. (2013). Repeatedly stressed rats have enhanced vulnerability to amygdala kindling epileptogenesis. Psychoneuroendocrinology *38*: 263–270.

Jones, S.A., Horiuchi, S., Topley, N., Yamamoto, N., and Fuller, G.M. (2001). The soluble interleukin 6 receptor: mechanisms of production and implications in disease. Faseb J *15*: 43–58.

Jung, J.E., Kim, G.S., and Chan, P.H. (2011). Neuroprotection by interleukin-6 is mediated by signal transducer and activator of transcription 3 and antioxidative

signaling in ischemic stroke. Stroke *42*: 3574–3579.

Jung, S., Jones, T.D., Lugo, J.N., Sheerin, A.H., Miller, J.W., D'Ambrosio, R., et al. (2007). Progressive dendritic HCN channelopathy during epileptogenesis in the rat pilocarpine model of epilepsy. Journal of Neuroscience *27*: 13012–13021.

Kalinski, P., Vieira, P.L., Schuitemaker, J.H.N., de Jong, E.C., and Kapsenberg, M.L. (2001). Prostaglandin E2 is a selective inducer of interleukin-12 p40 (IL-12p40) production and an inhibitor of bioactive IL-12p70 heterodimer. Blood *97*:.

Kan, A.A., de Jager, W., de Wit, M., Heijnen, C., van Zuiden, M., Ferrier, C., et al. (2012). Protein expression profiling of inflammatory mediators in human temporal lobe epilepsy reveals co-activation of multiple chemokines and cytokines. J Neuroinflammation *9*: 1–22.

Kapuscinski, J. (1995). DAPI: a DNA-specific fluorescent probe. Biotech Histochem *70*: 220–233.

Kato, N., Sato, S., Yokoyama, H., Kayama, T., and Yoshimura, T. (2005). Sequential changes of nitric oxide levels in the temporal lobes of kainic acid-treated mice following application of nitric oxide synthase inhibitors and phenobarbital. Epilepsy Research *65*: 81–91.

Kempermann, G. (2002). Why new neurons? Possible functions for adult hippocampal neurogenesis. Journal of Neuroscience *22*: 635–638.

Kennedy, M.B. (1995). Origin of PDZ (DHR, GLGF) domains. Trends Biochem. Sci. *20*: 350.

Khalil, N. (1999). TGF-β: from latent to active. Microbes and Infection *1*: 1255–1263.

Kikuchi, G. (1973). The glycine cleavage system: Composition, reaction mechanism, and physiological significance. Mol Cell Biochem *1*: 169–187.

Kikuchi, G., Motokawa, Y., Yoshida, T., and Hiraga, K. (2008). Glycine cleavage system: reaction mechanism, physiological significance, and hyperglycinemia. Proc. Jpn. Acad., Ser. B, Phys. Biol. Sci. *84*: 246–263.

Kilkenny, C., Browne, W., Cuthill, I.C., Emerson, M., and Altman, D.G. (2010). Animal Research: Reporting In Vivo Experiments: The ARRIVE Guidelines. The Journal of Gene Medicine *12*: 561–563.

Kim, E., and Sheng, M. (2004). PDZ domain proteins of synapses. Nature Reviews Neuroscience *5*: 771–781.

Kishore, U., and Reid, K.B.M. (2000). C1q: Structure, function, and receptors. Immunopharmacology *49*: 159–170.

Koh, S., Nguyen, S., Asarnow, R.F., LoPresti, C., Yudovin, S., Shields, W.D., et al. (2004). Five or more acute postoperative seizures predict hospital course and long-term seizure control after hemispherectomy. Epilepsia *45*: 527–533.

Krapfenbauer, K., Berger, M., Friedlein, A., Lubec, G., and Fountoulakis, M. (2001a). Changes in the levels of low-abundance brain proteins induced by kainic acid. Eur. J. Biochem. *268*: 3532–3537.

Krapfenbauer, K., Berger, M., Lubec, G., and Fountoulakis, M. (2001b). Changes in the brain protein levels following administration of kainic acid. Electrophoresis *22*: 2086–2091.

Krauss, G.L., Perucca, E., Ben Menachem, E., Kwan, P., Shih, J.J., Squillacote, D., et al. (2013). Perampanel, a selective, noncompetitive α-amino-3-hydroxy-5-methyl-4-isoxazolepropionic acid receptor antagonist, as adjunctive therapy for refractory partial-onset seizures: Interim results from phase III, extension study 307. Epilepsia *54*: 126–134.

Krizanac-Bengez, L., Kapural, M., Parkinson, F., Cucullo, L., Hossain, M., Mayberg, M.R., et al. (2003). Effects of transient loss of shear stress on blood–brain barrier endothelium: role of nitric oxide and IL-6. Brain Research *977*: 239–246.

Kumar, C., and Mann, M. (2009). Bioinformatics analysis of mass spectrometry-based proteomics data sets. FEBS Lett. *583*: 1703–1712.

Kürschner, V.C., Petruzzi, R.L., Golden, G.T., Berrettini, W.H., and Ferraro, T.N. (1998). Kainate and AMPA receptor binding in seizure-prone and seizure-resistant inbred mouse strains. Brain Research *780*: 1–8.

Kwan, P., and Brodie, M.J. (2004). Drug treatment of epilepsy: when does it fail and how to optimize its use? CNS Spectr *9*: 110–119.

Lassmann, H., Petsche, U., Kitz, K., Baran, H., Sperk, G., Seitelberger, F., et al. (1984). The role of brain edema in epileptic brain damage induced by systemic kainic acid injection. Nature *13*: 691–704.

Laszlo, F., Evans, S.M., and Whittle, B.J. (1995). Aminoguanidine inhibits both constitutive and inducible nitric oxide synthase isoforms in rat intestinal microvasculature in vivo. Eur. J. Pharmacol. *272*: 169–175.

Lawrence, C.W. (2002). Cellular roles of DNA polymerase ζ and Rev1 protein. DNA Repair *1*: 425–435.

Leckie, M.J., Brinke, A.T., Khan, J., Diamant, Z., O'Connor, B.J., Walls, C.M., et al. (2000). Effects of an interleukin-5 blocking monoclonal antibody on eosinophils, airway hyper-responsìveness, and the late asthmatic response. The Lancet *356*: 2144–2148.

Lehmann, T.N., Gabriel, S., Kovacs, R., Eilers, A., Kivi, A., Schulze, K., et al. (2000). Alterations of neuronal connectivity in area CA1 of hippocampal slices from temporal lobe epilepsy patients and from pilocarpine-treated epileptic rats. Epilepsia *41 Suppl 6*: S190–4.

Lehmkuhle, M.J., Thomson, K.E., Scheerlinck, P., Pouliot, W., Greger, B., and Dudek, F.E. (2009). A Simple Quantitative Method for Analyzing Electrographic Status Epilepticus in Rats. Journal of Neurophysiology *101*: 1660–1670.

Lehtimäki, K.A., Keränen, T., Palmio, J., Mäkinen, R., Hurme, M., Honkaniemi, J., et al. (2007). Increased plasma levels of cytokines after seizures in localization-related epilepsy. Acta Neurol Scand *116*: 226–230.

Lehtimäki, K.A., Peltola, J., Koskikallio, E., Keränen, T., and Honkaniemi, J. (2003a). Expression of cytokines and cytokine receptors in the rat brain after kainic acid-induced seizures. *110*: 253–260.

Lehtimäki, K.A., Peltola, J., Koskikallio, E., Keränen, T., and Honkaniemi, J. (2003b). Expression of cytokines and cytokine receptors in the rat brain after kainic acid-induced seizures. Brain Res. Mol. Brain Res. *110*: 253–260.

Lepreux, S., Bioulac-Sage, P., Gabbiani, G., Sapin, V., Housset, C., Rosenbaum, J., et al. (2004). Cellular retinol-binding protein-1 expression in normal and fibrotic/cirrhotic human liver: different patterns of expression in hepatic stellate cells and (myo)fibroblast subpopulations. J. Hepatol. *40*: 774–780.

Lewicki, M.S. (1998). A review of methods for spike sorting: the detection and classification of neural action potentials. Network *9*: R53–R78.

Lewis, G.P., and Fisher, S.K. (2003). Up-regulation of glial fibrillary acidic protein in response to retinal injury: its potential role in glial remodeling and a comparison to vimentin expression. Int. Rev. Cytol. *230*: 263–290.

Lévesque, M., and Avoli, M. (2013). The kainic acid model of temporal lobe epilepsy. Neurosci Biobehav Rev *37*: 2887–2899.

Li, A., Choi, Y.-S., Dziema, H., Cao, R., Cho, H.-Y., Jung, Y.J., et al. (2010). Proteomic profiling of the epileptic dentate gyrus. Brain Pathology *20*: 1077–1089.

Li, G., Bauer, S., Nowak, M., Norwood, B., and Tackenberg, B. (2011). Cytokines and epilepsy. Seizure *20*: 249–256.

Lindsay, K.W., Bone, I., and Fuller, G. (2010). Neurology and Neurosurgery Illustrated (Elsevier Health Sciences).

Lipton, S.A. (2004). Failures and Successes of NMDA Receptor Antagonists: Molecular Basis for the Use of Open-Channel Blockers like Memantine in the Treatment of Acute and Chronic Neurologic Insults. NeuroRx *1*: 101–110.

Lipton, S.A. (2007). Pathologically-activated therapeutics for neuroprotection: mechanism of NMDA receptor block by memantine and S-nitrosylation. Curr Drug Targets *8*: 621–632.

Lipton, S.A., and Stamler, J.S. (1994). Actions of redox-related congeners of nitric oxide at the NMDA receptor. Neuropharmacology *33*: 1229–1233.

Liu, X.-Y., Yang, J.-L., Chen, L.-J., Zhang, Y., Yang, M.-L., Wu, Y.-Y., et al. (2008). Comparative proteomics and correlated signaling network of rat hippocampus in the pilocarpine model of temporal lobe epilepsy. Proteomics *8*: 582–603.

Loddick, S.A., Turnbull, A.V., and Rothwell, N.J. (1998). Cerebral interleukin-6 is neuroprotective during permanent focal cerebral ischemia in the rat. J. Cereb. Blood Flow Metab. *18*: 176–179.

London, E.D., and Coyle, J.T. (2005). Specific binding of [3H]kainic acid to receptor sites in rat brain. Mol. Pharmacol. *15*: 492–505.

Lothman, E.W., Bertram, E.H., Kapur, J., and Stringer, J.L. (1990). Recurrent spontaneous hippocampal seizures in the rat as a chronic sequela to limbic status epilepticus. Epilepsy Research *6*: 110–118.

Löscher, W. (2002). Animal models of epilepsy for the development of antiepileptogenic and disease-modifying drugs. A comparison of the pharmacology of kindling and post-status epilepticus models of temporal lobe epilepsy. Epilepsy Research *50*: 105–123.

Löscher, W. (2011). Critical review of current animal models of seizures and epilepsy used in the discovery and development of new antiepileptic drugs. Seizure *20*: 359–368.

Löscher, W., and Brandt, C. (2010). Prevention or Modification of Epileptogenesis after Brain Insults: Experimental Approaches and Translational Research. Pharmacological Reviews *62*: 668–700.

Löscher, W., and Schmidt, D. (2012). Epilepsy: Perampanel-new promise for refractory epilepsy? Nature Reviews Neurology *8*: 661–662.

Löscher, W., Hörstermann, D., Hönack, D., Rundfeldt, C., and Wahnschaffe, U. (1993). Transmitter amino acid levels in rat brain regions after amygdala-kindling or chronic electrode implantation without kindling: Evidence for a pro-kindling effect of prolonged electrode implantation. Neurochemical Research *18*: 775–781.

Löscher, W., Wahnschaffe, U., Hönack, D., and Rundfeldt, C. (1995). Does prolonged implantation of depth electrodes predispose the brain to kindling? Brain Research *697*: 197–204.

Lyons, R.M., Gentry, L.E., Purchio, A.F., and Moses, H.L. (1990). Mechanism of

activation of latent recombinant transforming growth factor beta 1 by plasmin. The Journal of Cell Biology *110*: 1361–1367.

Ma, B., Zhang, K., Hendrie, C., Liang, C., Li, M., Doherty-Kirby, A., et al. (2003). PEAKS: powerful software for peptide de novo sequencing by tandem mass spectrometry. Rapid Commun. Mass Spectrom. *17*: 2337–2342.

MacDonald, P.N., Bok, D., and Ong, D.E. (1990). Localization of Cellular Retinol-Binding Protein and Retinol-Binding Protein in Cells Comprising the Blood-Brain Barrier of Rat and Human. Proceedings of the National Academy of Sciences of the United States of Ame *87*: 4265–4269.

MacEwan, D.J. (2002a). TNF ligands and receptors – a matter of life and death. Br. J. Pharmacol. *135*: 855–875.

MacEwan, D.J. (2002b). TNF receptor subtype signalling: differences and cellular consequences. Cell Signal *14*: 477–492.

Macias, M., Blazejczyk, M., Kazmierska, P., Caban, B., Skalecka, A., Tarkowski, B., et al. (2013). Spatiotemporal Characterization of mTOR Kinase Activity Following Kainic Acid Induced Status Epilepticus and Analysis of Rat Brain Response to Chronic Rapamycin Treatment. PLoS ONE *8*: e64455.

Maggio, N., Shavit, E., Chapman, J., and Segal, M. (2008). Thrombin Induces Long-Term Potentiation of Reactivity to Afferent Stimulation and Facilitates Epileptic Seizures in Rat Hippocampal Slices: Toward Understanding the Functional Consequences of Cerebrovascular Insults. J. Neurosci. *28*: 732–736.

Manaka, S., Ishijima, B., and Mayanagi, Y. (2003). Postoperative seizures: epidemiology, pathology, and prophylaxis. Neurol. Med. Chir. (Tokyo) *43*: 589–600– discussion 600.

Marat, A.L., Dokainish, H., and McPherson, P.S. (2011). DENN domain proteins: regulators of Rab GTPases. Journal of Biological Chemistry *286*: 13791–13800.

Marchi, N., Tierney, W., Alexopoulos, A.V., Puvenna, V., Granata, T., and Janigro, D. (2011). The Etiological Role of Blood-Brain Barrier Dysfunction in Seizure Disorders. Cardiovascular Psychiatry and Neurology *2011*: 1–9.

Matsuda, S., Wen, T.C., Morita, F., Otsuka, H., Igase, K., Yoshimura, H., et al. (1996). Interleukin-6 prevents ischemia-induced learning disability and neuronal and synaptic loss in gerbils. Neuroscience Letters *204*: 109–112.

Matsumoto, E.D., Margulis, V., Tunc, L., Taylor, G.D., Duchene, D., Johnson, B., et al. (2005). Cytokine response to surgical stress: comparison of pure laparoscopic, hand-assisted laparoscopic, and open nephrectomy. Journal of Endourology *19*:.

Maury, C.P., and Teppo, A.M. (1987). Immunodetection of protein composition in

cerebral amyloid extracts in Alzheimer's disease: enrichment of retinol-binding protein. J. Neurol. Sci. *80*: 221–228.

McCord, M.C., Lorenzana, A., Bloom, C.S., Chancer, Z.O., and Schauwecker, P.E. (2008). Effect of age on kainate-induced seizure severity and cell death. Neuroscience *154*: 1143–1153.

McKhann, G.M., II, Wenzel, H.J., Robbins, C.A., Sosunov, A.A., and Schwartzkroin, P.A. (2003). Mouse strain differences in kainic acid sensitivity, seizure behavior, mortality, and hippocampal pathology. Neuroscience *122*: 551–561.

McLin, J.P., and Steward, O. (2006). Comparison of seizure phenotype and neurodegeneration induced by systemic kainic acid in inbred, outbred, and hybrid mouse strains. European Journal of Neuroscience *24*: 2191–2202.

Mekada, K., Abe, K., Murakami, A., Nakamura, S., and Trimbos, J.B.M.Z. (2009). Genetic differences among C57BL/6 substrains. Experimental Animals *58*: 141–149.

Mering, von, C., Huynen, M., Jaeggi, D., Schmidt, S., Bork, P., and Snel, B. (2003). STRING: a database of predicted functional associations between proteins. Nucleic Acids Research *31*: 258–261.

Mering, von, C., Jensen, L.J., Snel, B., Hooper, S.D., Krupp, M., Foglierini, M., et al. (2005). STRING: known and predicted protein-protein associations, integrated and transferred across organisms. Nucleic Acids Research *33*: D433–7.

Mihály, A., and Bozóky, B. (1984). Immunohistochemical localization of extravasated serum albumin in the hippocampus of human subjects with partial and generalized epilepsies and epileptiform convulsions. Acta Neuropathol *65*: 25–34.

Milatovic, D., Gupta, R.C., and Dettbarn, W.D. (2002). Involvement of nitric oxide in kainic acid-induced excitotoxicity in rat brain. Brain Research *957*: 330–337.

Molloy, M.P., and Witzmann, F.A. (2002). Proteomics: technologies and applications. Brief Funct Genomic Proteomic *1*: 23–39.

Morrison, R.S., Kinoshita, Y., Johnson, M.D., Uo, T., Ho, J.T., McBee, J.K., et al. (2002). Proteomic analysis in the neurosciences. Mol. Cell Proteomics *1*: 553–560.

Mujumdar, R.B., Ernst, L.A., Mujumdar, S.R., Lewis, C.J., and Waggoner, A.S. (1993). Cyanine dye labeling reagents: sulfoindocyanine succinimidyl esters. Bioconjug. Chem. *4*: 105–111.

Müller, C.J., Bankstahl, M., Gröticke, I., and Löscher, W. (2009). Pilocarpine vs. lithium-pilocarpine for induction of status epilepticus in mice: Development of spontaneous seizures behavioral alterations and neuronal damage. Eur. J.

Pharmacol. *619*: 15–24.

Mülsch, A., Busse, R., Mordvintcev, P.I., Vanin, A.F., Nielsen, E.O., Scheel-Krüger, J., et al. (1994). Nitric oxide promotes seizure activity in kainate-treated rats. Neuroreport *5*: 2325–2328.

Nadal, A., Fuentes, E., Pastor, J., and McNaughton, P.A. (1995). Plasma albumin is a potent trigger of calcium signals and DNA synthesis in astrocytes. Proc. Natl. Acad. Sci. U.S.a. *92*: 1426–1430.

Nadler, J.V. (1981). Kainic acid as a tool for the study of temporal lobe epilepsy. Life Sciences *29*: 2031–2042.

Nadler, J.V., Perry, B.W., and Cotman, C.W. (1978). Intraventricular kainic acid preferentially destroys hippocampal pyramidal cells. Nature *271*: 676–677.

Nelson, E.J., Connolly, J., Connolly, J., McArthur, P., and McArthur, P. (2003). Nitric oxide and S-nitrosylation: excitotoxic and cell signaling mechanism. Biology of the Cell *95*: 3–8.

Niedermeyer, E., and de Silva, F.H.L. (2005). Electroencephalography: Basic Principles, Clinical Applications, and Related Fields. Lippincott Williams Wilkins.

Niespodziany, I., Klitgaard, H., and Margineanu, D.G. (1999). Chronic electrode implantation entails epileptiform field potentials in rat hippocampal slices, similarly to amygdala kindling. Epilepsy Research *36*: 69–74.

Nitiss, J.L. (2009). DNA topoisomerase II and its growing repertoire of biological functions. Nature Reviews Cancer *9*: 327–337.

Nitsch, C., and Klatzo, I. (1983). Regional patterns of blood-brain barrier breakdown during epileptiform seizures induced by various convulsive agents. Journal of Neuroscience *59*: 305–322.

Noachtar, S., and Rémi, J. (2009). The role of EEG in epilepsy: a critical review. Epilepsy & Behavior *15*: 22–33.

Nomura, Y., and Kitamura, Y. (1993). Inducible nitric oxide synthase in glial cells. Neuroscience Research 103–107.

Norenberg, M.D., and Martinez-Hernandez, A. (1979). Fine structural localization of glutamine synthetase in astrocytes of rat brain. Brain Research *161*: 303–310.

O'Neill, H.C., Orlicky, D.J., Hendry-Hofer, T.B., Loader, J.E., Day, B.J., and White, C.W. (2011). Role of Reactive Oxygen and Nitrogen Species in Olfactory Epithelial Injury by the Sulfur Mustard Analogue 2-Chloroethyl Ethyl Sulfide. Am J Respir Cell Mol Biol *45*: 323–331.

Ong, S.E., Foster, L.J., and Mann, M. (2003). Mass spectrometric-based approaches

in quantitative proteomics. Methods *29*: 124–130.

Palmieri, F. (2013). The mitochondrial transporter family SLC25: Identification, properties and physiopathology. Molecular Aspects of Medicine *34*: 465–484.

Parathath, S.R., Gravanis, I., and Tsirka, S.E. (2007). Nitric oxide synthase isoforms undertake unique roles during excitotoxicity. Stroke *38*: 1938–1945.

Parent, J.M., and Lowenstein, D.H. (2002). Seizure-induced neurogenesis: are more new neurons good for an adult brain? Prog. Brain Res. *135*: 121–131.

Park, J.-H., and Schuchman, E.H. (2006). Acid ceramidase and human disease. Biochim. Biophys. Acta *1758*: 2133–2138.

Park, K.K., Reuben, J.S., and Soliman, K.F. (2001). The role of inducible-nitric oxide in cocaine-induced kindling. Exp. Biol. Med. (Maywood) *226*: 185–190.

Parmentier, S., Böhme, G.A., Lerouet, D., Damour, D., Stutzmann, J.M., Margaill, I., et al. (1999). Selective inhibition of inducible nitric oxide synthase prevents ischaemic brain injury. Br. J. Pharmacol. *127*: 546–552.

Peltola, J., Palmio, J., Korhonen, L., Suhonen, J., Miettinen, A., Hurme, M., et al. (2000). Interleukin-6 and Interleukin-1 receptor antagonist in cerebrospinal fluid from patients with recent tonic–clonic seizures. Epilepsy Research *41*: 205–211.

Penkowa, M., Molinero, A., Carrasco, J., and Hidalgo, J. (2001). Interleukin-6 deficiency reduces the brain inflammatory response and increases oxidative stress and neurodegeneration after kainic acid-induced seizures. Nature *102*: 805–818.

Perillan, P.R., Chen, M., Potts, E.A., and Simard, J.M. (2002). Transforming growth factor-beta 1 regulates Kir2.3 inward rectifier K+ channels via phospholipase C and protein kinase C-delta in reactive astrocytes from adult rat brain. J. Biol. Chem. *277*: 1974–1980.

Perillo, N.L., Marcus, M.E., and Baum, L.G. (1998). Galectins: versatile modulators of cell adhesion, cell proliferation, and cell death. J Mol Med *76*: 402–412.

Perkins, D.N., Pappin, D.J., Creasy, D.M., and Cottrell, J.S. (1999). Probability-based protein identification by searching sequence databases using mass spectrometry data. Electrophoresis *20*: 3551–3567.

Persike, D.S., Lima, M.L., Amorim, R.P., Cavalheiro, E.A., Yacubian, E., Centeno, R.S., et al. (2012). Hippocampal proteomic profile in temporal lobe epilepsy. Journal of Epilepsy and Clinical Neurophysiology *18*: 53–56.

Peters, T.J. (1995). All About Albumin: Biochemistry, Genetics, and Medical Applications, 1995 San Diego (Academic Press).

Pérez-Asensio, F.J., Hurtado, O., and Burguete, M.C. (2005). Inhibition of iNOS

activity by 1400W decreases glutamate release and ameliorates stroke outcome after experimental ischemia. Neurobiology of Disease *18*: 375–384.

Picotti, P., Clément-Ziza, M., Lam, H., Campbell, D.S., Schmidt, A., Deutsch, E.W., et al. (2013). A complete mass-spectrometric map of the yeast proteome applied to quantitative trait analysis. Nature *494*: 266–270.

Pilz, R.B., and Casteel, D.E. (2003). Regulation of gene expression by cyclic GMP. Circ. Res. *93*: 1034–1046.

Pitkänen, A., and Lukasiuk, K. (2009). Molecular and cellular basis of epileptogenesis in symptomatic epilepsy. Epilepsy & Behavior *14*: 16–25.

Pitkänen, A., Schwartzkroin, P.A., and Moshé, S.L. (2005). Models of Seizures and Epilepsy. Academic Press 415–434.

Pont, F., Collet, A., and Lallement, G. (1995). Early and transient increase of rat hippocampal blood-brain barrier permeability to amino acids during kainic acid-induced seizures. Neuroscience Letters *184*: 52–54.

Porter, D.H., Cook, R.J., and Wagner, C. (1985). Enzymatic properties of dimethylglycine dehydrogenase and sarcosine dehydrogenase from rat liver. Arch. Biochem. Biophys. *243*: 396–407.

Probert, L., Akassoglou, K., Pasparakis, M., Kontogeorgos, G., and Kollias, G. (1995). Spontaneous inflammatory demyelinating disease in transgenic mice showing central nervous system-specific expression of tumor necrosis factor alpha. Proc. Natl. Acad. Sci. U.S.a. *92*: 11294–11298.

Przegaliński, E., Baran, L., and Siwanowicz, J. (1994). The role of nitric oxide in the kainate-induced seizures in mice. Neuroscience Letters *170*: 74–76.

Przegaliński, E., Baran, L., and Siwanowicz, J. (1996). The role of nitric oxide in chemically-and electrically-induced seizures in mice. Neuroscience Letters *217*: 145–148.

Pulman, J., Greenhalgh, J., and Marson, A.G. (1996). Antiepileptic drugs as prophylaxis for post-craniotomy seizures (Chichester, UK: John Wiley & Sons, Ltd).

Purves, D., Fitzpatrick, D., Katz, L.C., Lamantia, A.-S., McNamara, J.O., Williams, S.M., et al. (2001). Neuroscience 2nd edition.

Racine, R.J. (2002). Modification of seizure activity by electrical stimulation. II. Motor seizure. Electroencephalography and Clinical Neurophysiology *32*: 281–294.

Rao, R.S., Prakash, A., and Medhi, B. (2009). Role of different cytokines and seizure susceptibility: a new dimension towards epilepsy research. Indian J. Exp. Biol. *47*: 625–634.

Rattka, M., Brandt, C., and Löscher, W. (2013). The intrahippocampal kainate model of temporal lobe epilepsy revisited: Epileptogenesis, behavioral and cognitive alterations, pharmacological response, and hippoccampal damage in epileptic rats. Epilepsy Research *103*: 135–152.

Ravizza, T., Gagliardi, B., Noé, F., Boer, K., Aronica, E., and Vezzani, A. (2008). Innate and adaptive immunity during epileptogenesis and spontaneous seizures: Evidence from experimental models and human temporal lobe epilepsy. Neurobiology of Disease *29*: 142–160.

Ray, C.A., Bowsher, R.R., Smith, W.C., Devanarayan, V., Willey, M.B., Brandt, J.T., et al. (2005). Development, validation, and implementation of a multiplex immunoassay for the simultaneous determination of five cytokines in human serum. J Pharm Biomed Anal *36*: 1037–1044.

Rehni, A.K., Singh, T.G., Kalra, R., and Singh, N. (2009). Pharmacological inhibition of inducible nitric oxide synthase attenuates the development of seizures in mice. Nitric Oxide *21*: 120–125.

Riento, K., and Ridley, A.J. (2003). Rocks: multifunctional kinases in cell behaviour. Nat Rev Mol Cell Biol *4*: 446–456.

Rizzi, M., Perego, C., Aliprandi, M., Richichi, C., Ravizza, T., Colella, D., et al. (2003). Glia activation and cytokine increase in rat hippocampus by kainic acid-induced status epilepticus during postnatal development. Neurobiology of Disease *14*: 494–503.

Roch, C., Leroy, C., Nehlig, A., and Namer, I.J. (2002). Magnetic resonance imaging in the study of the lithium-pilocarpine model of temporal lobe epilepsy in adult rats. Epilepsia *43*: 325–335.

Rodeberg, D.A., Chaet, M.S., Bass, R.C., Arkovitz, M.S., and Garcia, V.F. (1995). Nitric oxide: An overview. The American Journal of Surgery *170*: 292–303.

Rogawski, M.A. (2011). Revisiting AMPA receptors as an antiepileptic drug target. Epilepsy Currents *11*: 56–63.

Rossman, K.L., Der, C.J., and Sondek, J. (2005). GEF means go: turning on RHO GTPases with guanine nucleotide-exchange factors. Nat Rev Mol Cell Biol *6*: 167–180.

Samuel, W. (2000). Epidemiology of Temporal Lobe Epilepsy. The Canadian Journal of Neurological Sciences *27*: S6–S10.

Sander, J.W. (2003). The epidemiology of epilepsy revisited. Curr Opin Neurol 1–6.

Satelli, A., and Li, S. (2011). Vimentin in cancer and its potential as a molecular target for cancer therapy. CMLS, Cell. Mol. Life Sci. *68*: 3033–3046.

Savitz, S.I., and Schäbitz, W.-R. (2012). Reviving neuroprotection using a new approach: targeting postsynaptic density-95 to arrest glutamate excitotoxicity. Stroke *43*: 3411–3412.

Schauwecker, P.E., and Steward, O. (1997). Genetic determinants of susceptibility to excitotoxic cell death: Implications for gene targeting approaches. Proc. Natl. Acad. Sci. U.S.a. *94*: 4103–4108.

Schmidt, D., and Löscher, W. (2003). How effective is surgery to cure seizures in drug-resistant temporal lobe epilepsy? Epilepsy Research *56*: 85–91.

Schroder, K., Hertzog, P.J., Ravasi, T., and Hume, D.A. (2004). Interferon-gamma: an overview of signals, mechanisms and functions. J. Leukoc. Biol. *75*: 163–189.

Schröder, W., Hinterkeuser, S., Seifert, G., Schramm, J., Jabs, R., Wilkin, G.P., et al. (2000). Functional and molecular properties of human astrocytes in acute hippocampal slices obtained from patients with temporal lobe epilepsy. Epilepsia *41 Suppl 6*: S181–4.

Schwartz, A.S., Yu, J., Gardenour, K.R., Finley, R.L., and Ideker, T. (2009). Cost-effective strategies for completing the interactome. Nature Methods *6*: 55–61.

Schwarze, S.R., Ho, A., Vocero-Akbani, A., and Dowdy, S.F. (1999). In vivo protein transduction: delivery of a biologically active protein into the mouse. Science *285*: 1569–1572.

Schwob, J.E., Fuller, T., Price, J.L., and Olney, J.W. (1980). Widespread patterns of neuronal damage following systemic or intracerebral injections of kainic acid: a histological study. Neuroscience *5*: 991–1014.

Seifert, G., Schilling, K., and Steinhäuser, C. (2006). Astrocyte dysfunction in neurological disorders: a molecular perspective. Nature Reviews Neuroscience.

Seiffert, E., Dreier, J.P., Ivens, S., Bechmann, I., Tomkins, O., Heinemann, U., et al. (2004). Lasting blood-brain barrier disruption induces epileptic focus in the rat somatosensory cortex. Journal of Neuroscience *24*: 7829–7836.

Seyfried, T.N., Robert, K.Y., and Glaser, G.H. (1980). Genetic analysis of audiogenic seizure susceptibility in C57BL/6J X DBA/2J recombinant inbred strains of mice. Genetics *94*: 701–718.

Shaftel, S.S., Carlson, T.J., Olschowka, J.A., Kyrkanides, S., Matousek, S.B., and O'Banion, M.K. (2007). Chronic interleukin-1beta expression in mouse brain leads to leukocyte infiltration and neutrophil-independent blood brain barrier permeability without overt neurodegeneration. Journal of Neuroscience *27*: 9301–9309.

Sharma, A.K., Reams, R.Y., Jordan, W.H., Miller, M.A., Thacker, H.L., and Snyder, P.W.

(2007). Mesial temporal lobe epilepsy: pathogenesis, induced rodent models and lesions. Toxicol Pathol *35*: 984–999.

Shiratori, Y., Hikiba, Y., Mawet, E., Niwa, Y., Matsumura, M., Kato, N., et al. (1994). Modulation of KC/gro protein (interleukin-8 related protein in rodents) release from hepatocytes by biologically active mediators. Biochemical and Biophysical Research Communications *203*: 1398–1403.

Shorvon, S.D. (2011). The etiologic classification of epilepsy. Epilepsia *52*: 1052–1057.

Simonian, N.A., Getz, R.L., Leveque, J.C., Konradi, C., and Coyle, J.T. (1996). Kainic acid induces apoptosis in neurons. Nature *75*: 1047–1055.

Sinha, S., Patil, S.A., Jayalekshmy, V., and Satishchandra, P. (2008). Do cytokines have any role in epilepsy? Epilepsy Research *82*: 171–176.

Sleigh, J., Harvey, M., Voss, L., and Denny, B. (2014). Ketamine – More mechanisms of action than just NMDA blockade. Trends in Anaesthesia and Critical Care *4*: 76–81.

Smirnova, M.G., Kiselev, S.L., Gnuchev, N.V., Birchall, J.P., and Pearson, J.P. (2002). Role of the pro-inflammatory cytokines tumor necrosis factor-alpha, interleukin-1beta, interleukin-6 and interleukin-8 in the pathogenesis of the otitis media with effusion. Eur. Cytokine Netw. 161–72.

Smith, K.A. (1988). Interleukin-2: inception, impact, and implications. Science *240*: 1169–1176.

Smith, M., Wilcox, K.S., and White, H.S. (2007). Discovery of antiepileptic drugs. Neurotherapeutics *4*: 12–17.

Sokrab, T.E., Kalimo, H., and Johansson, B.B. (1989). Endogenous serum albumin content in brain after short-lasting epileptic seizures. Brain Research *489*: 231–236.

Somera-Molina, K.C., Nair, S., Van Eldik, L.J., Watterson, D.M., and Wainwright, M.S. (2009). Enhanced microglial activation and proinflammatory cytokine upregulation are linked to increased susceptibility to seizures and neurologic injury in a 'two-hit' seizure model. Brain Research *1282*: 162–172.

Sperk, G. (1994). Kainic Acid Seizures in the Rat. Progress in Neurobiology *42*: 1–32.

Sperk, G., Lassmann, H., Baran, H., Kish, S.J., Seitelberger, F., and Hornykiewicz, O. (1983). Kainic acid induced seizures: neurochemical and histopathological changes. Neuroscience *10*: 1301–1315.

Sridharan, R. (2002). Epidemiology of epilepsy. Curr Sci *82*: 664–670.

Stafstrom, C.E. (2013). Jasper's Basic Mechanisms of the Epilepsies, 4th Edition. Neurology *81*: 1883–1884.

Stover, P., and Schirch, V. (1990). Serine hydroxymethyltransferase catalyzes the hydrolysis of 5,10-methenyltetrahydrofolate to 5-formyltetrahydrofolate. J. Biol. Chem. *265*: 14227–14233.

Subasi, A., and Erçelebi, E. (2005). Classification of EEG signals using neural network and logistic regression. Computer Methods and Programs in Biomedicine *78*: 87–99.

Sumanont, Y., Murakami, Y., Tohda, M., Vajragupta, O., Watanabe, H., and Matsumoto, K. (2006). Prevention of kainic acid-induced changes in nitric oxide level and neuronal cell damage in the rat hippocampus by manganese complexes of curcumin and diacetylcurcumin. Life Sciences *78*: 1884–1891.

Sun, H.-S., Doucette, T.A., Liu, Y., Fang, Y., Teves, L., Aarts, M., et al. (2008). Effectiveness of PSD95 inhibitors in permanent and transient focal ischemia in the rat. Stroke *39*: 2544–2553.

Suzuki, S., Tanaka, K., and Suzuki, N. (2008). Ambivalent aspects of interleukin-6 in cerebral ischemia: inflammatory versus neurotrophic aspects. J. Cereb. Blood Flow Metab. *29*: 464–479.

Szklarczyk, D., Franceschini, A., Kuhn, M., Simonovic, M., Roth, A., Minguez, P., et al. (2011). The STRING database in 2011: functional interaction networks of proteins, globally integrated and scored. Nucleic Acids Research *39*: D561–8.

Takatsu, K. (2004). Role of interleukin-5 in immune regulation and inflammation. Nippon Rinsho *62*: 1941–1951.

Taqatqeh, F., Mergia, E., Neitz, A., Eysel, U.T., Koesling, D., and Mittmann, T. (2009). More than a retrograde messenger: nitric oxide needs two cGMP pathways to induce hippocampal long-term potentiation. Journal of Neuroscience *29*: 9344–9350.

Tarroux, P. (1983). Analysis of protein patterns during differentiation using 2-D electrophoresis and computer multidimensional classification. Electrophoresis *4*: 63–70.

Taylor, A.W. (2009). Review of the activation of TGF-beta in immunity. J. Leukoc. Biol. *85*: 29–33.

Teleńczuk, B., Baker, S.N., Kempter, R., and Curio, G. (2015). Correlates of a single cortical action potential in the epidural EEG. NeuroImage *109*: 357–367.

Tomkins, O., Feintuch, A., Benifla, M., Cohen, A., Friedman, A., and Shelef, I. (2011). Blood-Brain Barrier Breakdown Following Traumatic Brain Injury: A Possible Role

in Posttraumatic Epilepsy. Cardiovascular Psychiatry and Neurology *2011*: 1–11.

Tomkins, O., Friedman, O., Ivens, S., Reiffurth, C., Major, S., Dreier, J.P., et al. (2007). Blood-brain barrier disruption results in delayed functional and structural alterations in the rat neocortex. Neurobiology of Disease *25*: 367–377.

Tomkins, O., Shelef, I., Kaizerman, I., Eliushin, A., Afawi, Z., Misk, A., et al. (2008). Blood-brain barrier disruption in post-traumatic epilepsy. J Neurol Neurosurg Psychiatry *79*: 774–777.

Townsend, D.M., and Tew, K.D. (2003). The role of glutathione-S-transferase in anti-cancer drug resistance. Oncogene *22*: 7369–7375.

Tracey, K.J., and Cerami, A. (1992). Tumor necrosis factor and regulation of metabolism in infection: role of systemic versus tissue levels. Proc. Soc. Exp. Biol. Med. *200*: 233–239.

Tracey, K.J., MD, Cerami, A., and D, P. (1994). Tumor necrosis factor: A pleiotropic cytokine and therapuetic target. Annu. Rev. Med.

Tsuchiya, K., and Kogure, S. (2011). Fast Fourier transformation analysis of kindling-induced afterdischarge in the rabbit hippocampus. Epilepsy Research *95*: 144–151.

Uva, L., Librizzi, L., Marchi, N., Noé, F., Bongiovanni, R., Vezzani, A., et al. (2008). Acute induction of epileptiform discharges by pilocarpine in the in vitro isolated guinea-pig brain requires enhancement of blood–brain barrier permeability. Nature *151*: 303–312.

V S Saxena, V.V.N. (2011). Nonpharmacological treatment of epilepsy. Annals of Indian Academy of Neurology *14*: 148–152.

Van Kampen, C., Gauldie, J., and Collins, S.M. (2005). Proinflammatory properties of IL-4 in the intestinal microenvironment. Am. J. Physiol. Gastrointest. Liver Physiol. *288*: G111–7.

Van Vliet, E.A., da Costa Araujo, S., Redeker, S., van Schaik, R., Aronica, E., and Gorter, J.A. (2007). Blood-brain barrier leakage may lead to progression of temporal lobe epilepsy. Brain *130*: 521–534.

Vazquez, A.J., Diamond, B.I., and Sabelli, H.C. (1975). Differential effects of phenobarbital and pentobarbital on isolated nervous tissue. Epilepsia *16*: 601–608.

Vezzani, A. (2004). Brain Inflammation and Seizures. Epilepsy Currents *4*: 73–75.

Vezzani, A., and Granata, T. (2005). Brain Inflammation in Epilepsy: Experimental and Clinical Evidence. Epilepsia *46*: 1724–1743.

Vezzani, A., Aronica, E., Mazarati, A., and Pittman, Q.J. (2013). Epilepsy and brain

inflammation. Experimental Neurology *244*: 11–21.

Vezzani, A., Balosso, S., and Ravizza, T. (2008). The role of cytokines in the pathophysiology of epilepsy. Brain, Behavior, and Immunity *22*: 797–803.

Vezzani, A., Conti, M., De Luigi, A., Ravizza, T., Moneta, D., Marchesi, F., et al. (1999). Interleukin-1beta immunoreactivity and microglia are enhanced in the rat hippocampus by focal kainate application: functional evidence for enhancement of electrographic seizures. Journal of Neuroscience *19*: 5054–5065.

Vezzani, A., Moneta, D., Richichi, C., and Aliprandi, M. (2002). Functional Role of Inflammatory Cytokines and Antiinflammatory Molecules in Seizures and Epileptogenesis. Epilepsia *43*: 30–35.

Vignali, D.A.A., and Kuchroo, V.K. (2012). IL-12 family cytokines: immunological playmakers. Nat Immunol *13*: 722–728.

Vilain, S., Cosette, P., Hubert, M., Lange, C., Junter, G.-A., and Jouenne, T. (2004). Comparative proteomic analysis of planktonic and immobilized Pseudomonas aeruginosa cells: a multivariate statistical approach. Analytical Biochemistry *329*: 120–130.

Vincent, A., Irani, S.R., and Lang, B. (2010). The growing recognition of immunotherapy-responsive seizure disorders with autoantibodies to specific neuronal proteins. Curr Opin Neurol *23*: 144–150.

Vincent, P., and Mulle, C. (2009). Kainate receptors in epilepsy and excitotoxicity. Nature *158*: 309–323.

Vodovotz, Y. (1997). Control of Nitric Oxide Production by Transforming Growth Factor-β1: Mechanistic Insights and Potential Relevance to Human Disease. Nitric Oxide *1*: 3–17.

Walker, M.C., White, H.S., and Sander, J.W.A.S. (2002). Disease modification in partial epilepsy. Brain *125*: 1937–1950.

Wallraff, A., Köhling, R., Heinemann, U., Theis, M., Willecke, K., and Steinhäuser, C. (2006). The impact of astrocytic gap junctional coupling on potassium buffering in the hippocampus. Journal of Neuroscience *26*: 5438–5447.

Wang, Q., Yu, S., Simonyi, A., Sun, G.Y., and Sun, A.Y. (2005). Kainic Acid-Mediated Excitotoxicity as a Model for Neurodegeneration. Mn *31*: 3–16.

Watanabe, S., Hayakawa, T., Wakasugi, K., and Yamanaka, K. (2014). Cystatin C protects neuronal cells against mutant copper-zinc superoxide dismutase-mediated toxicity. Cell Death & Disease *5*: e1497.

Watkins-Chow, D.E., Pavan, W.J., and Pavan, W.J. (2008). Genomic copy number and expression variation within the C57BL/6J inbred mouse strain. Genome Research

18: 60–66.

Waziri, A., Schevon, C.A., Cappell, J., Emerson, R.G., McKhann, G.M., and Goodman, R.R. (2009). Initial surgical experience with a dense cortical microarray in epileptic patients undergoing craniotomy for subdural electrode implantation. Neurosurgery *64*: 540–5– discussion 545.

Weinberg, M.S., Blake, B.L., and McCown, T.J. (2013). Opposing actions of hippocampus TNFα receptors on limbic seizure susceptibility. Experimental Neurology *247*: 429–437.

Weinstein, J.N., Myers, T.G., O'Connor, P.M., Friend, S.H., Fornace, A.J., Kohn, K.W., et al. (1997). An information-intensive approach to the molecular pharmacology of cancer. Science *275*: 343–349.

Wenzel, H.J., Woolley, C.S., Robbins, C.A., and Schwartzkroin, P.A. (2000). Kainic acid-induced mossy fiber sprouting and synapse formation in the dentate gyrus of rats. Hippocampus *10*: 244–260.

Wetherington, J., Serrano, G., and Dingledine, R. (2008). Astrocytes in the Epileptic Brain. Neuron *58*: 168–178.

White, A., Williams, P.A., Hellier, J.L., Clark, S., Edward Dudek, F., and Staley, K.J. (2010). EEG spike activity precedes epilepsy after kainate-induced status epilepticus. Epilepsia *51*: 371–383.

White, A.M., Williams, P.A., Ferraro, D.J., Clark, S., Kadam, S.D., Dudek, F.E., et al. (2006). Efficient unsupervised algorithms for the detection of seizures in continuous EEG recordings from rats after brain injury. Journal of Neuroscience Methods *152*: 255–266.

White, H.S. (2002). Animal models of epileptogenesis. Neurology *59*: S7–S14.

Wilgenbus, K.K., Hsieh, C.L., Lankes, W.T., Milatovich, A., Francke, U., and Furthmayr, H. (1994). Structure and localization on the X chromosome of the gene coding for the human filopodial protein moesin (MSN). Genomics *19*: 326–333.

Williams, P.A., Hellier, J.L., White, A.M., Staley, K.J., and Dudek, F.E. (2007). Development of Spontaneous Seizures after Experimental Status Epilepticus: Implications for Understanding Epileptogenesis. Epilepsia *48*: 157–163.

Williams, P.A., White, A.M., Clark, S., Ferraro, D.J., Swiercz, W., Staley, K.J., et al. (2009). Development of spontaneous recurrent seizures after kainate-induced status epilepticus. Journal of Neuroscience *29*: 2103–2112.

Willmore, L.J., Sypert, G.W., Munson, J.V., and Hurd, R.W. (1978). Chronic focal epileptiform discharges induced by injection of iron into rat and cat cortex. Science *200*: 1501–1503.

Wolf, H.K., Campos, M.G., Zentner, J., Hufnagel, A., Schramm, J., Elger, C.E., et al. (1993). Surgical Pathology of Temporal Lobe Epilepsy. Experience with 216 Cases. Journal of Neuropathology and Experimental Neurology *52*: 499–506.

Wolf, P., and Okujava, N. (1999). Possibilities of non-pharmacological conservative treatment of epilepsy. Seizure *8*: 45–52.

Wolpe, S.D., Davatelis, G., Sherry, B., Beutler, B., Hesse, D.G., Nguyen, H.T., et al. (1988). Macrophages secrete a novel heparin-binding protein with inflammatory and neutrophil chemokinetic properties. J Exp Med *167*: 570–581.

Wong, D., Dorovini-Zis, K., and Vincent, S.R. (2004). Cytokines, nitric oxide, and cGMP modulate the permeability of an in vitro model of the human blood–brain barrier. Experimental Neurology *190*: 446–455.

Wu, L., Niemeyer, B., Colley, N., Socolich, M., and Zuker, C.S. (1995). Regulation of PLC-mediated signalling in vivo by CDP-diacylglycerol synthase. Nature *373*: 216–222.

Wyss-Coray, T., Lin, C., Yan, F., Yu, G.Q., Rohde, M., McConlogue, L., et al. (2001). TGF-beta1 promotes microglial amyloid-beta clearance and reduces plaque burden in transgenic mice. Nat. Med. *7*: 612–618.

Xu, L., Zeng, L.-H., and Wong, M. (2009). Impaired Astrocytic Gap Junction Coupling and Potassium Buffering in a Mouse Model of Tuberous Sclerosis Complex. Neurobiology of Disease *34*: 291–299.

Xu, Z.-H., Otterness, D.M., Freimuth, R.R., Carlini, E.J., Wood, T.C., Mitchell, S., et al. (2000). Human 3′-Phosphoadenosine 5′-Phosphosulfate Synthetase 1 (PAPSS1) and PAPSS2: Gene Cloning, Characterization and Chromosomal Localization. Biochemical and Biophysical Research Communications *268*: 437–444.

Yamashita, T., Sawamoto, K., Suzuki, S., Suzuki, N., Adachi, K., Kawase, T., et al. (2005). Blockade of interleukin-6 signaling aggravates ischemic cerebral damage in mice: possible involvement of Stat3 activation in the protection of neurons. J Neurochem *94*: 459–468.

Youn, Y., Sung, I.K., and Lee, I.G. (2013). The role of cytokines in seizures: interleukin (IL)-1β, IL-1Ra, IL-8, and IL-10. Korean J Pediatr *56*: 271.

Yudkoff, M., Nissim, I., and Pleasure, D. (1988). Astrocyte Metabolism of [15N]Glutamine: Implications for the Glutamine-Glutamate Cycle. J Neurochem *51*: 843–850.

Yuen, T.G.H., Agnew, W.F., and Bullara, L.A. (1987). Tissue response to potential neuroprosthetic materials implanted subdurally. Biomaterials *8*: 138–141.

Zdanov, A., Schalk-Hihi, C., Gustchina, A., Tsang, M., Weatherbee, J., and Wlodawer,

A. (1995). Crystal structure of interleukin-10 reveals the functional dimer with an unexpected topological similarity to interferon gamma. Structure *3*: 591–601.

Zhou, L., and Zhu, D.-Y. (2009). Neuronal nitric oxide synthase: Structure, subcellular localization, regulation, and clinical implications. Nitric Oxide *20*: 223–230.

Zhu, C.-B., Blakely, R.D., and Hewlett, W.A. (2006). The Proinflammatory Cytokines Interleukin-1beta and Tumor Necrosis Factor-Alpha Activate Serotonin Transporters. Neuropsychopharmacology.

Zhu, Y., Roth-Eichhorn, S., Braun, N., Culmsee, C., Rami, A., and Krieglstein, J. (2000). The expression of transforming growth factor-beta1 (TGF-beta1) in hippocampal neurons: a temporary upregulated protein level after transient forebrain ischemia in the rat. Brain Research *866*: 286–298.

Zucker, D.K., Wooten, G.F., and Lothman, E.W. (1983). Blood-brain barrier changes with kainic acid-induced limbic seizures. Experimental Neurology *79*: 422–433.

Appendix

For loop script for splitting raw Spike2 data files into individual channels in text file using Python

```
for i in range(file_number, 0, -1):
               channel_raw = header_raw[-i]
              #looks for channel according to header
               channel = re.sub(re.compile('[A-Z a-z\"]'), '', channel_raw)
              #removes KA and leaves only the channel number
               file = open('{0}/channel{1}.txt'.format(file_directory, channel),
              'w')
              #create new text file i.e. channel1.txt
                file.close()
              #finish

               file_dict[count] = '{0}/channel{1}.txt'.format(file_directory,
              channel)
              #put name of text file into temporary storage structure
               count += 1
              #move on to next channel number


for x in file_dict:
                print('file = {0}'.format(file_dict[x]))
               #tells user which file accessing
                file = open('{0}'.format(file_dict[x]), 'a')
               #opens the accessed file
               for i in read[1:]:
              #reads data except header
                       j = i.split('\t')
                      #recognises each tab as a separate channel
                       j[-1] = j[-1].replace('\n', '')
                      #removes new line character
                         line = '{0}\n'.format(j[x])
                      #reads the relevant data entry point
                         file.write(line)
                      #writes the relevant data entry point into correct file
                file.close()
              #finish
```

For loop script for data filtering on EEGLAB toolbox using MATLAB

```
for days = start: final,

    hours_directory = sprintf('Day %d', days);
       #look for folder by day

    disp(hours_directory);
       #tells users which hour being analysed

    cd(hours_directory);
       #change directory to go into folder

    hours_folders = dir('*');
       #list all files in the folder

    disp(length(hours_folders))
       #tells user how many files there are in the folder

    for hours = 3: length(hours_folders),
       #only look in hours folder


        disp(hours_folders(hours).name);
              #tells user which hour folder is being analysed

        cd(hours_folders(hours).name)
              #change directory to folder being analysed

        j = dir('channel*.txt');
              #look for files called channel*.txt


        for i = 1: length(j),
              #go through each channel files

            disp(j(i).name);
              #tells user which channel/file is being analysed

            channel = strcat(j(i).name(1:2), j(i).name(8));
              #recognise channel in eeglab by ch*

            EEG =
pop_importdata('dataformat','ascii','nbchan',0,'data',j(i).name,'srate',100,'pnts',
0,'xmin',0);
            EEG.setname = channel;
            EEG = eeg_checkset( EEG );
            EEG = pop_eegfilt( EEG, 1, 0, [], [0]);
            EEG = eeg_checkset( EEG );
#internal command for eeglab data filtering

            filename = strcat(j(i).name(1:8), 'rejected.txt');
              #gives name as rejected.txt

            pop_export(EEG,filename,'erp','on','transpose','on');
              #saves rejected.txt file into folder

        end
        cd('../')
    end
    cd('../')
end
```

For loop script for counting local maxima using *findpeaks* toolbox in MATLAB

```
for days = start: finish,

    hours_directory = sprintf('Day %d', days);
       #look for the folder by day

    disp(hours_directory);
       #tells users which hour being analysed

    cd(hours_directory);
       #change directory to go into folder

    hours_folders = dir('*');
       #list all files in the folder

    for hours = 3: length(hours_folders);
       #only look in hours folder

        disp(hours_folders(hours).name)
              #tells user which hour folder is being analysed

        cd(hours_folders(hours).name)
              #change directory to folder being analysed

        j = dir('channel*rejected.txt');
              #look for files called channel*rejected.txt


        for i = 1:length(j),
              #go through each channel files

            disp(sprintf('Channel %s', j(i).name(8)));
              #display channel number on command window i.e. Channel 1

            channelselect = str2num(j(i).name(8));
              #find the channel number

            channel = strcat(j(i).name(1:2), j(i).name(8));
              #recognise as ch* i.e. ch1

            A = importdata(j(i).name);
              #import data

            chYpos=A(:,2);
              #create a new variable for second column called chYpos

            chYneg=chYpos*-1;
              #create a new variable called chYneg which flips chYpos upside down
            spk=findpeaks(chYpos,'minpeakheight',thresholds(channelselect));
              #calculate the number of local maxima above threshold in chYpos

            posspk=sum(spk>thresholds(channelselect));
              #count the number of local maxima above the threshold in chYpos

            spk=findpeaks(chYneg,'minpeakheight',thresholds(channelselect));
              #calculate the number of local maxima above the threshold in chYneg

            negspk=sum(spk>thresholds(channelselect));
              #count the number of local maxima above the threshold in chYneg

            disp(sprintf('posspk = %d', posspk));
              #display the number of local maxima in chYpos on command window

            disp(sprintf('negspk = %d', negspk));
              #display the number of local maxima in chYneg on command window

            manual_copy = input('press enter to continue');
```

```
            #display next result by pressing enter

        end
        cd('../')
    end
    cd('../')
end
cd('../')
```

Script for calculating coastline analysis using JAVA

- **Clean file**

```
writer = new BufferedWriter( new OutputStreamWriter(
                    new FileOutputStream(filename+"_cleanfile.txt"), "utf-8"));

            int evenCheck = 0;
            s.next();
            s.next();
            int test = 0;
            while(s.hasNext()) {

                if(evenCheck%2==0) {
                   String line = s.next();
                   if(line.equals("nan")) {

                       line = "0.000";
                   }
               writer.write(line+"\n");
```

- **Creating a 30-sec epoch of 3000 data points**

```
int numOfWindows = (int) Math.ceil(numberOfLines / 3000.0);
                System.out.println("Num windows: "+numOfWindows);

                int i = 0;
               double sumCoastLine = 0; //Make a sum of the coastLine results from
each window

               int windowSize = 3000;
                while(i<numOfWindows) {
                   double progress = (double) i/numOfWindows*100;

                   publish(progress*2);
           //update the size of the window
           if (i == numOfWindows-1) {

               windowSize = numberOfLines;
               System.out.println("Window size is: "+windowSize);
           }
           //Make window
           double[] window = wc.setWindow(i*3000, Seizure_Liverpool.filename +
"_cleanfile.txt", windowSize);
           double coastResult = cl.coast(window);

           sumCoastLine+=coastResult;
           output.add(Double.toString(coastResult));
```

Coastline analysis

```
double d = 0;
        for (int i = 1; i < data.length; i++) {
             d += (Math.abs(data[i]-data[i-1]));

        }
        return d;
```

Script for automatically listing all coastline data using Python

- **Fill up data in 120-datapoint window**

```
def read_file(root_directory, day, hours, coastline_files_list):

	clean = {}

	for channels in coastline_files_list:
		file = open('{0}/{1}/{2}/{3}'.format(root_directory, day, hours,
channels))
		#print('{0}/{1}/{2}/{3}'.format(root_directory, day, hours, channels))
		read = file.readlines()
		file.close()
		raw_data = read[1: -2]

		pre_clean = [''] * 120


		for i in range(len(raw_data)):
			entry = raw_data[i].strip()

			pre_clean[i] = entry

		clean[new] = pre_clean

	return(clean)
```

- **Automatically export data into excel per channel**

```
def export_to_excel(master, date_range):
	##Write script to export to an excel file

	multiplyer = date_range[1] - date_range[0] + 1
	i_range = 24 * multiplyer

	print(multiplyer, i_range)

	wb = openpyxl.Workbook(optimized_write = True)
	ws = wb.create_sheet(title='coastline by day')

	channel_list = []

	for channels in master:
		channel_list.append(channels)

	ordered_channels = sorted(channel_list)

	ws.append(ordered_channels)

	print('exporting')
	for i in range(i_range):
		for k in range(120):
			line = []
			for j in ordered_channels:

				line.append(master[j][i][k])


			new_line = []
			for individuals in line:
				try:
					new_line.append(float(individuals))
				except(ValueError):
					new_line.append(individuals)

			ws.append(new_line)


	wb.save('{0}/coastline_by_day.xlsx'.format(root_directory))
	print('\nComplete')
```